THE OHIO STATE UNIVERSITY

Studies of the Nonlinear Dynamics of Fluid Systems

C. David Andereck
Department of Physics

Grant No. N00014-89-J-1352
Contract No. N00014-86-K-0071
Final Report
Period Covered;

February, 1995

THE OHIO STATE UNIVERSITY

Studies of the Nonlinear Dynamics of Fluid Systems

C. David Andereck
Department of Physics

Grant No. N00014-89-J-1352
Contract No. N00014-86-K-0071
Final Report
Period Covered;
RF Project No. 721792

February, 1995

Table of Contents

I. Report Summary

Systems driven far from equilibrium are pervasive and important. Whether the specific external influence is heat flow (Rayleigh-Bénard convection in the lab, cloud layers in the atmosphere), centrifugal force (Taylor-Couette flow between rotating cylinders, flow along curved turbine blades), or reacting chemicals (Belousov-Zhabotinskii reaction, a brain), a striking feature of these systems is that they can generate patterns in space and in time, often as a result of an instability of some simple basic state. These patterns may be technologically useful or harmful, but in either case it is crucially important to understand the fundamental physics of the nonlinearities involved in order to control or to best utilize the particular system.

Some pattern features are common to large classes of systems; there is some universality in the behavior, regardless of the underlying system-specific physics. This understanding has come about largely through the application of simple model equations to carefully designed experiments. For example, it has been shown repeatedly in detailed, quantitative experiments, that *amplitude equations* (non-equilibrium versions of the Ginzburg-Landau equation, familiar from the mean field approximation for equilibrium phase transitions), are adequate to describe the behavior near the onset of the first pattern beyond the basic state. But this approach has a limited validity. Once a system has been driven away from a pattern's onset by a significant amount, amplitude equations do not work. An alternative which does not suffer from this limitation, *phase dynamics*, is an approach to the modeling of the long-wavelength, low-frequency excitations of a pattern. Phase dynamics is thus a *generalized hydrodynamics of patterns*; Taylor vortices or other fundamental pattern units such as convection cells or turbulent spirals are analogous to the atoms of equilibrium systems. Likewise, the excitations of these patterns are analogous to the modes of oscillation of an equilibrium system, such as phonons in a crystal lattice.

Under ONR support we carried out an experimental study of the *generalized hydrodynamic behavior of cellular patterns far from onset*. We showed the basic qualitative effectiveness of the phase dynamics approach in modeling this behavior for both ordered and turbulent flows in the Taylor-Couette system. Although the experiments involved a specific system, the phase equations that describe them are determined by the pattern symmetries, so the results should generalize to other systems.

In addition we performed a series of experiments on flows in the Taylor-Dean system, the flow between independently rotating concentric cylinders with a partially filled gap. By adjusting the rotation speeds of the two cylinders it is possible to tune the velocity profile across the gap over a wide range, and hence produce a large variety of flow patterns. We studied in detail several novel patterns and their evolution upon increasing the relevant control parameter.

Finally, in a different area entirely, we studied two distinct liquid crystal systems. The first was a liquid crystal layer subjected to a noisy control parameter, which resulted in a state diagram in which the statistical probability density characteristics served as the distinguishing feature of the different states. The second was a study of phase winding in a thin layer of a liquid crystal subjected to rotationally induced shear.

The outcome of this project is a better understanding of highly nonequilibrium ordered and turbulent patterns in both simple and complex fluid systems, and of the ability of phase dynamics to model long-wavelength low-frequency behaviors in some cases.

II. Dynamics in the Taylor-Couette System

1. Overview

The principal work of our laboratory has been on pattern formation and dynamics in the Taylor-Couette system, the flow between independently rotating concentric cylinders. This work was supported by ONR contract N00014-86-K-0071 and grant N00014-89-J-1352. We have extended the survey work begun by Coles(1965), and Andereck, Liu and Swinney (1986) into regions left unexplored in those previous studies. A now well-known result from all of these studies is that, approximately speaking, the base flow is unstable to time-independent Taylor vortices when the cylinders rotate in the same direction, and is unstable to spirals when they rotate in opposite directions. At least for the Taylor vortex flow, it had been clear for some time that by using different procedures for ramping the rotation speeds, different states of flow could be produced. The different states were characterized by different numbers of vortices, or otherwise stated, by the axial wavelength of the pattern. Coles (1965) had shown that different secondary flows could then result, depending on the axial wavelength of the vortex pattern. Andereck, Liu and Swinney (1986) took note of this and restricted their survey to those secondary flows arising for Taylor vortex patterns that were close to the critical wavelength. We have now undertaken a more detailed examination of the secondary flows when the axial wavelength is different from critical. Some of this work has appeared, notably that on our study of confined states (Baxter and Andereck (1986) (reproduced in Appendix A, on page A-1), Andereck and Baxter (1988)), as discussed in Section II.2. This experiment has now been interpreted in terms of a phase dynamics framework. We will also briefly describe, in Section II.3, our survey work on the co-rotating regime. An article on this work is in preparation (Hegseth, Baxter and Andereck (1995)).

In Section II.4 we will discuss our testing of the predictions of phase dynamics for Taylor vortices (Wu and Andereck (1991a) & A-5), wavy Taylor vortices (Wu and Andereck (1991b) & A-9) and turbulent Taylor vortices (Wu, Andereck and Brand (1992) & A-13). Phase dynamics is essentially the long-wavelength, low-frequency behavior of the phase of patterns, a hydrodynamic description of their modes that should apply far from onset. In Section II.5 we will describe our study of a highly turbulent pattern occurring in the counter-rotating cylinders regime, spiral turbulence. As part of this work we attempted to describe the spiral's behavior in terms of a simple phase equation (Hegseth, Andereck, Hayot and Pomeau (1989) & A-40). This was the first attempt to study the hydrodynamic behavior of anything other than simple, approximately periodic structures.

2. Confined States in the Taylor-Couette System

Confined states, which consist of traveling convection rolls in a small region, surrounded by a pattern-free background, have been found in electro-hydrodynamic and binary fluid convection. Baxter and Andereck (1986) (A-1) reported for the first time a different phenomenon, the appearance of confined states, or "dynamical domains", in co-rotating cylinders flows (see Andereck, Liu and Swinney (1986) for a survey of the primary flow states). The system is started with a Taylor vortex axial wavelength larger than critical, and then the inner cylinder speed is slowly ramped to a larger value. Typically, the flow changes from Taylor vortex flow to wavy vortex flow, to twists, to twists with wavy inflow boundaries, to dynamical domains, to uniform turbulent Taylor vortices, and then back to domains. The characteristic feature of a state with multiple dynamical domains is that there are *regions of differing axial wavelength along the axis of the system*, and hence differing secondary flows. A dramatic example of this is shown on page A-1, in which a large axial wavelength patch supports turbulent flow, while surrounded by laminar, wavy vortices. The growth of these regions is evident in a plot of the axial

wavelength of the individual vortex pairs, as shown in Figure 3 on page A-2. The initial uniform state is shown at ϵ (relative to Taylor vortex onset with the $R_o > 0$) of about 1.25 (inner cylinder Reynolds number Ri = 1000), the appearance of the first domains at about 1.62 ($R_i = 1300$), and the re-emergence of domains at about 2.38 ($R_i = 1900$).

Since this work was completed similar results have been obtained in slot convection by Dubois, Bergé and Petrov (1990), Dubois, DaSilva, Daviaud, Bergé and Petrov (1989) and Hegseth, Vince, Dubois and Bergé (1992). The patterns in their system are not always subject to the complicating secondary instabilities found for Taylor flows. In their case it is sometimes observed that the smaller rolls oscillate, but the same basic domain structure is observed in any case. In addition, some theoretical progress has been made in describing both the Bénard and Taylor confined states within the framework of phase dynamics by Brand and Deissler (1989), Brand (1990) and Deissler, Lee and Brand (1990), and in parametrically excited standing waves by Riecke (1990a & b). By including higher order terms in the phase equation they find a generalized potential with two local minima, each corresponding to a different wavevector, thus leading to the possibility of confined regions of different vortex sizes. Brand (1990) points out that pinning boundary conditions are probably necessary for observation of the confined states. In the absence of such boundaries the confined states should be at most neutrally stable.

3. Axial Wavelength Dependence of Flows in the Taylor System

One of the striking, and now well-established, features of nonlinear systems is the multiplicity of flow states possible for given values of the control parameters. This was recognized and emphasized by Coles (1965) in his ground-breaking study of the Taylor system, and in particular the wavy vortex state. Andereck, Dickman and Swinney (1983) and Andereck, Liu and Swinney (1986) showed that there were several new states of flow, all bifurcating from Taylor vortices, when the inner and outer cylinders rotate in the same direction. In these experiments the axial wavelength was kept near the critical value, recognizing that this would be the situation possibly most amenable to modeling, and closest to what might be considered the preferred set of transitions. It was clear at the time, as described in Andereck, Dickman and Swinney (1983), that the onset of secondary flows depended on the axial wavelength, but no attempt was made to study this in any systematic manner. Under ONR funding we made such a survey and found certain trends which have come under theoretical and numerical study (Nagata (1986), Nagata (1988) and Weisshaar, Busse and Nagata (1991)).

Experimentally there exist definite trends in the flow state diagrams. The usual wavy vortex flow is found for all of the average axial wavelengths we worked with, but "twisted" vortices are not found for small axial wavelengths. The twists are the only other primary instability for large wavelengths. The results on twisted vortices agree rather well with the numerical modeling of Weisshaar et al (1991). In Hegseth, Andereck and Baxter (1995) we describe some possible mechanisms of instability leading to the different flow states, wavy inflow boundaries, wavy outflow boundaries and twists, based on our observations of the axial wavelength dependences and some general input on the velocity field from numerical investigations.

4. Phase Dynamics of Taylor, Wavy and Turbulent Vortices

The Navier-Stokes equations of classical fluid dynamics in principle provide the appropriate fundamental framework for describing the behavior of any flow state that can be produced with Newtonian fluids, just as the partition function should fully describe the behavior of any equilibrium system. However, the direct solution of these problems is often impractical, particularly when dealing with spatially extended

systems. Therefore, various simplifications and approximations of these equations have been developed. One of the most successful is the Ginzburg-Landau expansion, which applies to equilibrium systems in the vicinity of a phase transition, and to nonequilibrium systems near a transition from one state to another. In the former case, it describes the behavior of the order parameter as, say, the temperature of the system is changed. In the latter case, the Ginzburg-Landau equation is recast as an amplitude equation, which describes the development of the amplitude of a pattern's velocity or concentration field near onset as some control parameter, such as an applied temperature gradient, is changed (see Ahlers (1991), Newell, Passot and Lega (1993), and Cross and Hohenberg (1993) for wide-ranging discussions of this formalism and its application to experiments). However, since this approach is applicable only near the onset of patterns, its overall usefulness is severely limited, since most of the parameter space for any given system usually is far from any pattern onset. Therefore, a different approach has been developed, usually called *phase dynamics* (see, for example, the seminal paper by Pomeau and Manneville (1979) and the recent general reviews by Brand (1988) and Cross and Hohenberg (1993)), which may apply to patterns both near and far from transitions. To begin our discussion, consider that a pattern may be described at its onset as having some characteristic critical uniform wavevector. Away from onset, if one thinks of a pattern as having locally an amplitude and a phase, the phase roughly speaking corresponding to the deviation of the pattern's wavevector from uniformity, then it is possible to write down equations describing the slow spatial and temporal dynamics of the phase itself. The practical advantages of this approach are three-fold:

- First, the phase equations are much simpler to solve than the Navier-Stokes equations.
- Second, they should be applicable far from the onset of patterns. Indeed, there is evidence that they apply even to turbulent flows (Wu, Andereck and Brand (1992) & A-13), where it is not at all clear that the amplitude equation formalism will be useful.
- Third, it is possible to write down phase equations by using the symmetries of the flow state under study. Since knowledge of the underlying microscopic processes, which determine the coefficients in the equation, is not essential, *the important qualitative results obtained for one system should generalize to similar patterns in quite different systems*. Thus, phase dynamics seeks to be a *generalized hydrodynamics of patterns*, in which the details of the microscopic interactions (described by the Navier-Stokes equations in our case) between the "atoms" of the system (rolls, cells) are smoothed over by looking only at long-wavelength, low-frequency behavior (which *is* generalized hydrodynamics, as discussed by Reichl (1980) and by Brand (1988)).

Our goal in this field must always be to produce a better understanding of pattern formation and dynamic behavior, and the onset of chaotic and turbulent flows. In this context, suppose that we have succeeded in writing down the generalized hydrodynamic equations for a given pattern. What should these equations tell us about that system? To answer this we appeal to our well-developed understanding of equilibrium systems. By analogy then, a uniform pattern near onset corresponds to a ground state, the zero temperature limit for that pattern. Most of the studies of patterns have concentrated on just this situation, the initial pattern that forms after increasing some control parameter. But the ground state is not the whole picture. Equilibrium systems support a spectrum of excitations, such as phonons, magnons and rotons, and the same should be true of patterns in nonequilibrium systems. Generalized hydrodynamics, as exemplified by phase dynamics, should yield both static pattern distortions and the dynamic excitations that correspond to the "zoo" of equilibrium excitations (Brand (1988)). From these we can determine the analogues of elastic constants and sound absorption. Such excitations may also play a roll in the transition to spatial-temporal chaos and turbulence, and in the final approach of a system to its steady state following some perturbation (Tabeling (1983) and Brand (1994)). Furthermore, changes in phase

diffusion coefficients signal the onset of pattern instabilities (for example, Fourtune, Rappel and Rabaud (1994) have found that the diffusion coefficient drops near the Eckhaus instability for a viscous fingering experiment, while it diverges rapidly near the onset of a parity-breaking instability). It is essential that we understand how patterns respond under changing external constraints and phase dynamics may give us a basic guide to this behavior. With ONR support we performed several experiments that examined these issues for several selected flow patterns, motivated in part by specific novel effects predicted by phase dynamics.

During the grant period we began an experimental study of the long-wavelength, low-frequency dynamics of several basic cellular and turbulent flow states in the Taylor-Couette system. Our intent was three-fold: to search for novel pattern behaviors, to test specific phase dynamics predictions for various flows and to investigate the applicability of this approach to turbulent flows. The importance of this work is clear, since unlike amplitude equations, the phase dynamics methodology should be useful far from the onset of an instability. But relatively few experiments have been performed that are capable of testing it. Pioneering work in this area has been performed in our laboratory.

The Taylor-Couette system produces a large variety of ordered and turbulent flow patterns (see Coles (1965), Snyder (1970), and Andereck, Liu and Swinney (1986). With the outer cylinder at rest the patterns are essentially as follows, with increasing rotation speed of the inner cylinder: purely azimuthal base flow, Taylor vortex flow (time-independent), wavy vortex flow (one frequency), modulated wavy vortex flow (two incommensurate frequencies), chaotic vortices (two frequencies and a noise component), and turbulent Taylor vortex flow. We studied experimentally the low-frequency, long-wavelength dynamics of Taylor vortices, wavy vortices and turbulent vortices by mechanically perturbing the pattern at one end of the cylinders and then capturing the response of the Kalliroscope-visualized vortices using a CCD array camera interfaced to a microcomputer. By plotting the vortex boundary positions as a function of time we extracted a great deal of information, including phase diffusion coefficients. In a real sense this procedure is analogous to the usual perturbative methods used in equilibrium systems. For example, phonons may be excited in crystals through inelastic neutron scattering or x-ray scattering. Some information about systems can be obtained by observing their steady-state behavior, but even more may be learned by observing their response to an external perturbation. We also applied the phase dynamics approach to spiral turbulence, and others have interpreted our work on confined states in terms of phase dynamics. Although our work already has ranged over several distinctly different types of flows and behaviors, much remains to be explored.

Our first experiments were on Taylor vortex flow, a state with only one phase variable ψ, associated with the positions of the vortices along the axis of the system. As predicted by Pomeau and Manneville (1979) and Tabeling (1983) the dynamics of Taylor vortices should be described by a simple one-dimensional diffusion equation:

$$\frac{\partial \psi}{\partial t} = D_{\parallel} \frac{\partial^2 \psi}{\partial z^2}$$

where $D_{\parallel}$ is a diffusion coefficient that depends on various parameters of the problem. To test these predictions in detail we applied sinusoidal and step perturbations to the flows through motion of one of the end boundaries of the system (see Figure 2a and Wu and Andereck (1991a) (A-5) and (1992a) (A-26); this method was adapted by Fourtune, Rappel and Rabaud (1994) for viscous fingering in the printer's instability). In the former case the vortices oscillated sinusoidally as well, but with an amplitude that dropped off exponentially with distance as the diffusion equation predicts (see Figure 5 on page A-31).

For a step function the response is proportional to the error function complement with an argument containing the distance of the vortex from the boundary over the square root of time. Our measurements confirmed the qualitative predictions from the phase diffusion equation. In addition the dependence of the diffusion coefficient on the base wavevector was consistent with the form given above, even though our experiment was performed outside the range of strict validity of the expression, and the values found for $D_{\|}$ are reasonably consistent with those computed by Dominguez-Lerma et al. (1984) and Riecke (1990c).

The next stage of our research concerned the phase dynamics of wavy vortex flow (WVF). As discussed by Brand and Cross (1983) there are two relevant phase variables in WVF, an axial variable ψ and an azimuthal variable φ associated with the positions of the waves on the vortices. They argued that these variables should be coupled through a pair of diffusion equations. When there is strong coupling the equations reduce to the characteristic form of wave equations, as for example the one for ψ:

$$\frac{\partial^2 \psi}{\partial t^2} - c^2 \frac{\partial^2 \psi}{\partial z^2} = 0$$

where c^2 depends on the coupling between the two phases. Thus we should see propagating modes in WVF, a qualitatively different behavior from that possible in Taylor vortex flow or related cellular flows such as those in Bénard convection. (This is akin to the situation in certain equilibrium systems. Consider, for example, liquid helium: For HeI heat transport is diffusive, while in HeII there are superfluid and normal fluid components and second sound, a ballistic transport of heat, can exist.) Of course, in the weak coupling limit the system behaves diffusively. Changing from the weak to the strong limit is achieved by increasing the vortex sizes, the number of azimuthal waves, and the wave amplitude, variables that are to some extent under experimental control.

Our principal result is that we have observed both propagating and diffusive modes in WVF. Figure 11 on page A-34 shows the oscillations of the averaged vortex boundaries in the diffusive (a) and propagating (b) limits. Figure 12a on page A-35 shows a plot of the amplitude vs axial position for the diffusive (x), propagating (□) and very low frequency propagating (●) behavior. End effects are important in the propagating case, leading to diffusive exponential decrease of the amplitude near the oscillating boundary, a region of relatively lower vortex wave amplitude. In summary, we have provided the first evidence for the existence of a propagating mode, as predicted by phase dynamics, in a system far from equilibrium. However, it is not the only system in which such modes may be expected. For example, a propagating mode with the same governing phase equation has been found in a theoretical investigation (Massaguer (1994)) of finite amplitude convection in a large aspect ratio system.

The phase dynamics approach has usually been thought of as applicable only to ordered patterns. Of course, chaotic and turbulent flows are abundant and it would be useful to have some ability to use simple equations that successfully describe at least large scale features of the flow. Therefore we decided to see if phase dynamics might apply to a turbulent state. It was a relatively straightforward extension of our work on Taylor vortices and WVF to go on to study turbulent vortices. The basic result is that for situations on the order of 20 times critical the phase perturbation behaves diffusively, if we take an average of the vortex boundary positions over a time scale long compared with the turbulent fluctuations, but small compared with the perturbation period (Wu, Andereck and Brand (1992) (A-13) and Wu and Andereck (1992a) (A-26)). The diffusion coefficient is more than an order of magnitude greater than for the Taylor vortex case, as shown by the much slower decrease in amplitude displayed in Figure 20a on page A-38. In this figure the x's represent turbulent Taylor vortices, while the □'s are from laminar

Taylor vortex flow. We attribute this to the enhanced momentum transport due to the turbulence.

To conclude, our experimental studies of the Taylor vortex system have confirmed phase dynamics predictions for more complex flows than previously studied. We have greatly extended the range of applicability of the phase dynamics approach by our work on turbulent vortices. Related work on phase dynamics of turbulent flow is discussed in the next section.

5. Spiral Turbulence and Phase Dynamics

Flows between counter-rotating cylinders are notably different from those we have just discussed. The primary bifurcation from the base flow, for large enough outer cylinder speed, is to laminar spirals rather than time-independent Taylor vortices. At large outer cylinder speeds the region of existence of the spirals is small (Andereck et al (1986)), and as the inner cylinder speed increases there is a subcritical instability to the extraordinary spiral turbulence pattern (Coles (1965), Coles and Van Atta (1966) and (1967), Van Atta (1966), and Andereck et al (1986)). Spiral turbulence, as shown in Figure 1 on page A-40, consists of a barber-pole pattern of laminar and turbulent bands that rotates at a well-defined angular velocity. It is particularly interesting among fluid dynamical patterns because it mixes the small scale (microscale) turbulent behavior with a well-ordered structure at large scales. It is the prototypical "coherent structure", examples of which have attracted much interest in recent years.

As is generally true for turbulent flows, the understanding of this pattern has been limited. Our experiments (Hegseth, Andereck, Hayot and Pomeau (1989) (A-40) and (1991) (A-44)) revealed some previously unobserved features of spiral turbulence, which have formed the basis for a phase dynamics model of the pattern. The work was carried out primarily with a $\Gamma=73$ system, much longer than in previous investigations. This permitted us to observe a variation in the pitch of the spiral (the angle with respect to the ends of the system) over the length of the system, the pitch being lower at the end of the system away from which the spiral appears to be moving. Furthermore, if the upper end of the system is a free surface the average pitch is dramatically different for spirals moving away from the free surface. These two basic observations can be incorporated in a phase dynamics model that should describe the slow time, long wavelength variations of the pattern. This equation is

$$\varphi_t(z,t) + v\varphi_z(z,t) = D\varphi_{zz}(z,t)$$

where we interpret φ as the mean azimuthal position of the spiral at height z and time t. (This is a phase in the sense that a uniform shift of φ has no dynamical effect, given the axisymmetry of Taylor-Couette flow.) v is the apparent axial velocity of the spiral in the laboratory frame and D is a phase diffusion coefficient. The basic solution is an exponential function of z plus a linear function of vt-z. Applying boundary conditions, which are assumed to be different at the "emitting" and "absorbing" ends, we have the general solution

$$\varphi(z,t) = \frac{w}{v}(vt-z) + \varphi_0 e^{(vz/D)}$$

where w and φ_0 are constants defined as

$$\varphi_0 = \frac{D}{v}\frac{\alpha-\beta}{1-e^{(vL/D)}}, \qquad \frac{w}{v} = \varphi_0\frac{v}{D} - \alpha$$

with $\alpha=\varphi_z$ and $\beta=\varphi_z$, the boundary conditions on φ. Should $\alpha=\beta$ then we would have a constant pitch. Since the top and bottom of the system are not symmetric with respect to the spiral we would not expect equality and hence the pitch variation with z. Also, with a free upper surface there is an even more extreme difference between α and β, which is born out by the experiment. Thus, we have been able to describe the large-scale variations in the spiral using an extremely simple phase dynamics modeling procedure.

A further result on spiral turbulence is that the spiral is relatively more unstable in longer systems. In fact, for R_o=-8000 (a higher speed than for the basic work discussed above) a simple spiral pattern could be found only at very low aspect ratios. At large Γ we found only a "broken" spiral, with coherence only on the order of a cylinder diameter or two. This instability is not contained within the phase dynamics model, and probably involves an influence of the secondary flow generated by the existence of the turbulent spiral.

III. Pattern Formation in the Taylor-Dean System

1. Introduction and Flow State Survey

The flow between rotating concentric cylinders is very special, having rotational symmetry as well as translational symmetry along the axis. This leads to definite restrictions on the types of flows that are possible, and on the detailed dynamics of those flows. We have conducted an investigation into the types of behavior possible if the rotational symmetry of the system is strongly broken, work which was supported by ONR Contract N00014-86-K-0071 and Grant N00014-89-J-1352 and a NATO travel grant. Breaking of the symmetry can be done in a variety of ways; our particular method was chosen because there are technological applications for variations of the flow, and because there were definite indications from previous work that interesting flows could be produced. The system consists of concentric rotating cylinders with the system axis horizontal. Instead of completely filling the gap with fluid, which would have simply reproduced the Taylor-Couette system, we only partially filled the system. This left an air gap at the top of the system, as shown in Figure 1 on page A-51. The fluid then responds to two influences, the rotation of the cylinders and the presence of the two free surfaces. In the region of the free surfaces the fluid must turn over, giving rise to a pressure driven flow back around the azimuthal direction. Thus we have a system which gives a combination of rotationally driven Couette flow and pressure driven Poiseuille flow around a curved channel, the so-called Dean flow. By rotating the cylinders at different rates it is possible to tune the base flow, away from the free surfaces, over a wide range of possibilities, and therefore select different types of instabilities for examination.

Early work on this system is represented by Brewster, Grosberg and Nissan (1959), who studied the linear stability of the flow and performed basic experiments with a small aspect ratio apparatus. Our work commenced with a survey of the possible flow states, but with a large aspect ratio to reduce the influence of the ends of the system. The results of this survey were reported in Mutabazi, Hegseth, Andereck and Wesfreid (1988) (A-50). The principal result was the mapping of the bifurcations from the base flow for the whole range of combinations of inner and outer cylinder speeds, as shown in Figure 2 on page A-52. In contrast to the case of Taylor-Couette flow, the initial instability with only the inner cylinder rotating is to time-dependent flow, the traveling inclined rolls. Stationary patterns are found with the outer cylinder rotating. The identification of the flows as "Dean" or "Taylor-Couette" relies on theoretical velocity field predictions made under a small gap approximation and ignoring free surface effects. In that approximation, a roughly linear profile was called Taylor-Couette like, and a parabolic profile was considered indicative of Dean flow since it was Poiseuille-like. An important aspect of the system is revealed in these profiles, namely that there may be more than one centrifugally unstable layer in the flow, a further contrast with the Taylor-Couette system and other simple systems. Some important aspects of the rich behavior of this system have subsequently been explored in our group, as detailed in the following sections.

2. Spatial-Temporal Pattern Modulations

Recently, systems which undergo a Hopf bifurcation from the base state have come under intense study, since the transition to spatial-temporal complexity may be more amenable to experimental and theoretical investigation than in, say, the Taylor-Couette system with the outer cylinder at rest. For Taylor-Dean flow, the traveling inclined rolls, which arise from the base flow via a Hopf bifurcation, indeed show a rapid increase in complexity with increasing inner cylinder rotation speed. We have carefully documented the transitions that occur and the characteristics of the states in Mutabazi, Hegseth, Andereck and Wesfreid (1990) (A-59) (see also Mutabazi, Wesfreid, Hegseth and Andereck (1991) (A-67)).

The initial instability is a supercritical Hopf bifurcation. The rolls that result (see Figure 2 on page A-61) are much stronger on one side of the system than the other. Theoretical and experimental evidence indicates that there are recirculation rolls near one of the free surfaces, but not the other (Normand, Mutabazi and Wesfreid (1991)), and this asymmetry may be affecting the roll pattern. In much of what follows we will assume that the rolls constitute a 1-dimensional pattern, but the asymmetry implies that the detailed behavior certainly cannot be quite that simple. Typically there will be a defect in the pattern separating right and left traveling rolls. The defect itself moves erratically along the axial direction. Close to onset, within a range of the reduced Reynolds number $\epsilon \in [0.013, 0.1]$, there is a long-wavelength modulation which becomes so pronounced that the roll velocity varies along the system and creation and annihilation events occur, leading to a weak phase turbulence. Such events have been found in binary-fluid convection (Kolodner, Bensimon and Surko (1988)) and electrohydrodynamic systems (Joets and Ribotta (1989)) as well.

At slightly higher ϵ the pattern undergoes a dramatic transition to a state modulated in space and time, with a wavelength of modulation that is about 3 rolls in extent. Again, the onset is free of hysteresis within our experimental uncertainty. This state and an associated space-time plot are shown in Figure 2b on page A-61. An interesting feature of this pattern is that the modulation envelope itself moves in the axial direction, but much more slowly than the rolls, as shown in the figure. The modulation also produces distortions of the rolls along their axes, suggesting there may be some relationship to the wavy spirals in the Taylor-Couette system with counter-rotating cylinders (Andereck, Liu and Swinney (1986)). Spatial correlation measurements before the onset of the 3-rolls modulated state show a smooth exponentially decreasing envelope, whereas in the modulated state there is a strong correlation only at distances of about 3 rolls. This phenomenon can be considered to be the generation of traveling patches or triplets, periodic in space and time, separated by laminar-like zones. Just as for the simple roll state at lower ϵ the roll-modulated pattern becomes subject to defect generation and eventually undergoes a transition to spatial-temporal disorder (see Figure 5 on page A-62). The origin of these modulations remains unknown. It is possible that it lies in competing instabilities in different sublayers of the flow, or in a wavy instability of the rolls themselves.

3. Transition From Time-Dependent to Stationary Patterns

Typical nonequilibrium systems undergo transitions to increasingly complex behaviors as the control parameter is increased. Eventually the flow becomes chaotic, possibly with spatial degrees of freedom excited, and then finally it may be called turbulent. Exceptions to this process are known. For example, in binary fluid mixtures there may be an initial transition to a traveling-waves state, followed by a subcritical instability to a stationary pattern upon an increase in the Rayleigh number (see Walden, Kolodner, Passner and Surko (1985)). We have found that, with only the outer cylinder rotating, the Taylor-Dean system undergoes a transition from a traveling roll state to a stationary roll pattern through a process described below (Mutabazi and Andereck(1991) & A-63, Fourtune, Mutabazi and Andereck(1992) & A-74).

Away from the end rings the flow consists of a purely azimuthal flow in the bulk, recirculation rolls near one free surface, and a boundary-layer flow near the other free surface. In the small-gap approximation the flow is parabolic, with an unstable layer of fluid between two stable layers. The unstable layer is in the Poiseuille region, thus indicating the instability will be of the Dean type. For very low rotation rates it is possible to detect Ekman cells near each end of the system. At higher rotation rates there are typically three regions in the flow: inclined rolls traveling to the right just outside the left Ekman region, laminar base flow, and inclined rolls traveling to the left just outside the right Ekman region. The

transition to this state is subcritical, with a hysteresis of about 13% in the control parameter. At still higher rotation rates the system fills with traveling rolls, both large wavelength and small. At about 20% above the onset of the first traveling rolls the flow becomes stationary and axisymmetric after a transient relaxation period. This transition is also subcritical, with a 20% hysteresis. The front between the traveling rolls and the stationary Dean rolls progresses at a finite velocity, of the order of 1 cm/s. The phase velocity of the traveling rolls has a large discontinuity at the transition.

We speculate that the time-dependent roll state may be a metastable phase driven ultimately by oscillations in the Ekman end regions. At some point the centrifugally driven instabilities in the bulk of the flow dominate and the stationary pattern can take over.

The transition from a traveling roll pattern to a stationary pattern appears to be unusual for a hydrodynamic system. It has been observed previously only for binary fluid convection. This behavior is also in contrast to that found in related systems. Pure Dean vortex flow in curved-channel Poiseuille flow consists at the onset of stationary almost axisymmetric rolls, except in the entrance region (for example, Ligrani and Niver (1988)). The transition to turbulence proceeds through successive instabilities of the rolls. In the Taylor-Couette system with the outer cylinder rotating there are no roll forming instabilities, just a turbulent transition for very large rotation rates. Moreover, for general rotation rates of the cylinders the only potentially related behavior is the reemergent periodicity found in the midst of turbulence (Walden and Donnelly (1979)). Linear stability theory does not show the basic features of the transition we have observed. It is possible that model equations with forcing might be used to mimic the influence of the Ekman end regions (as described in Fourtune, Mutabazi and Andereck (1992) & A-74).

4. Drift Instability and Second Harmonic Generation

Recently considerable attention has been given to one-dimensional extended systems in which oscillatory states as the first instability or as a secondary instability. It has been observed that the onset of a drifting pattern is sometimes associated with the appearance of a second harmonic in the stationary pattern. We have found such an instance in the Taylor-Dean system, where for rotation of both cylinders we find what seems to be a resonant 2:1 interaction between Dean rolls and Taylor vortices in adjacent fluid layers. These results are presented in Mutabazi and Andereck (1993) (A-81) and Mutabazi and Andereck (1995). Above the onset of the drift instability we found long-wavelength phase instabilities and eventually a wavelength-halving instability, which resulted in the appearance of small traveling rolls that eventually replace the original large Dean rolls. Several aspects of the complex dynamics of this system remain as theoretical challenges.

IV. Dynamics of Complex Fluids

1. Noise-Induced Effects in Liquid Crystals

The effects of imposing external noise on nonlinear systems has been investigated in diverse situations (see Horsthemke and Lefever (1984) and Griswold and Tough (1987)). Under certain conditions such systems may show extreme sensitivity to noise. In fact, it has been shown that *multiplicative* external noise can induce a variety of transitions, or affect those already present. A very interesting set of experiments has been performed on pattern-forming liquid crystal systems by Kai, Kai and Takata (1979), and Brand, Kai and Wakabayashi (1985). They found that imposing noise on the electrohydrodynamic instabilities shifted transition thresholds and stabilized the system against turbulence. However, quantitative agreement with existing theory was not possible, owing to the spatial complexity of the flow pattern. This difficulty has been overcome in our study of the Freedericksz transition of a nematic liquid crystal, which was suggested by the theoretical work of Horsthemke, Doering, Lefever and Chi (1985). The Freedericksz transition consists simply of a rotation of the nematic director under the influence of an imposed magnetic field; no roll pattern or other flow is generated. This simplifies the problem considerably, making possible a much more complete treatment than was possible for the electrohydrodynamic case. Our experimental results were reported in Wu and Andereck (1990) (A-86).

The apparatus consisted of a layer of the nematic liquid crystal MBBA, sandwiched between two parallel glass plates. The plates had been coated with polyvinyl alcohol and rubbed to form grooves which forced an approximate initial alignment of the director along a particular axis. The magnetic field was in the plane of the layer, perpendicular to the initial director orientation. The magnetic field produced a torque on the molecules due to their magnetic anisotropy. This torque tends to align the molecules in the direction of the field, and it is opposed by viscous and elastic torques. The equation of force balance is

$$\lambda_1 \partial_t \theta = K_{22} \partial_{zz} \theta + \chi_a H^2 \sin\theta\cos\theta$$

where $\theta(z,t)$ is the angle between the director and the x axis, λ_1 is the twist viscosity, K_{22} is the twist elastic constant, χ_a is the anisotropic susceptibility, and H is the applied magnetic field. The boundary conditions are $\theta(\pm d/2)=0$, where d is the sample thickness, which mean that the director is effectively pinned at the solid surfaces. With a slowly increasing H, we find that the director begins to rotate at a critical H; this is the Freedericksz transition for this geometry. Rotation of the director can be detected using a conoscopic microscope, which we coupled to a CCD array camera and image capture and processing system. The interference pattern turned with the rotation of the director, allowing determination of the value of θ moment by moment. Our interest was in adding a noise component to H, which turns it into a stochastic parameter. With suitable simplifications one can then solve the Fokker-Planck equation for the probability density functions that characterize the behavior of the director.

In our experiments we varied the average magnetic field, the correlation time of the noise, and its amplitude, and determined phase diagrams based on the observed transitions in the probability density functions of the rotation angle of the director. The imposed noise was dichotomous, a very special type, but one that was relatively easy to produce experimentally. The results are shown in the phase diagrams of Figure 2 on page A-88, in which we compare the experimental transition boundaries with those

predicted from analytic solutions of approximate equations and from numerical simulations we performed on the original equations. We found that the experiments and numerics agreed reasonably well for average magnetic field above H_c, while differing markedly below H_c, at least for large enough noise amplitude. This suggests that a more complete model, including possible spatial effects across the plane of the sample, and more realistic boundary conditions are used, potentially including boundary layers, might be necessary to account for all of our observations.

2. Phase Winding in Liquid Crystal Layers

In collaboration with P. E. Cladis of Bell Laboratories we performed an experiment on the formation of ring patterns in 2-d shear of a smectic-C liquid crystal layer. The shear was produced by inserting a small rotating rod into the center of a circular freely suspended film of 10E6. Upon rotation it was found that the resulting shear produced phase winding, the phase propagating outward from the rod. For low rotation rates and over small time intervals the phase progressed smoothly outward. However, under some conditions dislocations would form, which resulted in the onset of oscillations in the pattern. In a few cases this would actually collapse the ring pattern. At higher speeds still spatial-temporal chaos would result. These experimental observations were reported in Mutabazi, Finn, Gleeson, Goodby, Andereck and Cladis (1992) (A-90).

V. Conclusion

Pattern-forming nonequilibrium systems are a vital part of the natural and man-made world. It is critical to understand the physics of the pattern formation process itself, and of the behavior of the patterns once they are formed, in order to control or to best use a particular system. One of the key advances in this field has been the recognition that simple model equations, such as amplitude equations and phase equations, can provide much insight into the physics and give very precise qualitative and quantitative agreement with experimental observations. The amplitude equation approach has been repeatedly verified in diverse systems, but is limited in its range of applicability to near pattern onset. The phase dynamics approach is not so limited, but relatively few experiments have been performed that are capable of testing it. *One of the primary purposes of this project was to experimentally explore the long-wavelength, low-frequency limits of the dynamics of nonequilibrium patterns in various systems and, in the process, test the predictions of the phase dynamics approach as fully as possible.*

Pioneering experiments in our laboratory have shown the qualitative effectiveness of the phase dynamics approach in predicting the behavior of both ordered and turbulent vortex flows. Our experimental studies of the Taylor vortex system have confirmed several fundamental phase dynamics predictions for more complex flows than previously studied in other laboratories. We have obtained the first experimental evidence of a propagating phase mode. We have greatly extended the range of applicability of the phase dynamics approach by our work on turbulent vortices. We have even shown that phase dynamics may be used to describe the static deformations of a structure as exotic as spiral turbulence. Finally, we pioneered the work on pattern domains, which may also be a phase dynamics effect.

In addition to our work on phase dynamics we have also explored the novel flow phenomena found in the Taylor-Dean system, the flow between coaxial, horizontal cylinders with a partially-fluid-filled gap. By adjusting the rotation speeds of the two cylinders it is possible to vary dramatically the velocity profile across the gap. Our work has shown that this system has a flow regime diagram that is very different from that for simple Taylor-Couette flow. We have investigated a few areas of the diagram in detail. For example, with only the inner cylinder rotating, the initial transition is to traveling inclined rolls, which in turn undergo an instability to a short-wavelength amplitude modulation shortly after onset, followed by a transition to spatial-temporal chaos. Under some circumstances it is possible to produce two distinct Rayleigh unstable layers, separated by stable flow. This can give rise to resonant mode interactions leading to drift instabilities and other unique effects.

With the support of ONR we also began an investigation of the behavior of complex fluids, specifically liquid crystals. Our first project was on the effects of multiplicative external noise on one of the simplest transitions possible, the Freedericksz transition in a layer of nematic liquid crystal. It was found that various regimes of behavior could be produced by changing the characteristics of the noise. A second experiment, on the effects of shear flow on a freely suspended layer of smectic C liquid crystal, showed that ordered phase winding occurred so long as dislocations were not present. With dislocations, when rings of constant phase were broken, the behavior became disordered.

The outcome of this fundamental research program is a deeper understanding of the dynamics of highly nonequilibrium ordered and turbulent patterns, and a greatly enhanced appreciation for the advantages and limitations of phase dynamics as a description of some of their long-wavelength low-frequency behaviors. This project has laid the groundwork for new investigations, both theoretical and experimental, on the hydrodynamic behavior of patterns far from their onset in a variety of closed and open systems involving both simple and complex fluids.

VI. References

G. Ahlers, "Experiments with Pattern-Forming Systems," Physica D **51**, 421 (1991).

C. D. Andereck and G. W. Baxter, "An Overview of the Flow Regimes in a Circular Couette System," in *Propagation in Systems Far From Equilibrium*, edited by J. E. Wesfreid, et al (Springer-Verlag, New York, 1988), p. 315.

C. D. Andereck, R. Dickman and H. L. Swinney, "New Flows in a Circular Couette System With Co-Rotating Cylinders," Phys. Fluids **26**, 1395 (1983).

C. D. Andereck, S. S. Liu and H. L. Swinney, "Flow Regimes in a Circular Couette System With Independently Rotating Cylinders," J. Fluid Mech. **164**, 155 (1986).

G. W. Baxter and C. D. Andereck, "Formation of Dynamical Domains in a Circular Couette System," Phys. Rev. Lett. **57**, 3046 (1986).

H. R. Brand, "Phase Dynamics- A Review and a Perspective," in *Propagation in Systems Far From Equilibrium*, edited by J. E. Wesfreid, et al (Springer-Verlag, New York, 1988), p. 206.

H. R. Brand, "Confined States in Phase Dynamics," in *Nonlinear Evolution of Spatio-Temporal Structures in Dissipative Continuous Systems*, ed. by F. J. Busse and L. Kramer, (Plenum, New York,1990), p. 221.

H. R. Brand, private communication (1994).

H. Brand and M. C. Cross, "Phase Dynamics for the Wavy Vortex State of the Taylor Instability," Phys. Rev. A **27**, 1237 (1983).

H. R. Brand and R. J. Deissler, "Confined States in Phase Dynamics," Phys. Rev. Lett. **63**, 508 (1989).

H. R. Brand, S. Kai, and S. Wakabayashi, "External Noise Can Suppress the Onset of Spatial Turbulence," Phys. Rev. Lett. **54**, 555 (1985).

D. B. Brewster, P. Grosberg and A. J. Nissan, "The Stability of Viscous Flow Between Horizontal Concentric Cylinders," Proc. R. Soc. London, Ser. A **251**, 76 (1959).

D. Coles, "Transition in Circular Couette Flow," J. Fluid Mech. **21**, 385 (1965).

D. Coles and C. W. Van Atta, "Progress Report on a Digital Experiment in Spiral Turbulence," AIAA J. **4**, 1969 (1966).

D. Coles and C. W. Van Atta, "Digital Experiment in Spiral Turbulence," Phys. Fluids **10**, S120 (1967).

M. C. Cross and P. C. Hohenberg, "Pattern Formation Outside of Equilibrium," Rev. Mod. Phys. **65**, 851 (1993).

R. J. Deissler, Y. C. Lee and H. R. Brand, "Confined States in Phase Dynamics: The Influence of Boundary Conditions and Transient Behavior," Phys. Rev. A **42**, 2101 (1990).

M. A. Dominguez-Lerma, G. Ahlers and D. S. Cannell, "Marginal Stability Curve and Linear Growth Rate for Rotating Couette-Taylor Flow and Rayleigh-Bénard Convection," Phys. Fluids **27**, 856 (1984).

M. Dubois, P. Bergé and A. Petrov, "Properties of Quasi One-Dimensional Rayleigh-Bénard Convection," in *New Trends in Nonlinear Dynamics and Pattern-Forming Phenomena: The Geometry of Nonequilibrium*, edited by P. Huerre and P. Coullet, (Plenum, New York, 1990), p. 227.

M. Dubois, R. DaSilva, F. Daviaud, P. Bergé and A. Petrov, "Collective Oscillating Mode in a One-Dimensional Chain of Convective Rolls," Europhys. Lett. **8**, 135 (1989).

L. Fourtune, I. Mutabazi and C. D. Andereck, "A Model of the Disappearance of Time-Dependence in the Flow Pattern in the Taylor-Dean System," in *Ordered and Turbulent Patterns in Taylor-Couette Flow*, edited by C. D. Andereck and F. Hayot, (Plenum, New York, 1992), p. 91.

L. Fourtune, W.-J. Rappel, and M. Rabaud, "Phase Dynamics Near a Parity Breaking Instability," Phys. Rev. E **49**, R3576 (1994).

J. J. Hegseth, C. D. Andereck and G. W. Baxter, preprint (1995).
J. J. Hegseth, C. D. Andereck, F. Hayot and Y. Pomeau, "Spiral Turbulence and Phase Dynamics," Phys. Rev. Lett. **62**, 257 (1989).
J. J. Hegseth, C. D. Andereck, F. Hayot and Y. Pomeau, "Spiral Turbulence: Development and Steady State Properties," Eur. J. Mech. B/Fluids **10**, No. 2-Suppl., 221(1991).
J. Hegseth, J. M. Vince, M. Dubois and P. Bergé, "Pattern Domains in Rayleigh-Bénard Slot Convection," Europhys. Lett. **17**, 413 (1992).
A. Joets and R. Ribotta, "Localization and Defects in Propagative Ordered Structures," J. Phys. (Paris), Colloq. **50**, C3-171(1989).
P. Kolodner, D. Bensimon and C. M. Surko, "Traveling-Wave Convection in an Annulus," Phys. Rev. Lett. **60**, 1723 (1988).
P. M. Ligrani and R. D. Niver, "Flow Visualization of Dean Vortices in a Curved Channel With 40 to 1 Aspect Ratio," Phys. Fluids **31**, 3605 (1988).
J. M. Massaguer, "Large-Scale Flow and Pattern Drift in Finite Amplitude Convection," Phys. Fluids **6**, 2304 (1994).
I. Mutabazi and C. D. Andereck, "Transition From Time-Dependent to Stationary Flow Patterns in the Taylor-Dean System," Phys. Rev. A**44**, 6169 (1991).
I. Mutabazi and C. D. Andereck, "Drift Instability and Second Harmonic Generation in a One-Dimensional Pattern-Forming System," Phys. Rev. Lett. **70**, 1429 (1993).
I. Mutabazi and C. D. Andereck, preprint (1995).
I. Mutabazi, P. L. Finn, J. T. Gleeson, J. W. Goodby, C. D. Andereck, and P. E. Cladis, "Ring Pattern Formation in 2-d Shear of Freely Suspended Films of a Smectic C Liquid Crystal," Europhys. Lett. **19**, 391 (1992).
I. Mutabazi, J. J. Hegseth, C. D. Andereck and J. E. Wesfreid, "Pattern Formation in the Flow Between Two Horizontal Coaxial Cylinders With a Partially Filled Gap," Phys. Rev. A **38**, 4752 (1988).
I. Mutabazi, J. J. Hegseth, C. D. Andereck and J. E. Wesfreid, "Spatiotemporal Pattern Modulations in the Taylor-Dean System," Phys. Rev. Lett. **64**, 1729 (1990).
I. Mutabazi, J. E. Wesfreid, J. J. Hegseth and C. D. Andereck, "Recent Experimental Results in the Taylor-Dean System," Eur. J.Mech. B/Fluids **10**, No. 2-Suppl., 239 (1991).
M. Nagata, "Bifurcations in Couette Flow Between Almost Corotating Cylinders," J. Fluid Mech. **169**, 229 (1986).
M. Nagata, "On Wavy Instabilities of the Taylor-Vortex Flow Between Corotating Cylinders," J. Fluid Mech. **188**, 585 (1988).
A. C. Newell, T. Passot and J. Lega, "Order Parameter Equations for Patterns," Ann. Rev. Fluid Mech. **25**, 399 (1993).
Y. Pomeau and P. Manneville, "Stability and Fluctuations of a Spatially Periodic Convective Flow," J. Phys. (Paris) Lett. **40**, L609 (1979).
L. E. Reichl, *A Modern Course in Statistical Physics* (Texas, Austin, 1980).
H. Riecke, "Stable Wave-Number Kinks in Parametrically Excited Standing Waves," Europhys. Lett. **11**, 213 (1990a).
H. Riecke, "On the Stability of Parametrically Excited Standing Waves," in *Nonlinear Evolution of Spatio-Temporal Structures in Dissipative Continuous Systems,* ed. by F. H. Busse and L. Kramer, (Plenum, New York, 1990b), p. 437.
H. Riecke, private communication (1990c).
H. A. Snyder, "Waveforms in Rotating Couette Flow," Int. J. Non-Lin. Mech. **5**, 659 (1970).
P. Tabeling, "Dynamics of the Phase Variable in the Taylor Vortex System," J. Phys. (Paris) Lett. **44**, L665 (1983).
C. W. Van Atta, "Exploratory Measurements in Spiral Turbulence," J. Fluid Mech. **25**, 495 (1966).

R. W. Walden and R. J. Donnelly, "Reemergent Order of Chaotic Circular Couette Flow," Phys. Rev. Lett. **42**, 301 (1979).

R. W. Walden, P. Kolodner, A. Passner and C. M. Surko, "Traveling Waves and Chaos in Convection in Binary Fluid Mixtures," Phys. Rev. Lett. **55**, 496 (1985).

E. Weisshaar, F. H. Busse and M. Nagata, "Twist Vortices and Their Instabilities in the Taylor-Couette System," J. Fluid Mech. **226**, 549 (1991).

M. Wu and C. D. Andereck, "Phase Modulation of Taylor Vortex Flow," Phys. Rev. A **43**, 2074 (1991a).

M. Wu and C. D. Andereck, "Phase Dynamics of Wavy Vortex Flow," Phys. Rev. Lett. **67**, 1258 (1991b).

M. Wu and C. D. Andereck, "Phase Dynamics in the Taylor-Couette System," Phys. Fluids A **4**, 2432 (1992a).

M. Wu and C. D. Andereck, "Phase Dynamics in the Taylor-Couette System," in *Ordered and Turbulent Patterns in Taylor-Couette Flow*, edited by C. D. Andereck and F. Hayot, (Plenum, New York, 1992b), p. 75.

M. Wu, C. D. Andereck and H. R. Brand, "The Phase Dynamics of Turbulent Taylor Vortex Flow," Europhys. Lett. **19**, 587 (1992).

M. Wu and C. D. Andereck, "Effects of External Noise on the Fréedericksz Transition in a Nematic Liquid Crystal," Phys. Rev. Lett. **65**, 591 (1990).

Appendix A: Publications Resulting From This Grant

Confined States:

Phase Dynamics:

Taylor-Dean Flows:

Formation of Dynamical Domains in a Circular Couette System

G. William Baxter[a] and C. David Andereck
Department of Physics, The Ohio State University, Columbus, Ohio 43210
(Received 5 September 1986)

Novel flows between rotating concentric cylinders have been found in which domains of dynamically distinct behavior occur in spatially separate regions along the cylinders. Such flow states consist of Taylor vortices with a variety of secondary flows. The distinct secondary flows are correlated with variations in the axial wavelength of the vortex structure occurring over distances small compared with the system length. The results are compared with model systems that exhibit spatially nonuniform behavior and domain formation.

PACS numbers: 47.20.−k, 47.20.Tg

Much attention has been given in recent years to pattern formation and dynamic behavior in physical systems far from equilibrium. One of the most interesting results thus far is that the dynamics of certain small closed systems can be characterized by measurements at a single point in physical space. This is the case for the circular Couette system at low inner-cylinder speeds when the outer cylinder is at rest; measurements at different axial locations show the same dynamics.[1] Other studies at even lower inner-cylinder speeds have shown that end boundaries can induce smooth variations in Taylor-vortex sizes over distances comparable with the system length.[2-4] However, spatial and temporal properties of the flows can be quite different with the outer cylinder rotating[5-8] and therefore finite-length effects might also be different. We report here the first observations of spatial patterns, apparently induced by finite system size, which consist of stable, coexisting, dynamically distinct domains in flow between almost corotating cylinders (see Fig. 1). These domains are marked by different secondary flows and therefore a single-point measurement is insufficient to characterize the overall flow state. The secondary flows are correlated with pronounced, localized variations of the axial wavelength of the underlying Taylor-vortex structure. Such behavior is qualitatively different from that previously reported with the outer cylinder either at rest or rotating. In this Letter we will describe the conditions for occurrence of these unusual flows, give a preliminary characterization of them, and discuss the prospects for a theoretical treatment.

The system consists of concentric rotating cylinders, the inner one of black Delrin plastic (radius $r_i = 5.267$ cm) and the outer one of polished Plexiglas (radius $r_o = 5.965$ cm), giving a radius ratio $\eta \equiv r_i/r_o = 0.883$ and a gap $d \equiv r_o - r_i = 0.698$ cm. The upper and lower boundaries were formed by Teflon rings attached to the outer cylinder, typically a distance $h = 20.94$ cm apart, yielding an aspect ratio $\Gamma = h/d = 30.0 \pm 0.3\%$ (some runs were also made at $\Gamma = 70$). The cylinders were driven by Compumotor stepping motors with a rotation-rate precision of $\pm 0.01\%$; the inner-cylinder motor was connected to a PDP-11/73 computer which controlled both the ramping rate and data acquisition. The angular velocities Ω_i and Ω_o of the inner and outer cylinders are scaled in terms of Reynolds numbers $R_i = r_i d\,\Omega_i/\nu$ and $R_o = r_o d\,\Omega_o/\nu$, where ν is the kinematic viscosity of the fluid. The experiments were performed in a temperature-controlled room; the fluid temperature varied by no more than $\pm 0.1\,^\circ$C during a day. To visualize the flow we used 1%-by-volume Kalliroscope rheoscopic agent in distilled water.

Data acquisition involved several techniques. Basic data were obtained by use of a 28–85-mm variable focal length lens to form an image of the flow on a 1024-pixel charge-coupled device (CCD) linear array interfaced through CAMAC to the computer. A record of the overall visual appearance was kept with a time-lapse video recorder capable of storing 72 h of images from a closed-circuit television camera. The visual record was compared with the output of the CCD camera to estab-

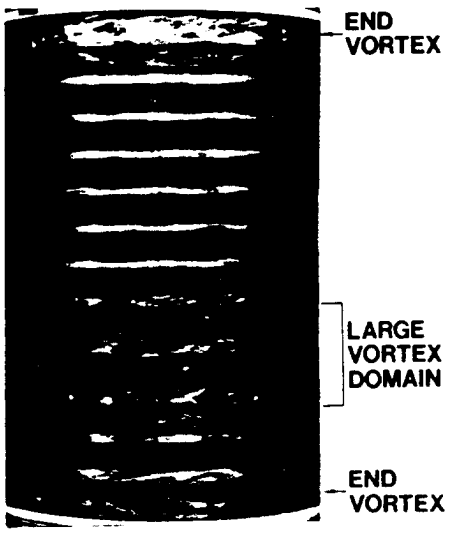

FIG. 1. Dynamical domain state for $\lambda = 2.5$, $R_o = 693$, $R_i = 1960$.

lish correlations between the secondary flows and the vortex sizes. Single-point time-series data were obtained with laser light reflected off the Kalliroscope flakes onto a photodiode detector; the resulting signal was digitized for processing with a fast-Fourier-transfrom routine. Finally, some vortex-size measurements were made with use of a cathetometer to check the CCD results.

Flow states were established with a specific average axial wavelength, defined as $\bar{\lambda}=2\Gamma/N$, where N is the number of Taylor vortices. For most of the work $\bar{\lambda}$ was 2.5, corresponding to 24 Taylor vortices in a system with aspect ratio 30. Various means may be used to produce the desired number of vortices[7,8]; for a fixed and low enough R_o, a quasistatic ramping of R_i from zero produces a $\bar{\lambda}$ of 2.0, but rapid ramping past the Taylor-vortex stability boundary can be used to produce a different $\bar{\lambda}$. Once the desired vortex wavelength was achieved the system was stabilized at the initial R_i and R_o until a uniform vortex size was achieved throughout the working space. R_i was then slowly ramped up under computer control through the regions of interest with CCD data obtained at regular intervals. This procedure was repeated over a range of R_o.

The CCD data were used to establish the degree of uniformity of the Taylor-vortex structure. To determine the local vortex size it was necesary to average over the secondary structures present on the vortices. These secondary flows might be waves on the boundaries between the vortices (wavy inflow or outflow boundary flows, or wavelets, small-amplitude waves on both boundaries), or waves internal to the vortices (twists), or combinations of these and small-scale noisy structure.[7,8] The CCD array rapidly takes 300 one-dimensional images (light-intensity profiles) aligned along the axis of the cylinders with each image covering the entire length of the system between the Teflon rings. Fifty of these axial slices are randomly chosen and then averaged. We are left with a nearly periodic signal in which minima correspond to vortex boundaries. The computer then locates the minima and determines the vortex sizes. The data presented here represent measurements of vortex-pair sizes since that is consistent with typical system behavior; similar secondary flows often occur in pairs of vortices sharing a common inflow boundary, and isolated vortices with secondary flows different from both nearest-neighbor vortices were not found. The cells adjacent to the top and bottom boundaries are consistently larger than the rest[7,8] and are excluded from the analysis. We have observed, however, that they vary little in size over the ranges of R_i and R_o considered here.

Our principal results are summarized in Figs. 2–4. Figure 2 is a section of the flow regime diagram for $\Gamma=30$, and $N=24$ [letters (b)–(f) refer to this figure]. We stress that N does not change in any of the transitions we discuss. For $550\lesssim R_o\lesssim 720$ the system progresses from uniform Taylor-vortex flow (b) to the twist pattern (d) as R_i is increased. At higher R_i waves form on the inflow boundaries between the vortices, and the vortex sizes gradually become nonuniform (e). In this range of R_i fluctuations are seen in vortex sizes and secondary flows. The fluctuations cease as the next transition is reached (f). Here the vortex-pair size distribution becomes bimodal, and the flows on the different-size vortices change (the particular secondary flow on a vor-

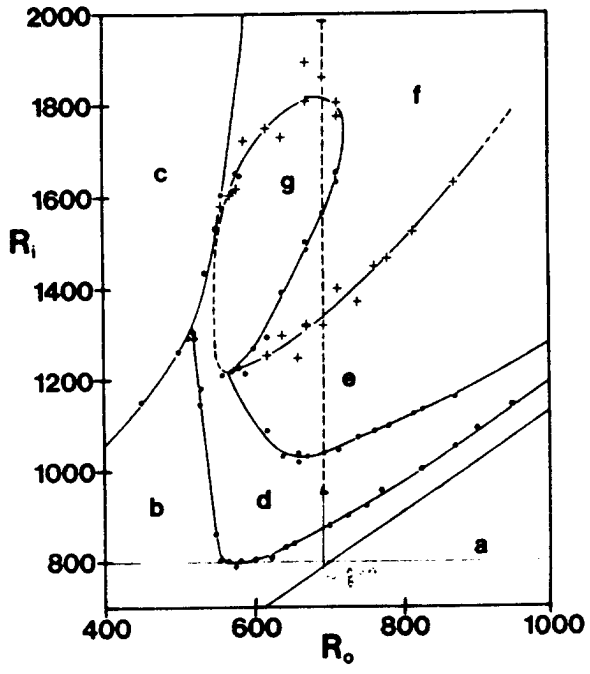

FIG. 2. Flow regime diagram for $\Gamma=30$, $\lambda=2.5$. The dashed line at $R_o=693$ gives the path along which the data of Fig. 3 were taken. The regions are as follows: (a) azimuthal flow, (b) Taylor-vortex flow, (c) wavy-vortex flow, (d) twists, (e) twists and wavy inflow boundaries, (f) dynamical domains, (g) uniform noisy wavelets and twists. Crosses indicate a transition to nonuniform behavior. Solid lines are present to guide the eye.

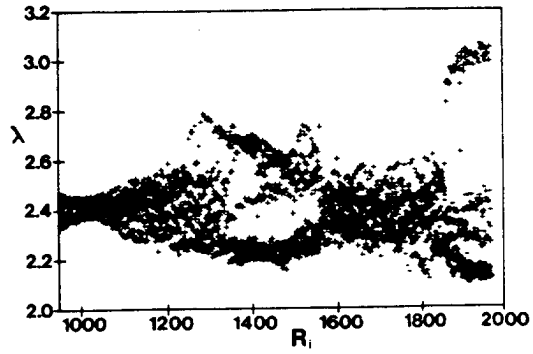

FIG. 3. Vortex-pair wavelengths obtained with a CCD array for $R_o=693$. Scatter in the uniform regimes is comparable with errors in computer fits of intensity minima in the raw data.

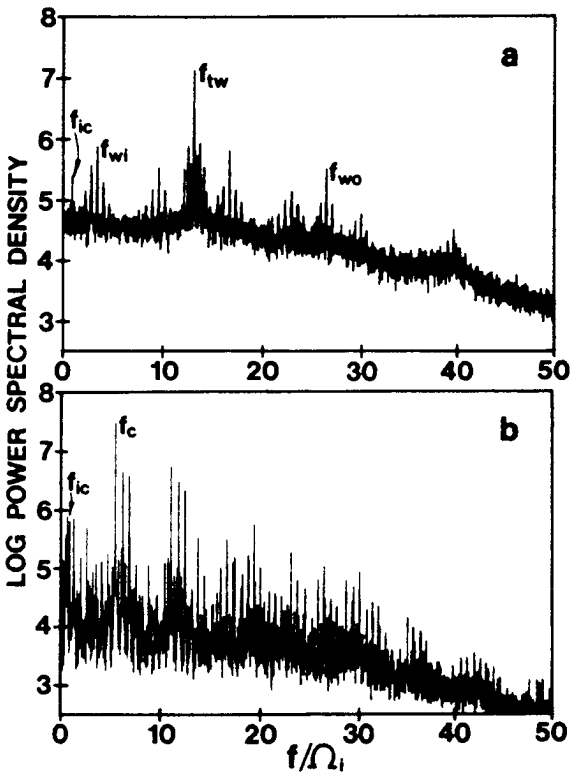

FIG. 4. Reflection spectra for a domain state with $R_o = 670$ and $R_i = 1900$. (a) Large vortices, (b) small vortices. Primary sharp features are labeled as follows: f_{tw}, twists; f_{wi}, wavy inflow boundaries; f_{wo}, wavy outflow boundaries; f_c, corkscrew; f_{ic}, inner cylinder. The background noise level is a factor of approximately 10 higher in (a) at high frequency.

tex depends sensitively on the vortex size, but the large vortices typically have twists, waves on both boundaries, and some small-scale noisy structure, while the small vortices may have no visually obvious secondary structure, or they may have a wave on the inflow boundary and weak twists). The large-vortex-pair axial wavelength λ [$\equiv$ (distance between outflow boundaries of the pair)/d] is found to be ~ 2.60, as compared with the small-pair λ of ~ 2.25. The 4 or 5 large vortex pairs are generally scattered throughout the system. As a result, significant wavelength variations occur over distances much smaller than the length of the cylinders. The onset of this regime is shown in Fig. 3, a plot of the local pair wavelength for $R_o = 693$. A persistent pattern with a distinct bimodal size distribution forms above $R_i \sim 1320$. At $R_i \sim 1560$ the system returns to axial uniformity (g). On every vortex in this regime there are weak twists, wavy inflow and outflow boundaries, and greater levels of small-length-scale noisy structure.

At $R_i \sim 1860$ the system again becomes unstable to domain formation (f) with the large-vortex-pair $\lambda \sim 3.0$ and the small-vortex-pair $\lambda \sim 2.2$. Figure 1 is typical of the visual appearance of such a flow state. The large vortices resemble those in the uniform regime (g) at lower R_i, with more pronounced small-scale structure, while flow in the small vortices appears to be relatively noise-free. Some small vortices may have periodic structures, such as a corkscrew pattern.[8] The spectra of Fig. 4 were obtained in this regime; the sharp features are different in the large and small vortices, and the broad background noise level is nearly an order of magnitude greater in the wide-vortex case. If $R_o > 720$, the nonuniformity sets in as for lower R_o, but the disparity between the largest and smallest vortices grows continuously until we reach the highly nonuniform flows shown in Fig. 1; no uniform regime interrupts the evolution. The uniform-nonuniform transitions all appear to be hysteretic, with ΔR_i as large as 125. For all values of R_o the flow gradually evolves at higher R_i to states in which the flow consists entirely of relatively uniform turbulent Taylor vortices.

Several points need to be emphasized about these flows. They are not transients; nonuniform flow states monitored for up to 48 h have never relaxed to a uniform state, although some rearrangement of the pattern can occur. They are also not due to cylinder defects since the domains do not always occur at the same locations when runs are duplicated. We have repeated some of the observations at various ramping rates; so long as our dimensionless average acceleration[9] $a^* \equiv (dR_i/dt)(Ld/\nu)$ was below ~ 20 no differences were noticed in either the flow states formed or the approximate onset of the instabilities. Some runs were made with $\Gamma = 70$ and $N = 56$ to look for aspect-ratio effects, and the same qualitative results were found as for $\Gamma = 30$. Some measurements were made at $\bar{\lambda} = 2.73$ and similar nonuniformities were found to occur; however, for $\bar{\lambda} = 2.31$ no evidence of domain formation has been found. In previous investigations at low R_i, Kalliroscope flakes have been shown to induce a nonuniform Taylor-vortex pattern with large vortices consistently at the top of the system.[10] The vortex-size irregularities in our experiments cannot be due to this effect since the largest vortex pairs occur at various locations along the cylinders during different runs. Our results were also independent of the visualant concentration. Finally, attempts were made to obtain data with a free upper surface, but the vortex at the upper surface was found to be unstable to splitting.

We know of no other closed system with behavior directly comparable to that reported here, but several systems do exhibit nonuniformities. The Eckhaus instability in an electrohydrodynamic system[11] leads to modulation of the roll pattern, but this is a transient effect. Intermediate-aspect-ratio Bénard convection has been found to occur with nonchaotic localized modes of oscillation.[12] There are instances in the circular Couette system in which the vortex structure is disrupted by the presence of turbators or dislocations near instabilities in which the number of vortices changes.[13] Vortex-size

variations have been reported near stability boundaries at low R_i when the outer cylinder is at rest,[2-4] but these are smooth variations in size (over distances comparable with the cylinder length[2]), with the central vortices larger than those near either end. At higher Reynolds numbers the onset of noisy small-scale structure occurs in the larger vortices near the center of the system[4] and spreads throughout the system as R_i increases. In contrast to these cases our system exhibits persistent, sharply defined coexisting domains of distinct dynamical behavior occurring over a large parameter range, and the secondary flows are correlated with abrupt wavelength variations in the primary-flow structure.

The origin of the domain states is only partially understood. In an ideal infinite system one might expect the vortices to be uniform,[14] althougth the preferred size might vary with R_i and R_o. In a finite system away from its preferred λ some vortex pairs may adjust their sizes at the expense of others. For the special case $R_o = 0$ this is observed to lead to changes in N, but for $R_o \neq 0$, N may not change and domains can form. It should be possible to study this by numerical examination of the stability of a vortex pair[14] with variable λ. A different approach is to construct model systems of coupled oscillators or 1D maps.[15-17] Such modes exhibit nonuniformities, and indeed Keeler and Farmer[17] have found coexisting chaotic and laminar domains as their system is forced away from its preferred wavelength. However, in contrast with our experiment, their model also predicts that in time the character of the individual domains will alternate between laminar and chaotic, and that there will be time intervals in which the entire system is laminar. While such a model has certain similarities to our experiments, it should only be taken as a starting point for the construction of models that more closely correspond to the actual flow.

In summary, we have found flow states in a finite-length circular Couette system in which dynamical domain formation occurs and very different levels of chaotic behavior coexist. The formation of the domains is governed by abrupt variations in the local axial wavelength of the Taylor vortices. We have argued that these effects may be related to the finite size of the system, but if so they are strikingly different from finite-size effects found in other nonequilibrium systems, including the Couette system with the outer cylinder at rest.

We would like to thank Tim DeVol and Donna Workman for assistance with the data analysis. We also thank H. Brand, J. D. Farmer, E. Siggia, and S. Zaleski for helpful discussions. This work was partially supported by the Office of Naval Research under Grant No. N00014-86-K-0071.

---

[a]Present address: Department of Physics, Duke University, Durham, NC 27706.

[1]A. Brandstäter, J. Swift, H. L. Swinney, A. Wolf, J. D. Farmer, E. Jen, and J. P. Crutchfield, Phys. Rev. Lett. **51**, 1442 (1983).

[2]K. Park, G. L. Crawford, and R. J. Donnelly, Phys. Rev. Lett. **51**, 1352 (1983).

[3]R. Heinrichs, G. Ahlers, and D. S. Cannell, Phys. Rev. Lett. **56**, 1794 (1986).

[4]G. P. King and H. L. Swinney, Phys. Rev. A **27**, 1240 (1983); G. P. King, Ph.D. dissertation, University of Texas, 1983 (unpublished).

[5]D. Coles, J. Fluid Mech. **21**, 385 (1965).

[6]H. A. Snyder, Int. J. Non-Lin. Mech. **5**, 659 (1970).

[7]C. D. Andereck, R. Dickman, and H. L. Swinney, Phys. Fluids **26**, 1395 (1983).

[8]C. D. Andereck, S. S. Liu, and H. L. Swinney, J. Fluid Mech. **164**, 155 (1986).

[9]K. Park, G. L. Crawford, and R. J. Donnelly, Phys. Rev. Lett. **47**, 1448 (1981).

[10]M. A. Dominguez-Lerma, G. Ahlers, and D. S. Cannell, Phys. Fluids **28**, 1204 (1985).

[11]M. Lowe and J. P. Gollub, Phys. Rev. Lett. **55**, 2575 (1985).

[12]R. W. Walden, P. Kolodner, A. Passner, and C. M. Surko, Phys. Rev. Lett. **44**, 242 (1984).

[13]R. J. Donnelly, K. Park, R. Shaw, and R. W. Walden, Phys. Rev. Lett. **44**, 987 (1980)

[14]M. Nagata, J. Fluid Mech. **169**, 229 (1986); P. Marcus, J. Fluid Mech. **146**, 45, 65 (1984).

[15]I. Waller and R. Kapral, Phys. Rev. A **30**, 2047 (1984).

[16]G. Oppo and R. Kapral, Phys. Rev. A **33**, 4219 (1986).

[17]J. D. Keeler and J. D. Farmer, to be published.

Phase modulation of Taylor vortex flow

Mingming Wu and C. David Andereck
Department of Physics, The Ohio State University, Columbus, Ohio 43210
(Received 5 November 1990; revised manuscript received 26 December 1990)

The phase dynamics of Taylor vortex flow close to onset was studied by applying a forced modulation to the upper boundary of a large-aspect-ratio concentric-cylinder system. Our experimental results show that the phase disturbances progress diffusively along the Taylor vortices in the axial direction. Values of the diffusion coefficients obtained experimentally are compared with those found in numerical computations. We also confirm the dependence of the diffusion coefficient on the wave vector of the Taylor vortices predicted by the general theoretical model of Pomeau and Manneville [J. Phys. (Paris) Lett. 40, L609 (1979)].

In the last decade, much attention has been given to the phase dynamics of patterns in hydrodynamic systems where the transition from a uniform state to a spatially periodic state occurs.[1-5] One of the classic examples is the Taylor-Couette system, which consists of fluid between two concentric cylinders with the inner one rotating. When the rotation frequency of the inner cylinder exceeds a threshold value, the spatially uniform circular Couette flow (CCF) changes to the axially periodic Taylor vortex flow (TVF). The flow pattern undergoes successive transitions as the inner cylinder rotation frequency increases further, leading eventually to turbulent flow. The characteristics of the flows in the Taylor-Couette system have been investigated extensively by visualizing the patterns and measuring the velocity profiles.[6] While the Navier-Stokes equation, in principle, provides a theoretical basis for understanding the experimental results,[7,8] the complexity of the equation often makes it difficult to compare with real laboratory situations, therefore necessitating the use of model equations. In particular, dynamics of patterns may be well reproduced with simplified model equations such as the Ginzburg-Landau equation.[9] In this spirit, it has been shown that phase variables (which might be associated with, for instance, the positions of rolls in the Taylor-Couette system) are governed by a simple diffusion equation[1] in the nonequilibrium systems that show spatially periodic structures after a supercritical bifurcation. This provides us with a very simple and direct way to study the slow, long-wavelength dynamics of Taylor vortices with theoretical understanding.

We have performed a detailed experimental study of the phase dynamics near the onset of TVF in a large-aspect-ratio concentric-cylinders system. The phase-diffusion coefficients were obtained by studying the responses of the Taylor vortices to the motion in the axial direction of the top boundary of the system. Two different boundary conditions were implemented in our experiments. In the first case the top boundary oscillated in the axial direction, while in the second case it was moved at a constant speed to a final position. In both cases the pattern disturbances traveled diffusively away from the boundary in the axial direction. The diffusion coefficients we obtained are consistent with the results of numerical computations[10,11] based on the Navier-Stokes equation. We also present experimental results on the dependence of the phase-diffusion coefficient on the wave vector of the Taylor vortices. We found that the diffusion coefficient decreased as the wave vector of the TVF deviated from q_c, the critical wave vector for TVF.[12] These results are consistent with the phase-diffusion model.[1]

The control parameter for the Taylor-Couette system with the outer cylinder at rest is the Taylor number T. It is defined as $T=(\Omega_i r_i d/\nu)(d/r_i)^{1/2}$, where Ω_i is the inner cylinder rotation frequency, r_i is the inner cylinder radius, d is the gap between the inner and outer cylinders, and ν is the kinematic viscosity. When T exceeds the threshold T_c, the flow changes from a uniform CCF to a periodic TVF. In the vicinity of T_c, the lowest order of, for example, the radial velocity field has the form $u(r,z,t)=A(z,t)e^{iq_c z}u(r)$, where $u(r)$ is the eigenfunction, z is the axial position, and q_c is the critical wave vector corresponding to the lowest T_c.[12] The amplitude $A(z,t)$ can then be rewritten as $|A(z,t)|e^{i\phi(z,t)}$, where $\phi(z,t)$ is the phase variable associated with the slow space and time variations in A. ϕ has been predicted[3] to obey a diffusion equation

$$\frac{\partial\phi}{\partial t}=D_{\parallel}\frac{\partial^2\phi}{\partial z^2} \tag{1}$$

where

$$D_{\parallel}=\frac{\xi_0^2}{\tau_0}\frac{(\epsilon-3\xi_0^2q^2)}{(\epsilon-\xi_0^2q^2)}, \tag{2}$$

and τ_0 is the perturbation amplitude growth rate, ξ_0 is the correlation length, $\epsilon=(T-T_c)/T_c$ is the distance to the onset of TVF, $q=\tilde{q}-q_c$, $\tilde{q}$ is the wave vector of the TVF.

Our experiment is conducted in concentric cylinders with the outer one fixed. The inner cylinder radius $r_i=5.262$ cm, the outer cylinder radius $r_0=5.965$ cm, the length between collars initially is 49.5 cm, and therefore the radius ratio $\eta=0.882$ and the aspect ratio $\Gamma=L/(r_0-r_i)=70.4$. The inner cylinder is driven by a Compumotor stepper motor. The working fluid is a solution of double distilled water and 44% glycerol by weight. 1% by volume of Kalliroscope AQ1000 is added for visualization. The forced modulation is added through moving the top collar of the system [see Fig. 1(a)]. A stepper motor can move the collar a maximum distance of 1 cm. The visualized TVF pattern is viewed with a 512×480 pixel CCD

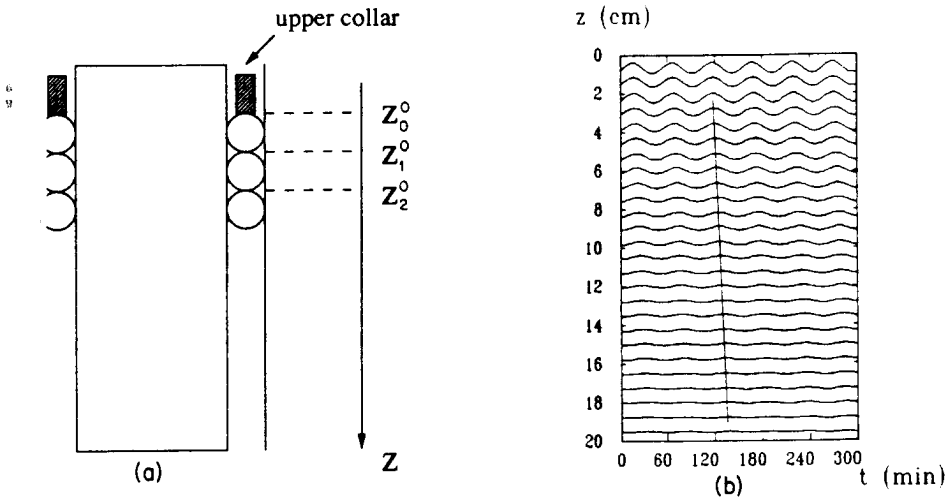

FIG. 1. (a) Schematic diagram of the experimental geometry. (b) Node line locations of TVF subjected to the periodic boundary modulation, t represents time and z is the distance from the top collar. The solid line traces the shift in phase from vortex to vortex.

camera which is connected to an image processor. The light intensity of a vertical line of the pattern is recorded and the positions of the node lines are determined by finding minima of the light intensity profile. For a typical situation we have a resolution of 34 pixels per vortex.

In the first type of experiment, the top collar oscillated in the axial direction. We found that the phase at $z=0$ exactly follows the top collar's motion due to the fact that the period of the modulation $T \gg d^2/\nu$, the diffusion time through a vortex. (Typically, $T=3040$ s and $d^2/\nu=12.3$ s.) This provided the following boundary condition

$$\phi|_{z=0}=\phi_0 \sin(\omega t)\,. \tag{3}$$

Here ϕ_0 and ω are the modulation amplitude and frequency. Solving Eq. (1) with the above boundary condition, we obtain

$$\phi(z,t)=\phi_0 e^{-\alpha z}\sin(\omega t-\beta z)\,, \tag{4}$$

$$\alpha=\beta=\left(\frac{\omega}{2D_{\parallel}}\right)^{1/2}. \tag{5}$$

Assuming z_n is the location of the nth vortex node line, then $\phi(z_n,t)+\tilde{q}z_n=n\pi$, therefore

$$z_n=[n\pi-\phi_0 e^{-\alpha z}\sin(\omega t-\beta z)]/\tilde{q}$$

$$\simeq z_n^0-\phi_0 e^{-\alpha z_n^0}\sin(\omega t-\beta z_n^0)/\tilde{q}\,, \tag{6}$$

where z_n^0 is the location of the vortex node line without modulation and $z_n^0=n\pi/\tilde{q}$. Equation (6) shows that the node lines oscillate sinusoidally, their amplitudes decrease along the axial direction, and a phase shift occurs between the neighboring node line motions.

In the second experiment, we moved the top collar to a final position at a constant speed, which leads to the approximate boundary condition

$$\phi|_{z=0}=\phi_0 H(t)\,. \tag{7}$$

Here $H(t)$ is the step function, 0 for $t<0$, 1 for $t\geq 0$. It deviates from the real boundary condition owing to the finite time (typically 48 s) for the collar to reach its final position, but our analysis showed that this deviation is negligible in the region far from the boundary (three or

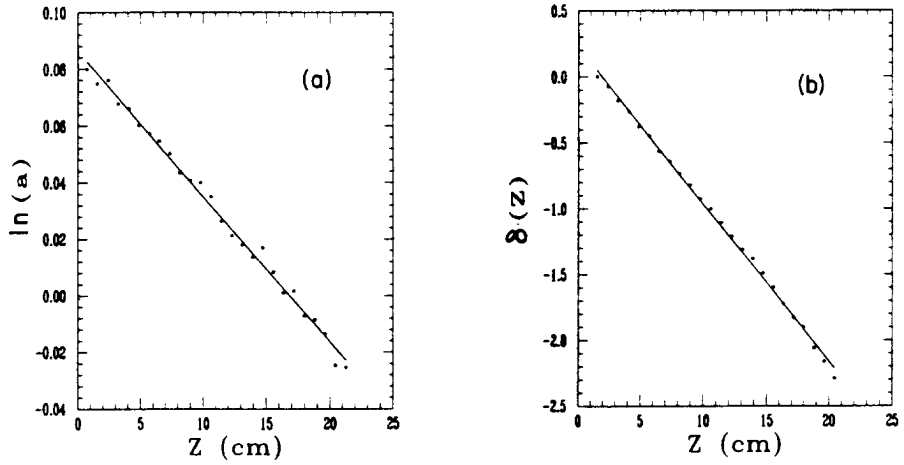

FIG. 2. Dots represent the experimental data and the solid lines are derived from the fit to the diffusion model. (a) a is the amplitude of each node line motion. (b) δ is the phase shift of the node line motion.

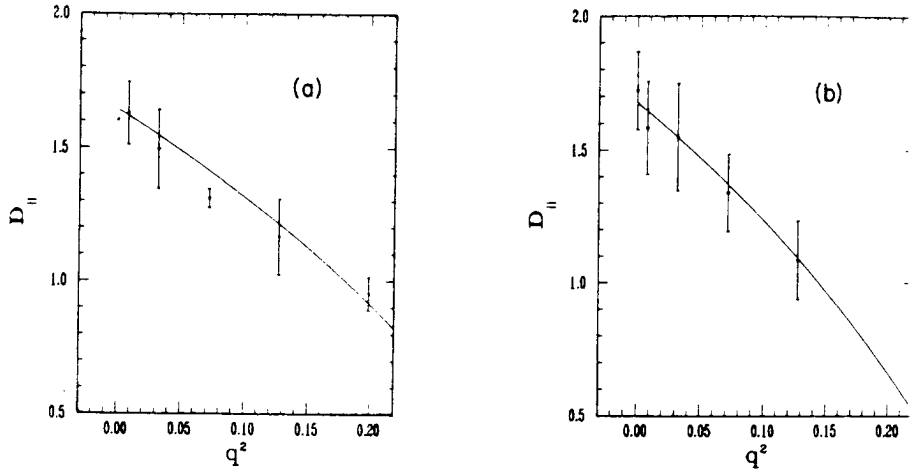

FIG. 3. Relation between $D_\parallel$ and the square of the wave vector, q^2, for: (a) the periodic modulation case; (b) the step-function modulation case. Dots represent the experimental data and the solid lines are the fits to Eq. (2).

more vortices away from the collar). Substituting the above boundary condition in Eq. (1) and following the same procedure as described for the periodic modulation, we find that the location of the nth vortex node line is given by

$$z_n = z_n^0 - d_0 \mathrm{erfc}\left(\frac{z_n}{2(D_\parallel t)^{1/2}}\right) \simeq z_n^0 - d_0 \mathrm{erfc}\left(\frac{z_n^0}{2(D_\parallel t)^{1/2}}\right), \quad (8)$$

where d_0 is the distance that the top collar moves and erfc is the error function complement.

In the periodic modulation case, the sinusoidal motion of the upper collar has a typical amplitude of $d_0/d = 0.480$ and a period of 3040 s. For each set of data, the inner cylinder rotation frequency is adjusted to the TVF region and left about 1 h (our measurements showed that it took about 30 min for our system to reach a steady state). Two hours after starting the modulation, we began recording a vertical line image of the flow pattern every 2 min for 5 h. Figure 1(b) is a typical data set. The response of each node line is a sinusoidal function of time, with an amplitude and phase shift as predicted by Eq. (6). By fitting this data set with the following equation

$$z_n = z_n^0 - a\sin(\omega t - \delta), \quad (9)$$

where a and δ are the amplitude and the phase of the node line motion, we found that $\ln a$ and δ were linearly related to z_n^0 as shown in Fig. 2(a) and 2(b). The slopes of the lines give us values of α and β from Eq. (6), and hence the value of $D_\parallel$. The variations of α and β were within 20%. The resultant value of $D_\parallel$ was found to be independent of the modulation period. Repeating the experiment with a different Taylor vortex wave vector we found that $D_\parallel$ decreased when the wave vector q deviated from q_c. Figure 3(a) shows a typical dependence of $D_\parallel$ on q. The correlation length ξ_0 and correlation time τ_0 can be obtained by fitting this with Eq. (2). The values for this case are listed in Table I.

In the step function case, the upper collar moves at a constant speed (about 0.125 mm/s) to a final position in 48 s, which leads to an aspect ratio increase of 0.853. The response time of each vortex increased with distance of the vortex from the top boundary. For instance, the relaxation time for the 2nd vortex boundary to reach halfway to its steady-state position is 31.1 s after the collar comes to rest, while that of the 3rd vortex boundary is 71.9 s. In this case, the approximation of Eq. (7) is valid for the vortices beyond the three adjacent to the collar. The same data acquisition technique is used here. The light intensity profile of a vertical line is recorded every 12 s after the modulation is added. A typical data set took 40 min. Figure 4 shows a sample result. Fitting this data with the equation

$$z_n = z_n^0 - d_0 \mathrm{erfc}\left(\frac{s_n}{\sqrt{t}}\right), \quad (10)$$

TABLE I. Values of $D_\parallel$ from our experiments, for $\tilde{q} = 3.25$ and $\eta = 0.882$; calculated values of ξ_0 and τ_0 for $\eta = 0.90$ from Ref. 10; and $D_\parallel$ for $\tilde{q} = 3.30$ and $\eta = 0.85$ from Ref. 11.

$D_\parallel$	ξ_0	$1/\tau_0$	ϵ	Source of data
1.63 ± 0.12	0.260	24.3	0.0740	periodic modulation
1.59 ± 0.07	0.293	18.9	0.0740	periodic modulation
1.54 ± 0.20	0.288	19.3	0.0621	constant modulation
1.58 ± 0.17	0.301	17.4	0.0829	constant modulation
	0.382	13.109		Ref. 10
1.70			0.070	Ref. 11

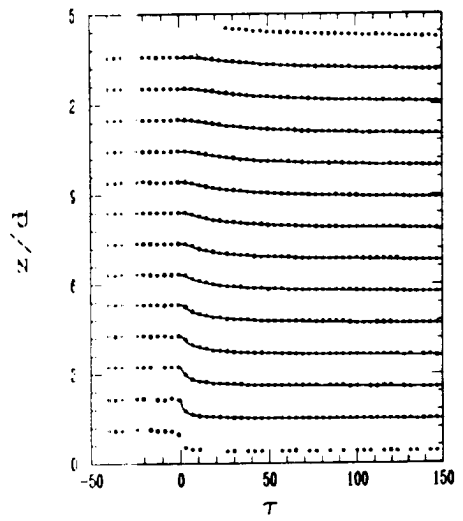

FIG. 4. Node line locations of TVF subjected to the step-function boundary modulation. Modulation is added at $\tau=0$ $[\tau=t/(d^2/\nu)]$. Dots represent the experimental data and solid lines are the error function fits to the data.

where $s_n=z_n^0/2(D_\parallel)^{1/2}$ according to Eq. (8), we obtain s_n as a linear function of z_n^0. Therefore, $D_\parallel$ is evaluated by the slope of s_n and z_n^0. Repeating this process for different TVF wave vectors, we obtained a relation between $D_\parallel$ and wave vector similar to that found in the case of periodic modulation. The results are shown in Fig. 3(b). The resultant values of ξ_0 and τ_0 are shown in Table I in comparison with those from the periodic cases and numerical computations.[10,11] Our values of ξ_0 and τ_0 differ from the numerical values of Ref. 10, while $D_\parallel$ from Ref. 11 is within our error bars for three cases. In both numerical cases, the geometry studied was similar to ours. That we differ with Ref. 10 suggests we may be operating somewhat beyond the range of applicability of Eq. (2), which is, strictly, only appropriate for $\epsilon\rightarrow 0$. Further experiments with ϵ smaller than 0.06 would be needed to verify this.

As shown in Fig. 3(a) and 3(b), the range of wave vectors accessible to us is limited due to the large radius ratio of our system. According to the Eckhaus theory,[12] there are larger stable wave-vector regions of TVF in a small radius ratio system, since it is possible to go to higher ϵ before reaching a wavy instability. Therefore, it is expected that an experiment in a small radius ratio system will show a more profound dependence of $D_\parallel$ upon the wave vector.

In summary, our experimental results have confirmed the basic features of the phase diffusion model proposed by Pomeau and Manneville[1] near the onset of TVF. We studied the phase-diffusion process under two distinct types of modulation and obtained consistent results. In both cases, the phase variables diffused along the Taylor vortices in the axial direction. The measured diffusion coefficients decreased when the Taylor vortex wave vector deviated from q_c.

We express our special thanks to Innocent Mutabazi for many useful discussions. We also thank Doug Dolfinger for developing the modulation apparatus. This work was supported by the Office of Naval Research, under Contract No. N00014-86-K-0071 and Grant No. N00014-89-J-1352.

[1]Y. Pomeau and P. Manneville, J. Phys. (Paris) Lett. **40**, L609 (1979).

[2]J. E. Wesfreid and V. Croquette, Phys. Rev. Lett. **45**, 634 (1980).

[3]P. Tabeling, J. Phys. Lett. **44**, 665 (1983).

[4]H. Brand and M. C. Cross, Phys. Rev. A **27**, 1237 (1983).

[5]M. Lucke and D. Roth, Z. Phys. B **78**, 147 (1990).

[6]H. L. Swinney and R. DiPrima, in *Hydrodynamic Instabilities and the Transition to Turbulence*, 2nd ed., edited by H. L. Swinney and G. P. Gollub (Springer, Berlin, 1985), p. 139.

[7]P. S. Marcus, J. Fluid Mech. **146**, 45 (1984).

[8]P. S. Marcus, J. Fluid Mech. **146**, 65 (1984).

[9]A. C. Newell, J. A. Whitehead, J. Fluid Mech. **38**, 279 (1969). For application to the Taylor-Couette system see R. Graham and J. A. Domaradzki, Phys. Rev. A **26**, 1572 (1982), and references therein.

[10]M. A. Dominguez-Lerma, G. Ahlers, and D. S. Cannell, Phys. Fluids **27**, 856 (1984).

[11]H. Riecke (private communication); see also a related paper, H.-G. Paap and H. Riecke (unpublished).

[12]G. Ahlers, D. S. Cannell, and M. A. Dominguez-Lerma, Physica **23D**, 202 (1986).

Phase Dynamics of Wavy Vortex Flow

Mingming Wu and C. David Andereck
Department of Physics, The Ohio State University, Columbus, Ohio 43210
(Received 17 April 1991)

The phase dynamics of wavy vortex flow is studied by applying a forced modulation to the upper boundary of a large-aspect-ratio concentric cylinders system. The experimental results are consistent with a model based on coupled phase equations. We find that the perturbations propagate as traveling waves parallel with the axis of the system when there is a strong coupling between the axial and azimuthal phase variables, and diffusively for weak coupling. The propagating wave speed is measured for a range of Reynolds numbers.

PACS numbers: 47.20.−k, 47.30.+s

Considerable attention has been given to patterns formed in such nonequilibrium systems as Rayleigh-Bénard convection and Taylor-Couette flow. These studies have typically been concerned with the properties of these patterns under steady-state conditions, e.g., wavelengths, wave speeds, and space-time variations. Much less is known about the responses of such patterns to external perturbations [1–7]. The importance of this may be seen by a simple analogy with solids: It is possible to determine their crystallographic characteristics alone, but the elastic properties revealed by detailed phonon studies are essential for a complete understanding of the structure and its underlying atom-atom interactions. In this Letter we present the results of an experimental investigation of the response to perturbations of a particular nonequilibrium pattern which arises in the Taylor-Couette system. The slow perturbations give rise to long-wavelength excitations, either diffusive or propagating, which will be discussed within the framework of the phase dynamics theory of Brand and Cross [4].

The Taylor-Couette system [8] consists of fluid between two concentric cylinders with the inner one rotating. The flow pattern undergoes successive transitions as the cylinder's angular velocity Ω increases. When the Reynolds number R ($\propto \Omega$) exceeds a threshold value R_c, the spatially uniform circular Couette flow changes to the axially periodic Taylor vortex flow (TVF). The first time-dependent regime, wavy vortex flow (WVF), in which an azimuthal wave is superimposed on the TVF, occurs for slightly greater R in a large-radius-ratio system. The phase dynamics in the Taylor vortex case (i.e., one phase variable) is now well established. The behavior can be described by a simple diffusion model [1–3,5,6]. The experiments reported here concern wavy vortex flow, which is described by *two* phase variables: One variable, ψ, is related to the axial position variations of the vortices and the other, ϕ, to the azimuthal wave phase. Brand and Cross [4] proposed that the dynamics in this case is governed by coupled diffusion equations with the coupling strength proportional to the azimuthal wave vector. They predict richer dynamics than for the Taylor vortex case, but experimental support for this picture has been lacking until now.

To study the phase dynamics of wavy vortex flow, we impose a periodic modulation at one end of the cylinders and the responses of the vortices are recorded. The variations of ψ diffuse along the cylinders for small vortex size, small azimuthal wave number m, and small azimuthal wave amplitude, and propagate otherwise. We show that the diffusion coefficient for ψ increases with decreasing vortex size, while the coupling between neighboring vortices increases with increasing azimuthal wave vector and wave amplitude. The values of the traveling wave speed are found to increase with the rotation frequency of the cylinder.

The control parameter of our system is the Reynolds number $R=\Omega r_i d/\nu$, where r_i (=5.262 cm) is the inner-cylinder radius, d (=0.703 cm) is the gap between the inner and outer cylinders, and ν is the kinematic viscosity. We scale lengths by d and time by d^2/ν (12 sec). The average aspect ratio $\Gamma=L/d=70.4$, where L is the length of the cylinder. The working fluid is bounded by two Teflon rings. The lower ring is tightly fitted to the outer cylinder, while there is a 0.8-mm gap between the top ring and both the inner and outer cylinders. The upper ring is supported by the traversing mechanism responsible for driving the axial oscillation of the ring. This mechanism is driven by a stepper motor under computer control [5,9]. 1% by volume of Kalliroscope AQ1000 is added to the fluid for visualization. The visualized flow pattern is viewed with a 512×480 pixel charge-coupled-device camera which is connected to an image processor. The light intensity of a vertical line of the pattern is recorded and the positions of the vortex boundary lines are determined by finding minima of the light intensity profile. The vortex boundary line positions change on two time scales, the slow time T_1 (corresponding to the slow top boundary oscillation, which has a typical period of several minutes) and the fast time T_2 (corresponding to the azimuthal wave motion of period $\simeq 1$ sec). We define $\bar{z}_n(T_1)$ to be the average boundary line position change of the nth vortex due to the slow top boundary modulation. Thus, $\psi=q\bar{z}_n(T_1)$, where q is the axial wave vector. To obtain $\bar{z}_n(T_1)$, we take about 100 consecutive line profiles (covering about 10 azimuthal waves) in 7 sec, find the intensity minima, and then average out the azimuthal wave

motion. For a typical situation we have a resolution of 30 pixels per vortex.

We first measured $\bar{z}_n(T_1)$ at $\epsilon=0.140$ [$\epsilon=(R-R_c)/R_c$], slightly above the onset of WVF, where the azimuthal wave number $m=3$. A typical result is shown in Fig. 1(a). The amplitude of $\bar{z}_n(T_1)$ decreases exponentially along the system axis [Fig. 2(a)], which is indicative of diffusion, and there is a linear phase shift between oscillations of neighboring vortices [Fig. 2(b)]. Upon further increasing the rotation frequency, the system reaches a new stable state with $m=7$ at $\epsilon=0.813$. For modulation period $T=53.3$, $\bar{z}_n(T_1)$ reveals an axially propagating wave in the middle section of the cylinders, as shown in Fig. 1(b). The complete amplitude of $\bar{z}_n(T_1)$ versus axial position is shown as the □ data symbols in Fig. 2(a). Diffusive behavior is observed in the vortices near the top collar of the cylinders ($0<z<10$). These end vortices have a small azimuthal wave amplitude, evidently leading to a relatively weaker coupling between the axial and azimuthal phase variables than in the bulk.

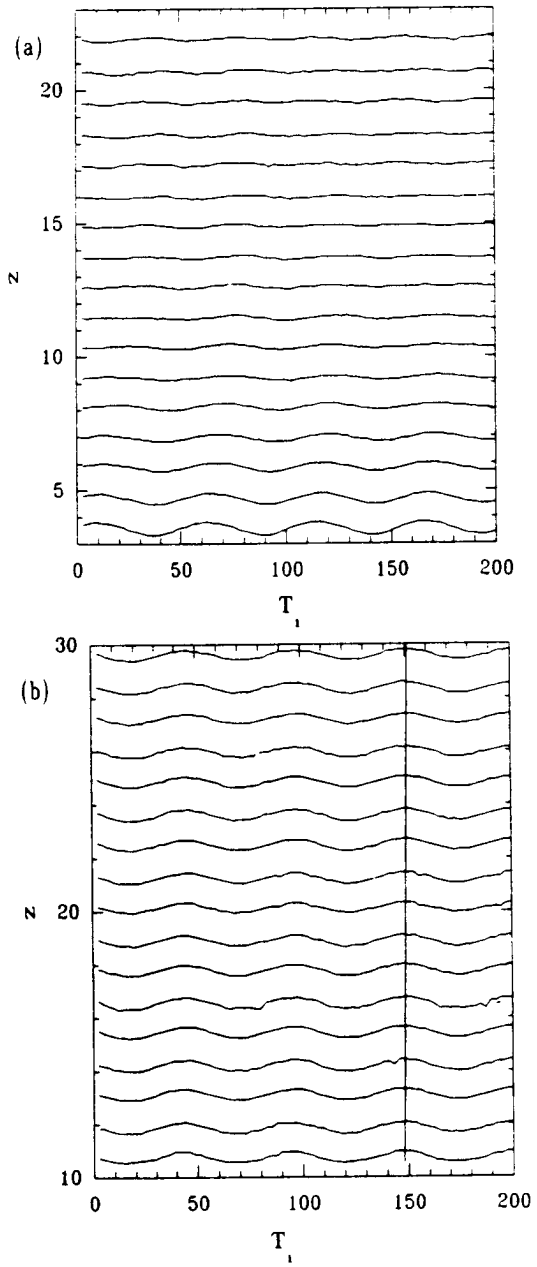

FIG. 1. Responses of the axial phase variable $\bar{z}_n(T_1)$ to a modulation of period $T=53.3$. Number of vortices $N=60$. (a) $m=3$, $\epsilon=0.140$; (b) $m=7$, $\epsilon=0.813$. The straight line traces the shift in phase from vortex to vortex.

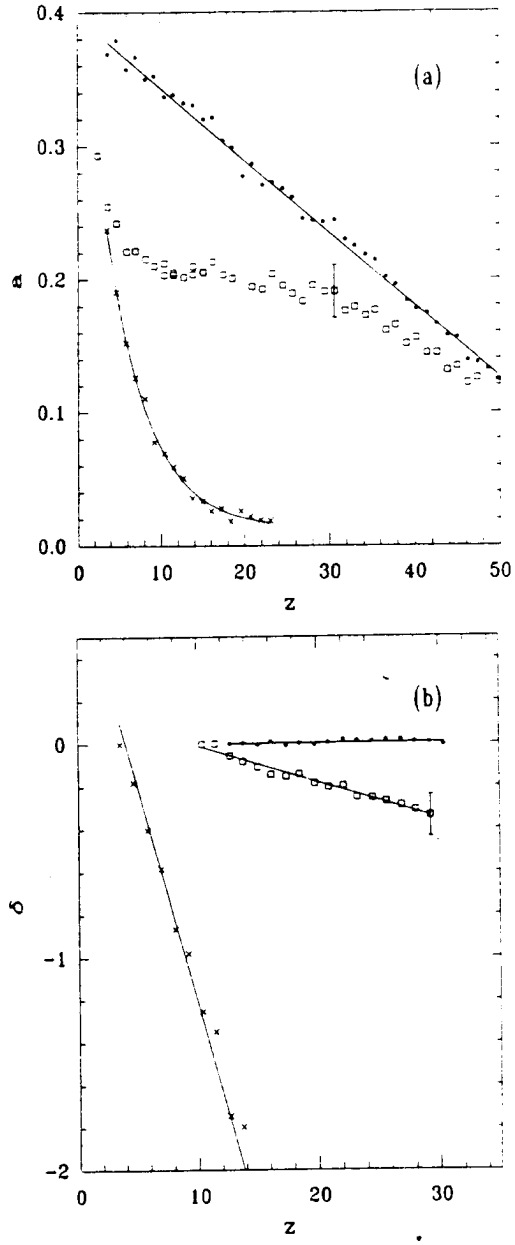

FIG. 2. (a) Amplitude and (b) phase shift δ of $\bar{z}_n(T_1)$ vs axial position. The bar represents the largest error of all the data points. ×: $m=3$, $N=60$, $\epsilon=0.140$, $T=53.3$; □: $m=7$, $N=60$, $\epsilon=0.813$, $T=53.3$; ●: $m=7$, $N=60$, $\epsilon=0.813$, $T=207$. The solid lines are fits to the data, either linear or exponential.

A second contributing factor is that vortices near the collar are ~3% smaller than in the middle region. The diffusive behavior near the collar is consistent with the observation, discussed below, that the diffusion coefficient is larger for smaller vortices. In our experiment the axial range of the constant-amplitude propagation region varied with modulation period, ϵ, and vortex size: Faster modulation, larger ϵ, and larger vortex size lead to a longer constant-amplitude region. The phase shift δ of neighboring $\bar{z}_n(T_1)$ in this region has a linear dependence on the axial position [□ line of Fig. 2(b)]. The falloff of the $\bar{z}_n(T_1)$ amplitude in the lower end of the cylinders [$z > 30$ in Fig. 2(a)] is evidently a finite-length effect. The phase shift in this region is a linear function of the axial position with a slope close to that of the phase shift line for the traveling wave in the middle of the system.

For $T = 207$ [● line of Fig. 2(a)], the amplitude of $\bar{z}_n(T_1)$ is linearly related to the axial position. Its slope, scaled by the oscillation amplitude of the upper ring, is $0.0137 \simeq 1/\Gamma$. This is a typical solution of a propagating wave equation where the wavelength is much longer than the length of the system. The corresponding phase shift between neighboring $\bar{z}_n(T_1)$ [● line of Fig. 2(b)] is zero, which means that the modulation is slow enough for each vortex to respond simultaneously.

The vortex-size dependence of the phase dynamics was explored in some detail. Figure 3 shows the amplitude of $\bar{z}_n(T_1)$ along the axis for the same ϵ and m, but different vortex size. The amplitude decreases more rapidly in the $N = 60$ state than in the $N = 54$ state, indicating the diffusion coefficient is larger for small vortices. Similar behavior is found in Taylor vortex flow [5].

The slope of $\delta(z)$ gives the traveling wave vector K, and in turn the value of the traveling wave speed c. In Fig. 2(b), we obtained $c = 7$ (or 0.4 cm/sec), which shows this is a very soft system compared with sound propagation in liquids or solids. The computed wavelength is about 365.

We have measured the traveling wave velocity c in the middle section of the cylinders as a function of ϵ in the strong-coupling regime (see Fig. 4). c is shown below to be proportional to the coupling strength. For a wavy state with fixed m and N, the increase of ϵ corresponds (roughly) to increasing azimuthal wave amplitude. Thus the increase of c with ϵ (see Fig. 4) implies that the coupling strength increases with the azimuthal wave amplitude. c can also be evaluated from the amplitude equation [4] close to the onset of TVF. However, the calculated value shows only a very small dependence on ϵ, changing from 0.63 to 0.65 for a variation of ϵ from 0.5 to 1.5. This difference is not unreasonable as the amplitude equation approach is useful only close to the onset of TVF. Further theoretical work is necessary to explain the dependence of c on ϵ.

We can understand many of our observations within the theoretical framework of the coupled linearized phase equations [4]. Based on symmetry arguments and consideration of sufficiently slow variations in space and time, Brand and Cross proposed that the dynamics of the phase variables ψ and ϕ of the wavy vortex flow is governed by the following equations:

$$\frac{\partial \psi}{\partial t} = D_1 \frac{\partial^2 \psi}{\partial z^2} + C_1 \frac{\partial \phi}{\partial z}, \quad \frac{\partial \phi}{\partial t} = D_2 \frac{\partial^2 \phi}{\partial z^2} + C_2 \frac{\partial \psi}{\partial z}, \qquad (1)$$

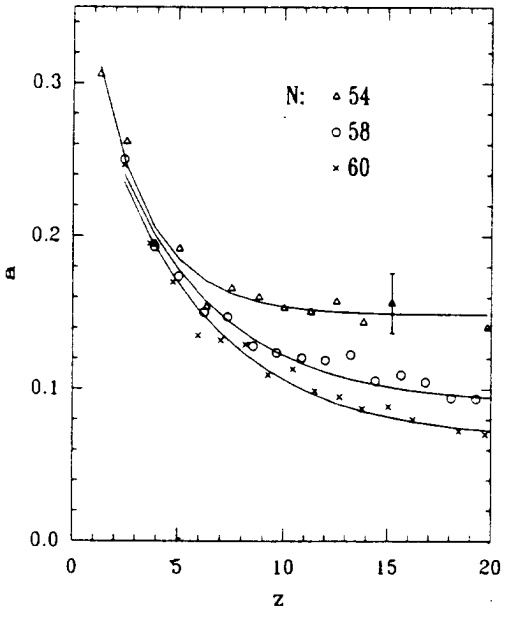

FIG. 3. Amplitude a of $\bar{z}_n(T_1)$ vs axial position for different vortex sizes. The bar represents the largest error of all the data points. $T = 28$, $\epsilon = 0.813$, $m = 7$, and N as indicated. The solid lines are exponential fits to the data.

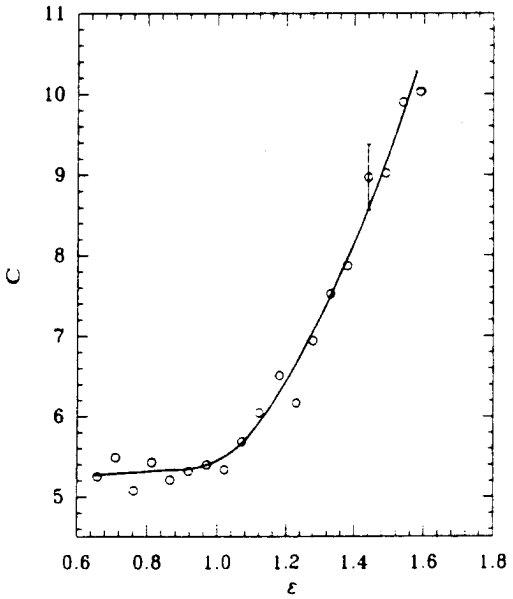

FIG. 4. Values of traveling wave speed c vs ϵ for $m = 8$, $N = 54$, and $T = 20$. The bar represents the largest error of all the data points. The solid line is drawn to guide the eye.

where D_1 and D_2 are the diffusion coefficients for the axial and azimuthal directions, $C_1, C_2 \propto q_y$, and z is along the axis. D_1, D_2, C_1, C_2 can be evaluated by the amplitude equation near the onset of TVF [4]. From this equation, we expect that for a Taylor vortex state ($q_y = 0$, $C_1 = C_2 = 0$) or for a small-q_y wavy vortex state (leading to small C_1, C_2), ψ can be described by a diffusion equation, while for a large q_y, ψ is governed by a propagating wave equation:

$$\frac{\partial^2 \psi}{\partial t^2} - c^2 \frac{\partial^2 \psi}{\partial z^2} = 0. \tag{2}$$

Here $c = (C_1 C_2)^{1/2}$.

The phase at $z = 0$ exactly followed the collar's oscillatory motion since the modulation period is much larger than d^2/ν, the diffusion time through a vortex (typically, $T \cong 53$). Therefore we have the following boundary condition:

$$\psi|_{z=0} = \psi_0 \sin(\omega t), \tag{3}$$

where ψ_0 and $\omega = 2\pi/T$ are the modulation amplitude and frequency. To compare with our experiment, Eq. (1) is solved with the above boundary equation in two distinct regimes. The first is the weak-coupling regime where $C_1 C_2 \ll \omega |D_1 - D_2|$. The solution has the form

$$\psi(z,t) = \psi_0 e^{-\alpha z} \sin(\omega t - \alpha z), \tag{4}$$

$$\alpha = (\omega / 2D_1)^{1/2}. \tag{5}$$

This behavior was observed in Taylor vortex flow [5], where $C_1, C_2 = 0$, and in small-m wavy vortex flow [for example, $m = 3$; see the $\times$ lines of Figs. 2(a) and 2(b)]. Using Eqs. (4) and (5), the slope of the line in Fig. 2(b) gives $D_1 \cong 1.4$. By comparison, for Taylor vortex flow [5] we found values of D ranging from 1.6 to 1.1, depending on the axial wave vector.

The second is the strong-coupling regime where $C_1 C_2 \gg 2\omega(D_1 + D_2)$. The solution then has the form

$$\psi(z,t) = \psi_0 \sin(\omega t - Kz), \tag{6}$$

where $K = \omega/c$. This corresponds to the large-m wavy state ($m = 7$, 8, or 9) where strong coupling exists. A typical example is shown in Figs. 2(a) and 2(b). We were not able to study the phase dynamics of the $m = 4$, 5, and 6 states due to difficulties with analysis of their very large amplitude waves. For these intermediate-m states we might expect an overdamped mode [4].

To summarize, we have studied the phase dynamics of wavy vortex flow and observed both diffusive and propagating modes. These results are consistent with the coupled-phase-equation picture of Brand and Cross [4]. The measured traveling wave speed and its strong dependence on the Reynolds number remains a challenge for the theory.

We thank H. Brand for carefully reading the manuscript and Z. H. Wang, F. Hayot, and I. Mutabazi for helpful discussions. This work was supported by the Office of Naval Research, under Contract No. N00014-86-K-0071 and Grant No. N00014-89-J-1352.

[1] Y. Pomeau and P. Manneville, J. Phys. (Paris), Lett. **40**, L609 (1979).
[2] J. E. Wesfreid and V. Croquette, Phys. Rev. Lett. **45**, 634 (1980).
[3] P. Tabeling, J. Phys. (Paris), Lett. **44**, L665 (1983).
[4] H. Brand and M. C. Cross, Phys. Rev. A **27**, 1237 (1983).
[5] M. Wu and C. D. Andereck, Phys. Rev. A **43**, 2074 (1991).
[6] H. Riecke, Phys. Fluids A (to be published).
[7] M. Lucke and D. Roth, Z. Phys. B **78**, 147 (1990).
[8] H. L. Swinney and R. DiPrima, in *Hydrodynamic Instabilities and the Transition to Turbulence*, edited by H. L. Swinney and G. P. Gollub (Springer, Berlin, 1985), 2nd ed., p. 139.
[9] Details of the traversing system will be presented elsewhere.

EUROPHYSICS LETTERS 1 August 1992

Europhys. Lett., **19** (7), pp. 587-592 (1992)

The Phase Dynamics of Turbulent Taylor Vortex Flow.

M. WU(*), C. D. ANDERECK(*) and H. R. BRAND(**)

(*) *Department of Physics, The Ohio State University - Columbus, OH 43210*
(**) *FB 7, Physik, Universität Essen - D-4300 Essen 1, Germany*

(received 9 December 1991; accepted in final form 23 June 1992)

PACS. 47.20 – Hydrodynamic stability and instability.
PACS. 47.30 – Rotational flow and vorticity.
PACS. 05.70 – Thermodynamics.

Abstract. – We study the phase dynamics of turbulent Taylor vortex flow by applying a forced modulation to the upper boundary of a large-aspect-ratio system of concentric cylinders. The experiment shows that the axial phase variable of the turbulent Taylor vortex flow is a deterministic variable and its dynamics can be described by a simple diffusion model. The resultant diffusion coefficient of the turbulent Taylor vortex flow is about an order of magnitude larger than that of laminar/regular Taylor vortex flow. We argue that the approach of phase dynamics can also be applied to turbulent flows as long as there is, on sufficiently long-time scales, a coherent structure discernable in the system.

The concept of phase dynamics, the analogue of hydrodynamics for large-aspect-ratio pattern forming nonequilibrium systems, which is concerned with the long-wavelength, low-frequency modulations of patterns, has turned out to be the most suitable macroscopic approach for spatially periodic patterns *far above onset* of an instability over the last few years [1]. Phase dynamics has been studied in particular for one-dimensional [2-9] as well as for two-dimensional nonequilibrium systems [4, 10]. In both cases, phase dynamics gives rise to simple model equations, making it possible to compare theoretical and experimental results directly. In this paper, we present an experimental study of phase dynamics in a turbulent flow, where nevertheless long-range spatial coherence exists. A diffusion model is proposed to explain the experimental results obtained. In addition we discuss for which other flows showing locally turbulent, irregular or rapidly oscillating behavior the concept of phase dynamics could be used.

The Taylor-Couette system investigated experimentally consists of two rotating concentric cylinders with fluid confined in between. The control parameter of the system is the Reynolds number $R \equiv \Omega r_i d/\nu$, where Ω is the rotation rate of the inner cylinder (for fixed outer cylinder), r_i is the radius of the inner cylinder, d is the gap between the cylinders, and ν is the kinematic viscosity of the fluid. The fluid displays various spatially periodic structures as R increases. The succession of flow pattern instabilities with increasing R is: uniform circular Couette flow, axially periodic Taylor vortex flow (TVF), wavy vortex flow, modulated wavy vortex flow, weakly turbulent flow, and turbulent Taylor vortex flow (TTVF) [11].

The phase dynamics for the Taylor-Couette system describes the slow temporal and spatial changes of the wavelength in the axial and the azimuthal direction. The phase dynamics of a one-phase variable case, the Taylor vortex flow, has been studied extensively

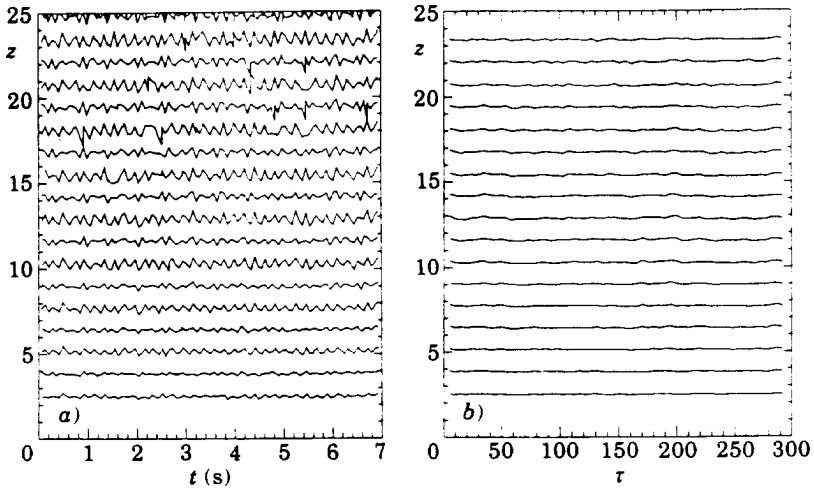

Fig. 1. – Space-time diagram of a turbulent Taylor vortex flow with $\varepsilon = 19.7$, $N_p = 27$, *a*) before and *b*) after averaging. We note the different scale on the abscissa in *a*) and *b*). The total time interval plotted in *b*) is about 500 times (*i.e.* nearly three orders of magnitude) as long as that plotted in *a*).

and found to be well described by a simple diffusion equation [2, 4-9]. A more recent experimental study of phase dynamics for a two-phase variable case, the wavy vortex flow [10], shows that it is described by coupled diffusion equations, as proposed by Brand and Cross [4]. In this manuscript, we present experimental work on phase dynamics in turbulent vortex flow and suggest a model to describe the results. A sinusoidal forcing is added to the top collar of the Taylor-Couette system. The perturbations to the wavelength of the first vortex diffuse along the cylindrical axis and the resultant diffusion coefficient is found to be more than an order of magnitude larger than that of regular Taylor vortex flow.

Our experiment is conducted for two concentric cylinders with the outer one fixed. The radius of the inner cylinder is $r_i = 5.262$ cm and that of the outer cylinder $r_o = 5.965$ cm. The inner-cylinder rotation frequency is controlled by a Compumotor stepper motor (model M83-93) which is precise to 0.001 Hz. The motor is interfaced through a Compumotor indexer to a PDP-11/73 computer. The working fluid region is bounded at both ends by Teflon rings. The lower-end ring is a tight fit with the outer cylinder and leaves a gap of 0.8 mm to the inner cylinder. The upper ring is controlled by a traversing mechanism [12] and it can oscillate along the axial direction over a maximum distance of 1 cm. The upper teflon ring has a gap of ~ 0.8 mm to both inner and outer cylinders. In this way, the fluid can move past the ring when the ring oscillates. The distance between the two teflon rings initially (before the modulation is added) is 49.5 cm, and therefore the average aspect ratio $\Gamma = L/(r_o - r_i) = 70.4$. The working fluid is a solution of doubly distilled water and 44% glycerol by weight, which has a $\nu = 4.0$ cs. 1% by volume of Kalliroscope AQ1000 is added for visualization. All the numbers in this paper are dimensionless unless indicated otherwise. Lengths are scaled by the gap $d(= r_o - r_i = 0.703$ cm), and the time is scaled by d^2/ν, which is 12.3 s in our system.

The TTVF is obtained by increasing the inner-cylinder rotation rate to $\varepsilon = (R - R_c)/R_c \sim 20$ for a state with number of vortex pairs $N_p = 27$. It consists of highly turbulent flow on a small scale, while the wavy vortex boundaries persist. Walden and Donnelly studied the time series of the vortex boundary in a similar state and found that its Fourier spectrum had a peak frequency (~ 1% larger than the cylinder rotation frequency Ω) embedded in a noise band [13]. Thus, the position of a vortex boundary $z_n(\tau)$, where τ is just time scaled by d^2/ν,

is a stochastic variable and the number of phase variables involved might be unclear at first sight. However, if we study the flow pattern further, we find that the axial phase variable (related to the *average* vortex boundary positions) is a deterministic variable. The space-time diagram of turbulent vortex boundaries is shown in fig. 1*a*). The vortex boundaries fluctuate on a time scale of 0.1 s. If we average the vortex boundary positions over longer times, *e.g.*, of length of ~ 7 s (to average out the azimuthal wavy fluctuations), and record the average vortex boundary positions $\bar{z}_n(\tau)$ every 60 s, $\bar{z}_n(\tau)$ remains constant for at least three hours (see fig. 1*b*)). This shows that the average vortex position is a deterministic variable even though the flow inside each vortex is turbulent. Under these specific experimental conditions we find that long-range spatial correlations exist in an ε range of $19 \div 22$ for an $N_p = 26$ state. The ε range increases with the vortex size. It should, however, be possible to detect coherent vortices over a much larger range of ε [14].

Comparing fig. 1*a*) and *b*), we see that averaging over a time scale that is much shorter than all time scales of interest for the small-frequency behavior relevant for phase dynamics, a temporally averaged coherent pattern emerges. From inspection of fig. 1*b*) we also see that this temporally averaged pattern shows a spatially well-defined coherent vortex flow with long-range spatial correlations. We note that the vortex wavelengths of the averaged pattern as well as the characteristic length scales for the spatial variations during modulations are much larger than the turbulent spatial fine structure observed within the turbulent Taylor vortices, thus satisfying the requirement of a clear-cut separation of length scales necessary for the phase dynamics approach. These requirements are described more fully following the discussion of our results.

The experimental procedure is as follows. The cylinder rotation rate is carefully tuned until a steady TTVF is formed. The upper collar, controlled by a stepper motor, oscillates sinusoidally along the cylindrical axis. The amplitude of oscillation is about 0.5. Twenty minutes after the boundary modulation is added, the camera begins to take data. A light intensity profile of the flow pattern along a vertical line is grabbed and digitized by an image processor, and the vortex boundaries are located by finding the minima of the intensity profile. The vortex boundary positions change on two time scales, the fast time scale (~ 0.1 s) related to the azimuthal wavy fluctuations, and the slow time scale T related to the top

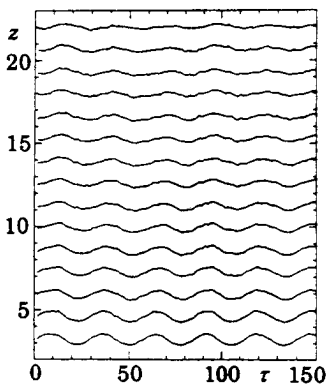

Fig. 2.

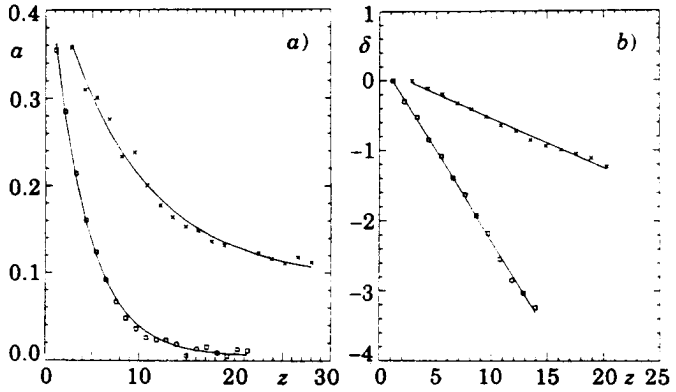

Fig. 3.

Fig. 2. – Responses of the axial phase variable $\bar{z}_n(\tau)$ to a modulation of period $T = 27.6$. The turbulent wavy vortex flow is at $\varepsilon = 19.7$, $N_p = 26$.

Fig. 3. – *a*) Amplitude a and *b*) phase shift δ of $\bar{z}_n(\tau)$ *vs.* axial position for a modulation period of $T = 27.6$. □ Taylor vortex flow, $\varepsilon = 0.075$, $N_p = 33$; × turbulent Taylor vortex flow, $\varepsilon = 19.7$, $Np = 26$. The solid lines are exponential (*a*)) and linear (*b*)) fits to the data.

boundary modulation (the period of modulation $T = 27.6$ in the experiment). As described above, the average vortex boundary position $\bar{z}(\tau)$ is obtained by averaging out the fast azimuthal wavy fluctuations. $\bar{z}_n(\tau)$ is usually recorded once every 20 s for approximately half an hour, yielding 90 data segments, about 15 for each modulation period.

A typical time series of $\bar{z}_n(\tau)$ is shown in fig. 2. The amplitude of $\bar{z}_n(\tau)$ drops off exponentially (see fig. 3*a*)) and the phase shift of the neighboring $\bar{z}_n(\tau)$ has a linear dependence on the axial position (see fig. 3*b*)). This phenomenon is similar to the case of Taylor vortex flow [8], in which the phase dynamics is described by a diffusion model.

Assume ψ, directly proportional to $\bar{z}_n(\tau)$, is the averaged axial phase variable, then the simplest diffusion model gives

$$\frac{\partial \psi}{\partial \tau} = D_{\parallel} \frac{\partial^2 \psi}{\partial z^2}, \tag{1}$$

where $D_{\parallel}$ is the diffusion coefficient, and z is along the system axis. The oscillation of the upper collar provides the boundary condition as

$$\psi|_{z=0} = \psi_0 \sin(\omega\tau), \tag{2}$$

where ψ_0 and ω are the modulation amplitude and frequency. In the experiment we have used $T = 27.6$, that is $\omega \approx 2\pi/T \approx 0.228$. Solving eq. (1) with the above boundary condition, we obtain

$$\psi(z, \tau) = \psi_0 \exp[-\alpha z] \sin(\omega\tau - \beta z), \tag{3}$$

$$\alpha = \beta = \sqrt{\frac{\omega}{2D_{\parallel}}}. \tag{4}$$

This indicates that the amplitude of $\bar{z}_n(\tau)$ drops off exponentially and the phase shift between neighboring $\bar{z}_n(\tau)$ is linearly related to the axial position z, which is in agreement with fig. 3*a*) and *b*). From the slope of the line in fig. 3*b*), the diffusion coefficient can be evaluated by eq. (4), which is about 25 in this case. The diffusion coefficients show no significant dependence on the modulation frequency for sufficiently small modulation frequencies.

The amplitude and phase shift of $\bar{z}_n(\tau)$ of TTVF are plotted in comparison with the same quantities for TVF (fig. 3*a*), 3*b*)). In fig. 3*a*), the amplitude drops off more rapidly for the TVF than that of the TTVF. In fig. 3*b*) the phase shift of TVF has a steeper slope than that of TTVF. By applying the analysis described by eqs. (1)-(4) to the TVF data (see also [8]) we find that the diffusion coefficient for a TTVF is larger than TVF; the ratio is ~ 14 for our choice of parameters. The ratio would vary, of course, depending upon the values of ε and axial wavelength. We note, however, that the variation of D as a function of ε for our set of parameter values and the accessible ε range of $19 < \varepsilon < 22$ for TTVF is negligible and within the experimental error for D ($\pm$ 20%). The variation of D for TTVF has not been determined either experimentally or theoretically before (see ref. [5-9] for discussions of the variation of D for TVF). Therefore, our comparison is intended simply to represent the significant enhancement of D caused by the turbulent flow. The large phase diffusion coefficient of the TTVF can be attributed to the efficient momentum transport of the turbulent fluctuations of the TTVF [15]. A similar turbulence-enhanced phenomenon for kinetic coefficients has been observed for mass transport in turbulent Taylor-Couette flow at even higher Reynolds numbers [16]. The more efficient momentum transport appears to lead in both cases to a faster exchange of information about the concentration of a passive scalar (mass transport) and about the temporally averaged wavelength of the pattern (phase diffusion) and thus to larger effective transport coefficients in both cases.

The results just described bring us naturally to the question of how generally the model of a one-dimensional phase diffusion equation is applicable to flows showing locally already turbulent behavior. Or to phrase the question even more generally: what has phase dynamics

to say about flow patterns that are locally turbulent, but which still have regular features in an averaged sense? And what are the necessary conditions concerning the time and length scales involved? As a first step we go back to systems close to thermodynamic equilibrium and recall the analysis leading to the derivation of hydrodynamic equations in such a system (see ref. [17]). For example, consider nematic liquid crystals. In those the positions of the constituents still show short-range order, whereas the molecules align on average spontaneously parallel to a certain direction characterized by a unit vector, the so-called director [18], and thus show broken orientational symmetry. The director is already a quantity which is averaged over many molecules in space and over many collision times temporally. That is, close to equilibrium the hydrodynamic equations one is writing down are already averaged over the shorter time and length scales.

What we suggest here is to use the same approach for the TTVF state and similar states. That is, we consider equations for the average location of, *e.g.*, the vortex boundary between neighboring vortices, assuming that the fluctuations in this location are fast compared to the time scales one is interested in. The phase entering eq. (1) is thus already a smoothed-out version of the actual phase. The same applies to the time τ entering the time derivative and the coordinate z entering the spatial derivative. It is very important to keep in mind, however, under which conditions such a phase equation for a locally already turbulent pattern could make sense. Necessary ingredients for this to be the case include a clear-cut separation of length and time scales. That means, for example, well-defined vortices for the averaged pattern, which has been averaged over fairly short times. Also all time scales one is interested in must be long compared to the time scale over which one is averaging. Similarly, the length scales one can investigate must be large compared, *e.g.*, to the vortex wavelength, as is already the usual case for phase dynamics. In addition the amplitude of the coherent pattern of interest should not vary strongly and/or abruptly, in particular zeros in the modulus of the amplitude would invariably lead to an immediate breakdown of the very concept of phase dynamics. The systems for which the averaging discussed here could make sense include, aside from the TTVF studied in this manuscript, turbulent spirals as they have been investigated by various groups [19-21]. In this case the occurrence of a propagating mode as predicted from phase dynamics for laminar spirals [22] can also be expected for the turbulent pattern. Furthermore, one must keep in mind the possibility of mean-flow effects, when one is applying phase dynamics to locally turbulent patterns, but this feature is similar to that already present for periodic flows. Another candidate for which the type of averaging procedure outlined could be applicable is slot convection in simple fluids. There one observes [23] well above onset that there are localized variations in the wavelength. Sometimes one finds, in addition, localized spatio-temporal oscillations of the interface between neighboring rolls. In case these oscillations, which are rather rapid, could be averaged out similarly to the rapid irregular waves discussed in this manuscript, one might again be able to use a phase equation for the description of this state. In this case this is an even more challenging question as the distribution of wavelengths requires a nonlinear phase equation, which bears a great resemblance to spinodal decomposition, for its description [24].

In conclusion, the phase dynamics of TTVF has been studied experimentally. A sinusoidal perturbation is added to the top collar of the apparatus in the TTVF state and the disturbances are found to diffuse along the axis of the system. A diffusion model is proposed for the phase dynamics in TTVF. The measured diffusion coefficient of TTVF is found to be ~ 14 times larger than that of regular TVF for our particular choice of parameters. Finally we have critically discussed to what extent patterns showing locally turbulent, irregular or rapidly oscillating behavior could be amenable to a phase dynamics treatment in an average sense with respect to the variables.

It will be most interesting to measure the variation of the phase diffusion coefficient D as a function of ϵ in the TTVF regime for a set of parameter values which allow for a large range of existence (in ϵ) of turbulent Taylor vortices and to see *a*) whether there is a simple scaling law, $D = \epsilon^{\gamma}$, and *b*) to find out whether the phase diffusion coefficient shows any singular behavior as the transition to featureless turbulence is approached. Another important issue for future research is the question of how the diffusion coefficient varies as a function of ϵ for a scalar (such as the concentration investigated in ref. [16]) *vs.* that of a vectorial quantity (such as linear momentum or wave vector as investigated here).

* * *

We thank G. D. BAO, F. HAYOT and M. DUBOIS for many useful discussions. CDA thanks the Office of Naval Research for supporting the experimental work described here. HRB thanks the Deutsche Forschungsgemeinschaft for supporting his work.

REFERENCES

[1] BRAND H. R., in *Propagation in Systems for from Equilibrium*, edited by J. E. WESFREID *et al.* (Springer, New York, N.Y.) 1988, p. 206; in *Patterns, Defects and Instabilities*, edited by D. WALGRAEF and N. M. GHONIEM (Kluwer, Amsterdam) 1990, p. 25.
[2] POMEAU Y. and MANNEVILLE P., *J. Phys. (Paris) Lett.*, 40 (1979) L-609.
[3] WESFREID J. E. and CROQUETTE V., *Phys. Rev. Lett.*, 45 (1980) 634.
[4] BRAND H. and CROSS M. C., *Phys. Rev. A*, 27 (1983) 1237.
[5] TABELING P., *J. Phys. (Paris) Lett.*, 44 (1983) L-665.
[6] AHLERS G., CANNELL D. S. and DOMINGUEZ-LERMA M. A., *Physica D*, 23 (1986) 202.
[7] GERDTS U., Ph.D. Thesis, Universität Kiel (1985).
[8] WU M. and ANDERECK C. D., *Phys. Rev. Rapid Commun. A*, 43 (1991) 2074.
[9] PAAP H.-G. and RIECKE H., *Phys. Fluids A*, 3 (1991) 1519.
[10] WU M. and ANDERECK C. D., *Phys. Rev. Lett.*, 67 (1991) 1258.
[11] SWINNEY H. L. and DI PRIMA R., *Instabilities and Transitions in Flow Between Concentric Rotating Cylinders*, in *Hydrodynamic Instabilities and the Transition to Turbulence*, 2nd edition, edited by SWINNEY H. L. and GOLLUB J. P. (Springer, Berlin-Heidelberg-New York) 1985, p. 139.
[12] WU M. and ANDERECK C. D., preprint (1991); WU M., Ph.D. Thesis, The Ohio State University (1991), unpublished.
[13] WALDEN R. W. and DONNELLY R. J., *Phys. Rev. Lett.*, 42 (1979) 301.
[14] SMITH G. P. and TOWNSEND A. A., *J. Fluid Mech.*, 123 (1982) 187.
[15] TENNEKES H. and LUMLEY J. L., *A First Course in Turbulence* (The MIT Press, Cambrdige, Mass. and London, England) 1972.
[16] TAM W. Y. and SWINNEY H. L., *Phys. Rev. A*, 36 (1987) 1374.
[17] FORSTER D., *Hydrodynamic Fluctuations, Broken Symmetry and Correlation Functions* (Benjamin, New York, N.Y.) 1975.
[18] DE GENNES P. G., *The Physics of Liquid Crystals* (Clarendon Press, Oxford) 1974.
[19] COLES D., *J. Fluid Mech.*, 21 (1965) 385.
[20] ANDERECK C. D., LIU S.S. and SWINNEY H. L., *J. Fluid Mech.*, 164 (1986) 155.
[21] HEGSETH J. J., ANDERECK C. D., HAYOT F. and POMEAU Y., *Phys. Rev. Lett.*, 62 (1989) 257.
[22] BRAND H. R., *Phys. Rev. A*, 31 (1985) 3454.
[23] DUBOIS M., BERGÉ P. and PETROV A., in *New Trends in Nonlinear Dynamics and Pattern Forming Phenomena*, edited by P. HUERRE and P. COULLET (Plenum, New York, N.Y.) 1991, p. 227; HEGSETH J. J., VINCE J. M., DUBOIS M. and BERGÉ P., *Europhys. Lett.*, 17 (1992) 413.
[24] BRAND H. R. and DEISSLER R. J., *Phys. Rev. A*, 41 (1990) 5478.

PHASE DYNAMICS IN THE TAYLOR-COUETTE SYSTEM

Mingming Wu and C. David Andereck

Department of Physics
The Ohio State University
Columbus, Ohio 43210

INTRODUCTION

In principle, the flows in the Taylor-Couette system can be understood as solutions of the Navier-Stokes equation [1, 2, 3]. Unfortunately the complexity of the equation often makes it difficult to compare with laboratory results, thus necessitating the use of model equations [4, 5, 6, 7]. A typical example is the successful use of amplitude equations [4] for the states close to the onset of the first supercritical bifurcations. The amplitude equation is derived from the basic equations by the expansion of a small amplitude of the structure. In the amplitude equation, the phase variable and amplitude are two independent variables. For a case where the wavelength has slow time and space variation, the amplitude is slaved to the phase variable and the amplitude equation can be simplified to a phase equation [5, 6, 7]. For a flow pattern that is far above its onset, the amplitude equations are no longer valid, but the equations for the phase variables still are.

In this paper, we give an overall summary of our experimental studies on phase dynamics in the Taylor-Couette system. Section 2 gives the experimental setup and the data acquisition technique. Section 3 contains the experimental results on the phase dynamics of Taylor vortex flow, wavy vortex flow and turbulent wavy vortex flow, along with their theoretical models.

EXPERIMENTAL SETUP

Our experiment is conducted in two concentric cylinders with the outer one fixed. The radius of the inner cylinder is $r_i = 5.262cm$, the outer one $r_o = 5.965cm$. The cylinder rotation rate is controlled by a Compumotor stepper motor(model M83-93) which is precise to 0.001 Hz. A PDP-11/73 is interfaced through the Compumotor indexer to control the stepper motor. The working fluid region is bounded at both ends by Teflon rings. The upper ring touches neither the outer nor the inner cylinder, and is controlled by a traversing mechanism. The ring is able to oscillate along the axial direction over a maximum distance of 1cm under the control of a Compumotor stepper motor. The distance between the Teflon rings initially (before the modulation is added) is 49.5cm, and therefore the average aspect ratio $\Gamma = \frac{L}{r_o - r_i} = 70.4$. The working fluid is a solution of double distilled water and 44% glycerol by weight. 1% by volume of Kalliroscope AQ1000 is added for visualization. The flow pattern is viewed with a 512 × 480 pixel CCD camera which is connected to an image processor. The

Ordered and Turbulent Patterns in Taylor-Couette Flow
Edited by C.D. Andereck and F. Hayot, Plenum Press, New York, 1992

image data file can be saved in a micro-computer and later transferred to a VAX 8650 for further analysis.

EXPERIMENTAL AND THEORETICAL STUDIES OF THE PHASE DYNAMICS IN THE TAYLOR-COUETTE SYSTEM

The controlling parameter of the Taylor Couette system is the Reynolds number ($\propto \Omega$, the inner cylinder rotation frequency). When R exceeds a threshold value R_c, the spatially uniform circular Couette flow (CCF) changes to the axially periodic Taylor vortex flow(TVF). The first time-dependent regime, wavy vortex flow(WVF), in which an azimuthal wave is superimposed on the TVF, occurs for slightly greater R in a large radius ratio system. If R is increased further, the flow will pass the weakly turbulent region and reach the turbulent wavy vortex flow (TWVF). The azimuthal wavy boundary lines persist in the TWVF as in the case of WVF, but each vortex contains well developed turbulent flow [8].

The phase variables of interest are directly related to the positions of the vortex boundaries. For TVF, one phase variable ψ, the axial phase variable, is used to describe the position variations of the vortex boundary. For WVF, the azimuthal phase variable ϕ is introduced to describe the azimuthal wave motion. In the case of TWVF, it is not evident how many phase variables are involved. Our study only concerns the axial phase variable ψ, which relates to the average vortex boundary position in the axial direction.

In order to study the phase dynamics of the flow patterns, a sinusoidal forcing is applied to the upper ring of the system. Responses of the vortex boundaries to the modulation are recorded by the computer. The following gives a detailed experimental and theoretical descriptions of the phase dynamics in the three flow regimes.

Taylor Vortex Flow

Assume z_n^0 and z_n are the n^{th} vortex boundary positions before and after the modulation is added. Then $z_n^0 = \frac{n\pi}{\tilde{q}}$ and $\psi(z_n, t) = (z_n^0 - z_n)\tilde{q}$, where $\tilde{q}$ is the axial wavevector. We adjust the cylinder rotation frequency until a stationary TVF pattern is formed. The flow pattern is set for 30 minutes before the upper ring oscillation begins. The image processor starts to take data 2 hours after the modulation is added. The vertical line profile of the flow pattern is taken every 2 minutes for 5 hours. The vortex boundary position $z_n(z_n^0, t)$ is obtained by locating the minima of the light intensity profile. Fig. 1 is a typical data set. The response of each node line is a sinusoidal function of time. The amplitude (in ln scale) and the phase of the node line motion are linearly related to the axial position (Fig. 2a , Fig. 2b).

The above observations are understood by a simple diffusion model:

$$\frac{\partial \psi}{\partial t} = D_{\|} \frac{\partial^2 \psi}{\partial z^2} \tag{1}$$

where $D_{\|}$ is the diffusion coefficient in the axial direction.

We found that the phase at $z = 0$ exactly follows the top collar's motion due to the fact that the period of the modulation $T \gg d^2/\nu$, the diffusion time through a vortex. (typically, T = 3040sec. and d^2/ν = 12.3sec.) This provides the following boundary condition:

$$\psi|_{z=0} = \psi_0 sin(\omega t) \tag{2}$$

Here ψ_0 and ω are the modulation amplitude and frequency. Solving Eqn. 1 with the above boundary condition, we obtain:

$$z_n = z_n^0 - a \sin(\omega t - \delta)/\tilde{q} \tag{3}$$

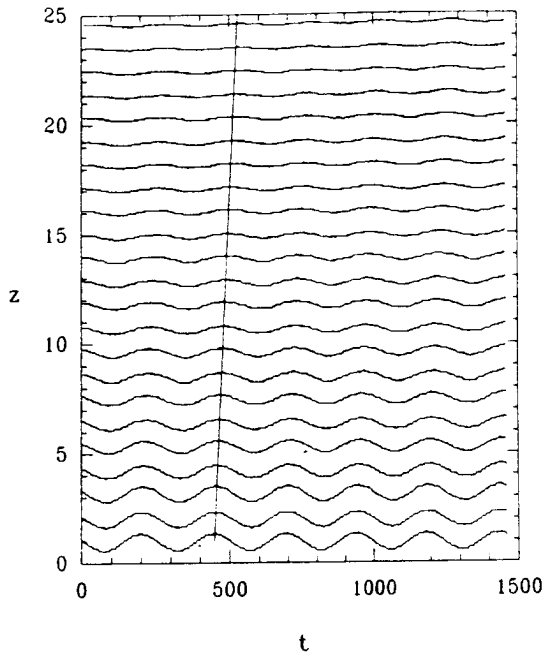

Figure 1. Node line locations of TVF subjected to the periodic boundary modulation, t represents time and z is the distance from the top collar. The solid line traces the shift in phase from vortex to vortex.

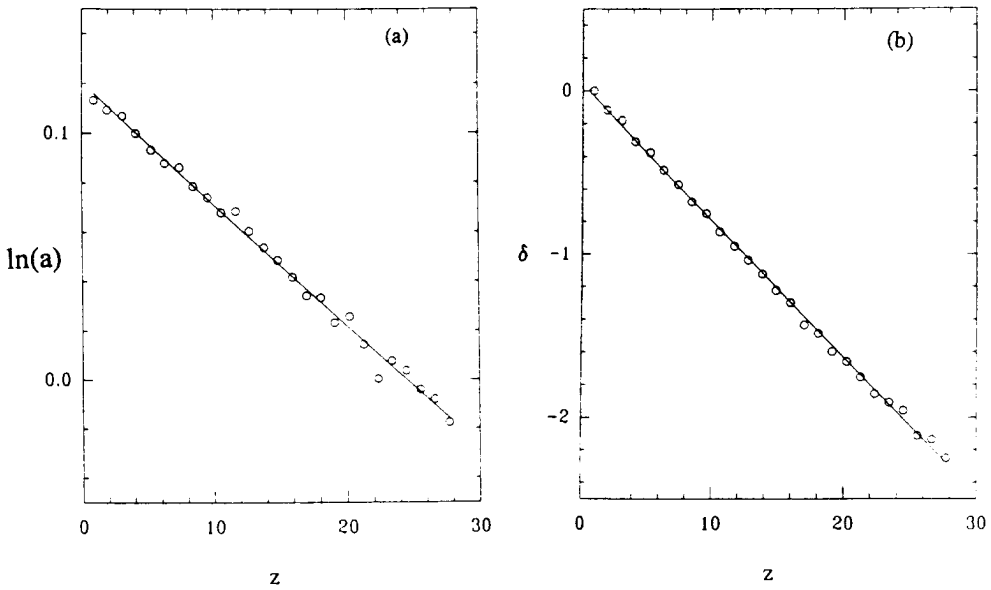

Figure 2. Circles are the experimental data and the solid lines are from the fit to the diffusion model. (a) a is the amplitude of each node line motion. (b) δ is the phase shift of the node line motion.

where $a = (\psi_0/\tilde{q})e^{-\alpha z_n^0}$, $\delta = \beta z_n^0$, a and δ are the amplitude and the phase of the node line motion, and:

$$\alpha = \beta = \sqrt{\frac{\omega}{2D_{||}}} \tag{4}$$

The fact that lna and δ are linearly related to z_n^0 is consistent with our experimental results shown in Fig. 2a and Fig. 2b. The slopes of the lines give us values of α and β and hence the value of $D_{||}$ from Eqn. 4. The variations of α and β from our experiment were within 20%. A more detailed description of the phase dynamics in TVF can be found in Ref. [9].

Wavy Vortex Flow

The phase dynamics of the wavy vortex flow is complicated by the introduction of the second phase variable ϕ, thus leading to richer possibilities. Our experimental study has been limited to the dynamics of ψ. A somewhat different approach will be needed to study the dynamics of ϕ and further work on this matter is important for fully understanding the phase dynamics in WVF.

In contrast with the Taylor vortex flow, the vortex boundary position in the lab frame $z_n(z,t)$ now changes on two time scales, the slow time T_1 (corresponding to the slow boundary perturbation, which has a typical period of several minutes) and the fast time T_2 (corresponding to the azimuthal wave motion of period $\simeq$ 1 sec.). Averaging out the azimuthal wave motion, we have $\psi = \tilde{q}(\bar{z}_n(T_1) - \bar{z}_n^0)$, where $\bar{z}_n^0$ is the average vortex boundary position without modulation. In order to obtain $\bar{z}_n(T_1)$, we take about 100 consecutive line profiles (covering about 10 azimuthal waves) in 7 sec., find the intensity minima along each vertical line, then average out the azimuthal wave motion for each node line. We repeat the above process at a time interval of 20 or 30 sec. depending on the modulation period T. In general, 10 data points are taken in a period T.

$\bar{z}_n(T_1)$ is measured for flow states with different m. A m=3 state is obtained by increasing ϵ slightly above the onset of TVF, $\epsilon = 0.140$. A typical result is shown in Fig. 3a. The amplitude of $\bar{z}_n(T_1)$ decreases exponentially along the system axis, and there is a linear phase shift between oscillations of neighboring vortices. Upon further increasing the rotation frequency, the system reaches a new stable state with $m = 7$ at $\epsilon = 0.813$. In order to obtain $m = 7$ with the same vortex number N, the rotation frequency is changed rapidly from $\epsilon = 0.140$ to $\epsilon = 0.813$. For the same modulation period $T = 53.3$, $\bar{z}_n(T_1)$ reveals an axially propagating wave in the middle section of the cylinders, as shown in Fig. 3b.

The above observations can be explained within the theoretical framework of the coupled phase equations proposed by Brand and Cross [7]. Based on their symmetry analysis, ψ and ϕ are governed by:

$$\begin{aligned} \frac{\partial \psi}{\partial t} &= D_{||}\frac{\partial^2 \psi}{\partial z^2} + C_{||}\frac{\partial \phi}{\partial z} \\ \frac{\partial \phi}{\partial t} &= D_{\perp}\frac{\partial^2 \phi}{\partial z^2} + C_{\perp}\frac{\partial \psi}{\partial z} \end{aligned} \tag{5}$$

where z is along the axial direction, $D_{||}$ and $D_{\perp}$ are the diffusion coefficients for the axial and azimuthal directions, $C_{||}, C_{\perp} \propto q_y$ and represent the coupling between the azimuthal wave motion and the axial vortex position change. These coefficients can be derived from the amplitude equation near the onset of TVF.

For the weak coupling case where $C_1 C_2 \ll |D_1 - D_2|\omega$, the coupled equations can be simplified to a diffusion model. Fig. 3a shows that for a small q_y, the small $C_{||}, C_{\perp}$ case, the phase dynamics is similar to the case of TVF. The diffusion coefficient can be evaluated by Eqn. 4 and it is $\sim$1.4.

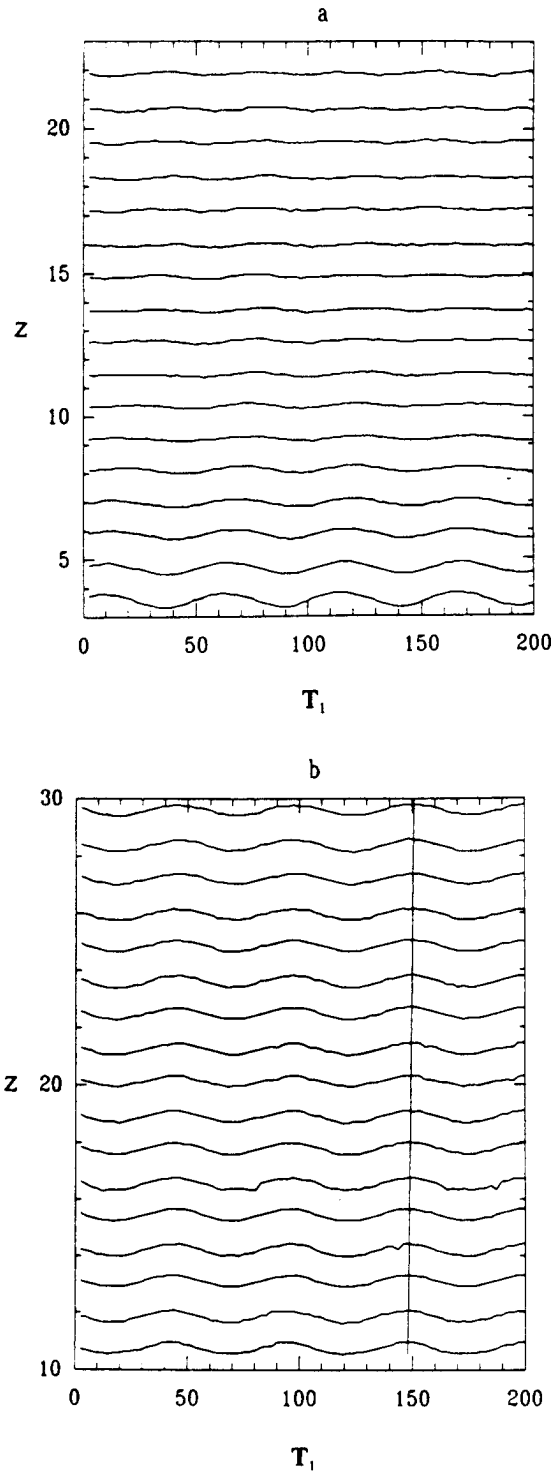

Figure 3. Responses of the axial phase variable $\bar{z}_n(T_1)$ to a modulation of period T = 53.3. Number of vortices N=60. (a) m=3, ϵ = 0.140; (b) m=7, ϵ = 0.813. The straight line traces the shift in phase from vortex to vortex.

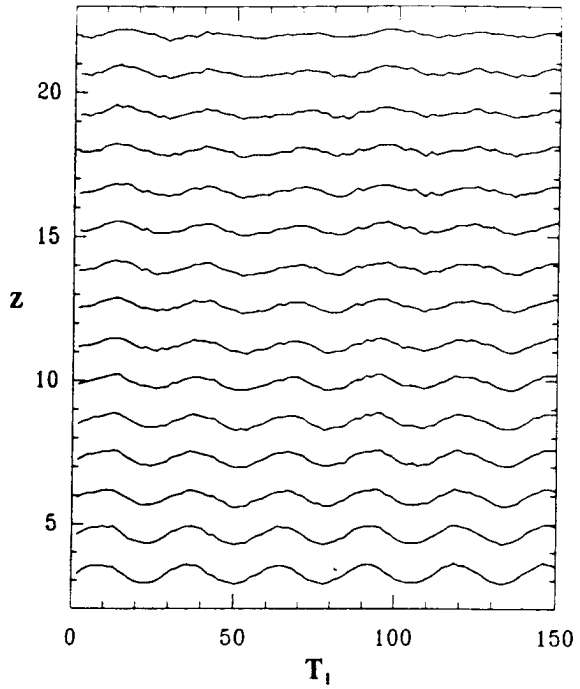

Figure 4. Responses of the axial phase variable $\bar{z}_n(T_1)$ to a modulation of period T = 27.6. The flow state has ϵ = 19.7, N=52.

For the strong coupling case where $C_{||}C_{\perp} \gg 2\omega(D_{||} + D_{\perp})$, Eqn. 5 is decoupled into a simple traveling wave equation:

$$\frac{\partial^2\psi}{\partial t^2} - c^2\frac{\partial^2\psi}{\partial z^2} = 0 \tag{6}$$

where $c = \sqrt{C_{||}C_{\perp}}$. This is confirmed by our observation in the large q_y (m=7) flow pattern and its traveling wave behavior is shown in Fig. 3b. For more details on the phase dynamics of WVF, see Ref. [10].

Turbulent Wavy Vortex Flow

The average vortex boundary position $\bar{z}_n$ of TWVF is measured with the same data acquisition technique as in the wavy vortex flow. A typical time series of $\bar{z}_n(T_1)$ is shown in Fig. 4. The amplitude drops off exponentially and the phase shift of neighboring vortex boundaries has a linear dependence on the axial position. This indicates that the phase dynamics in TWVF can be described by a simple diffusion model. A diffusion coefficient is evaluated by Eqn. 4 from the slope of the line (phase vs. axis). It is about 18 in this case and about 10 times larger than that of TVF.

CONCLUSION

We have studied the phase dynamics both experimentally and theoretically in the TVF, WVF and TWVF. The phase dynamics in TVF and TWVF can be described by a simple diffusion model, while that of WVF is governed by a coupled diffusion model.

We thank H. Brand for persistent encouragement during this project and Z. H. Wang, F. Hayot and I. Mutabazi for helpful discussions. This work was supported by the Office of Naval Research, under contract N00014-86-K-0071 and grant N00014-89-J-1352.

References

[1] P. S. Marcus, J. Fluid Mech. 146, 45(1984)

[2] P. S. Marcus, J. Fluid Mech. 146, 65(1984)

[3] M. Nagata, J. Fluid Mech., **169**, 229(1986), and **188**, 585(1988)

[4] A. C. Newell, J. A. Whitehead, J. Fluid Mech., 38, 279(1969) For application to the Taylor-Couette system see R. Graham and J. A. Domaradzki, Phys. Rev. A 26, 1572(1982) and references therein

[5] Y. Pomeau and P. Manneville, J. Phys. Lett. 40, L609 (1979)

[6] P. Tabeling, J. Phys. Lett. 44, L665 (1983)

[7] H. Brand and M. C. Cross, Phys. Rev. **A**, 27, 1237(1983)

[8] R. W. Walden, R. J. Donnelly, Phys. Rev. Lett. 42, 301(1979)

[9] M. Wu, C. D. Andereck, Phys. Rev. **A**, Rapid Comm., 43, 2074(1991)

[10] M. Wu, C. D. Andereck, Phys. Rev. Lett. (1991), in press

Phase dynamics in the Taylor–Couette system

Mingming Wu and C. David Andereck
Department of Physics, The Ohio State University, Columbus, Ohio 43210

(Received 23 December 1991; accepted 26 May 1992)

The phase dynamics of flows in the Taylor–Couette system have been studied by applying a forced modulation to the upper boundary of a large aspect ratio concentric cylinder system. In a one phase variable case, the Taylor vortex flow, the perturbations diffuse along the axial direction and the pattern's response is well described by a simple diffusion model. In a two phase variable case, the wavy vortex flow, the perturbations either propagate as traveling waves or diffuse, depending on the coupling between the axial and azimuthal phase variables. In the turbulent Taylor vortex flow, where spatial coherence coexists with the turbulent flow, the phase dynamics of the coherent structure are described by a diffusion model with a diffusion coefficient an order of magnitude larger than for the laminar Taylor vortex flow.

I. INTRODUCTION

Considerable attention has been given to spatially periodic patterns formed in nonequilibrium fluid-dynamical systems such as Taylor–Couette flow,[1] Rayleigh–Bénard convection,[2] viscous fingering,[3] and mixing layers of two immiscible fluids.[4] In general, each system is controlled by an external stress R. When R exceeds a threshold value R_c, the system undergoes a transition from a spatially uniform state to a periodic state, thereby breaking the translational invariance of the system. A typical example is the Taylor–Couette system, in which the fluid is confined between two concentric rotating cylinders (see Fig. 1). The control parameter is the Reynolds number R ($\propto \Omega$, the inner cylinder rotation frequency). When R is small, the flow in an infinitely long system has only an azimuthal velocity component, and it is called simply circular Couette flow (CCF). When R exceeds R_c, a centrifugal instability gives rise to Taylor vortex flow (TVF) out of the base CCF. In TVF, the velocity field consists of a sequence of pairs of counter-rotating vortices stacked along the cylinders [see Fig. 2(a)]. The velocity field varies with distance from the system axis, periodically along the system axis, and is constant in the azimuthal direction. The first time-dependent regime, wavy vortex flow (WVF), in which an azimuthal traveling wave is superimposed on the TVF, occurs for slightly greater R in a large radius ratio system [see Fig. 2(b)]. Upon further increasing R, the flow first becomes quasiperiodic, then weakly turbulent or chaotic, and eventually reaches a turbulent Taylor vortex flow (TTVF) in which the vortex boundaries are embedded in a turbulent background [see Fig. 2(c)]. The vortex sizes are typically somewhat greater than those in TVF. The vortex boundaries become difficult to discern when R/R_c is increased to ~ 700,[5] which is well above the range of R considered here.

In principle, all the above phenomena may be understood using the Navier–Stokes equation.[6–10] However, the complexity of the equation has thus far made it impractical to generate full numerical solutions for comparison with the potentially huge number of laboratory situations. Furthermore, it is not always easy to extract the physical insights needed for a deep understanding of the flow patterns from such numerical solutions. Therefore, model equations are of considerable importance. For example, amplitude equations[11–14] can describe the dynamics of the states close to the onset of the first supercritical bifurcation. Amplitude equations are derived from the Navier–Stokes equation (or other basic equations) by the expansion of a small amplitude of the emerging structure. Many interesting features of laboratory generated Taylor–Couette flows are contained in this class of model equations.[15,16]

In an amplitude equation approach, the phase and amplitude are independent variables. For a case where the wavelength has slow time and space variations, the amplitude is slaved to the phase variable and the amplitude equation can be simplified to a phase equation. For flow patterns further above the onset of Taylor vortex flow the amplitude equation is no longer useful, but the equations for phase variables are presumed still valid.

Pomeau and Manneville[17] and Kuramoto[18] introduced the method of phase dynamics for treating nonequilibrium systems. A simple phase diffusion equation was derived from the Swift–Hohenberg equation. This phase equation can be applied to a nonequilibrium system that undergoes a supercritical bifurcation and forms a spatially periodic pattern. Pomeau and Manneville applied their theory to the weakly nonlinear regime (near the onset of the convection state) of the Rayleigh–Bénard (RB) system. A phase diffusion equation was derived for the RB system and the diffusion coefficient was found to depend on the wave vector of the convective rolls and the distance above the threshold of convection. Following this, Wesfreid and Croquette[19] and Croquette and Schosseler[20] studied experimentally the phase dynamics near the onset of the convection state in the RB system. A modulation, forced by periodic injection of fluid, was imposed on the RB system and the responses of the convective rolls were studied. Their results partially confirmed the validity of the phase diffusion model in the RB system. Tabeling[21] applied the Pomeau–Manneville formalism to the Taylor–Couette sys-

 0899-8213/92/112432-14$04.00

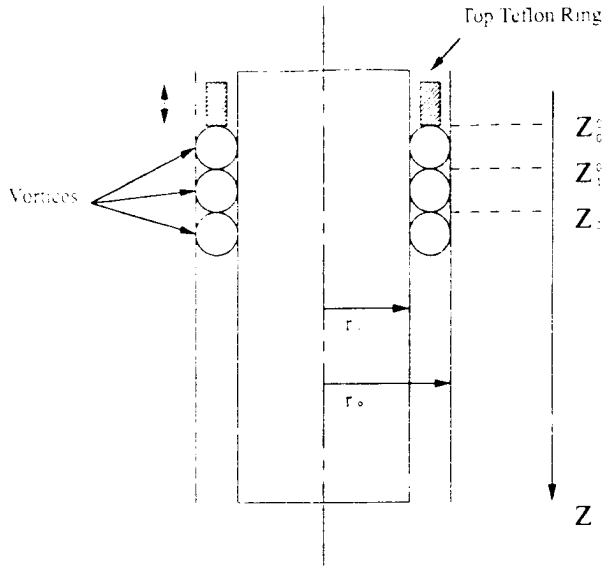

FIG. 1. Schematic diagram of the Taylor–Couette system, $r_i = 5.262$ cm, $r_o = 5.965$ cm, and aspect ratio $\Gamma = 70$.

tem and obtained a similar phase diffusion equation near the onset of TVF. He showed that the diffusion coefficient depends on the Taylor vortex wave vector and the distance above threshold (which was true also for the RB system). In addition, Tabeling suggested that Snyder's experimental results from a small aspect ratio Taylor–Couette system showed evidence of phase diffusive behavior.[21,22] In Snyder's experiment, the flow state was perturbed in a spatially uniform manner (a sudden increase of the inner cylinder frequency) and the adjustments of the cell boundaries were observed. It was found that the cell sizes exponentially relaxed to their final values, which was consistent with

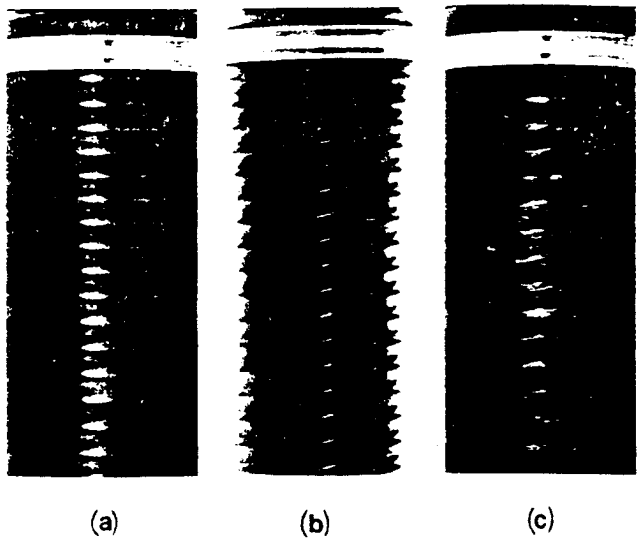

FIG. 2. Representative flow regimes: (a) TVF at $\epsilon = 0.140$ and $Np = 30$, where N_p is the number of vortex pairs, (b) WVF at $\epsilon = 0.813$, $Np = 30$, and $m = 7$, where m is the number of waves in the azimuthal direction, and (c) TTVF at $\epsilon = 19.7$ and $Np = 28$.

Tabeling's calculation. However, the relaxation time, which is inversely proportional to the diffusion coefficient, did not seem to depend on the distance from TVF onset or the average wave vectors of the vortices, although this was not a primary point of his investigation. Following Tabeling's work, numerical simulations of the phase dynamics near the onset of the TVF have been performed.[23] In the simulations, one end boundary of the system was moved to its final position with various speed profiles and the responses of the vortices were studied. Phase diffusive behavior was found in the region far from the boundary. An experimental study of the phase dynamics in TVF was carried out by Gerdts,[24,25] in a small aspect ratio ($\Gamma \sim 20$) system. As in the simulations, the first vortex was compressed by moving the upper collar of the Taylor–Couette system and the responses of the vortices in the bulk were studied. The results showed diffusive behavior and the measured diffusion coefficients were found to depend on the wave vector.

While a significant amount of work has been done on phase dynamics for the one phase variable case,[17–26] much less attention has been paid to the two phase variable situation.[27–31] Based on a symmetry analysis, and using a slow time and space variation approximation, Brand and Cross proposed that the proper description for wavy vortex flow involved *coupled* diffusion equations.[27–29] They predicted a propagating phase mode in the strong coupling limit and a diffusive mode in the weak coupling regime. The diffusion coefficients and coupling coefficients can be evaluated only for states close to the onset of TVF, although the equations themselves are valid for states far above TVF onset.

Phase dynamics has usually been thought of as only applicable to well-ordered spatial patterns. However, there are circumstances throughout fluid dynamics in which relatively coherent structures exist, embedded in a background of turbulence. It is reasonable to ask whether phase dynamics might be relevant for describing the behavior of those coherent structures, ignoring the small-scale fluctuations. It is in this spirit that we have studied phase dynamics for turbulent Taylor vortices. Specifically, we have asked whether phase equations can be used to describe the slow temporal and spatial changes of the coherent structures in TTVF (where the coherent structures are the Taylor vortices themselves)? Theoretical and experimental work on this problem has been lacking until now.

An overall experimental study of phase dynamics in the Taylor–Couette system is presented in this paper. Brief reports of some of these experimental results have appeared.[26,30–32] Section II provides the theoretical background. Section III describes the experimental setup and the data acquisition techniques, as well as the experimental results on phase dynamics in TVF, wavy vortex flow, and turbulent Taylor vortex flow. Section IV summarizes our work.

II. THEORETICAL BACKGROUND

The control parameter for the Taylor–Couette system with the outer cylinder at rest is the Reynolds number R,

defined as $R=\Omega_i r_i d/\nu$, where Ω_i is the inner cylinder rotation rate, r_i is the inner cylinder radius, d is the gap between the inner and outer cylinders, and ν is the kinematic viscosity. When R exceeds the threshold R_c (neglecting Ekman effects near the ends of a finite system), the flow changes from a uniform circular Couette flow (CCF) to a spatially periodic Taylor vortex flow (TVF). In the vicinity of T_c, the velocity field can be described as

$$\begin{aligned}&\mathbf{V}_{\mathrm{TVF}}(\mathbf{r},t)=\mathbf{V}_{\mathrm{CC}}(\mathbf{r},t)+\mathbf{v}(\mathbf{r},t),\\&\mathbf{v}(\mathbf{r},t)=A(z,t)\mathbf{v}(r)e^{iq_c z}+A^*(z,t)\mathbf{v}^*(r)e^{-iq_c z},\end{aligned}\tag{1}$$

where $\mathbf{V}_{\mathrm{CC}}(\mathbf{r},t)$ and $\mathbf{V}_{\mathrm{TVF}}(\mathbf{r},t)$ are the velocity fields for CCF and TVF, $\mathbf{v}(\mathbf{r},t)$ is the perturbation velocity field, $\mathbf{v}(r)$ is the eigenfunction of the velocity field, q_c is the critical wave vector corresponding to the lowest T_c, and $A(z,t)$ is the complex amplitude which retains only the slow time and space variations. The amplitude equation can be derived by the general procedure of Newell and Whitehead,[12] it is

$$\tau_0\frac{\partial A}{\partial t}=\epsilon A+\xi_0^2\frac{\partial^2 A}{\partial z^2}-g|A|^2A,\tag{2}$$

where τ_0 is the perturbation amplitude growth rate, ξ_0 is the correlation length, z is the coordinate in the axial direction, g is a factor relating to the scale of A, and $\epsilon=(R-R_c)/R_c$ is the distance to the onset of TVF.

Because of the periodicity of the TVF in the axial direction, $A(z,t)$ can be written in the form[16]

$$A(z,t)=A_0e^{iqz}e^{i\sigma t},\tag{3}$$

where $q=\tilde{q}-q_c$, $\tilde{q}$ is the wave vector of the TVF, and σ is the growth rate of the perturbation. A steady state for $\epsilon>\xi_0^2q^2$ is obtained by substituting Eq. (3) into Eq. (2), with the result being

$$A_0=\sqrt{(\epsilon-\xi_0^2q^2)/g}.\tag{4}$$

However, this solution is not stable over the whole range of q. The stability of A_0 may be determined by assuming $A(z,t)=\overline{A(z,t)}e^{i\Psi}$ where

$$\overline{A(z,t)}=A_0+a(z,t),\quad \Psi=qz+\psi(z,t);\tag{5}$$

$a(z,t)$ and $\psi(z,t)$ are small perturbations of the steady solution A_0e^{iqz}. A standard linear stability analysis of Eq. (2) with the above assumptions gives

$$\frac{\partial\psi}{\partial t}=D_{\parallel}\frac{\partial^2\psi}{\partial z^2},\tag{6}$$

where

$$D_{\parallel}=\frac{\xi^2}{\tau_0}\frac{(\epsilon-3\xi_0^2q^2)}{(\epsilon-\xi_0^2q^2)}.\tag{7}$$

The steady state A_0 is stable when the diffusion coefficient is positive. Therefore instability occurs in the range $\xi_0^2q^2<\epsilon<3\xi_0^2q^2$. Here $\epsilon<3\xi_0^2q^2$ produces the Eckhaus instability.[16,33–35]

If we increase R further, the rotational symmetry of the TVF is broken and a new pattern emerges, wavy vortex flow (WVF). Therefore, a second phase variable ϕ is introduced to describe the phase of the azimuthal wave motion. A more precise definition of ψ and ϕ can be seen by examining the form of the amplitude of the wavy vortex flow:

$$A=|B|e^{i\psi}+i|C|e^{i\psi}(e^{i(q_y y+\phi)}+\text{c.c.}),\tag{8}$$

where q_y is the azimuthal wave vector, y is the azimuthal position, B and C are constants, and $C\to 0$ at ϵ_w, the onset of WVF. Brand and Cross[27] proposed coupled diffusion equations to describe the phase dynamics in WVF according to a symmetry analysis. The equations for WVF must be invariant under two symmetry operations: (1) $z\to -z$, $\psi\to-\psi$, $\phi\to\phi$; and (2) $y\to -y$, $q_y\to -q_y$, $\psi\to\psi$, $\phi\to-\phi$. Thus they argue that the appropriate phase equations are

$$\begin{aligned}\frac{\partial\psi}{\partial t}&=D_1\frac{\partial^2\psi}{\partial z^2}+C_1\frac{\partial\phi}{\partial z},\\\frac{\partial\phi}{\partial t}&=D_2\frac{\partial^2\phi}{\partial z^2}+C_2\frac{\partial\psi}{\partial z},\end{aligned}\tag{9}$$

where z is along the system axis, D_1 and D_2 are the diffusion coefficients for the axial and azimuthal directions, and C_1, $C_2\propto q_y$ represent the coupling strength between axial and azimuthal motion. The coefficients can be derived following the same procedure as in the case of TVF close to onset.

Assume the phase variable ψ (and also ϕ through the coupling of the equations) is perturbed by a term proportional to $\exp[i(Kz-\omega t)]$, and substitute into Eq. (9). We then eliminate terms in ϕ and find the following relation between K and ω:

$$\begin{aligned}K^2&=\frac{i\omega(D_1+D_2)-C_1C_2+\sqrt{\Delta}}{2D_1D_2},\\\Delta&=C_1^2C_2^2\left(1-\frac{2i\omega(D_1+D_2)}{C_1C_2}-\frac{(D_1-D_2)^2\omega^2}{C_1^2C_2^2}\right).\end{aligned}\tag{10}$$

For the strong coupling case, i.e., $C_1C_2\gg 2\omega(D_1+D_2)$, we have $K=\omega/c$, where $c=\sqrt{C_1C_2}$. Equation (9) in this case has the characteristic form of a wave equation:

$$\frac{\partial^2\psi}{\partial t^2}-c^2\frac{\partial^2\psi}{\partial z^2}=0.\tag{11}$$

For the weak coupling limit, where $C_1C_2\ll|D_1-D_2|\omega$, we have $K^2=-i\omega/D_1$ or $K^2=-i\omega/D_2$, a typical situation for a diffusion process. In Taylor vortex flow, $C_1=C_2=0$, the weak coupling condition is trivially satisfied, and the diffusion model for TVF is recovered.

With sufficient increase in ϵ the flow becomes chaotic or weakly turbulent. As ϵ is increased still further, the flow becomes increasingly turbulent. The vortices remain as large-scale structures (similar in size to the laminar Taylor vortices), periodically stacked along the axis of the system. The vortex boundaries fluctuate quasiregularly with a period of $\sim 1/\Omega_i$. The number of phase variables involved in this case is uncertain. However, we have found that the *average* vortex boundary position is a well-defined, deter-

ministic variable. We argue that a phase equation approach would still be valid for such a coherent structure of vortices embedded in an otherwise locally turbulent flow.

A possible analogy for motivating a phase dynamics approach for TTVF is in the hydrodynamic equations for certain equilibrium systems.[32] For example, consider nematic liquid crystals.[36] In nematics the positions of the constituents show short range order, whereas the molecules align on average spontaneously parallel to a certain direction characterized by a unit vector, the director, and thus show broken orientational symmetry. The director is a quantity which is averaged over many molecules in space and over many collision times. That is, close to equilibrium the hydrodynamic equations are already averaged over the shorter time and length scales. We argue that this approach would be useful for the TTVF and similar flows. That is, we consider equations for the average location of the vortex boundary between neighboring vortices, assuming that the fluctuations of the vortex boundaries are fast compared to the time scales in which we are interested. After the fast fluctuations are averaged out, the coherent structure left is similar to TVF. Therefore, we predict that the slow perturbations to the coherent structure will diffuse along the axis of the system in a manner analogous to the case of TVF.

III. EXPERIMENTAL TECHNIQUE AND RESULTS

A. Experimental setup

Our experiment was conducted in two concentric cylinders with the outer one fixed (see Fig. 1). The inner cylinder was made of black Delrin plastic with radius $r_i=5.262$ cm and the outer cylinder was of Plexiglas with inner radius $r_o=5.965$ cm, which gave a radius ratio $\eta=r_i/r_o=0.882$. (For further details on the basic system, see Ref. 37.) The inner cylinder rotation frequency was controlled by a Compumotor stepper motor (model M83-93) which is precise to 0.001 Hz. A PDP-11/73 was interfaced through the Compumotor indexer to control the stepper motor. The working fluid region was bounded at both ends by Teflon rings. The lower end ring fit snugly against the outer cylinder, with a gap of ~ 0.8 mm to the inner cylinder. The upper ring was attached to a traversing mechanism, described later, which allowed the ring to oscillate along the axial direction over a maximum amplitude of ± 0.5 cm. There were gaps of ~ 0.8 mm between the upper Teflon ring and both the inner and outer cylinders. In this way, the fluid could move past the ring when it oscillated. The distance between the two Teflon rings initially (before the modulation was added) was 49.5 cm, and therefore the average aspect ratio $\Gamma=L/(r_o-r_i)=70.4$. The working fluid was a solution of double distilled water and 44% glycerol by weight, which has a kinematic viscosity $\nu=4.0$ cS. Temperature regulation in the room was within 1 °C, with the fluid temperature itself varying by a few tenths of a degree. One percent by volume of Kalliroscope AQ1000 was added for visualization. The fluid could be used for at least two months before it deteriorated.

The flow pattern was viewed under room illumination

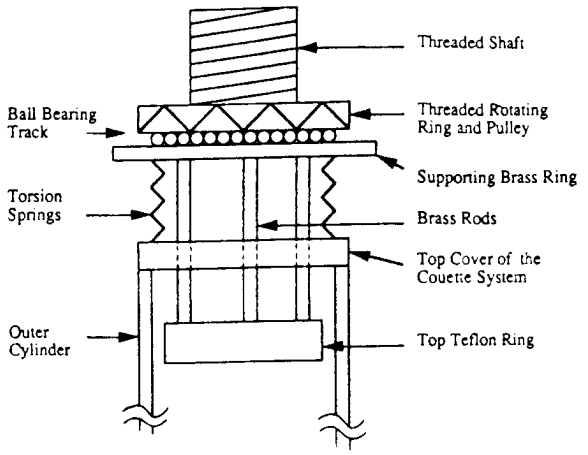

FIG. 3. Schematic diagram of the modulation device that provides the vertical movement of the upper collar of the Taylor–Couette system.

with a 512×480 pixel CCD camera (Javelin Model JE-7242 Newvichip) that was connected to an image processor (Imaging Technology FG-1024). For a typical situation, this camera and processor provided a resolution of 34 pixels per vortex. The image processor board was installed in a PC-AT (Everex System 1800). The board digitized a picture of the flow pattern and the PC recorded the light intensity profile along a vertical line. A C language program was used along with the software package HALO (Imaging Technology) for the frame grabbing and basic processing. The positions of the vortex boundaries were determined by finding the local minima of the light intensity profile. In a normal data taking process, we recorded the intensity profile of a vertical line in the dynamic memory of the PC, found the minima, and saved their locations into a data file. The data files were then transferred by ethernet to a VAX 8650 system for data analysis (curve fitting or plotting).

The oscillation of the upper ring was controlled by a traversing mechanism. A schematic diagram of this device is shown in Fig. 3. It consisted of two basic parts. The lower part was a plate connected to the moving Teflon ring. The connections were made by three $\frac{1}{8}$ in. brass rods running through the top cover of the concentric cylinders system. The plate was supported against gravity by three torsional springs that were mounted on the top cover. The upper rotating ring was connected to the supporting plate by a ball bearing track. The upper ring was threaded on the inside and a pulley was mounted on the outside. A timing belt connected the pulley with a Compumotor M83-93 stepper motor. The translations of the rotating ring produced the vertical displacement, which was transmitted to the upper Teflon collar by the supporting plate and the three brass rods. Four rotations of the stepper motor produced a 1 mm displacement of the upper collar. The stepper motor was controlled by a Compumotor indexer, which was controlled in turn by a PDP-11/73 computer. A safety stop was designed with the joy stick input of the indexer to prevent the motor from overrunning the range, thereby damaging itself and the system.

All the numbers in the following are dimensionless unless otherwise indicated. Lengths are scaled by the gap d ($=r_o-r_i=0.703$ cm), and times are scaled by d^2/ν, which is ~ 12.3 sec in our system.

B. Experimental results

1. Taylor vortex flow

A TVF pattern [Fig. 2(a)] is obtained by increasing the rotation speed slightly above the critical $R_c=112$. Two types of perturbations, induced by motion of the upper ring, were applied to the pattern, either a sinusoidal forcing or a step function forcing. The responses of the vortex boundary positions to the perturbations were then recorded as a function of time.

The axial phase variable ψ is directly proportional to the vortex boundary position variation. Assuming $z_n(z,t)$ is the nth vortex boundary position in the axial direction, and $z_n^0=n\pi/\tilde{q}$ is the vortex boundary position before the upper ring oscillates, then the phase of the amplitude at the nth vortex boundary $=(\Psi+q_c z)|_{z=z_n}=\psi(z_n,t)+\tilde{q}z_n=n\pi$. This gives

$$z_n=z_n^0-\psi(z_n,t)/\tilde{q}, \tag{12}$$

which shows that the axial phase variable is directly proportional to the vortex boundary position variation. In the sinusoidal modulation case, the phase at $z=0$ exactly followed the collar's motion, which follows from the fact that the period of the modulation $T\gg d^2/\nu$, the diffusion time through a vortex, where T is typically several thousand seconds. This resulted in the following boundary condition:

$$\psi|_{z=0}=\psi_0\sin(\omega t). \tag{13}$$

Here $\psi_0/\tilde{q}$ and ω are the modulation amplitude and frequency. Solving Eq. (6) with the above boundary condition, we obtain

$$\psi(z,t)=\psi_0 e^{-\alpha z}\sin(\omega t-\beta z), \tag{14}$$

$$\alpha=\beta=\sqrt{\omega/2D_\parallel}\,. \tag{15}$$

Substituting $\psi(z_n,t)$ into Eq. (12) gives

$$\begin{aligned} z_n&=z_n^0-\psi_0 e^{-\alpha z_n}\sin(\omega t-\beta z_n)/\tilde{q}\\ &\simeq z_n^0-\psi_0 e^{-\alpha z_n^0}\sin(\omega t-\beta z_n^0)/\tilde{q}. \end{aligned} \tag{16}$$

Equation (16) shows that the vortex boundary position is a sinusoidal function of time, the amplitude of the motion decreases exponentially along the axial direction, and the phase shift between neighboring vortices has a linear dependence on the axial position. The diffusion coefficient can be evaluated from the parameters α and β, and α and β should have the same value according to Eq. (15).

In the second experiment, the upper collar is moved to a final position at a constant speed, which leads to the approximate boundary condition:

$$\psi|_{z=0}=\psi_0 H(t), \tag{17}$$

where $H(t)$ is the step function, 0 for $t<0$, 1 for $t\geq 0$. This is an *approximate* boundary condition owing to the finite time (typically 48 sec) for the collar to reach its final position, but analysis of our data shows that this approximation has a negligible effect in the region beyond a few vortex diameters from the boundary. However, by imposing a step function, we are measuring the reaction of the flow pattern to a modulation with a wide frequency band instead of just a single frequency. The fact that phase dynamics should only be valid for slow temporal and spatial changes indicates that the step function experiment may not be as accurate as in the sinusoidal function case. The advantage of the step function is that it takes about 40 min to take one set of data compared with 6 h in the sinusoidal case. This enabled us to collect several data sets (~ 10) for each flow state and thus obtain an average value for $D_\parallel$.

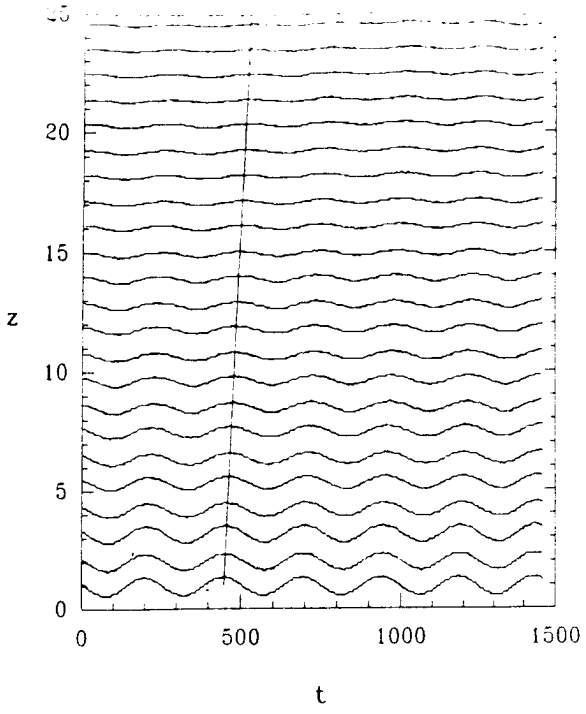

FIG. 4. Vortex boundary locations of TVF subjected to the periodic boundary modulation ($T=247$), t represents time and z is the axial position. $z=0$ is the location of the upper collar. The solid line traces the shift in phase from vortex to vortex.

Substituting Eq. (17) into Eq. (6), we obtain $z_n(z,t)$ as

$$\begin{aligned} z_n(z,t)&=z_n^0-d_0\,\mathrm{erfc}(z_n/2\sqrt{D_\parallel t})\\ &\simeq z_n^0-d_0\,\mathrm{erfc}(z_n^0/2\sqrt{D_\parallel t}), \end{aligned} \tag{18}$$

where d_0 is the distance that the upper collar moves and erfc is the complement of the error function.[38]

In the periodic modulation case, the sinusoidal motion of the upper collar had a typical amplitude of $d_0/d=0.480$ and a period of 3040 sec. Before commencing the oscillation, the TVF was left at least an hour so that the flow reached its steady state (this occurs in our system in about half an hour). Two hours after the oscillation of the upper ring began, light intensity profiles along a vertical line were recorded once every 2 min for a period of 5 h. Figure 4 is a typical data set.

The response of each vortex boundary is necessarily a sinusoidal function of time, with an amplitude and phase shift as predicted by Eq. (16). By fitting the data with the following equation

$$z_n = z_n^0 - a \sin(\omega t - \delta), \tag{19}$$

where a and δ are the amplitude and the phase of the vortex boundary motion, we found that $\ln a$ and δ were linearly related to z_n^0, as shown in Fig. 5. The slopes of the lines yield α and β, from Eq. (15), and in turn $D_\parallel$. The variation of α and β for different runs was less than 20%.

For a TVF, the Ekman pumped end rolls are normally larger than the rolls in the center of the cylinder. It has been suggested that, for finite cylinders, α should always be smaller than β,[39] as found by taking the effect of the Ekman rolls as a perturbation in the derivation of the phase equations from the amplitude equation. This is consistent with our observations, as shown in Fig. 6. A detailed calculation is underway to attempt to verify this assertion. (To compute the diffusion coefficient we have used only the β values, which, coming from the phase shifts, are more precisely determined.)

Repeating the above experiment with different modulation frequencies, we found that the diffusion coefficient is, within our experimental uncertainty, independent of modulation frequency. These results are summarized in Table I.

The diffusion coefficient depends on the Taylor vortex wave vector, as suggested by the Pomeau–Manneville diffusion model. From the Eckhaus instability curve, we know there is a limited range of stable states of TVF for a fixed ϵ. The detailed history of the adjustment of Ω_i selects the particular Np within the stable range. Our procedure for obtaining a stable TVF state with different Np for a fixed ϵ is as follows. For $q=q_c$ (or $Np=35$ in our system), we increase the inner cylinder rotation rate very slowly (in about 20 min) from 0 to the desired ϵ. For a larger Np ($Np>35$) state, Ω_i is increased abruptly from 0 to the selected ϵ. For a smaller Np ($Np<35$) value, a stable wavy vortex state is obtained first and any defects that may form are given time to annihilate or otherwise leave the flow. Finally, Ω_i is adjusted to the ϵ chosen for the experiment. Here $D_\parallel$ was measured with several different wave vectors and it was found to decrease when the wave vector q deviated from q_c. Figure 7 shows the typical dependence of $D_\parallel$ on the vortex wave vector. The correlation length ξ_0 and correlation time τ_0 are obtained by fitting this with Eq. (7). These results are summarized in Table II.

In the step function modulation case, the upper collar moves at about 0.125 mm/sec to a final position in 48 sec, thereby increasing the aspect ratio by 0.853. The data acquisition technique used for the oscillatory case was used here as well. The light intensity profile along a vertical line was recorded once every 12 sec over a period of 40 min after the oscillation was started. Figure 8 shows a sample result. From this plot we can see that the response time of each vortex increases with the distance of the vortex from the upper boundary. For instance, the time for the second vortex boundary to reach halfway to its steady-state position was 31.1 sec after the collar came to rest, while the third vortex boundary took 71.9 sec. In this case at least, the approximation of Eq. (17) is valid for the vortices beyond the three adjacent to the collar. Fitting the data with the equation

$$z_n = z_n^0 - d_0 \operatorname{erfc}(s_n/\sqrt{t}), \tag{20}$$

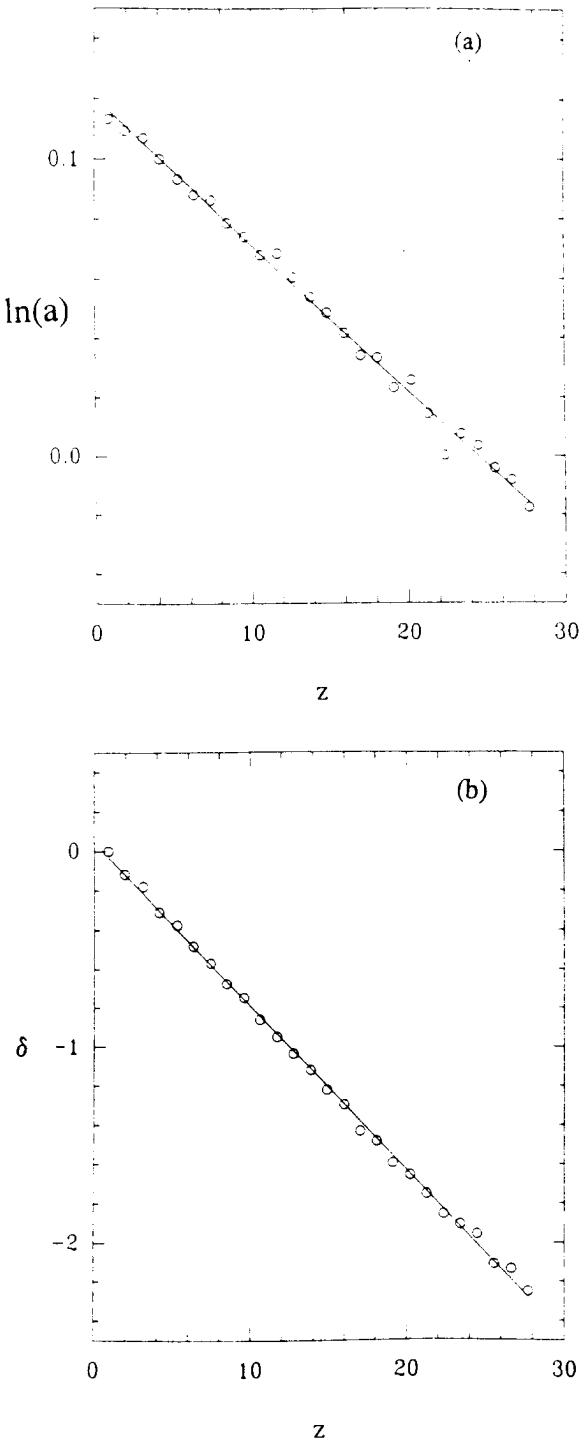

FIG. 5. The circles are the experimental data and the solid lines are from the fit to the diffusion model. (a) a is the amplitude of each vortex boundary motion; (b) δ is the phase shift of the vortex boundary motion.

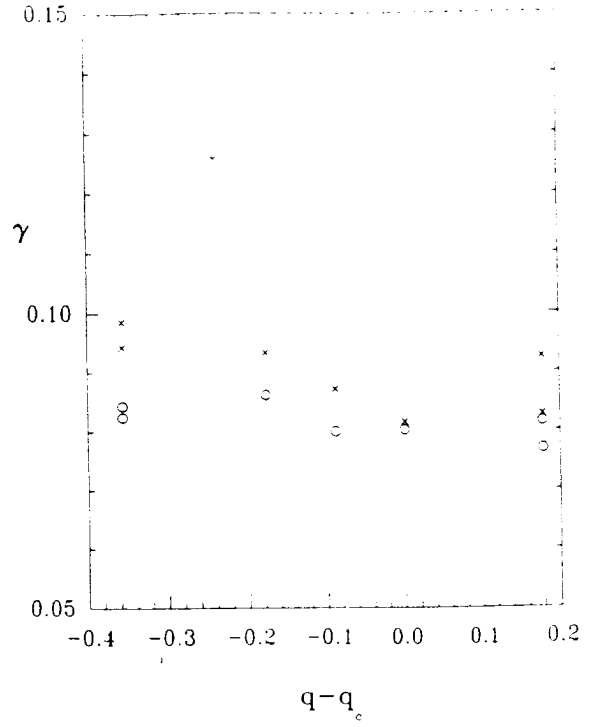

FIG. 6. The difference between β and α due to the Ekman rolls; γ is α for (○) and β for (×).

where $s_n = z_n^0/2\sqrt{D_\parallel}$ according to Eq. (18), we obtain s_n as a linear function of z_n^0, as shown in Fig. 9. The slope of the line in Fig. 9 gives the value of $D_\parallel$. Repeating this process for different TVF wave vectors, we obtained a relation between $D_\parallel$ and the wave vector similar to that found under periodic modulation, as shown in Fig. 7(b). The resulting values of ξ_0 and τ_0 are compared in Table II with those from the periodic cases and numerical simulations.[40,41] Our values for ξ_0 and τ_0 differ from the values in Ref. 40, while $D_\parallel$ from Ref. 41 is within our error bars for three cases. In both numerical cases, the system geometry studied was similar to ours. That we differ with Ref. 40 suggests we may have been operating outside their numerical limit of $\epsilon \to 0$. Further experiments with ϵ smaller than 0.06 may yield better agreement.

As shown in Fig. 7, the range of wave vectors accessible to us is limited due to the large radius ratio of our system. According to the Eckhaus theory,[16,33–35] the range of stable wave vectors for TVF is larger for a smaller radius ratio system where it is possible to go to higher ϵ before reaching the wavy instability. Therefore, it is expected that an experiment in such a system will show a greater dependence of $D_\parallel$ on the wave vector.[24]

TABLE I. Values of the diffusion coefficients obtained from e ents with different modulation period T for a TVF state with and $\epsilon=0.074$.

$D_\parallel$	1.33	1.02	1.28	1.13
T	88.5	175.0	278.0	312.0

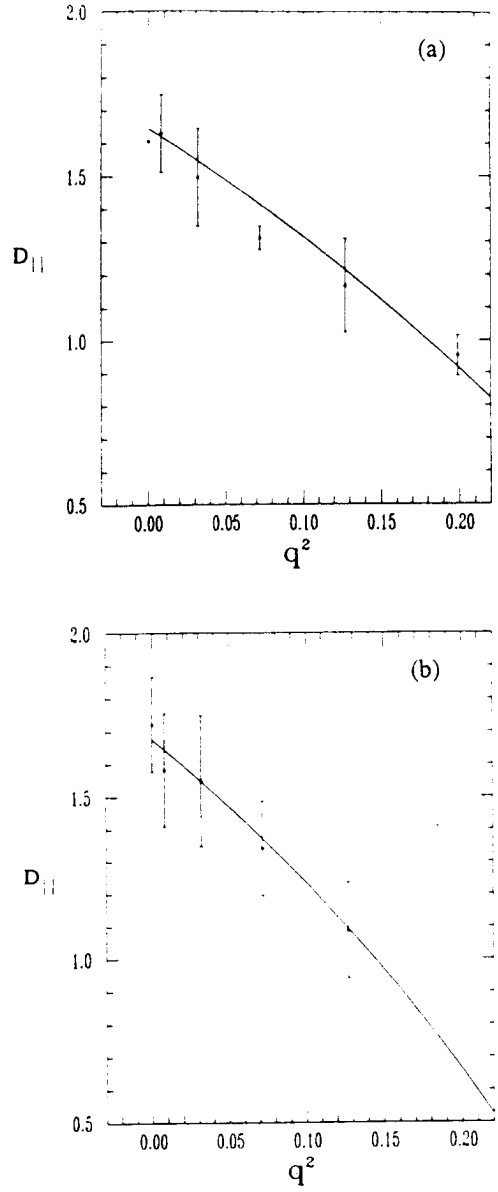

FIG. 7. Relation between $D_\parallel$ and the square of the wave vector, q^2, for (a) the periodic modulation case; (b) the step function modulation case. Dotted lines are the experimental data and the solid lines are the fits using Eq. (7).

2. Wavy vortex flow

A wavy vortex flow [Fig. 2(b)] can be obtained in a large radius ratio system by increasing the Reynolds number to slightly above the onset of TVF. The onset of WVF is at $\epsilon_\omega = 0.223$ for our system. The data acquisition process is complicated by the azimuthal wave motion of the vortex boundary. The vortex boundaries move on two time scales, the slow time T (corresponding to the slow upper boundary oscillation, with a period of several minutes) and the fast time T_1 (corresponding to the azimuthal wave motion of period $\simeq 1$ sec). We define $\bar{z}_n(\tau)$ to be the average boundary position of the nth vortex due to the slow upper boundary modulation, where τ is real time scaled by d^2/ν. Thus, $\psi = q[\bar{z}_n(\tau) - \bar{z}_n^0]$, where q is the axial wave vector.

The procedure for obtaining $\bar{z}_n(\tau)$ is as follows. We

TABLE II. Values of the correlation length and time for TVF from our experiments and the numerical simulations.[40,41] The diffusion coefficients are for $Np=35$.

D	ξ_0	$1/\tau_0$	ϵ	Source of data
1.63 ± 0.12	0.260	24.3	0.0740	periodic modulation
1.59 ± 0.07	0.293	18.9	0.0740	periodic modulation
1.54 ± 0.20	0.288	19.3	0.0621	constant modulation
1.58 ± 0.17	0.301	17.4	0.0829	constant modulation
	0.382	13.109		Ref. 40
1.70			0.070	Ref. 41

first take about 100 consecutive line profiles (covering approximately ten azimuthal waves) in 7 sec and find the intensity minima. A typical space-time diagram of the wavy vortex boundary positions is shown in Fig. 10. The data file records locations of minima of the vertical lines (z_n,t). Our interest is in the average position of each vortex boundary. Thus we need to rearrange our data file, putting the locations of each vortex boundary together, and then averaging the locations for each line. The following technique is used to sort out the locations of each vortex boundary. The original data (locations of vortex boundaries) are put into an array, $S(z,t)$, where z is the axial position and t is time:

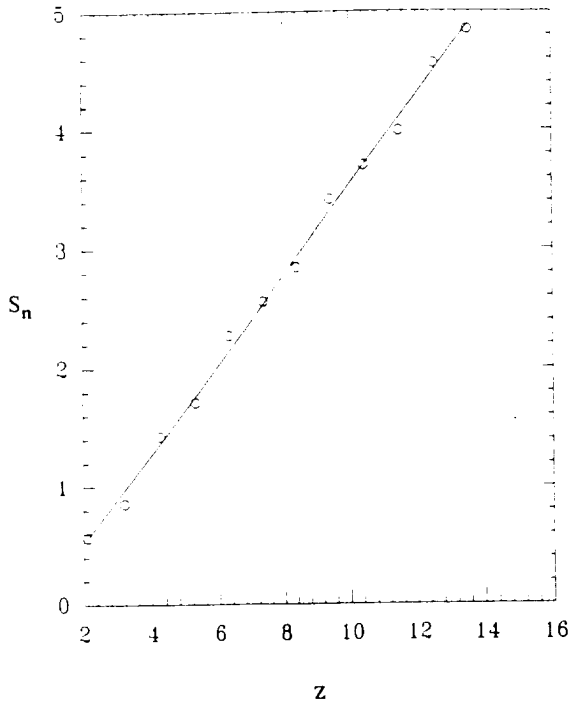

FIG. 9. Relation between s_n and the axial position z for a TVF state at $\epsilon=0.062$, $Np=34$.

$$S(z,t)=1, \quad \text{when } (z,t) \text{ is located at the vortex boundary,}$$
$$=0, \quad \text{otherwise.} \tag{21}$$

The numbers $S(z,t)$ over the time range (a typical time range is ~ 7 sec) at a fixed z value are then added together.

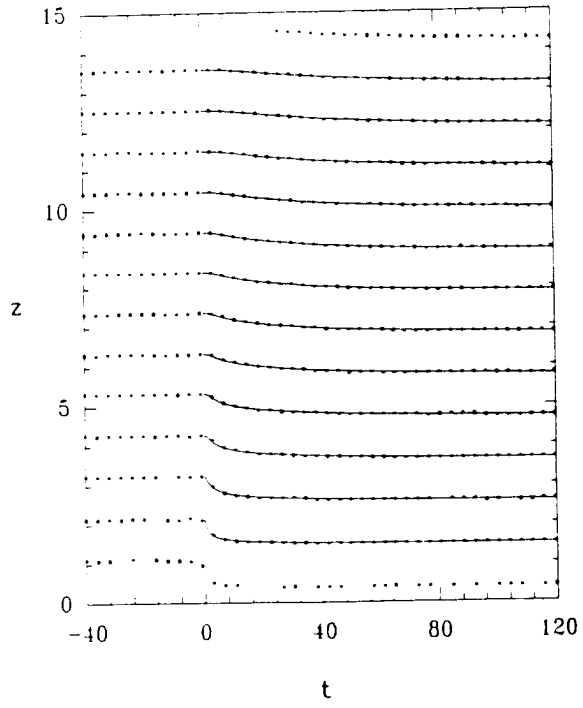

FIG. 8. Vortex boundary locations of TVF subjected to the step function boundary modulation. Modulation is added at $t=0$. Dotted lines are the experimental data and solid lines are the error function fits to the data.

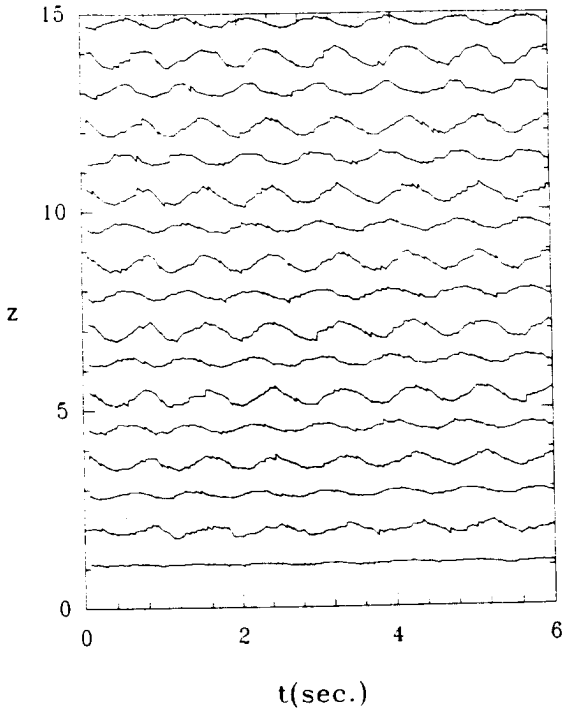

FIG. 10. Space-time diagram of wavy vortex boundary positions at $\epsilon=0.813$, $Np=27$, $m=7$.

When the sum equals 0, it means that a particular z value locates the separation region of two vortex boundaries. Different vortex boundaries are thus identified and the azimuthal wave motions are averaged out along each vortex boundary to obtain $\bar{z}_n(\tau)$. This technique becomes more difficult to apply when the vortex boundary motions overlap in the axial direction (for instance, in the case of modulated wavy vortex flow) since our method can no longer separate each vortex boundary. In order to find $\bar{z}_n(\tau)$ in such a case we would need to fit $S(z,t)$ with a series of sinusoidal functions. Further work will be necessary to study the phase dynamics in either modulated wavy vortex flow or large amplitude wavy vortex flow.

We first discuss our measurements of $\bar{z}_n(\tau)$ for flow states with different m. An $m=3$ state was obtained by increasing ϵ slightly above the onset of TVF, to $\epsilon=0.140$. A typical result is shown in Fig. 11(a). The amplitude of $\bar{z}_n(\tau)$ decreases exponentially with distance from the boundary [Fig. 12(a)], and there is a linear phase shift between oscillations of neighboring vortices [Fig. 12(b)]. These are characteristics of a diffusive mode, as shown by Eq. (16). The diffusion coefficient in this case is ~ 1.4, comparable to that for TVF. Increasing ϵ to 0.813, the system reaches a new stable state with $m=7$. In order to obtain $m=7$ with the same Np, ϵ must be changed rapidly from 0.140 to 0.813. With the same modulation period as for the $m=3$ case, $T=53.3$, there is an axially propagating wave in the middle region of the cylinders, as shown in the space-time plot of Fig. 11(b), evidently described by $\bar{z}_n-\bar{z}_n^0 \propto \sin(kz-\omega t)$, with small damping.[27] The complete amplitude of $\bar{z}_n(\tau)$ versus axial position is shown as the □ data points in Fig. 12(a). We identify the behavior in the central region, from $z\sim 7$ to ~ 35 as a propagating mode because (1) the amplitude is roughly constant over many vortices, in contrast to the diffusive case; and (2) the phase shift δ of neighboring $\bar{z}_n(\tau)$ in this region depends linearly on the axial position [□ line of Fig. 12(b)], which is to be expected for a traveling wave but not a standing wave.

The behavior in the end regions for $T=53.3$ is rather different from that in the bulk. Diffusive behavior is observed in the vortices near the *upper* (oscillating) collar of the cylinders ($0<z<10$). We attribute this to two effects. First, the azimuthal wave amplitude a_w (i.e., in the absence of our imposed perturbation) decreases rapidly near each end of the system from its value in the bulk. The relation between a_w and z is shown in Fig. 13. The healing length for a_w is about the size of three or four pairs of vortices. It decreases with increasing ϵ. The small a_w at the ends evidently weakens the coupling between ψ and ϕ, thereby contributing to the diffusive behavior near the collars. Second, the vortices near the collar are $\sim 3\%$ smaller than in the middle region. The diffusive behavior near the collar is consistent with the observation, discussed below, that the diffusion coefficient is relatively larger for smaller vortices. The falloff of the $\bar{z}_n(\tau)$ amplitude in the *lower* end of the cylinders [$z>30$ in Fig. 12(a)] is evidently a finite length effect. The phase shift in this region is also a linear function of the axial position with a slope close to that of the phase shift line for the traveling wave in the middle of the system.

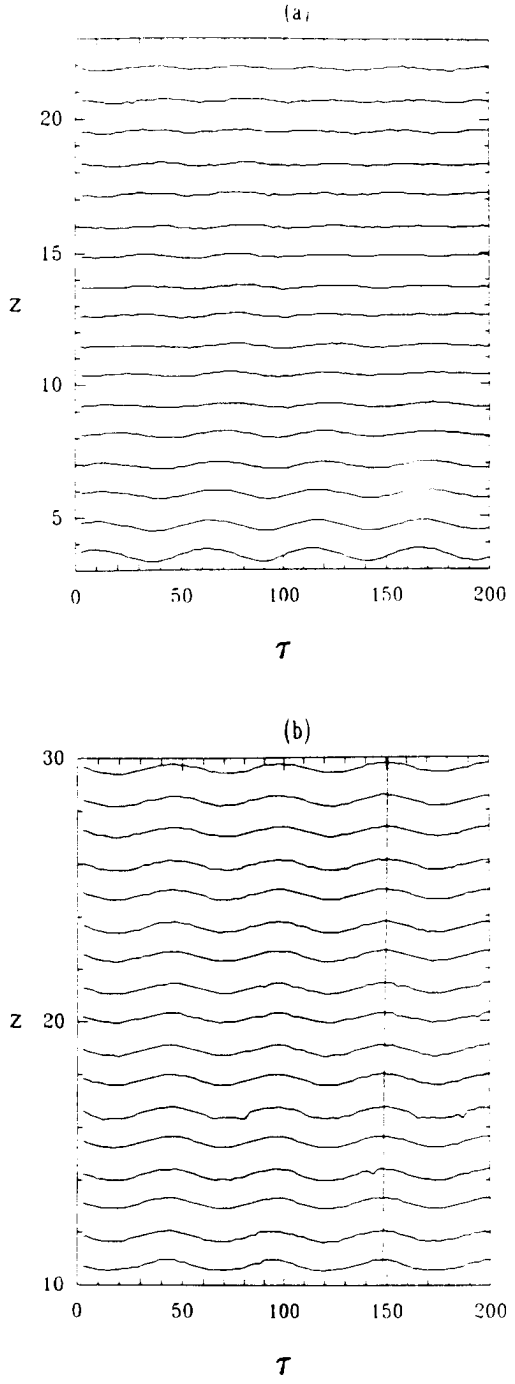

FIG. 11. Responses of the axial phase variable $\bar{z}_n(\tau)$ to a modulation of period $T=53.3$. $Np=30$, (a) $m=3$, $\epsilon=0.140$; (b) $m=7$, $\epsilon=0.813$. The straight line traces the shift in phase from vortex to vortex.

The effects of modulation frequency on the phase dynamics were also studied. Figures 12(a) and 14 show that for a fast modulation, the amplitude drops off more rapidly near the upper collar than for a slower modulation. This is consistent with the diffusion model, where $a \propto \exp[-\sqrt{(\omega/2D_\parallel)}z]$. The constant amplitude region where the propagating mode exists shortens as the modulation frequency decreases, and it finally collapses into a straight line for very long periods of oscillation. For example, for modulation period $T>101$ [* and □ lines of Fig.

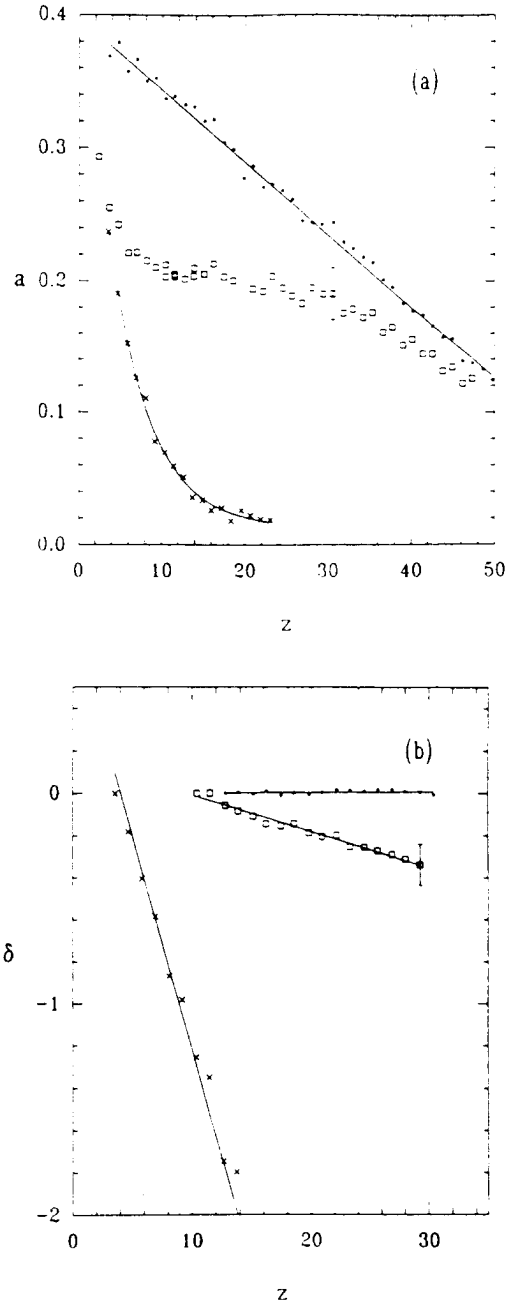

FIG. 12. Amplitude (a) and phase shift (b) of $\bar{z}_n(\tau)$ versus axial position. The bar represents the largest error of all the data points. ×: $m=3$, $Np=30$, $\epsilon=0.140$, $T=53.3$; □: $m=7$, $Np=30$, $\epsilon=0.813$, $T=53.3$; ●: $m=7$, $Np=30$, $\epsilon=0.813$, $T=207$. The solid lines are fits to the data.

14, and the × data points of Fig. 12(a)], the amplitude decreases linearly with z, with a slope $0.0137 \sim 1/\Gamma$. The slope here is scaled by the maximum amplitude of the oscillation of the upper collar. This is a typical solution of a propagating wave equation when the wavelength is much longer than the system itself. The corresponding phase shift between neighboring $\bar{z}_n(\tau)$ (* and □ lines of Fig. 15) is zero, which means that the modulation is slow enough for each vortex to respond essentially simultaneously. (The discontinuities in Fig. 15 come from the fact that the data were taken separately from different sections of the flow pattern in order to obtain higher resolution. The pattern is

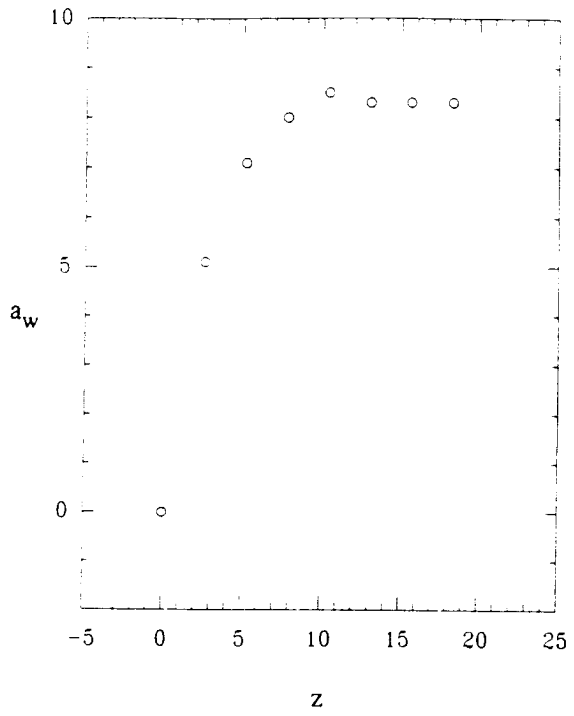

FIG. 13. Azimuthal wave amplitude a_w versus the axial position z, $z=0$ is the position of upper collar, and the WVF state is at $\epsilon=0.813$, with $Np=27$ and $m=7$.

sectioned into three parts, $0<z<19$, $19<z<38$, and $38<z<54$.)

The vortex size dependence of the phase dynamics was also investigated. Figure 16 shows the amplitude of $\bar{z}_n(\tau)$

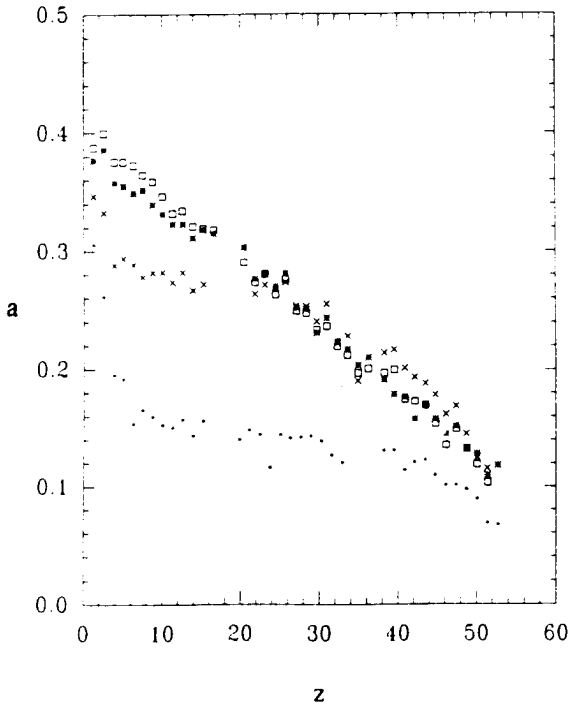

FIG. 14. Amplitude versus z for the state $\epsilon=0.813$, $Np=27$, and $m=8$, for different modulation periods: $T=27.6$ for ●; 52.0 for ×; 101 for *; 207 for □.

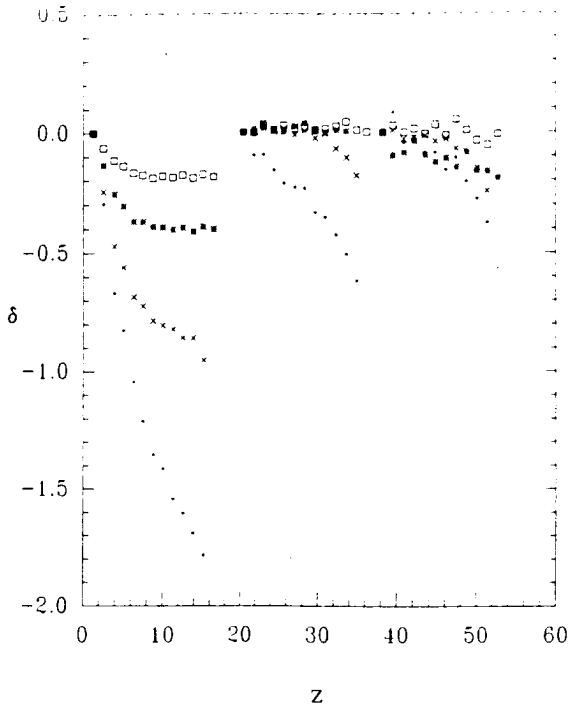

FIG. 15. Phase versus z for the state $\epsilon=0.813$, $Np=27$, and $m=8$, for different modulation periods: $T=27.6$ for ●; 52.0 for ×; 101 for *; 207 for □.

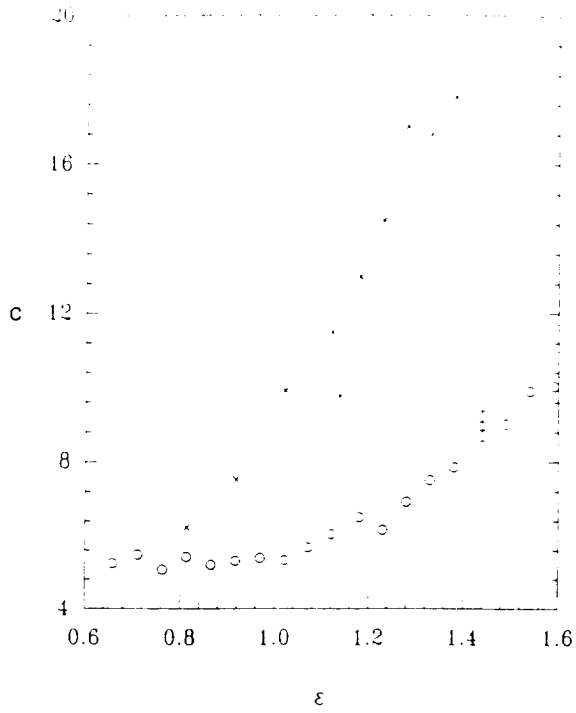

FIG. 17. Values of traveling wave speed c vs ϵ for $m=8$, $Np=27$, and $T=20$ for ○, 27.6 for ×. The bar represents the largest error of all the ○ data points.

along the axis for the same ϵ and m, but different vortex sizes. The amplitude decreases more rapidly for $Np=30$ than for $Np=27$, showing the diffusion coefficient is larger relative to the coupling coefficients for smaller vortices.

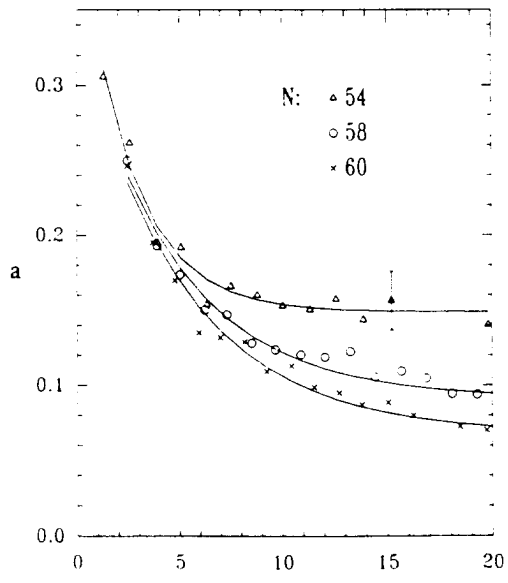

FIG. 16. Amplitude a of $\bar{z}_n(\tau)$ versus axial position for different vortex sizes. The bar represents the largest error of all the data points. $T=28$, $\epsilon=0.813$, $m=7$, and $N(=2Np)$ as indicated. The solid lines are exponential fits to the data.

Compare this with the behavior found in Taylor vortex flow (see Fig. 7 and Ref. 26).

The slope of $\delta(z)$ vs z yields the traveling wave vector K, and in turn the wavelength, which is about 365 for the conditions of the □ data points of Fig. 12(b), longer than the system. Knowing K we can compute the traveling wave speed c. For this representative case we obtain the value of $c=7$ (or 0.4 cm/sec), which shows this is a very soft system compared with sound propagation in liquids or solids.

Having established that a propagating mode exists for the strong coupling case, i.e., for large vortices, large azimuthal wave number and large wave amplitudes, we can ask further questions about the nature of the propagation. For example, we measured the traveling wave velocity c in the middle section of the cylinders as a function of ϵ (see Fig. 17). For a wavy state with fixed m and N, increasing ϵ corresponds (roughly) to increasing azimuthal wave amplitude. Thus the increase of c with ϵ in Fig. 17 implies that the coupling strength increases with the azimuthal wave amplitude. Wave speed c can also be evaluated from the amplitude equation[27] close to the onset of TVF. However, the calculated value shows only a weak dependence on ϵ, changing from 0.63 to 0.65 for a variation of ϵ from 0.5 to 1.5. This difference is not unreasonable as the amplitude equation approach should be useful only for very small ϵ. Further theoretical work is necessary to understand the ϵ dependence of c.

The traveling wave speeds for states with fixed N and m were measured for different modulation frequencies. Figure 17 shows that the measured c is larger for the lower frequency case. This indicates that either the actual disper-

sion relation is not linear or the linear phase equations are not sufficient to explain the experiment in quantitative detail. Further work is clearly needed to determine the dispersion relation in the wavy state.

The intermediate states $m=4,5,6$ are obtainable and stable, but the azimuthal wave amplitude is so large that neighboring vortices overlap in the axial direction and as a result our basic data analysis program is not capable of finding the average vortex boundary positions. Therefore, no results have been obtained in this region. This is a rather interesting problem to be explored experimentally. As pointed out by Brand,[27,42] the phase dynamics in this region should give rise to an overdamped mode.

3. Turbulent Taylor vortex flow

We turn now to the behavior of coherent structures in a turbulent flow, the TTVF [Fig. 1(c)]. A TTVF is formed when ϵ is increased to $\epsilon_T \sim 20$ for a vortex pair $Np=26$ state. The threshold for this state, ϵ_T, is not critical for our purposes, but appears to vary with the vortex size, being lower for larger vortices (i.e., smaller Np). A representative space-time diagram of the vortex boundary positions is shown in Fig. 18(a). The vortex boundaries fluctuate on a time scale of ~ 0.1 sec. Walden and Donnelly[43] studied the time dependence of a similar state and found that its Fourier spectrum had a peak frequency $\sim 1\%$ larger than the cylinder rotation frequency Ω_i embedded in a noise band. The peak was apparently related to the presence of waves on the vortices. The presence of noise suggests that the vortex boundary position is a stochastic variable and, therefore, the number of phase variables involved might be unclear at first sight. However, we found that the *average* vortex boundary $\bar{z}_n^0$ is a *deterministic* variable in a limited range of ϵ values (for $Np=27$, $15<\epsilon<19$). Here *average* means averaging out the fast fluctuations along the azimuthal direction. We average the vortex boundary positions over a longer time scale than that associated with the turbulent fluctuations, e.g., ~ 7 sec, and record the average vortex boundary positions $\bar{z}_n(\tau)$ once every 60 sec. We find that $\bar{z}_n(\tau)$ is constant for at least 3 h [see Fig. 18(b)]. This indicates that TTVF possesses strong spatial coherence even though the flow itself is certainly turbulent. Our focus, then, is on the response of the *coherent structure* to the very slow perturbation imposed on the system.

The basic experimental approach and data acquisition technique is the same as that for TVF and WVF. So, a sinusoidal forcing is added to the system through the upper collar and the responses of the average vortex boundary positions $\bar{z}_n(\tau)$ are measured. A line profile of the TTVF pattern is recorded and the vortex boundaries are located by finding the minima of the light intensity profile. Here z_n varies on two distinct time scales, the fast time turbulent fluctuations ($T_1 \sim 0.1$ sec), and the slow time variation ($T \sim 5$ min) due to the oscillation of the upper collar. The technique described in Sec. III B 2 is used to average out the fast fluctuations. A typical time series of $\bar{z}_n(\tau)$ is shown in Fig. 19. The amplitude drops off exponentially and the phase shift of the boundary line motions varies linearly with the axial position, as shown in Fig. 20. This indicates

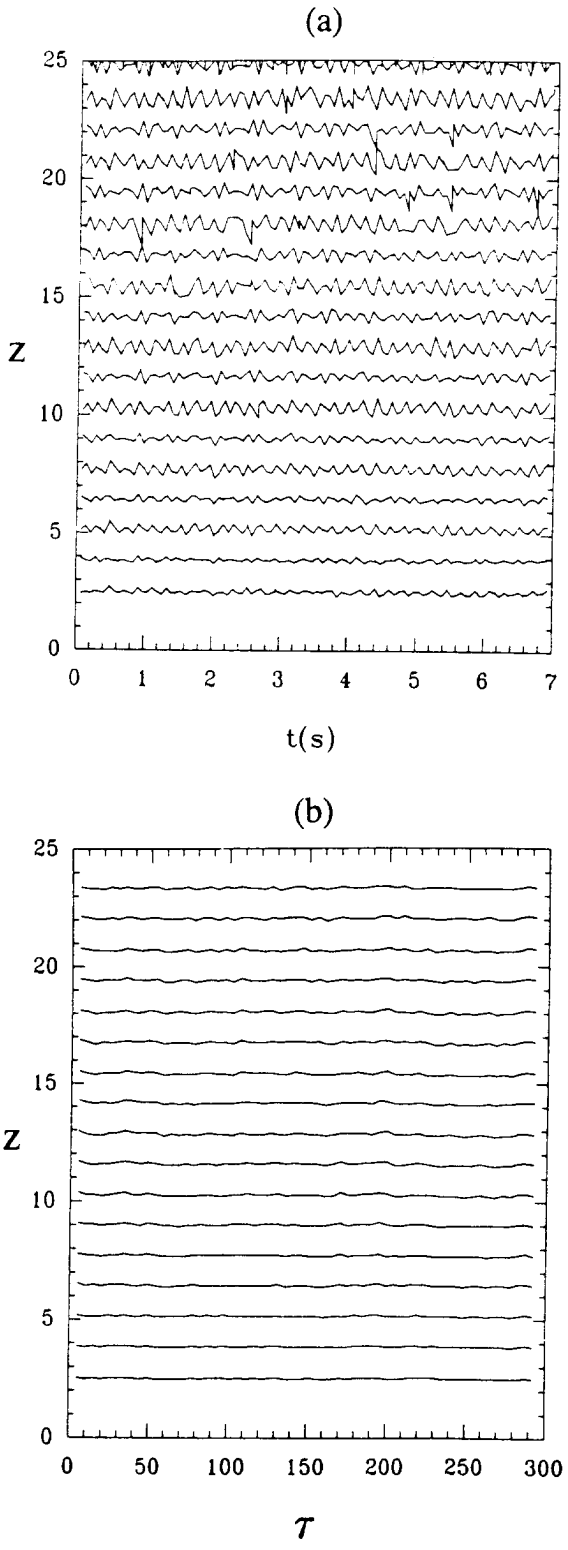

FIG. 18. Space-time diagram of the boundary positions of a turbulent Taylor vortex flow with $\epsilon=19.7$, $Np=27$, before (a) and after (b) averaging.

that the phase dynamics in TTVF can be described by a simple diffusion model, as suggested in Sec. II. From the slope of the line in Fig. 20(b), the diffusion coefficient can be evaluated by Eq. (15), which is about 24 in this case.

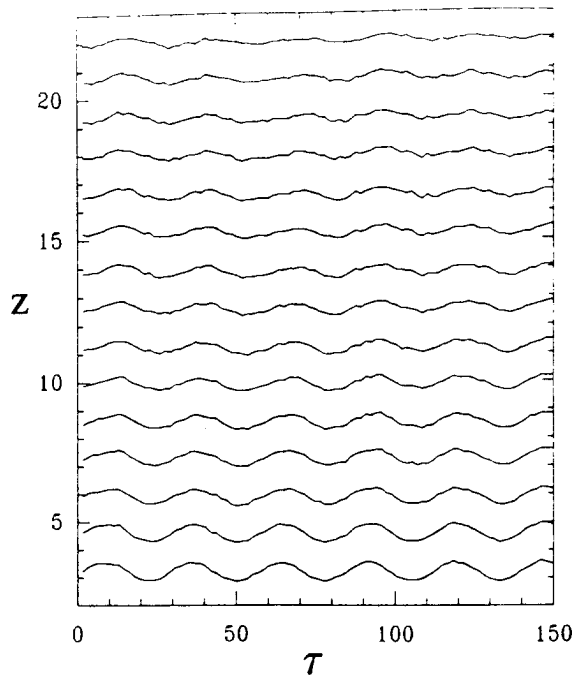

FIG. 19. Responses of the axial phase variable $\bar{z}_n(\tau)$ to a modulation of period $T=27.6$. The TTVF has $\epsilon=19.7$ and $Np=26$.

The amplitude and phase shift of $\bar{z}_n(\tau)$ of TTVF are plotted in comparison with those for TVF (Fig. 20). Figure 20(a) shows that the amplitude drops off more rapidly for the TVF than for the TTVF. Figure 20(b) shows that the phase shift for TVF has a steeper slope than that for TTVF. Both results indicate that the diffusion coefficient for TTVF is larger than for TVF, the ratio being ~ 14 for the particular parameters we have selected. We attribute the large diffusion coefficient of the TTVF to the efficient momentum transport of the turbulent fluctuations of the TTVF.[44] It will be interesting to explore the dependence of the diffusion coefficient on ϵ, particularly at very high ϵ as the vortices become less well defined. It will also be useful to compare the results on phase diffusion, which involves vector quantities such as momentum, with scalar diffusion in TTVF.[45]

IV. CONCLUSION

We have studied the phase dynamics of three distinct regimes of flow in the Taylor–Couette system, the TVF, WVF, and TTVF. A forced modulation was added through motions of the upper collar of the system and the responses of the vortex positions to the modulation were studied. The phase dynamics in TVF was found to be well described by a simple one phase variable diffusion model. The measured diffusion coefficients were found to decrease as the wave vector deviated from its critical value. In WVF, the perturbation propagates along the cylinder as a traveling wave when the coupling between the axial and azimuthal phase variables is strong, and diffuses otherwise. This is understood within a theoretical framework of coupled diffusion equations. In TTVF, the phase dynamics of

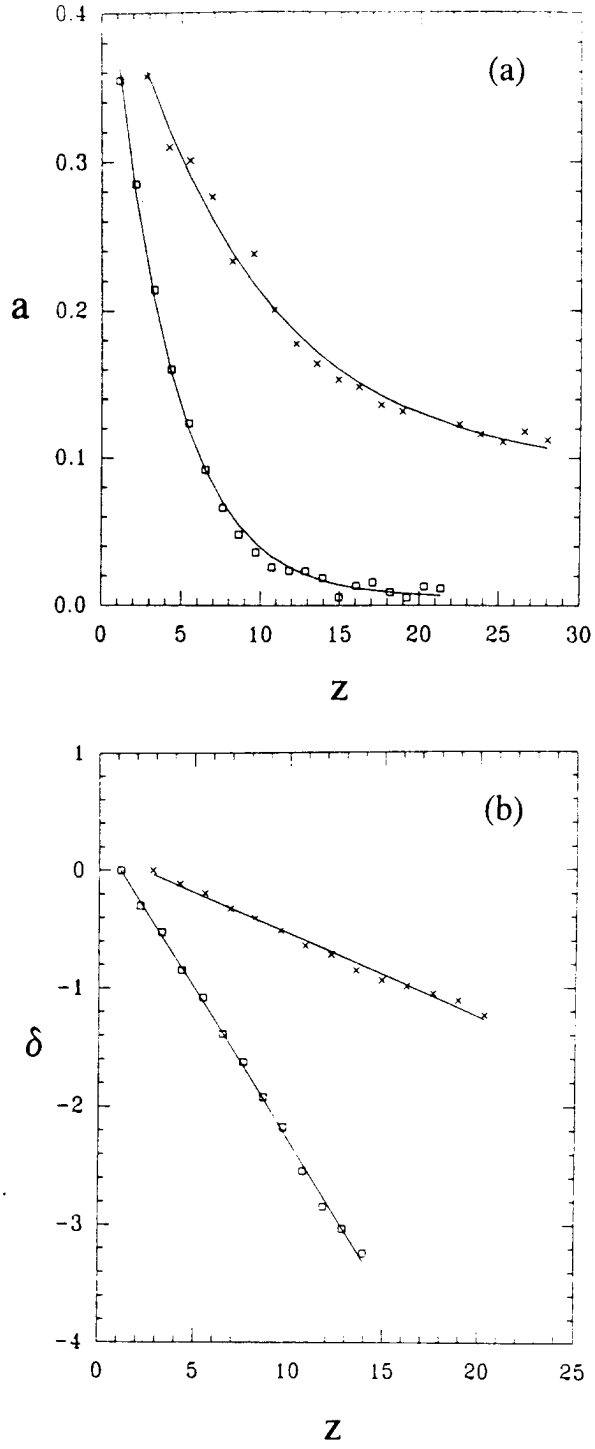

FIG. 20. (a) Amplitude and (b) phase shift of $\bar{z}_n(\tau)$ vs z for a modulation period $T=27.6$. × data are for a TTVF state with $\epsilon=19.7$ and $Np=26$; □ data are for a TVF state with $\epsilon=0.075$ and $Np=33$.

the coherent structure of vortices was found to be similar to that of TVF, being described in an average sense by a one phase variable diffusion model. The measured diffusion coefficient is more than an order of magnitude larger than that for TVF, apparently a result of the turbulence enhanced momentum transport. In summary, we have established that the phase dynamics approach is valid for patterns with more than one-dimensional periodicity, and that

it can deal with turbulent flows as well. This extension of phase dynamics into a turbulent regime suggests that it will be a useful tool for attacking a wider range of problems than previously thought possible.

ACKNOWLEDGMENTS

We thank H. Brand for many enlightening discussions and encouragements through this project. We also thank Z. H. Wang, F. Hayot, and I. Mutabazi for helpful discussions.

This work was supported by the Office of Naval Research, under Contract No. N00014-86-K-0071 and Grant No. N00014-89-J-1352.

[1] H. L. Swinney and R. DiPrima, "Instabilities and transitions in flow between concentric rotating cylinders," in *Hydrodynamic Instabilities and the Transition to Turbulence*, edited by H. L. Swinney and G. P. Gollub, 2nd ed. (Springer-Verlag, Berlin, 1985), p. 139.

[2] H. Bénard, "Les tourbillons cellulaires dans une nappe liquide transportant de la chaleur par convection en regime permanent," Ann. Chim. Phys. 7, Ser. 23, 62 (1901). For recent reviews, see F. H. Busse, "Transition to turbulence in Rayleigh–Bénard convection," in Ref. 1, p. 97.

[3] Y. Couder, "Growth patterns: from stable curved fronts to fractal structures," in *Chaos, Order and Patterns*, edited by R. Artuso, P. Cvitanović, and G. Casati (Plenum, New York, 1991), p. 203.

[4] C. Ho and P. Huerre, "Perturbed free shear layers," Annu. Rev. Fluid Mech. **16**, 365 (1984).

[5] G. P. Smith and A. A. Townsend, "Turbulent Couette flow between concentric cylinders at large Taylor numbers," J. Fluid Mech. **123**, 187 (1982).

[6] P. S. Marcus, "Simulation of Taylor–Couette flow. Part 1. Numerical methods and comparison with experiment," J. Fluid Mech. **146**, 45 (1984).

[7] P. S. Marcus, "Simulation of Taylor–Couette flow. Part 2. Numerical results for wavy-vortex flow with one travelling wave," J. Fluid Mech. **146**, 65 (1984).

[8] A. Davey, R. C. DiPrima, and J. T. Stuart, "On the instability of Taylor vortices," J. Fluid Mech. **31**, 17 (1968).

[9] M. Nagata, "Bifurcations in Couette flow between almost corotating cylinders," J. Fluid Mech. **169**, 229 (1986); "On wavy instabilities of the Taylor-vortex flow between corotating cylinders," *ibid.* **188**, 585 (1988).

[10] S. Chandrasekhar, *Hydrodynamic and Hydromagnetic Stability* (Dover, New York, 1981).

[11] H. Yahata, "Temporal development of the Taylor vortices in a rotating fluid," Prog. Theor. Phys. Suppl. **64**, 176 (1978); "Temporal development of the Taylor vortices in a rotating fluid II," Prog. Theor. Phys. **61**, 791 (1979).

[12] A. C. Newell and J. A. Whitehead, "Finite bandwidth, finite amplitude convection," J. Fluid Mech. **38**, 279 (1969). For application to the Taylor–Couette system see R. Graham and J. A. Domaradzki, "Local amplitude equation of Taylor vortices and its boundary condition," Phys. Rev. A **26**, 1572 (1982) and references therein.

[13] P. Hall, "Evolution equations for Taylor vortices in the small-gap limit," Phys. Rev. A **29**, 2921 (1984).

[14] H. Yahata, "Slowly varying amplitude of the Taylor vortices near the instability point," Prog. Theor. Phys. **57**, 347 (1977).

[15] G. Pfister and I. Rehberg, "Space-dependent order parameter in circular Couette flow transitions," Phys. Lett. A **83**, 19 (1981).

[16] G. Ahlers, D. S. Cannell, M. A. Dominguez-Lerma, and R. Heinrichs, "Wavenumber selection and Eckhaus instability in Couette–Taylor flow," Physica D **23**, 202 (1986).

[17] Y. Pomeau and P. Manneville, "Stability and fluctuations of a spatially periodic convective flow," J. Phys. Lett. (Paris) **40**, L609 (1979).

[18] Y. Kuramoto, "Phase dynamics of weakly unstable periodic structures," Prog. Theor. Phys. **71**, 1182 (1984).

[19] J. E. Wesfreid and V. Croquette, "Forced phase diffusion in Rayleigh–Bénard convection," Phys. Rev. Lett. **45**, 634 (1980).

[20] V. Croquette and F. Schosseler, "Diffusive modes in Rayleigh–Bénard structures," J. Phys. (Paris) **43**, 1183 (1982).

[21] P. Tabeling, "Dynamics of the phase variable in the Taylor vortex system," J. Phys. Lett. (Paris) **44**, L665 (1983).

[22] H. A. Snyder, "Wave-number selection at finite amplitude in rotating Couette flow," J. Fluid Mech. **35**, 273 (1969).

[23] M. Lücke and D. Roth, "Structure and dynamics of Taylor vortex flow and the effect of subcritical driving ramps," Z. Phys. B **78**, 147 (1990).

[24] H. Paap and H. Riecke, "Drifting vortices in ramped Taylor vortex flow. Quantitative results from phase equation," Phys. Fluids A **3**, 1519 (1991).

[25] U. Gerdts, Ph.D. thesis, Universit Kiel, 1985.

[26] M. Wu and C. D. Andereck, "Phase modulation of Taylor vortex flow," Phys. Rev. A **43**, 2074 (1991).

[27] H. R. Brand and M. C. Cross, "Phase dynamics for the wavy vortex state of the Taylor instability," Phys. Rev. A **27**, 1237 (1983).

[28] H. R. Brand, "Nonlinear phasedynamics for the spatially periodic states of the Taylor instability," Prog. Theor. Phys. **71**, 1096 (1984).

[29] H. R. Brand, "Phase dynamics—a review and perspective," in *Propagation in Systems Far from Equilibrium*, edited by J. E. Wesfreid, H. R. Brand, P. Manneville, G. Albinet, and N. Boccara (Springer-Verlag, New York, 1988), p. 206.

[30] M. Wu and C. D. Andereck, "Phase dynamics of wavy vortex flow," Phys. Rev. Lett. **67**, 1258 (1991).

[31] M. Wu and C. D. Andereck, "Phase dynamics in the Taylor–Couette system," in *Ordered and Turbulent Patterns in Taylor–Couette Flow*, edited by C. D. Andereck and F. Hayot (Plenum, New York, 1992).

[32] M. Wu, C. D. Andereck, and H. R. Brand, "The phase dynamics of turbulent Taylor vortex flow," to appear in Europhys. Lett. (1992).

[33] W. Eckhaus, *Studies in Nonlinear Stability Theory* (Springer-Verlag, New York, 1965).

[34] D. S. Cannell, M. A. Dominguez-Lerma, and G. Ahlers, "Experiments on wave number selection in rotating Couette-Taylor flow," Phys. Rev. Lett. **50**, 1365 (1983).

[35] L. Ning, G. Ahlers, and D. S. Cannell, "Wave-number selection and traveling vortex waves in spatially ramped Taylor–Couette flow," Phys. Rev. Lett. **64**, 1235 (1990).

[36] P. G. De Gennes, *The Physics of Liquid Crystals* (Clarendon, Oxford, 1974).

[37] J. Hegseth, Ph.D. thesis, The Ohio State University, 1990.

[38] M. Abramowitz and I. E. Stegun, *Handbook of Mathematical Functions with Formulas, Graphs and Mathematical Tables* (U. S. Government Printing Office, Washington, DC, 1964), p. 297.

[39] M. Lücke and D. Roth (private communication, 1991).

[40] M. A. Dominguez-Lerma, G. Ahlers, and D. S. Cannell, "Marginal stability curve and linear growth rate for rotating Couette–Taylor flow and Rayleigh–Bénard convection," Phys. Fluids **27**, 856 (1984).

[41] H. Riecke (private communication, 1990). The method of computation is described in Ref. 24.

[42] H. R. Brand (private communication, 1991).

[43] R. W. Walden and R. J. Donnelly, "Reemergent order of chaotic circular Couette flow," Phys. Rev. Lett. **42**, 301 (1979).

[44] H. Tennekes and J. L. Lumley, *A First Course in Turbulence* (MIT Press, Cambridge, MA, 1972).

[45] W. Y. Tam and H. L. Swinney, "Mass transport in turbulent Couette–Taylor flow," Phys. Rev. A **36**, 1374 (1987).

Spiral Turbulence and Phase Dynamics

John J. Hegseth, C. David Andereck, F. Hayot, and Y. Pomeau[a]
Department of Physics, Ohio State University, 174 West 18th Avenue, Columbus, Ohio 43210
(Received 22 August 1988)

Hysteretic spiral turbulence is a remarkable phenomenon of coexistence of turbulent and laminar domains in Taylor-Couette flow. We observe and measure for the first time a nonuniform pitch in long geometries and its dependence on boundary conditions at the cylinder ends, and we explain these results within the framework of phase dynamics. We also discuss the influence of secondary flow on the azimuthal width of the spiral.

PACS numbers: 47.20.−k, 47.30.+s

Spiral turbulence—the coexistence of laminar and turbulent spiral regions in Taylor-Couette flow—is highlighted by Feynman[1] as an example of the richness of phenomena described by the Navier-Stokes equations (see Fig. 1). Spiral turbulence has been extensively studied by Coles[3] and its existence region for a particular geometry mapped out in the (R_o,R_i) plane of Taylor-Couette flow between concentric rotating cylinders. Here R_o and R_i are proportional to the angular velocities Ω_o and Ω_i of the outer and inner cylinder, respectively [$R_o=b(b-a)\Omega_o/\nu$ and $R_i=a(b-a)\Omega_i/\nu$, where a is the radius of the inner and b is the radius of the outer cylinder, and ν is the kinematic viscosity]. Subsequently Van Atta,[4] at one point in the parameter space, measured the pitch of the spiral and mapped its profile in a plane perpendicular to the cylinder axes.

Spiral turbulence is particularly interesting among all fluid instabilities, because it mixes short scale (or microscale) turbulence and a well ordered structure at large scales. It is the prototype of the "coherent structures" of great interest in fluid mechanics in recent years.[5] In this Letter we report new measurements of spiral turbulence, in particular of the spiral pitch, for different boundary conditions, and propose a theoretical approach in the spirit of Feynman[1] "to find the qualitative content of the Navier-Stokes equations." The novel observation that the pitch varies along the axis fits well into a phase dynamics approach, which—we believe—is here applied for the first time to a situation with sustained microscale turbulence. In addition the well-known[3,4] observation that the turbulent spiral is of finite azimuthal width, will be explained as resulting from the subcritical character of the flow and its boundedness in the azimuthal direction.

It is important to stress the subcritical character of the laminar-spiral turbulence transition, which leads to large hysteretic effects.[2,3] As shown by one of us,[6] subcritical instabilities in general should lead to expanding or contracting turbulent domains in laminar flow. For the finite Taylor-Couette system, this cannot be the whole story. In fact, large-scale Poiseuille flow in the laminar region is generated by Reynolds stress in the turbulent region. The case of weakly inclined, supercritical Taylor vortices was worked out by Hall,[7] who completed previous work[8] on amplitude equations. In Hall's work[7] the backflow is proportional to an integral over azimuthal angle involving the square of the amplitude, which itself is proportional to the Reynolds stress.[9] The theory for the subcritical case has not yet been worked out, however; the same basic mechanism must be at work, and this allows for a qualitative understanding. The backflow

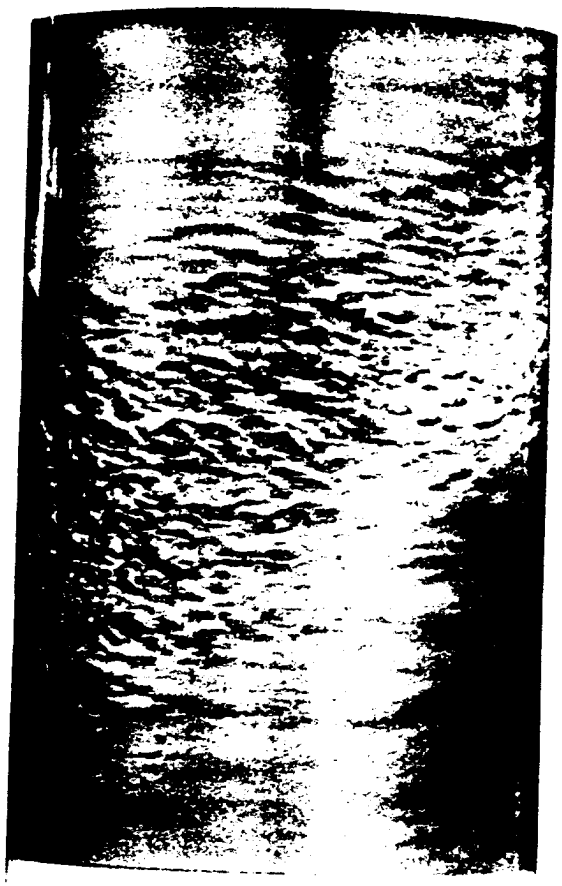

FIG. 1. Spiral turbulence for fixed upper and lower boundaries, aspect ratio 30, $R_o=-3000$, $R_i=700$ (from Ref. 2).

counteracts the velocity of expansion of the turbulent spot until the latter stops. The matching of azimuthal Reynolds numbers (the relevant length being the azimuthal width of each region) for laminar and turbulent flow (assumed to have the same average velocity) leads at onset to roughly equal azimuthal width of each region, up to the mismatch between molecular and turbulent viscosities in the respective regions.

The experimental apparatus used here has been largely described in a previous paper.[10] In brief, the geometric parameters of our system are the radius ratio $a/b = 0.882$ and the aspect ratio $\Gamma = L/(b-a)$, which can be as large as 73. The cylinder speeds were controlled by Compumotor stepping motors with a rotation-rate precision of $\pm 0.01\%$. The working fluid in all cases was distilled water, with visualization of the pattern accomplished by the addition of 1% by volume Kalliroscope polymeric flakes. With a free upper surface the fluid level may be changed continuously while the cylinders rotate. Perturbation experiments in the hysteretic regime were carried out by our injecting fluid into completely laminar flow through a small hole (0.15 cm diam) in the side of the Plexiglas outer cylinder. Approximately 0.1 cm^3 of fluid is injected over a time of less than 0.03 sec, while monitoring the visualized flow with a television camera mounted on a rotating table. The angular velocity of the table was set equal to the expected velocity of the turbulent spots (and ultimately the turbulent spiral). Measurements of the pitch were made by use of a multiple detector reflectance technique. At two points along the axis, light from He-Ne lasers is focused on the fluid and the reflected light detected by photodiodes, the output of which is digitized and sent to our PDP-11/73 computer for analysis. The time delay between the two signals, together with the distance between the detectors, yields the pitch.

We have followed the azimuthal and axial expansions of a spot created at the midpoint of the cylinder in the manner described above. The spot created expands initially much faster (~ 2 times) in the azimuthal direction than in the axial one as shown in Fig. 2. The azimuthal expansion stops as soon as about half of the perimeter length is reached, i.e., from our point of view as soon as there is sufficient backflow. The spot then breaks into two spots in the axial direction, which propagate axially and azimuthally, their width being always approximately that of the final spiral. These spots may then undergo further splitting and subsequent growth. The different pieces eventually connect and construct a spiral. The presence of axial propagation shows that the backflow has in fact a complex three-dimensional structure.

Spiral turbulence is found over a wide range of R_0 and R_i. We limited our detailed survey to the hysteretic regime. We have found that for $\Gamma = 73$ persistent spirals occurred only for $R_o > -4000$, and that at $R_o = -8000$ no large scale organized structure was apparent. In this

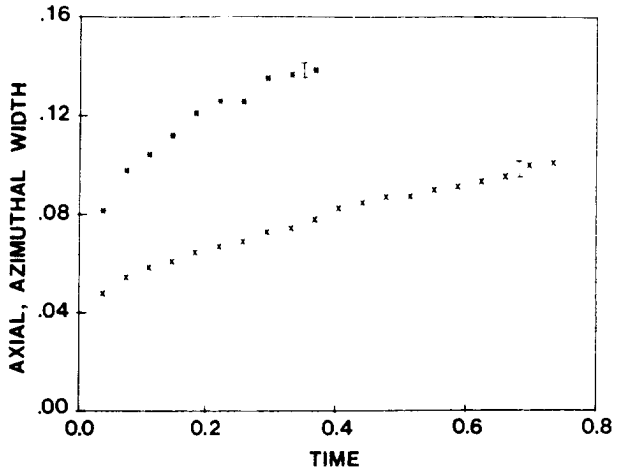

FIG. 2. Axial (×) and azimuthal (*) widths of turbulent spots for $R_o = -3000$, $R_i = 770$. The widths are scaled by the average perimeter length of 35.3 cm, and the time by the outer cylinder period of 0.91 sec. Fits to the first seven points in each case yields initial front velocities of 1.78 cm/sec for the axial case and 3.86 cm/sec for the azimuthal case. Representative error bars are shown for each case.

case a "broken" spiral pattern is found, i.e., the pattern may be locally a spiral, but the helicity changes over an axial distance of the order of the cylinder diameters. Some regions may not show even local spirals, just turbulent patches. This same incoherent state is found with either free or rigid upper boundary. A simple spiral pattern does not emerge until the aspect ratio is lowered to ≈ 28. Measurements on the simple spirals at large aspect ratio were therefore confined to $R_o \approx -3000$. As shown in Fig. 3 these spirals were *always* observed to have a pitch that varied with axial position. We take first the case in which the top and bottom boundaries are rigid and move with the outer cylinder. If the outer cylinder, as viewed from *above,* rotates clockwise, then a right-handed spiral would have a *lower* pitch near the *bottom* of the cylinder than near the *top,* while a left-handed spiral has a *larger* pitch near the bottom that at the top. If the outer cylinder rotates counterclockwise, then, consistent with the first observations, a right-handed spiral would have a *lower* pitch at the *top* of the cylinder than at the bottom, while a left-handed spiral would have a *larger* pitch at the top than at the bottom. In other words, the pitch is lower near the end away from which the spiral appears to be moving. The average pitch depends only weakly on R_i. Its value is compatible with that measured previously.[4] With a free upper surface the picture changes dramatically. For a counterclockwise rotation of the outer cylinder, a right-handed spiral looks much the same as for the rigid-rigid boundary condition case, while a left-handed spiral has a much lower average pitch. In the former case the spiral wraps around the cylinder approximately twice, while in the

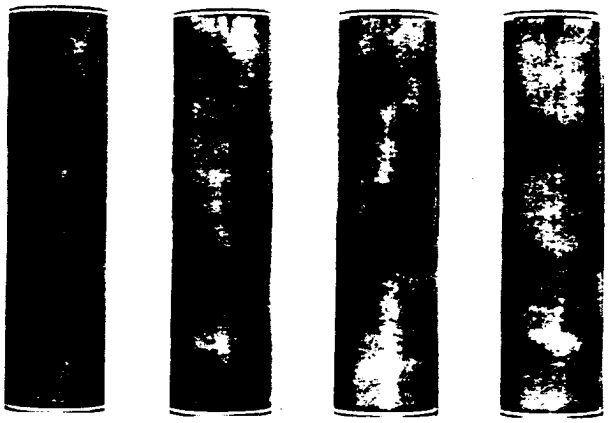

FIG. 3. Spiral turbulence with $\Gamma \cong 73$, $R_o = -3000$, $R_i = 950$, and outer cylinder rotating counterclockwise viewed from above. The turbulent band always turns in the direction of rotation of the outer cylinder. (a) and (b) have rigid upper boundaries, (c) and (d) have free upper boundaries. In (a) and (c) the spirals propagate downward and have lower pitch at the top. In (b) and (d) the spirals propagate upward and have lower pitch at the bottom. There is a substantial average pitch difference between (c) and (d) as discussed in the text. Typical pitch angles for case (b) are $19° \pm 1°$ at the bottom and $44° \pm 6°$ at the top, while for (d) they are $16° \pm 0.5°$ at the bottom and $29° \pm 2°$ at the top.

latter case it wraps around 3 times. In all of these cases the spiral pitch persisted over many hours of observation and was reproducible from run to run.

We shall now attempt a simple phase-dynamics approach to describe the observed pitch of the turbulent spiral and its variations, compatible with the symmetries of the problem.

Let $\varphi(z,t)$ be the mean azimuthal position of the spiral at height z and time t. We treat φ as a real quantity, its periodicity does not matter for the present purpose. The quantity φ is a phase in the sense that a uniform shift of φ has no dynamical effect, because of the axisymmetry of Taylor-Couette flow. The simplest possible form of a phase equation then takes the same form as that considered by Pocheau *et al.*,[11] for representing the effect of transverse flow on Rayleigh-Benard roll structure, namely,

$$\varphi_t + v\varphi_z = D\varphi_{zz} . \tag{1}$$

We shall postpone considerations of boundary conditions, and note that Eq. (1) has a family of solutions

$$\varphi = w(vt - z)/v + \Phi(z) , \tag{2}$$

where w is a constant of integration and v is the apparent axial velocity of the spiral in the laboratory frame. $\Phi(z)$ is considered below. The value of the pitch is undetermined, as is the wave number of the Rayleigh-Benard rolls in the phase equation of Ref. 11. The absolute value of the pitch should be allowed to vary in a band, as the roll wave number. This can be taken into account[11] by the introduction of a pitch dependence in D [cf. (1)]. We shall neglect this in our simple approach, as well as any velocity dependence on pitch. The function $\Phi(z)$ in (2) is the solution of $v\Phi_z = D\Phi_{zz}$ and thus of the form

$$\Phi(z) = \varphi_0 \exp(vz/D) . \tag{3}$$

The only boundary conditions compatible with phase invariance are $\varphi_z = \alpha$ at one end (say $z = 0$) and $\varphi_z = \beta$ at the other end ($z = L$). Parameters α and β, which describe the locally imposed pitch, could be computed in principle within the framework of a complete amplitude equation. Similar coefficients have been calculated by Cross[12] in a different context. Those terms should take into account the interaction between the Ekman layer and the finite amplitude solution.

We do not expect α and β to be the same, because of the structure of turbulence within the spiral. The observed splitting of a spot into two, one moving upwards, one downwards, reflects itself in the end in the existence of spirals of either helicity. It corresponds to a spontaneous axial symmetry breaking, which should be associated with a difference in the internal structure of the spots, made of progressive finite amplitude waves moving axially in either direction. As the fluid outside the spiral is linearly stable against those waves, they only propagate within spiral boundaries, being emitted at one side and absorbed at the other. This view is consistent with the observed asymmetry between leading and trailing edges of the spiral azimuthal profile.[4] Consequently, waves are emitted at one end of the spiral and absorbed at the other, which leads to α being different from β. A full picture would need an extension of the results in Ref. 6 to complex amplitudes of progressive waves.

We note that the same symmetries as above would be present for spiraling Taylor vortices.[7,8] There too the pitch would be nonuniform, at least for large aspect ratios. On the other hand, the subtle dependence of wavelength (here pitch) upon boundary conditions[13] for steady structures such as Rayleigh-Benard rolls near threshold, does not seem to be relevant for inclined Taylor vortices. This is because their phase is always increasing or decreasing when measured at the boundary. Thus this phase cannot be taken as a relevant constant parameter for constraining the wavelength of the structure. The general solution of Eq. (2) is thus

$$\varphi(z,t) = w(vt - z)/v + \varphi_0 \exp(vz/D) . \tag{4}$$

Here φ_0 and w are determined by boundary conditions at $z = 0$ and $z = L$,

$$\varphi_0 = \frac{D}{v} \frac{\alpha - \beta}{1 - \exp(vL/D)} , \quad \frac{w}{v} = \varphi_0 \frac{v}{D} - \alpha . \tag{5}$$

There is then a continuous variation of the pitch φ_z between α and β. The experimental results show that $\alpha \neq \beta$,

generically. If $\alpha = \beta$, then from (5), $\varphi_0 = 0$ and one obtains the solution of constant pitch $\varphi(z,t) = -a(vt - z)$. We note that Eq. (1) is invariant under the symmetry

$$\begin{pmatrix} z \to -z \\ v \to -v \end{pmatrix},$$

which relates two possible spirals of opposite helicity. This, however, also interchanges boundary conditions and therefore a spiral that in one helicity is compressed at the bottom and expanded at the top shows the opposite behavior in the other helicity. These features are evident in the experimental data.

However, once the symmetry between bottom and top is broken, as in the case when the top interface is a free surface and the bottom one rigid, there is no reason based on symmetry that the two spirals of opposite helicity are related. For the free-rigid case, this is what the data show. The data moreover show that for one of the helicities the pitch is relatively insensitive to whether the upper surface is rigid or free.

Phase dynamics thus provides a simple framework in which to discuss the pitch of spiral turbulence, its axial variation, and dependence on boundary conditions.

A final remark is the following: As reported above, at $R_o = -8000$ a simple spiral pattern only emerges at low aspect ratio. There is an apparent contradiction between this result and the stable spiral solutions of Eq. (1), which exist at any cylinder length L. However, the greater L, the less stable the spiral becomes, because the least stable perturbation decays as $\exp(-D\pi^2/L^2)t$. We conjecture that for large aspect ratio the spiral becomes unstable against a secondary instability, not included in the phase dynamics approach, and which involves coupling with complex secondary flow.[14] This conjecture is reinforced by the fact that the typical correlation length for a broken turbulent spiral is of the order of the cylinder diameter, which also characterizes the large scale flows.

This work was supported by the Office of Naval Research (Contract No. N00014-86-K-0071), the Department of Energy (Contract No. DE-FG02-88ER13916.A000), and by a CNRS Programme International de Cooperation Scientifique.

---

[a]Permanent address: Laboratoire de Physique Statistique, associé CNRS, Ecole Normale Supérieure, 24, rue Lhomond, 75005 Paris, France.

[1]R. P. Feynman, *Lecture Notes in Physics* (Addison-Wesley, Reading, MA, 1964), Vol. 2.

[2]C. D. Andereck, S. S. Liu, and H. L. Swinney, J. Fluid Mech. **164**, 155 (1986).

[3]D. Coles, J. Fluid Mech. **21**, 385 (1965).

[4]C. W. Van Atta, J. Fluid Mech. **25**, 495 (1966). See also D. Coles and C. W. Van Atta, Phys. Fluids **10**, S120 (1967); D. Coles and C. W. Van Atta, AIAA J. **4**, 1969 (1966).

[5]A. K. M. F. Hussein, Phys. Fluids **26**, 2816 (1983), and references therein.

[6]Y. Pomeau, Physica (Amsterdam) D **23**, 1 (1986), and in Proceedings of the Conference on Fluctuations and Instabilities, Chile, 1987, edited by E. Tirapegui and L. Villaroel (Reidel, Dordrecht, to be published).

[7]P. Hall, Phys. Rev. A **29**, 2921 (1984).

[8]P. Tabeling, J. Phys. Paris, Lett. **44**, L665 (1983); H. Brand and M. C. Cross, Phys. Rev. A **27**, 1237 (1983).

[9]A. Davey, L. M. Hocking, and K. Stewartson, J. Fluid Mech. **63**, 529 (1974).

[10]G. W. Baxter and C. D. Andereck, Phys. Rev. Lett. **57**, 3046 (1986).

[11]A. Pocheau, V. Croquette, P. Le Gal, and C. Poitou, Europhys. Lett. **3**, 915 (1987).

[12]M. C. Cross, Phys. Rev. Lett. **57**, 2935 (1986).

[13]Y. Pomeau and S. Zaleski, J. Phys. Paris, Lett. **44**, 135 (1983); M. C. Cross, P. G. Daniels, P. C. Hohenberg, and E. D. Siggia, J. Fluid Mech. **127**, 155 (1983).

[14]The explicit coupling between large scale flow and phase dynamics in a Rayleigh-Benard system at low to moderate Prandtl number has been considered by A. Pocheau, C.R. Acad. Sci. **306**, 331 (1988), and by A. C. Newell, in *Propagation in Nonequilibrium Systems*, edited by J. E. Wesfreid, H. R. Brand, P. Manneville, G. Albinet, and N. Boccara (Springer-Verlag, Berlin, 1988), p. 122.

Eur. J. Mech., B/Fluids, 10, n° 2 - Suppl., 221-226, 1991

Spiral turbulence: development and steady state properties

J. HEGSETH

S.P.S.R.M.-C.E.N. Saclay, 91191 Gif-sur-Yvette Cedex, France

C. D. ANDERECK and F. HAYOT

Department of Physics, Ohio State University,
174, West 18th Avenue, Columbus, Ohio 43210, U.S.A.

Y. POMEAU

Laboratoire de Physique Statistique, associé C.N.R.S., École Normale Supérieure,
24, rue Lhomond, 75005 Paris, France

Abstract. We present observations and measurements of a non-uniform pitch of the turbulent spiral in long geometries and discuss its dependence on boundary conditions at the cylinder ends, the helicity of the spiral, and the sense of rotation of the outer cylinder. We attempt to describe these results within the framework of phase dynamics which is applied here for the first time -we believe- to a structure with sustained microscale turbulence. We also discuss the influence of secondary flow on the azimuthal and axial width of the spiral and suggest that the small scale turbulence consists of propagating finite amplitude nonlinear waves.

Spiral turbulence consists of laminar and turbulent regions in Taylor-Couette flow which coexist to form a spiral (see Figure 1a). It occurs in the coaxial cylinder system when the outer cylinder rotates rapidly while the inner cylinder rotates in the opposite sense at a lower rate (large $|-R_o|$ and a comparatively low R_i, where R_i (R_o) is the inner (outer) cylinder Reynolds number based on the gap between the cylinders, d, and the cylinder velocity [Andereck et al, 1986]). Spiral turbulence is particularly interesting because it mixes small scale (or microscale) turbulence and a well ordered structure at large scales, i.e. it is a coherent turbulent structure. Furthermore, this structure occurs in a confined system, allowing the study of turbulence without many of the difficulties found in open flow systems. The observation that the pitch varies along the axis fits well into a phase dynamics approach, which to our knowledge is here applied for the first time to a situation with sustained microscale turbulence. This simplified approach is in the spirit of Feynman [Feynman, 1964] "to find the qualitative content of the Navier-Stokes equations." We also show that the finite azimuthal width [Coles, 1965] [Van Atta, 1966] of the turbulent spiral is a result of the subcritical character of the flow and the bounded azimuthal geometry of the Taylor-Couette system.

The apparatus used here has been described elsewhere [Baxter and Andereck, 1986] [Hegseth et al, 1989]. We have performed perturbation experiments in the hysteretic regime in which a small amount of fluid is quickly injected through a small hole into laminar Couette flow. The initial axial and azimuthal

EUROPEAN JOURNAL OF MECHANICS, B FLUIDS, VOL. 10, N° 2-SUPPL., 1991
0997-7546/91/221 6/$ 2.60/

velocities of the spreading of the turbulent front were then determined [H et al, 1989]. We have also made space-time diagrams of the spiral [Mutabazi et al, 1990]. The light reflected from the visualized flow was focused onto an axially oriented line of 1024 pixels to be digitized once every 0.14 seconds.

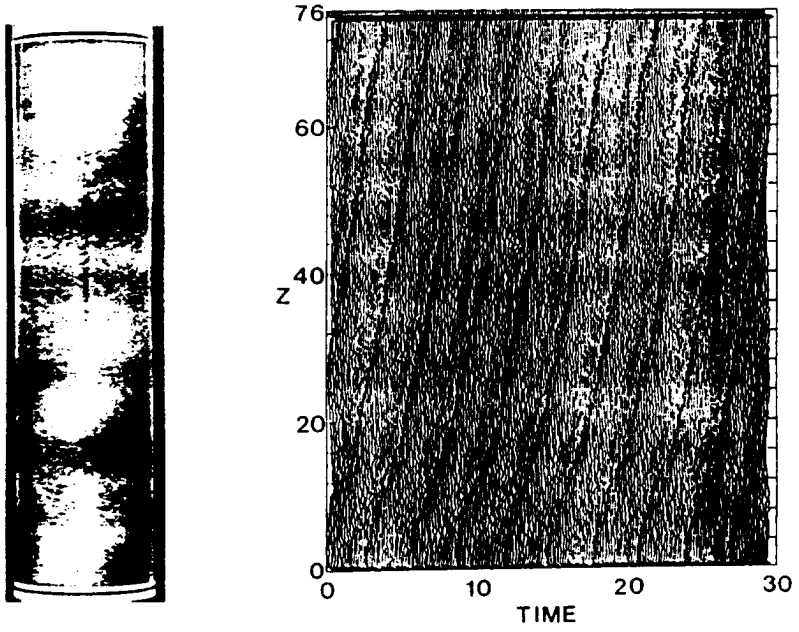

a b

Figure 1

a) Spiral turbulence with $\Gamma = 73$, $R_o = -3000$, $R_i = 950$, and outer cylinder rotating clockwise viewed from above. The turbulent band always turns in the direction of rotation of the outer cylinder. The boundaries on the top and bottom are rigid and the spiral appears to be traveling upward. b) Space-time diagram of spiral turbulence for the same configuration and parameters as in Figure 1a. Time is scaled by the outer cylinder rotation period and the axial position, Z, is scaled by the gap, d. The emitting side is at the bottom (axial position $\approx$0) and the absorbing side is at the top (axial position $\approx$76).

The laminar flow to spiral turbulence transition is characterized by large hysteretic effects [C, 1965] [A et al, 1986], which implies that this transition is a subcritical bifurcation. Subcritical bifurcations in flows with infinite domains can lead to either expanding or contracting turbulent domains in laminar flow [Pomeau, 1986]. This argument requires the existence of a potential functional in which there are at least two minima corresponding to a metastable (a local minimum but not a global minimum) and a stable state (the global minimum). The existence of such a potential functional is, however, an

uncommon occurrence in fluid dynamics. The case of spiral turbulence, as seen in the laboratory frame of reference, shows that this analysis does not hold since we have both an expanding turbulent domain at the front face of the spiral and a contracting turbulent domain at the rear face.

Coles and Van Atta [Coles and Van Atta, 1966] measured the 6 components of Reynolds stress as a function of the azimuth in the rest frame of the spiral at the mean radius. They found four components of Reynolds stress that are zero in the laminar region and increase to their maximum values in the center of the turbulent region. The other two components of Reynolds stress are negligibly small. This periodic variation in the Reynolds stress produces a periodic forcing on the mean flow. This suggests that a large scale Poiseuille flow in the laminar region is generated by the change in Reynolds stress in the turbulent region. A similar backflow generating process in weakly inclined supercritical Taylor vortices has been explicitly worked out by Hall [Hall, 1984]. Hall, who completed previous work [Tabeling, 1983] [Brand and Cross, 1983] on amplitude equations, found that the backflow is proportional to an integral over the azimuthal angle involving the square of the amplitude, which itself is proportional to the Reynolds stress. The theory for the subcritical case has not yet been worked out, but, the same basic mechanism is probably at work, and this allows for a qualitative understanding. The backflow counteracts the velocity of expansion of the turbulence until the latter stops, i.e., the backflow generated by the Reynolds stress slows down the mean flow until a transition to laminar flow occurs at the rear face. The turbulence generates a backflow which acts on the turbulence limiting its growth. Similar feedback effects have been found [Thual and Fauve, 1988] in subcritical transitions to nonlinear traveling waves using a fifth order Ginzburg-Landau equation. Thual and Fauve found that when a potential functional exists (which is the case when all the coefficients in this Ginzburg-Landau equation are real) the stable state would expand at the expense of the metastable state. In the case where a potential functional does not exist (when the third order and the fifth order coefficients are complex) they found a localized structure, i.e. the nonlinear traveling wave solution and the null solution coexist in spatially separated regions with a stationary interface separating the two. Other studies of the subcritical bifurcations in the Ginzburg-Landau equation show simular behavior [Thual and Fauve, 1990] [Van Saarloos and Hohenberg, 1990] [Hakim et al, 1990]. The turbulent flow in spiral turbulence, as seen in its rest frame, is such a localized structure which occurs after a subcritical transition. Thual and Fauve reasoned that the localization was due to the amplitude-dependence of the wave frequency (which is a general property of nonlinear waves). The spatial shape of an amplitude envelope of a pulse of waves affects the frequencies of the waves in the pulse which in turn affects the pulse's shape. This feedback between the pulse's shape and wave frequencies works to limit the growth of the pulse. Davey et al [Davey et al, 1974] studied weakly nonlinear three dimensional disturbances in Poiseuille flow and found that spatial variations in the amplitude of these disturbances generate pressure gradients. They found the lowest order Ginzburg-Landau equation for a special case. The induced pressure gradient, in this special case, is shown to contribute to the complex constant which couples the amplitude of the nonlinear wave solution to its frequency. This suggests that there may be a physical connection between the feedback mechanism of the backflow described above and the feedback mechanism of Thual and Fauve for localized structures in subcritical phenomena.

We found stable spirals of both helicities in a wide range of R_o and R_i at the lower aspect ratios $\Gamma = 30$ and a fixed upper surface (Γ, the aspect ratio, is the radio of the cylinder length, L, to the gap, d). We found that the pitch stays constant at $\sim 30°$ for these R_o's and R_i's. This, however, was not the case for larger aspect ratios, in fact, at $\Gamma = 73$ persistent spirals occurred only for $R_o = -3000$. At $R_o = -8000$ no large scale coherent structure was seen at any R_i. At this R_o there were local

spiral-like structures with the helicity changing sign over an axial distance of the order of the cylinder diameters. Because these spiral-like structures would not alway connect to make V-shaped structures, these turbulent patches formed a "broken" spiral pattern. Sometimes the turbulence would not form local spirals or V-shaped structures, just turbulent patches.

Since we are interested in simple spirals we made measurements only at $R_o = -3000$ for large aspect ratios. We found that these spirals always have a pitch that varied with axial position as shown in Figure 1. The manner in which this variation occurred depended on the end boundary condition, the helicity of the spiral, and the sense of rotation of the spiral [H et al, 1989]. We found that the pitch is always lower near the end away from which the spiral appears to be moving. With a free upper surface the pitch varies in the same manner but the variation in the pitch is not as large and there are also differences in the average pitch [H et al, 1989].

We videotaped the azimuthal and axial expansions of a spot created at the midpoint of the cylinder (to prevent end conditions from affecting the front velocity) in the rest frame of the spiral. After the spot is generated by the perturbation it initially expands much faster (~2 times) in the azimuthal direction than in the axial direction [H et al, 1989]. The turbulent spot stops its azimuthal expansion as soon as it is about as wide as half of the perimeter length. This is evidently the width at which there is sufficient backflow to stop the spot's growth [H et al, 1989]. The spot, however, continues to grow along the cylinder axis for ~2 seconds, when it breaks into two spots separated axially. These two spots continue to propagate axially in the rest frame of the spiral, with their widths always remaining approximately that of the final spiral. At still later times these spots propagate both axially and azimuthally. They may also undergo further splitting and subsequent growth. The different pieces eventually connect in a complicated process and construct a spiral. The presence of axial propagation shows that the backflow has in fact a complex three-dimensional structure. This is consistent with the measurements of Coles and Van Atta [C & V, 1966] which show both a periodic axial mean flow and a periodic azimuthal mean flow of comparable magnitude in the rest frame of the spiral at the mean radius. This mean flow is tangential to the spiral at the leading edge and nearly normal to the spiral at the trailing edge with a stagnation point in the center of the turbulence. This shows that the Reynolds stress drives both a mean azimuthal and a mean axial flow. The axial backflow limits the growth of the spot axially just as the azimuthal backflow limits the growth of the spot azimuthally. The boundary conditions at the ends of the spiral change this configuration somewhat, i.e., the axial mean flow is zero at a rigid boundary and a free surface. Figures 1b shows a space-time diagram corresponding to the picture in Figure 1a. The darker regions show the leading edge of the spiral and the changes in slope of these phase lines indicate changes in the axial speed of the spiral. The end effects must modify the periodicity of the axial component of the mean flow and this in turn may generate a larger scale mean flow. It has been found [Pocheau et al, 1987] that mean flows modify the wavelength of Rayleigh-Benard rolls and a similar mechanism may be working here to change the pitch. This suggests that a simple phase dynamics approach, similar to the one used for Rayleigh-Benard rolls, may be used here to describe the observed pitch of the turbulent spiral and its variations.

We first introduce the real phase field $\varphi(z,t)$, which is the mean azimuthal position of the periodic spiral at height z and time t. The quantity φ is a phase in the sense that a uniform shift of φ has no dynamical effect on the periodic turbulent spiral pattern because of the axisymmetry of Taylor-Couette flow. We assume that the phase equation has the same form as considered previously [P et al, 1987], [Brand, 1985] i.e.

$$\varphi_t + v\varphi_z = D\varphi_{zz}.$$

Equation (1) has a family of solutions consisting of the base state (no phase variation) plus a phase variation, i.e.

$$\varphi = \frac{w}{v}(vt - z) + \Phi(z) \qquad 2$$

where w is a constant of integration (which we would identify as the frequency of the spiral in its base state) and v is the apparent axial velocity of the spiral in the laboratory frame when there is no phase variation. Equation (1) expresses the fact that the spiral relaxes diffusively in its rest frame. $\Phi(z)$, the variation of the phase, and the boundary conditions, which apparently cause the phase variation, are considered below. The value of the pitch is undetermined, as is the wave number of the Rayleigh-Benard rolls in the phase equation [P et al, 1987]. Just as the roll wave number is allowed to vary within the Eckhaus stable band [P et al, 1987], the absolute value of the pitch should be allowed to vary within a stable pitch band. This can be taken into account [P et al, 1987] by introducing a pitch dependence in D(cf (1)).

Because the phase can only be known to within an arbitrary constant it cannot be used as a boundary condition. However, as stated above, the pitch is undetermined and in fact the only boundary conditions compatible with phase invariance are $\varphi_z = \alpha$ at one end (say $z = 0$) and $\varphi_z = \beta$ at the other end ($z = L$). Parameters α and β describe the local pitch which the boundary conditions impose. α and β could, in principle, be computed within the framework of a complete amplitude equation. Cross [Cross, 1986] calculated similar coefficients in a different context.

The general solution of equation (1) is

$$\varphi(z,t) = \frac{w}{v}(vt - z) + \varphi_0 \exp\frac{v}{D}z. \qquad 3$$

Here φ_0 and w are determined by boundary conditions at $z = 0$ and $z = L$

$$\varphi_0 = \frac{D}{v}\frac{\alpha - \beta}{1 - \exp vL/D}, \quad \frac{w}{v} = \varphi_0\frac{v}{D} - \alpha. \qquad 4$$

This describes how the pitch, φ_z, varies continuously between α and β. The experimental results as shown in Figure 1 show that $\alpha \neq \beta$. If $\alpha = \beta$, then from (4), $\varphi_0 = 0$ and one obtains the solution of constant pitch $\varphi(z,t) = -\alpha(vt - z)$. Equation (1) is invariant under the symmetry $\binom{z \to -z}{v \to -v}$ which relates two possible spirals of opposite helicity. This symmetry operation also interchanges boundary conditions and therefore a spiral that in one helicity is compressed at the bottom and expanded at the top, shows the opposite behavior in the other helicity. These features are evident in the experimental data [H et al, 1989]. However, in the case when the top interface is a free surface and the bottom one rigid the above symmetry is broken and there is no reason based on symmetry for the two spirals of opposite helicity to be related. For the free-rigid case, this is what the data shows [H et al, 1989]. The data also shows that when the spiral appears to move upward the pitch is relatively insensitive to whether the upper surface is rigid or free [H et al. 1989].

We have argued that the large scale spiral structure is a result of the backflow limiting the growth of the turbulence in the axial and azimuthal directions. In the perturbation experiment we observed that the spot alway split into two parts, one moving upwards, one downwards. This splitting and subsequent propagation suggests that the two spots consist of progressive finite amplitude waves moving axially, in the rest frame of the spiral, in either direction. In other words, the initial spot which is made of up moving and down moving waves splits into two spots, one consisting primarily of up moving waves and the other consisting primarily of down moving waves. This separation of the two types of

waves corresponds to a spontaneous axial symmetry breaking. The final spiral which forms after a few minutes consists primarily of either up moving or down moving waves, which accounts for the existence of spirals of either helicity. As the fluid outside the spiral is linearly stable against these waves, they only propagate within the spiral boundaries, being emitted at one side and absorbed at the other. This view is consistent with the observed asymmetry between leading and trailing edges of the spiral azimuthal profile [V, 1966]. Consequently, waves are emitted at one end of the spiral and absorbed at the other, which leads to α being different from β. A full picture would need an extension of previous results [P, 1986] to complex amplitudes of progressive waves. Figure 1b illustrate the differences between the emitting side and the absorbing side. The difference is most pronounced when the free upper surface is an emitter [Hegseth, 1990].

In conclusion, we found that the pitch of the spiral is lower near the end away from which the spiral appears to be moving. Phase dynamics, for periodic structures with the symmetry of the spiral, gives a simple description of this pitch variation. We have visualized the initial spreading of the pattern and made space-time diagrams which, together with previous results, have given us a physical picture of the spiral. The Reynolds stress in the turbulence generates an azimuthal and axial backflow which limits the azimuthal and axial extent of the turbulence accounting for the spiral shape. The internal structure of the turbulence is evidently made of progressive finite amplitude waves that propagate either up or down along the axis with one end of the spiral being the emitter of the waves (the end with the compressed pitch) and the other end being the absorber of the waves (the end with expanded pitch).

References

C. D. Andereck, S. S. Liu, and H. L. Swinney, J. Fluid Mech. **164**, 155 (1986).

G. W. Baxter, C. D. Andereck, Phys. Rev. Lett. **26**, 1395 (1986).

H. R. Brand, M. C. Cross, Phys. Rev. A **27**, 1237 (1983).

H. R. Brand, Phys. Rev. A **31**, 3454 (1985).

D. Coles, J. Fluid Mech. **21**, 385 (1965).

D. Coles, C. W. Van Atta, AIAA J., **4**, 1969 (1966).

M. C. Cross, Phys. Rev. Lett. **57**, 2935 (1986).

A. Davey, L. M. Hocking, and K. Stewartson, J. Fluid Mech. **63**, 529 (1974).

R. P. Feynman, *Lecture Notes in Physics, Vol. II* (Addison-Wesley, Reading, 1964).

V. Hakim, P. Jakobsen, and Y. Pomeau, Europhys. Lett. **11**, 19 (1990).

P. Hall, Phys. Rev. A **29**, 2921 (1984).

J. J. Hegseth, C. D. Andereck, F. Hayot, and Y. Pomeau, Phys. Rev. Lett. **62**, 257 (1989).

J. Hegseth, *Spatiotemporal Patterns In Flow Between Two Independently Rotating Cylinders*, Ph.D. Thesis, Ohio State University (1990).

I. Mutabazi, J. J. Hegseth, C. D. Andereck, and J. E. Westfreid, Phys. Rev. Lett. **64**, 1729 (1990).

A. Pocheau, V. Croquette, P. LeGal, and C. Poitou, Europhys. Lett. **3**, 915 (1987).

Y. Pomeau, Physica D, **23**, 1, (1986).

P. Tabeling, J. Phys. Lett. (Paris) **44**, 665 (1983).

O. Thual, and S. Fauve, J. Phys. Lett. (Paris) **49**, 1829 (1988).

O. Thual, and S. Fauve, Phys. Rev. Lett. **64**, 282 (1990).

C. W. Van Atta, J. Fluid Mech. **25**, 495 (1966).

W. van Saarloos, and P. C. Hohenberg, Phys. Rev. Lett. **64**, 749 (1990).

Pattern formation in the flow between two horizontal coaxial cylinders with a partially filled gap

Innocent Mutabazi,* John J. Hegseth, and C. David Andereck
Department of Physics, Ohio State University, 174 West 18th Avenue, Columbus, Ohio 43210

Jose E. Wesfreid
Laboratoire d'Hydrodynamique et Mécanique Physique, Ecole Supérieure de Physique et de Chimie Industrielles de la Ville de Paris, 10 rue Vauquelin, 75231 Paris Cédex 05, France

(Received 29 February 1988)

Flow between two horizontal coaxial cylinders with a partially filled gap is subject to several types of centrifugal instabilities which lead to the formation of a variety of spatial patterns. An experimental investigation has shown that there are five distinct branches of primary instabilities occurring in the system and that four codimension-2 points are easily reached. Theoretical predictions are in qualitative agreement with the observations.

I. INTRODUCTION

The behavior of systems far from equilibrium has been the subject of intense investigation over the last several years. Of particular interest has been the manner in which spatial patterns arise. Pattern formation may be driven by a wide variety of mechanisms, including temperature gradients, concentration gradients, and centrifugal effects. Centrifugal instabilities[1,2] occur in flow with curved streamlines, and they play an important role in many problems of practical importance. Two of the best known examples are the Taylor-Couette instabilities, which occur in the flow between two concentric rotating cylinders, and the Taylor-Gortler instabilities, which occur in the boundary layer on a concave wall. The Taylor-Couette and Taylor-Gortler instabilities have been extensively investigated both theoretically and experimentally (see Refs. 3–5 and references therein). However, a third class, the Dean instabilities,[6] which occur in the presence of a pressure gradient along a curved channel (Poiseuille flow), has received much less attention.

Here, we present a simple system in which it is possible to realize the main centrifugal instabilities by an appropriate choice of control parameters. We consider two horizontal coaxial cylinders of radii r_i and r_o, which rotate independently with angular velocities Ω_i and Ω_o for the inner and the outer cylinder, respectively. When the gap between the cylinders is completely filled with fluid, we have the classical Taylor-Couette problem. When the gap is partially filled and both cylinders rotate there exists a combination of Taylor-Couette flow (caused by the differential rotation of the cylinders) and Poiseuille flow (caused by the backflow induced by the presence of the horizontal free surfaces). As the system control parameters are varied, the base flow instabilities will change from those associated with Taylor-Couette to those associated with Dean. Under some conditions one might expect to see flow patterns that result from competition between instabilities. In other cases boundary layers on the curved surfaces may give rise to Taylor-Gortler instabilities.[7] We will not discuss the last any further since boundary layer instabilities are apparently not dominant for the range of system parameters chosen. The relevant control parameters are the ratio of angular velocities $\mu=\Omega_o/\Omega_i$ and the Taylor number.

In Sec. II we will summarize the few related experimental and theoretical results which have been reported so far. In Sec. III we describe our experimental procedure and in Sec. IV we report the results obtained. Section V is a comparison of the experimental results with the present theory. Finally, we will conclude with suggested directions for future work.

II. PREVIOUS WORK

The flow between two horizontal coaxial cylinders with a partially filled gap was first investigated by Brewster and Nissan[8] in 1958. They deduced approximate velocity fields for laminar flow with only the inner cylinder rotating, and they measured the critical angular velocity and the wave number of the resulting rolls. In 1959, Brewster, Grosberg, and Nissan[9] considered the critical conditions for the formation of vortices between the cylinders in three cases: when the gap is filled with fluid and the flow is caused by the rotation of the inner cylinder (Taylor-Couette problem), when the flow is produced by pumping around the annular space (Dean problem), and when the liquid is driven by the rotation of the inner cylinder and forced to reverse its flow at a free surface. Their results for the Dean problem were in satisfactory agreement with the theoretical values for the threshold of the instability and the wave number of the vortices. They considered also the combination of the pumping of fluid around the annular space and the rotation of the inner cylinder. They obtained the interesting result that, in the neighborhood of a particular value of the ratio of the pumping flow rate to the rotation flow rate, the critical value of the control parameter has an abrupt change, and

the wavelength of the vortices has a discontinuity. The competition between the destabilization of the Couette and Poiseuille layers in the basic flow was invoked to explain this anomalous behavior.

DiPrima,[10] using a Galerkin method, calculated the stability diagram for the combined Couette-Poiseuille problem and introduced a parameter λ which measures the relative importance of the pumping flow compared to the flow driven by the rotation of the inner cylinder. He found that the neutral stability curve (using the principle of exchange of stabilities, which assumes that the instability that occurs is stationary) exhibits a discontinuity for $\lambda=\lambda_c=-3.667$. Hughes and Reid[11] found, by numerically integrating the stability equations, that, in the vicinity of λ_c, the marginal stability curve presents two minima with different values of wave numbers. Raney and Chang[12] relaxed the restrictions of the principle of exchange of stabilities and found that, in the vicinity of λ_c, the marginal stability curve consisted of two stationary loops connected by an oscillatory branch at the absolute minimum of the control parameter. They came to the conclusion that in the neighborhood of λ_c, an oscillatory instability might occur. No experimental verification of this result has been reported so far, perhaps because of the difficulty of realizing a well-controlled flow with external pumping.

Mutabazi, Peerhossaini, and Wesfreid[7] have reported experimental results for the case of a partially filled gap with only the inner cylinder rotating. They emphasized the oscillatory character of the observed structures and found a lower value of the threshold of instability than that claimed by Brewster and Nissan.[8] In another paper Mutabazi *et al.*,[13] describe the quantitative characteristics of the oscillatory structures. Recently, Mutabazi, Normand, Peerhossaini, and Wesfreid[14] have solved the linear stability problem for axisymmetric perturbations in the flow between two co-rotating cylinders with a partially filled gap. They found that at the instability threshold in such a system it is possible to detect oscillatory or stationary rolls depending on the ratio of the angular velocities μ. The intersection points (codimension-2 points) of the oscillatory and stationary branches in the diagram (μ, T_c), where T_c is the critical value of the Taylor number considered as the control parameter of the flow, were predicted to be experimentally accessible. We report here the results of an initial test of these predictions.

III. EXPERIMENTAL PARAMETERS AND PROCEDURES

The system considered in our experiment has been previously used in the investigation of Taylor-Couette instabilities and is described in Baxter and Andereck.[15] It consists of two horizontal coaxial cylinders, the inner one made of black Delrin plastic (radius $r_i=5.262$ cm) and the outer one made of polished Plexiglas (radius $r_o=5.965$ cm). So the radius ratio $\eta=0.882$ and the gap is given by $d=r_o-r_i=0.703$ cm. Teflon rings attached to the outer cylinder define the left and right boundaries for the liquid and produce an aspect ratio (working space length/gap) $\Gamma=68$. The cylinders were driven by Compumotor stepping motors with a rotation-rate resolution of 0.001 Hz. The angular velocities Ω_i and Ω_o of the inner and outer cylinders are scaled in terms of Reynolds numbers $R_i=\Omega_i r_i d/\nu$ and $R_o=\Omega_o r_o d/\nu$, where ν is the kinematic viscosity of the working fluid. As shown in Fig. 1, the gap is filled only about $\frac{2}{3}$ full with distilled water to avoid communication between the two sides of the system. The rotation of the cylinders typically induces no significant film on the walls. The experiments were performed in a controlled environment room; the fluid temperature varied by no more than 0.1 °C. Visualization of the flow states has been accomplished with a mixture of 1% by volume Kalliroscope AQ1000 in water. Interpretation of structures observed in the flow with polymeric flakes is based on the following: a dark area indicates flow along the observer's line of sight, while a light area indicates flow perpendicular to the line of sight. However, the asymmetry between the radial inflow and outflow boundaries can produce confusion between the wavelength and roll size of patterns if one boundary is much less distinct than the other.

Data acquisition involved two techniques. Flow frequencies were determined from a single point time series obtained with laser light reflected off the Kalliroscope flakes onto a photodiode detector. The resulting signal was digitized for processing with a fast Fourier transform (FFT) routine. Spatial data were obtained by eye and by using a 28–85-mm variable focal length lens to form an image of the visualized flow on a 1024-pixel charge-coupled device (CCD) linear array interfaced through CAMAC to the computer. The line of 1024 pixels is oriented parallel to the cylinder axis. The output consists of intensity maxima and minima which correspond to the centers of the rolls and inflow and outflow boundaries, respectively. Analysis of the intensity plots yields the vortex sizes and hence the wavelength of the structure.

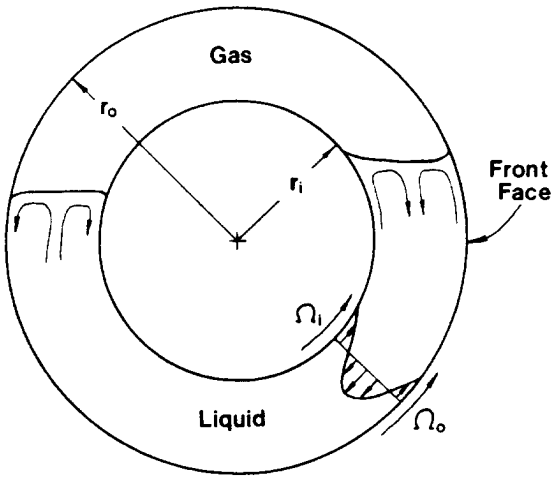

FIG. 1. Schematic cross section of the apparatus. The "front face" is defined to mean that the observer sees the inner cylinder rotating upward as shown. The outer cylinder can rotate in either direction. Qualitative pictures of the flow near the free surfaces are shown, along with the fully developed velocity profile away from these surfaces.

IV. RESULTS

The transitions from unperturbed flow to the various critical states are summarized in Fig. 2. The observations were made from the front face (as defined in Fig. 1), while the rear face was viewed simultaneously, when needed, by a video camera and monitor. The system control parameters are the Reynolds numbers R_i and R_o (defined above), respectively, for the inner and the outer cylinders [the base flow may also be specified by the angular velocities ratio μ and the Taylor number defined as $T=(\Omega_i r_i d/\nu)(d/r_i)^{1/2}$ but the first pair of parameters has the advantage of being more easily controlled in an experiment]. For our experiments the two sets of parameters are related as follows: $\mu=0.882R_o/R_i$ and $T=0.366R_i$ (or $R_i=2.736T$ and $R_o=3.102\mu T$). In presenting our results we will scale wavelengths by d, velocities by ν/d, and frequencies by ν/d^2.

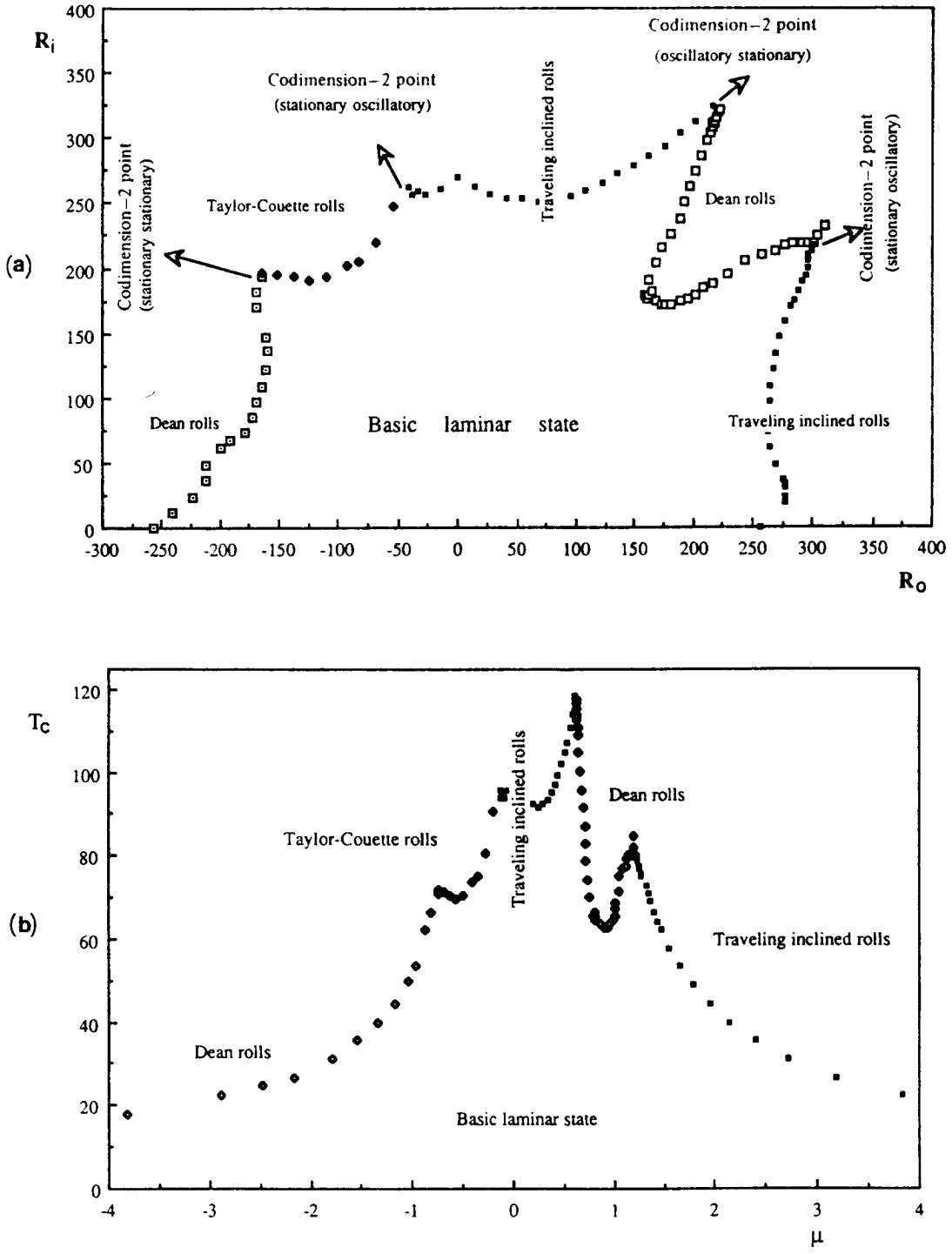

FIG. 2. (a) Diagram of primary flow transitions in the (R_0, R_i) space. (b) Diagram of primary flow transitions in the (μ, T) space.

A. Base flow

The fully developed base flow between two infinite horizontal coaxial cylinders with a partially filled gap is azimuthal (except in the neighborhood of the free surfaces) if the entrance angle θ_e is small compared to the filling angle θ_f ($\approx 4\pi/3$ for our experiment). The entrance angle is given, for $\mu=0$, by[13] $\theta_e=\Omega_i d^2/9\pi^2\nu=2f_i/9\pi$, where f_i is the scaled frequency of rotation of the inner cylinder. Then the condition for assuming fully developed azimuthal base flow is $f_i \ll f_o=9\pi\theta_f/2$. For our experimental case $f_o=67.1$. We have worked in the range $0.5\le f_i\le 15.5$, with $f_c\le 7.2$ for all the transitions. At these rotation frequencies we can consider our base flow to be essentially azimuthal. The azimuthal velocity profile is given by[16] $V(r)=Ar\ln r+Br+C/r$, where $A=(1/2\rho\nu)\partial P/\partial\theta$ is related to the azimuthal pressure gradient and the coefficients B and C are obtained from the boundary conditions on the cylindrical walls. The flow rate conservation across a given radial section (θ=constant plane) gives the value of A. We get

$$A=\frac{2[2(\Omega_i-\Omega_o)r_i^2r_o^2\ln(r_o/r_i)+(\Omega_o r_o^2-\Omega_i r_i^2)(r_o^2-r_i^2)]}{(r_o^2-r_i^2)^2-4r_i^2r_o^2[\ln(r_o/r_i)]^2}, \tag{1}$$

$$B=\frac{(\Omega_o r_o^2-\Omega_i r_i^2)-A(r_o^2\ln r_o-r_i^2\ln r_i)}{r_o^2-r_i^2}, \tag{2}$$

$$C=\frac{[\Omega_i-\Omega_o+A\ln(r_o/r_i)]r_i^2r_o^2}{r_o^2-r_i^2}. \tag{3}$$

The coefficient A in $V(r)$ is zero in the classical Couette problem (fully filled gap). The velocity profile is a superposition of the Couette flow imposed by the rotation and the Poiseuille flow in a curved channel produced by the azimuthal pressure gradient. This superposition is well seen in the small-gap approximation. For the purposes of our experiment, we will use the small-gap approximation ($\eta\to 1$) and introduce a characteristic velocity ν/d to obtain the quadratic trinomial in x [with $x=(r-r_i)/d$]:

$$V(x)=3(R_i+R_o)x^2-2(2R_i+R_o)x+R_i. \tag{4}$$

This profile possesses up to two nodal surfaces (surfaces of zero azimuthal velocity) between the two cylinders situated at

$$x=\frac{2R_i+R_o\pm\sqrt{R_i^2+R_iR_o+R_o^2}}{3(R_i+R_o)}. \tag{5}$$

Figure 3 gives the velocity profiles for different values of the parameters R_i and R_o. Examination of these base flows reveals the possibility for centrifugal instabilities. To a first approximation the centrifugally unstable regions will be those in which the inviscid Rayleigh circulation criterion ($d/dr\,|\,\Omega r^2\,|<0$) holds, as noted in the figure. The presence of viscosity modifies this simple picture, but the basic instabilities remain. These have been examined numerically by Mutabazi *et al.*[14]

B. Stationary patterns

For R_o in the ranges of -257--35 and 160–257, the base flow is typically unstable to formation of a pattern of time-independent vortices. (The behavior near $R_i=0$ is rather different and will be discussed at length in Sec. IV E.) They have no significant azimuthal variation, except very near the free surfaces, and are of uniform size along the cylinder, with a dimensionless wavelength of the vortex pairs (defined as λ/d) of about 2.4 in the corotating case and approximately 2.45 in the counterrotating flows [see Figs. 4(a) and 4(b)]. The patterns for $-257<R_o<-175$ and for $160<R_o<270$ are clearly observed and therefore are most likely forming near the outer cylinder. The analysis of the approximate base flow profile suggests that these are Dean rolls.[14] For $-257\le R_o\le -170$, Rayleigh's criterion applied to the profile of Fig. 3(a) shows that the potentially unstable layer in the gap is contained within the Poiseuille flow region, which will therefore give rise to Dean rolls. For $160\le R_o\le 270$ numerical results[14] show that the rolls should be confined to the outer unstable layer, which again is part of a Poiseuille flow region, indicating these are also Dean rolls. Slightly beyond the onset of the instability, subharmonics intervene, leading to rather complex patterns.

For $-170<R_o<-35$, the rolls are difficult to observe, being apparently localized near the inner cylinder, and they do not strengthen significantly as R_i is increased. These are probably Taylor-Couette vortices [Fig. 4(c)] because the destabilized layer near the inner cylinder has a velocity profile [see Fig. 3(c)] which is Couette-like rather than Poiseuille-like. The transition between these theoretical profiles occurs near the experimental codimension-2 point at $R_i=197$ and $R_o=166$. For R_o from -175 to -170, the rolls appear first in the rear face. This branch has been explored in two ways, both by fixing R_o and changing R_i, and by fixing R_i and changing R_o, and the results were essentially the same. The Dean rolls and Taylor-Couette rolls are both unstable to time-dependent patterns (traveling inclined rolls; see Sec. IV B) when R_i is increased for fixed R_o, except, of course, for

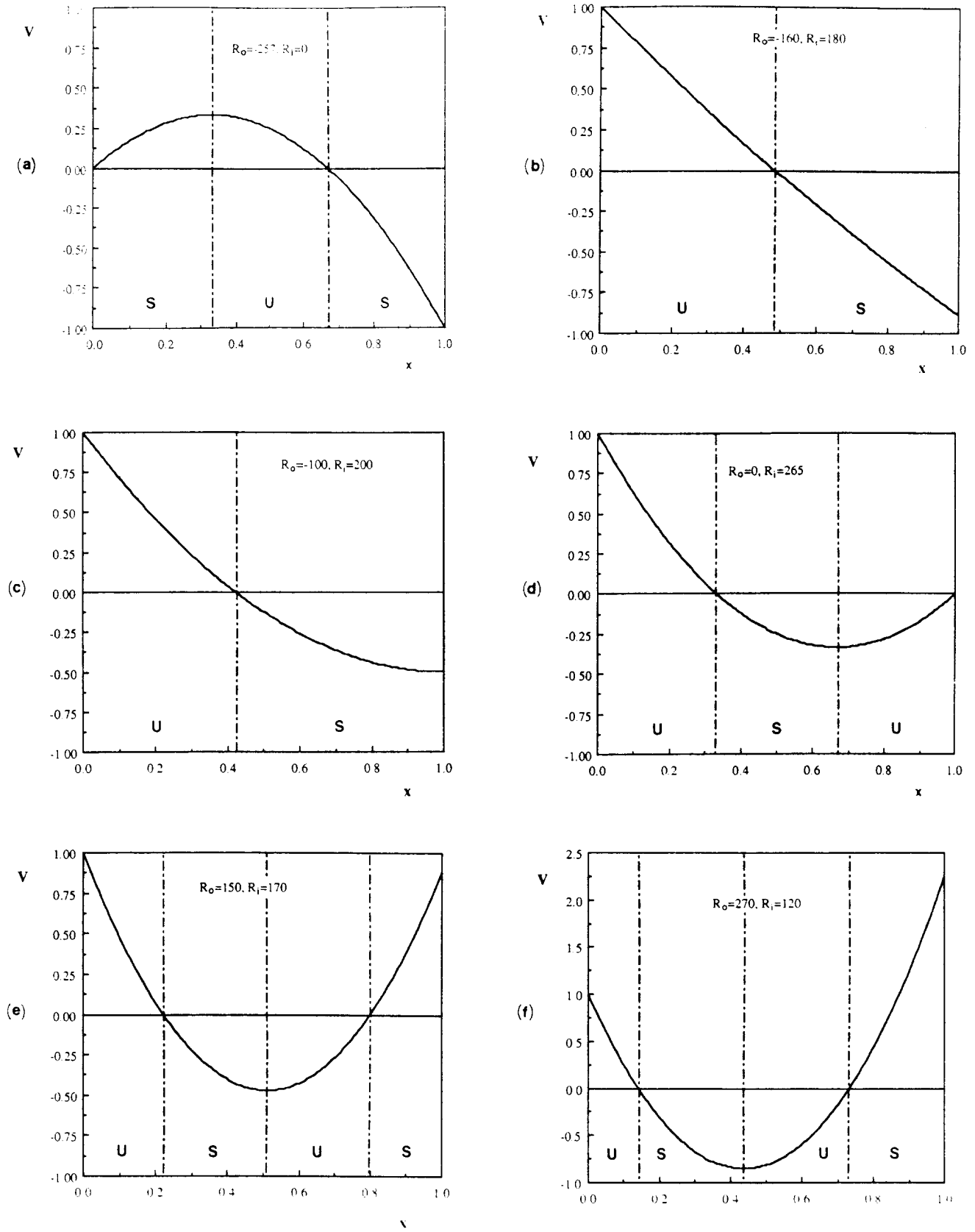

FIG. 3. Base flow velocity distributions near instability thresholds (flow patterns arising from the base flow instabilities are indicated in parentheses): (a) only outer cylinder rotating, (b) counter-rotating cylinders (Dean rolls), (c) counter-rotating cylinders (Taylor-Couette rolls), (d) only inner cylinder rotating (traveling inclined rolls), (e) co-rotating cylinders (Dean rolls), (f) co-rotating cylinders (traveling inclined rolls). *S* and *U* indicate Rayleigh stable and unstable layers, respectively. The fluid velocities have been normalized to the outer cylinder velocity in (a) and the inner cylinder velocity in (b)–(f).

R_o from 150 to 200, in which case the base flow is regained before traveling rolls form.

C. Time-dependent patterns

Traveling spirals (or, technically, traveling inclined cells, since a complete spiral is not really possible owing to the presence of the free surfaces) [Fig. 4(c)] appear at threshold for R_o in the ranges -30–210 and 265–300. They form at an angle of about 20° with the vertical and propagate along the cylinder axis with a constant velocity. The dimensionless roll propagation velocity, scaled by ν/d, is approximately 29 (0.4 cm/sec). Figure 5 shows

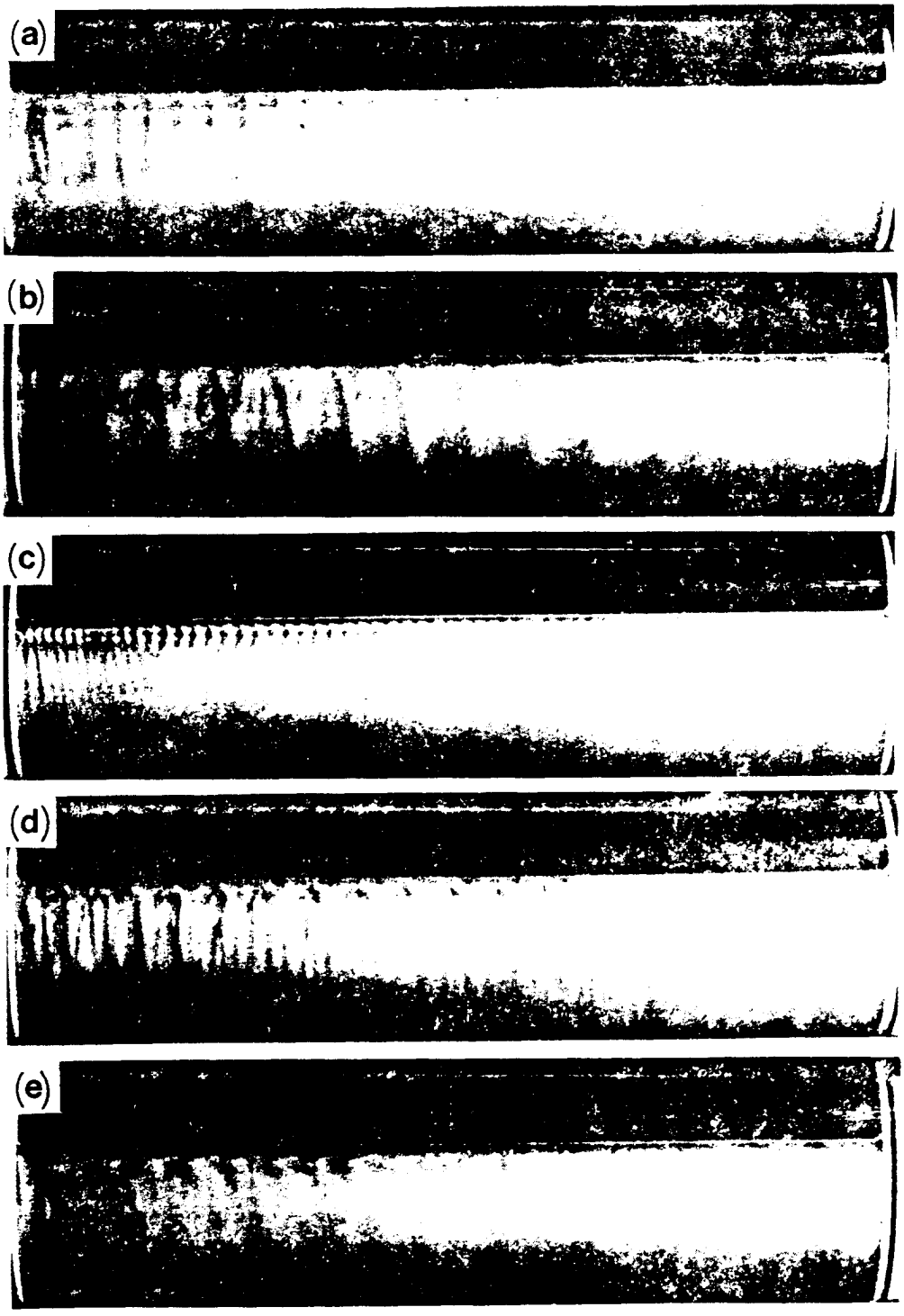

FIG. 4. States observed for different values of control parameters: (a) Dean rolls, $R_o = 220$, $R_i = 195$, (b) Taylor-Couette rolls, $R_o = -136$, $R_i = 252$, (c) inclined traveling rolls, $R_o = 70$, $R_i = 280$, (d) Dean rolls for only the outer cylinder rotating, $R_o = 320$, $R_i = 0$, (e) coexisting inclined and Dean rolls, $R_o = -45$, $R_i = 265$.

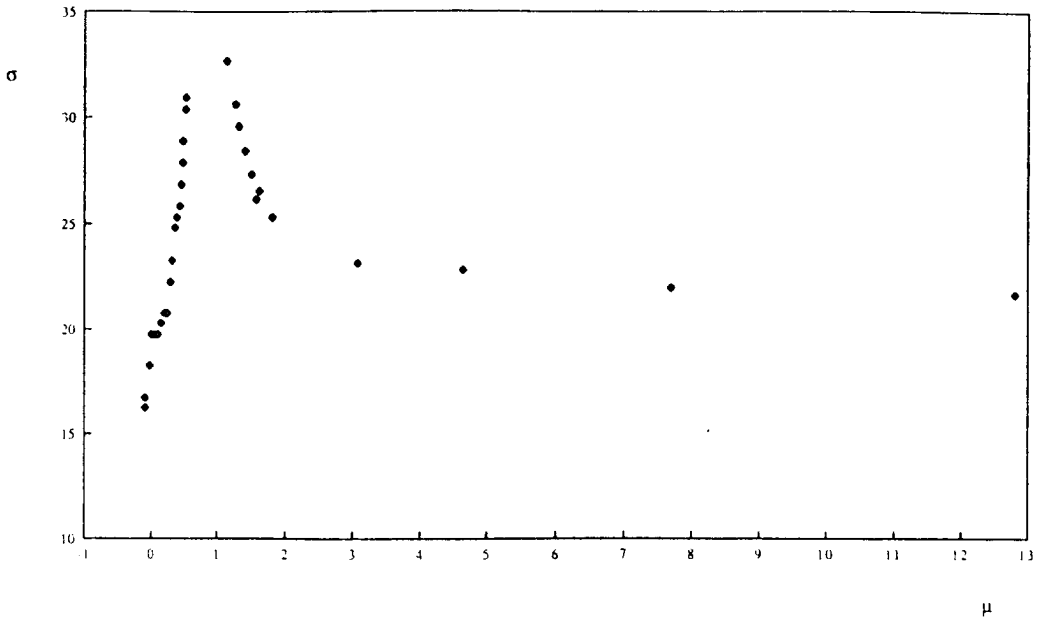

FIG. 5. The frequency σ of traveling inclined rolls vs μ the ratio of the angular velocities of the two cylinders. σ is the measured frequency in Hertz scaled by d^2/ν. The region between the two branches corresponds to the stationary patterns. The ends of the two branches correspond to the codimension-2 points.

the frequency as a function of the angular velocities ratio μ. It is interesting that there is no preferred propagation direction for the rolls; they may move from either left to right or right to left, but the relationship of the tilt direction to the direction of propagation is always the same. Occasionally there may be inclined rolls with opposite tilt and propagation direction existing simultaneously in different regions along the cylinder. Usually one will occupy almost the entire length with the other confined near one end. Although in principle standing waves formed by counterpropagating rolls may exist we have not yet observed this effect. The inclined rolls become much weaker partway around the cylinder, with greatest strength near the front face. It is possible that the presence of the free surfaces accounts for this by imposing an entrance length region on the fully developed Couette and Poiseuille profile.[7] Above threshold the rolls become clearly visible all the way from the front to the back free surface, corresponding to a decrease of the entrance length.

D. Laminar state-inclined rolls-laminar state-stationary patterns transition

There are two bands of R_o values (from 155 to 210 and from 257 to 300) for which the instability differs as R_i is increased. In the first band, when R_i is increased from about 160, the instability sets in as stationary axisymmetric rolls, but at higher R_i they disappear and the flow becomes laminar, without any structures. At still higher values of R_i inclined rolls form. In the second band the instability sets in as a traveling pattern. Upon increasing R_i the pattern disappears and the base laminar flow reappears. At still larger R_i stationary axisymmetric rolls form in the flow. The roll size is the same as that for the stationary patterns for R_o in the range 160–257. It is interesting to notice that if we plot the phase diagram [Fig. 2(a)] in terms of the parameters T and μ [Fig. 2(b)], the transition, for fixed μ and increasing T, is directly from the base state to inclined rolls or to the stationary Dean rolls.

E. Codimension-2 points

The traveling inclined roll state and the stationary state branches intersect at three oscillatory-stationary codimension-2 points. Preliminary inspections of the neighborhoods of these points have proved quite interesting. There are often mixed states of stationary and traveling rolls. Sometimes the traveling rolls are near the right end and the stationary rolls are near the left end (or vice versa), or the traveling rolls may coexist with the stationary rolls in the same region [see Fig. 4(e)]. The Dean and Taylor-Couette branches intersect in another codimension-2 point (stationary-stationary). Near that point rolls which were clearly visible at the outer cylinder wall become less distinct as the unstable region develops near the inner cylinder wall.

In all cases the system was brought to just beyond the instability threshold and then allowed to settle for many gap diffusion times d^2/ν, following which the process was repeated. It might be possible that these states near the codimension-2 points are transients: waiting for a very long time, the system may pass to a pure state like those prevailing further from the immediate neighborhood of the codimension-2 point, but this has not been established, owing to practical difficulties with Kalliroscope solution lifetime limits. Further work will be necessary to achieve a coherent picture of these complex flows.

F. Inner cylinder at rest, outer cylinder rotating

When the inner cylinder is at rest and the outer cylinder is rotating, there is some difficulty in establishing the onset of the instability. End effects dominate the flow. Large spiral-like vortices propagating away from each end virtually fill the system. They are most prominent on the side with the outer cylinder moving upward. On the other side at $R_o = 257$ weak stationary Dean rolls form and coexist with the end-effect rolls. Increasing R_o to 300 establishes Dean rolls on both sides of the system, and the end effects become less apparent [Fig. 4(d)]. It is then possible to decrease R_o to 272 and retain the axisymmetric state. After establishing Dean rolls throughout, one can then increase R_i slowly and observe various transitions. Two cases arise: when the cylinders are counter-rotating, these rolls persist but become weaker in the back face. For co-rotating cylinders, the Dean rolls are observed to be asymmetric, weaker in the front face than in the back, until $R_i \simeq 12$, at which point traveling inclined rolls appear in the front face. The transition between Dean rolls and inclined rolls in this region has not been thoroughly explored.

V. DISCUSSION OF RESULTS

The stationary states of the diagram (R_o, R_i) may be understood at least qualitatively if one applies the Rayleigh stability criterion to the base flow velocity profile. In fact, from Fig. 3, one sees that the velocity profile may be considered as a superposition of linear Couette and Poiseuille profiles. Depending on the critical Reynolds number for the different sublayers, the onset of instability for the whole system will begin in that sublayer with the minimal critical value. The inclined roll states might be understood as the result of the competition between the mechanisms of destabilization of the Couette and Poiseuille sublayers. In fact, we see in Fig. 3 that the inclined rolls exist for those values of R_i and R_o for which the base velocity field has two potentially unstable sublayers, while the stationary states develop for the case when the base velocity profile has only one potentially unstable sublayer. The Dean rolls which emerge for R_o in the range 160–300 appear to be an exception to this and they may be seen as intermediate between the inclined roll and laminar states. It is also interesting to remark that the system is always linearly unstable with either the inner or the outer cylinder at rest, while for the classical Taylor-Couette system the flow is linearly stable when the inner cylinder is at rest. The result obtained for the case with only the inner cylinder rotating agrees with the results found previously and reported in Refs. 7 and 13.

The presence of an oscillatory branch in between two distinct stationary branches has been predicted,[14] but the observed critical values were quite different from those calculated. In particular, the oscillatory branch was predicted to exist between the codimension-2 points at $R_o = 142$, $R_i = 483$ and $R_o = 216$, $R_i = 489$. (Theoretical critical values have been omitted from Fig. 2 since they are quite large compared with the experimental values.) Several assumptions were made in developing the initial theory, among which are the small gap approximation, the infinite cylinder length, and the axisymmetric perturbations (even though the system itself breaks the azimuthal symmetry). Nevertheless, the predicted frequency is of the same order as that observed in the experiment. For stationary states, axisymmetric perturbations may still suffice to describe the behavior far from the free surfaces. However, the use of axisymmetric perturbations for the oscillatory states appears to cause more serious difficulties. In fact, in this case we observe nonaxisymmetric patterns with angular wave number m [from perturbations in $\exp i(st + qz + m\theta)$] different from zero. An important feature in this kind of system is that noninteger values for m are allowed, in contrast to the classical Taylor-Couette case when propagating nonaxisymmetric structures arise. If we define

$$m = \frac{2\pi \left[\frac{r_o + r_i}{2} \right] \tan\alpha}{d\lambda} , \tag{6}$$

then we find that the experimental value for m is approximately 14 for $\mu = 0$, corresponding to an inclination angle $\alpha = 19°$ and a wavelength $\lambda = 1.22$ (0.86 cm). For $\mu = 0.22$ the experimental value for m is 13.4. We note that the λ we have used is equal to the distance along the axis between successive dark boundaries. We are so far unable to distinguish inflow from outflow boundaries owing to the weak nature of the flows, and this presents us with an ambiguity. The observed boundaries in most cases are equally dark (as determined visually and with image analysis), which is indicative that they may be of the same type, i.e., all inflow or all outflow. In a few cases a set of very weak dark lines can just be detected, apparently revealing that the wavelength is only half that given by the strong dark lines. We are led to the tentative conclusion that either one boundary is much weaker than the other and is thus normally not visible, or that there may exist unobserved weak counter-rotating cells existing next to the inner cylinder. This is a matter that will await resolution in future experiments. It is possible that the value of m may change with both the values of R_i and R_o and the filling volume ratio. Indeed, preliminary experiments[17] have shown that m decreases slightly with a continuous increase of the filling fraction, although the critical Taylor number is unchanged. The Ekman cells induced by the Teflon end rings have a nonaxisymmetric profile and will affect, as a perturbation, the bulk flow. This influence is probably more important near the line $\mu = -1$ (where the velocity gradients are larger) and lower at the line $\mu = 1$. The entry length near the free surfaces, caused by the growth of a boundary layer, may be affecting the inclined rolls since near threshold they are most prominent on only one side, but evidently this is not so important for the Dean or Taylor-Couette rolls.

We emphasize that further transitions have been observed in the system for values of the parameters R_i and R_o beyond the instability thresholds, but they have not yet been quantitatively characterized.

VI. CONCLUSION

We have shown that the flow between two horizontal coaxial rotating cylinders with a partially filled gap is very rich in nonequilibrium patterns. We have found a variety of different structures extending over wide ranges of the external control parameters R_o and R_i. Five primary instability branches and four codimension-2 points have been directly observed. Approximate characteristics of the states (threshold control parameter values, frequency of inclined rolls at threshold, and wavelengths) have been determined. However, our results indicate the need for further, more extensive, investigations. Theoretically, account must be taken of nonaxisymmetric perturbations, a finite gap, and nonlinearities. The last is no doubt important in the vicinity of the codimension-2 points, where mixed-mode patterns have been observed. It may also be important to explore the effect of radius ratio changes. Experimentally it would be desirable to establish the details of the flows in the codimension-2 point neighborhoods,[18] search for possible changes in tilt and propagation velocity of the inclined rolls as functions of R_o and R_i,[19] and explore the behavior of the various flows as the system is driven beyond threshold into chaotic or weakly turbulent states. The last is potentially quite interesting since this system breaks the rotational symmetry of the circular Couette flow, thus undoubtedly changing the dynamics in a profound way, even for the flows bifurcating from the Taylor-like rolls.

ACKNOWLEDGMENTS

We would particularly like to thank Diane Jacobs for her help in programming and Kalliroscope management. I.M. wishes to thank all the staff of the Nonlinear Dynamics Laboratory of the Department of Physics of the Ohio State University for all that they did to make his stay pleasant. We also express our gratitude to Christiane Normand for assistance in checking numerical results. This work was supported in part by the Office of Naval Research under Contract No. N00014-86-K0071 and the French Ministry of Cooperation (CIES) which supported the travel expenses of I.M.

---

*Permanent address: Laboratoire d'Hydrodynamique et Mecanique Physique, Ecole Supérieure de Physique et de Chimie Industrielles de la Ville de Paris, 10 rue Vauquelin, 75231 Paris Cédex 05, France.

[1]S. Chandrasekhar, *Hydrodynamic and Hydromagnetic Stability* (Oxford University, London, 1961), Chaps. VII and VIII.

[2]P. G. Drazin and W. H. Reid, *Hydrodynamic Stability* (Cambridge University, Cambridge, 1981), Chap. 3.

[3]R. C. DiPrima and H. L. Swinney, in *Hydrodynamic Instabilities and the Transition to Turbulence*, Vol. 45 of *Topics in Applied Physics*, edited by H. L. Swinney and J. P. Gollub (Springer, New York, 1981), Chap. 6.

[4]C. D. Andereck, S. S. Liu, and H. L. Swinney, J. Fluid Mech. **164**, 155 (1986).

[5]H. Peerhossaini, Thèse de Doctorat et Sciences, Université de Paris VI, 1987.

[6]W. R. Dean, Proc. R. Soc. London, Ser. A **121**, 402 (1928).

[7]I. Mutabazi, H. Peerhossaini, and J. E. Wesfreid, in *Propagation in Systems Far From Equilibrium, Proceedings in Physics*, edited by J. E. Wesfried and H. R. Brand (Springer, New York, in press).

[8]D. B. Brewster and A. H. Nissan, Chem. Eng. Sci. **7**, 215 (1958).

[9]D. B. Brewster, P. Grosberg, and A. H. Nissan, Proc. R. Soc. London, Ser. A **251**, 76 (1959).

[10]R. C. DiPrima, J. Fluid. Mech. **6**, 462 (1959).

[11]T. H. Hughes and W. H. Reid, Z. Angew. Math. Phys. **7**, 573 (1964).

[12]D. C. Raney and T. S. Chang, Z. Angew. Math. Phys. **22**, 680 (1971).

[13]I. Mutabazi, H. Peerhossaini, J. E. Wesfreid, and C. D. Andereck (unpublished).

[14]I. Mutabazi, C. Normand, H. Peerhossaini, and J. E. Wesfreid (unpublished).

[15]G. W. Baxter and C. D. Andereck, Phys. Rev. Lett. **57**, 3046 (1986).

[16]S. Chandrasekhar, *Hydrodynamic and Hydromagnetic Stability* (Oxford University, London, 1961), pp. 350–359.

[17]Experiments performed at the Weizmann Institute, Rehovot (Israel) [J. E. Wesfreid (personal communication)].

[18]G. Iooss, in *Trends in Applications of Pure Mathematics to Mechanics*, Vol. 249 of *Lecture Notes in Physics*, edited by E. Kröner and K. Kirchgässner (Springer-Verlag, Berlin, 1986), p. 297.

[19]W. F. Langford, R. Tagg, E. J. Kostelich, H. L. Swinney, and M. Golubitsky, Phys. Fluids **31**, 776 (1988).

Spatiotemporal Pattern Modulations in the Taylor-Dean System

Innocent Mutabazi,[a] John J. Hegseth, and C. David Andereck
Department of Physics, Ohio State University, 174 West 18th Avenue, Columbus, Ohio 43210

Jose E. Wesfreid
Laboratoire d'Hydrodynamique et Mécanique Physique,
Ecole Supérieure de Physique et de Chimie Industrielles de Paris, 10, rue Vanquelin,
75231 Paris CEDEX 05, France
(Received 1 December 1989)

Flow between two horizontal coaxial cylinders with a partially filled gap is investigated for the case when the primary instability forms a pattern of traveling inclined rolls which is simply periodic in space and time. Slightly above the onset, there is a second instability which results in a periodic modulation of the rolls with an axial wavelength of ~ 3 rolls and a lower frequency. Both the traveling inclined rolls and the ~ 3-roll-modulation pattern exhibit long-wavelength, low-frequency phase modulations and associated defects.

PACS numbers: 47.20.−k

The transition to turbulence remains one of the major problems of nonlinear physics which is still not well understood. In the last few years, considerable effort has been devoted to the problem of the formation of cellular patterns, and their subsequent evolution to disorder, in fluid systems far from equilibrium such as Rayleigh-Bénard convection and Taylor-Couette flow, as well as many other hydrodynamic, mechanical, and physicochemical systems.[1,2] In such cases, the bifurcation from the base state occurs via a stationary or an oscillatory instability (Hopf bifurcation). Recently, attention has been drawn to systems in which the transition from the base state occurs via a Hopf bifurcation, in which case the transition to spatial-temporal complexity may be more accessible for experimental characterization and theoretical treatment. Such systems include convection in binary mixtures[3] and in liquid crystals,[4] the Taylor-Couette system with counter-rotating cylinders,[5] the Taylor-Dean system,[6] chemical reactions,[7,8] and plastic deformation with negative-strain-rate sensitivity.[9]

We report the first observation of an unusual transition sequence in the behavior of a hydrodynamic system with well controlled centrifugal instabilities, the Taylor-Dean system. The system consists of flow between two horizontal coaxial rotating cylinders with a partially filled gap. The flow patterns observed depend on the inner- and outer-cylinder rotation speeds, which we rescale as our dimensionless control parameters, the inner- and outer-cylinder Reynolds numbers R_i and R_o. Depending on the value of R_o selected, the flow evolves upon increasing R_i to either a stationary axisymmetric-roll pattern or a traveling-inclined-roll pattern (Hopf bifurcation).[6] We investigate here the behavior of the traveling-roll pattern when the outer cylinder is at rest and R_i is slowly increased. Just above the onset, a phase variation in the pattern produces a long-wavelength modulation and time-dependent pattern defects are generated. At higher rotation speeds, the pattern undergoes an unusual periodic short-wavelength amplitude modulation with an envelope size of ~ 3 rolls. While investigation of different extended one-dimensional systems with a Hopf bifurcation as the first transition has led to interesting results such as solitary-wave-like behavior[10–12] or isolated patches of traveling rolls,[13–16] we know of no other system with traveling patterns at onset which undergoes such a short-wavelength modulation. The aim of this Letter is to present the main characteristics of this novel traveling pattern, and describe its evolution toward spatial-temporal complexity.

The Taylor-Dean system may be understood (and distinguished from the Taylor-Couette system) by observing that the partial filling of the gap between the cylinders produces two horizontal surfaces. When the cylinders rotate they drive the fluid toward a free surface. To reverse the direction of the flow the free surface induces a pressure gradient along the azimuthal direction (Fig. 1). As a result, the flow sufficiently far away from the free surfaces can be regarded as a combination of Couette flow, from the rotation of the cylinders, and Poiseuille flow, due to the azimuthal pressure gradient. The traveling-roll pattern may then arise as a result of the competition between centrifugal instabilities of the Couette and Poiseuille components of the flow.[17]

Our system consists of two horizontal coaxial cylinders, the inner cylinder made of black Delrin plastic with an outer radius $r_o = 4.486$ cm and the outer cylinder made of Duran glass with an inner radius $r_i = 5.080$ cm. The gap between the cylinders is $d = r_o - r_i = 0.594$ cm and the cylinders are independently driven as described elsewhere.[6] The radius ratio $\eta = 0.883$ is large enough for the small-gap approximation to be reasonable. Teflon rings are attached to the inner surface of the outer cylinder a distance $L = 53.40$ cm apart, giving an aspect ratio $\Gamma = L/d = 90$. The fluid is water with 1%

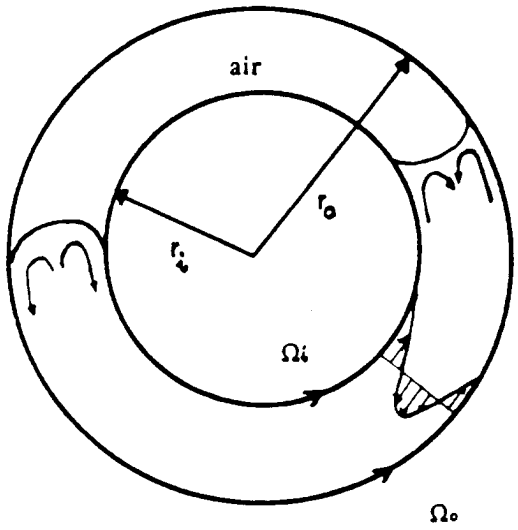

FIG. 1. Sketch of the experimental geometry: Corotating cylinders with a partially filled gap. The front face is defined to be the one in which the inner cylinder is rotating upward.

Kalliroscope AQ1000 for visualization. We have fixed the filling-level fraction $n=\theta_f/2\pi$ at 0.75.[6] (The instability threshold depends only weakly on n. For $n\in[0.5, 0.8]$ the variation of R_{ic} is within the experimental precision ($\simeq 1\%$).)

We define inner- and outer-cylinder Reynolds numbers as follows: $R_i=2\pi f_i r_i d/\nu$ and $R_o=2\pi f_o r_o d/\nu$, respectively, where f_i and f_o are the inner- and outer-cylinder rotation frequencies. The dimensionless control parameter is $\epsilon=(R_i-R_{ic})/R_{ic}$, where R_{ic} is the inner-cylinder Reynolds number at onset of the traveling inclined rolls for a given R_o. The flow-pattern frequencies are scaled with the inverse of the radial diffusion time $\tau_r=d^2/\nu \approx 36$ s, the wavelengths are scaled by the gap size d, and the velocities are scaled by the radial diffusion velocity ν/d.

Frequency measurements at a single position in the flow have been made by the light-reflectance technique described elsewhere.[6] Spatial information is obtained using a 28–35-mm variable-focal-length lens to image the flow pattern onto a 1024-pixel charge-coupled-device (CCD) linear array. The array is controlled by a CAMAC module, which also serves as the data gateway to our PDP-11 computer. This system is able to continuously process up to one frame every 0.07 s. The output of the CCD camera gives the instantaneous reflected light intensity along the axis of the cylinders, the maxima corresponding to roll centers and the minima corresponding to inflow and outflow boundaries. Space-time diagrams are then produced by displaying intensity versus axial position plots at regular intervals along a time axis. We have also used a high-intensity white-light source to illuminate a thin cross section of the flow to visualize the internal processes in the structures.

The initial instability to traveling rolls is, within our experimental limits, a supercritical Hopf bifurcation. The intensity of the rolls decreases along the azimuth such that they are weaker in the rear face than in the front face. This may be connected to the presence of a horizontal recirculation roll at the front free surface. The rolls are inclined $\sim 20°$ from the vertical (Fig. 2). The wavelength of the rolls along the cylinders' axis is $\lambda=1.416$. At onset the rolls have no preferred direction and may move either left or right. The direction of propagation is the same as the roll inclination direction. Light sheet visualization through the gap shows that the rolls exist near the outer cylinder. Above threshold both right- and left-traveling rolls may exist separated by a vertical (noninclined) defect line. The defect line is not necessarily in the middle of the cylinder axis; in fact, it moves in an erratic fashion with a velocity of about 50 times less than that of the rolls. Such defect lines are inherent to traveling-wave patterns.[18]

We have measured the frequencies of the traveling rolls (from power spectra) as a function of R_i, as shown in Fig. 3. Near the onset, for a fixed R_o, the fundamental frequency f of the traveling rolls increases almost linearly with R_i. Measurements of the frequency at different points along the axis show that for $\epsilon\approx 0.013$, and above, there is a local frequency of the pattern. This can also be seen in Fig. 2 where the phase lines of the rolls are curved. Close to onset, after either a left- or right-traveling roll pattern has grown to a length of ~ 30 rolls, a long-wavelength modulation appears which generates this phase variation. The wavelength of this modulation decreases from ~ 30 to ~ 10 rolls as R_i increases. For $\epsilon\in[0.02,0.1]$ the frequency and roll-velocity variation becomes strong. High-velocity rolls occasionally collide with low-velocity rolls, resulting in the loss of a roll. The collision gives rise to a damped modulation moving in a direction opposite to the traveling rolls. Roll creation events have also been observed [as can be deduced from Fig. 2(a)]. Similar roll creation and destruction events have been observed in binary-fluid convection[14] and in electrohydrodynamic systems.[19]

Increasing R_i, the flow undergoes a second instability which results in a short-wavelength modulation of the traveling waves [Fig. 2(b)]. The onset is nonhysteretic, within our experimental precision of $\simeq 1\%$. It manifests itself as a roll-intensity modulation with a nonsymmetric envelope of wavelength $\Lambda=4.11$ and lower frequency f_2 of about 0.7 for $R_o=0$. The size of an individual roll changes as it travels through the modulation envelope. This ~ 3-roll (short-wavelength) modulation appears for $-45<R_o<45$ with a threshold varying as shown in Fig. 4. The modulation envelope moves with a velocity depending on the value of R_o.

The short-wavelength modulations produce distortions of each roll along its axis [Fig. 2(b)]. This suggests that the short-wavelength modulation may be analogous to the wavy spirals in the counter-rotating Taylor-Couette system.[5] Given the axial velocities in the data of Fig.

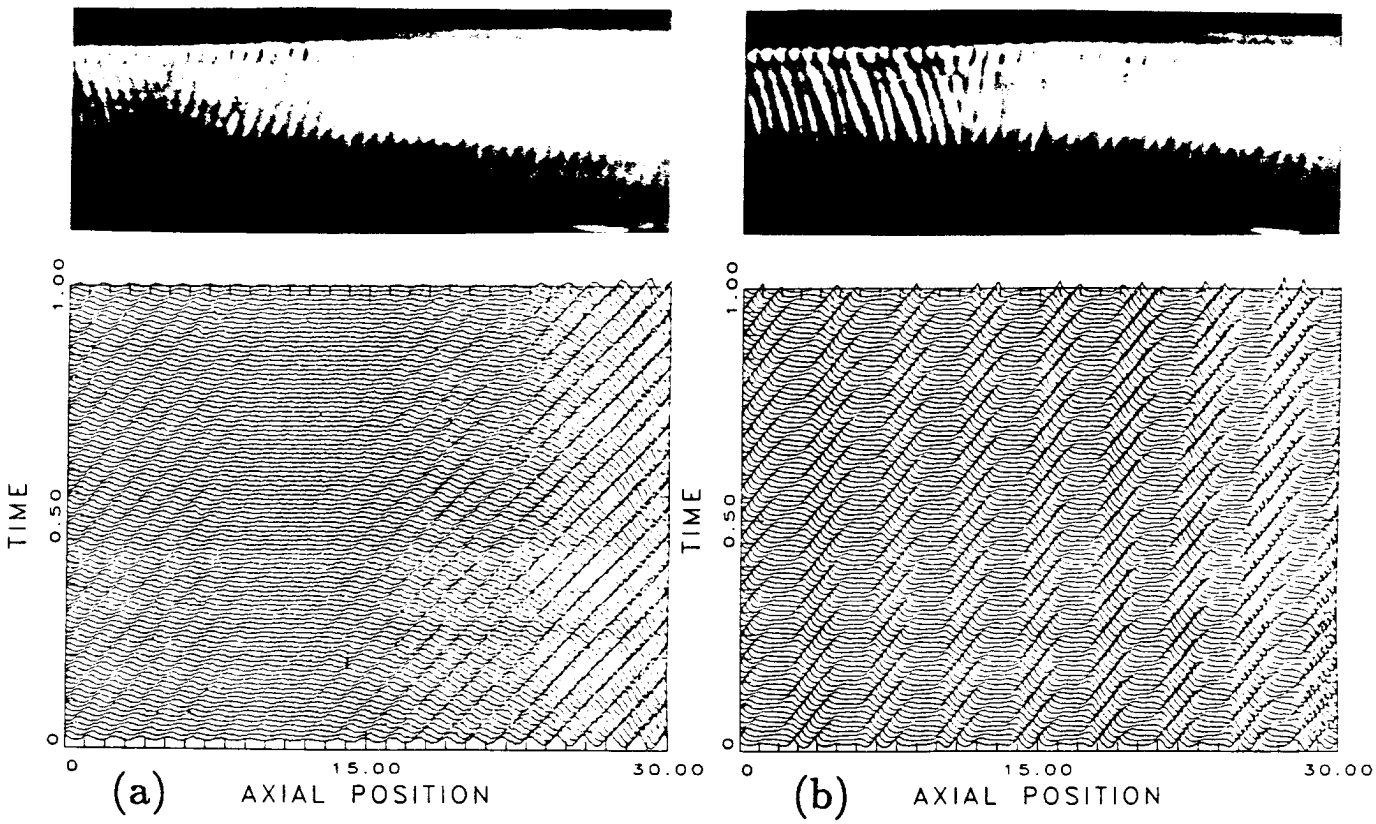

FIG. 2. Photographs of the traveling-roll patterns viewed from the front face (the top of each view being a free horizontal surface) and their space-time diagrams: (a) traveling-inclined-roll pattern near threshold at $R_i = 263$ and $R_o = 0$. (b) Short-wavelength (~3-roll) -modulation pattern at $R_i = 303$ and $R_o = 0$.

2(b), and the 20° inclination angle, there should be ≈ 2.9 azimuthal waves. We observe $\simeq 2$ waves in the front face while the third may remain unseen because of the decreasing intensity of the rolls along the azimuth.

We measured the time-averaged spatial intensity-intensity correlation function of the rolls along the axis for $R_o = 0$. Time averaging of individual spatial autocorrelations was done over a time of $\simeq 40\tau_r$ and had the effect of removing the

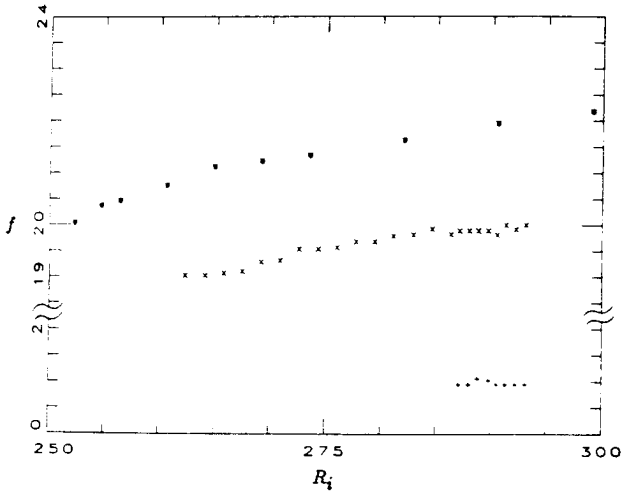

FIG. 3. Fundamental and secondary frequencies as functions of R_i: fundamental frequency for $R_o = 0$ (×), for $R_o = 39$ (*), and the secondary frequency for $R_o = 0$ (+).

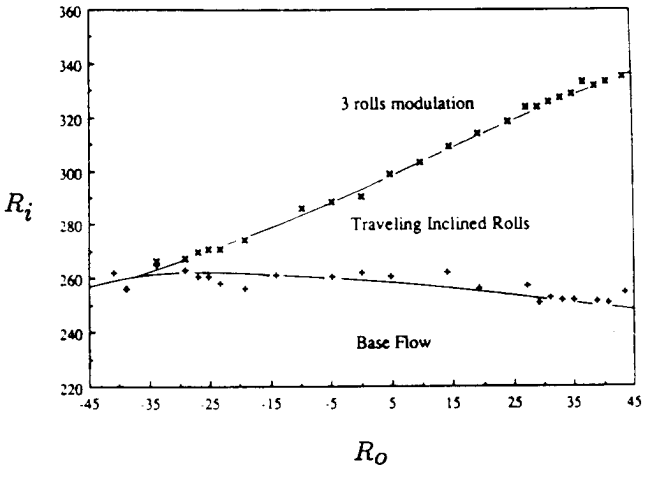

FIG. 4. Phase diagram (R_o, R_i) for the threshold of the inclined-traveling-roll pattern, and the short-wavelength-modulation pattern. The solid lines are guides to the eye.

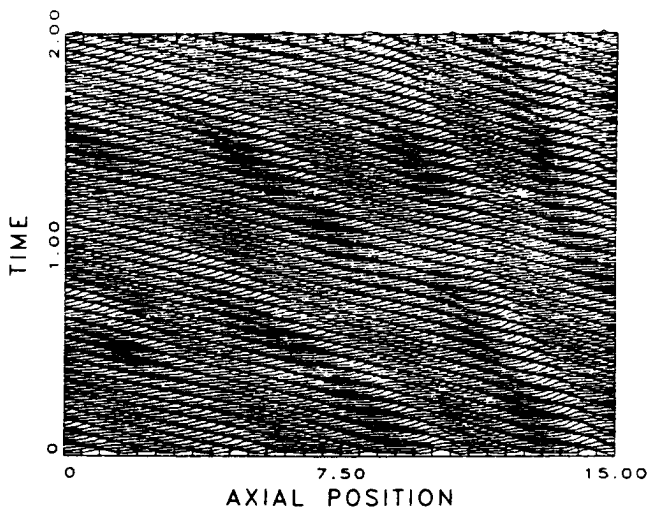

FIG. 5. The ~3-roll pattern at $R_i = 308$, $R_o = 0$. The traveling rolls are separated by propagating envelopes which exhibit phase modulations and defects.

long-range correlation. Before the onset of the short-wavelength modulation, the envelope of this correlation function decreases smoothly within an exponential envelope with a characteristic length of about 2.6. After the short-wavelength modulation appears, the correlation remains strong only at distances of 3 rolls. This reflects the varying roll size and apparent strength within a modulation wavelength. This phenomenon can be considered as the generation of traveling patches (triplets) periodic in space and in time separated by periodic laminarlike zones. As in the case of the initial traveling-roll pattern, the roll-modulated pattern may exhibit spatiotemporal defects (Fig. 5). At these and higher R_i values the correlation function drops rapidly to zero beyond one roll wavelength.

To summarize, for a large-aspect-ratio Taylor-Dean system, the traveling inclined rolls observed at the onset of instability, undergo, after the onset of a long-wavelength modulation associated with defects, a novel short-wavelength modulation with an axial wavelength of ~3 rolls. This modulation may be generated either by competing instabilities in different layers or by a wavy instability of the rolls. This short-wavelength-modulation pattern strongly distorts individual rolls and exhibits a long-wavelength modulation associated with defects. This transition to the ~3-roll-modulation pattern is not far from the onset of the primary instability, making this system a good candidate for investigating the transition to weakly turbulent states.

We thank Christiane Normand and Yves Pomeau for interesting suggestions. I.M. thanks the staff of the Nonlinear Dynamics Laboratory for all that they provided him during his stay at Ohio State University. This work has been supported by the Office of Naval Research and NATO.

[a]Present address: Laboratoire d'Hydrodynamique et Mécanique Physique, Ecole Supérieure de Physique et de Chimie Industrielles de Paris, 10, rue Vauquelin, F-75231 Paris CEDEX 05, France.

[1]*Cellular Structures in Instabilities,* edited by J. E. Wesfreid and S. Zaleski, Lecture Notes in Physics Vol. 210 (Springer-Verlag, Berlin, 1984).

[2]*Propagation in Systems Far from Equilibrium,* edited by J. E. Wesfreid, H. R. Brand, P. Manneville, G. Albinet, and N. Boccara, Springer Series in Synergetics Vol. 41 (Springer-Verlag, Berlin, 1988).

[3]P. Kolodner and C. M. Surko, Phys. Rev. Lett. **61**, 842 (1988).

[4]I. Rehberg, S. Rasenat, and V. Steinberg, Phys. Rev. Lett. **62**, 756 (1989).

[5]C. D. Andereck, S. S. Liu, and H. L. Swinney, J. Fluid Mech. **164**, 155 (1986).

[6]I. Mutabazi, J. J. Hegseth, C. D. Andereck, and J. E. Wesfreid, Phys. Rev. A **38**, 4752 (1988).

[7]Y. Kuramoto, *Chemical Oscillations, Waves and Turbulence,* Springer Series in Synergetics Vol. 19 (Springer-Verlag, Berlin, 1984).

[8]Z. Nagy-Ungvarai and S. C. Müller, in *Propagation in Systems Far from Equilibrium* (Ref. 2), p. 100.

[9]Y. Estrin and L. P. Kubin, Res Mech. **23**, 197 (1988).

[10]M. Rabaud, S. Michalland, and Y. Couder, Phys. Rev. Lett. **64**, 184 (1990).

[11]A. Simon, J. Bechhoefer, and A. Libchaber, Phys. Rev. Lett. **61**, 2574 (1988).

[12]G. Faivre, S. de Chivigné, C. Guthmann, and P. Kurowski, Europhys. Lett. **9**, 779 (1989).

[13]P. Kolodner, C. M. Surko, and H. Williams, Physica (Amsterdam) **37D**, 319 (1989).

[14]P. Kolodner, D. Bensimon, and C. M. Surko, Phys. Rev. Lett. **60**, 1723 (1988).

[15]R. Henrichs, G. Ahlers, and D. S. Cannell, Phys. Rev. A **35**, 2761 (1987).

[16]V. Steinberg, J. Fineberg, E. Moses, and I. Rehberg, Physica (Amsterdam) **37D**, 359 (1989).

[17]I. Mutabazi, C. Normand, H. Peerhossaini, and J. E. Wesfreid, Phys. Rev. A **39**, 763 (1989).

[18]L. Gil and J. Lega, in *Propagation in Systems Far from Equilibrium* (Ref. 2), p. 164.

[19]A. Joets and R. Ribotta, J. Phys. (Paris), Colloq. **50**, C3-171 (1989).

Transition from time-dependent to stationary flow patterns in the Taylor-Dean system

Innocent Mutabazi and C. David Andereck
Department of Physics, Ohio State University, 174 W 18th Avenue, Columbus, Ohio 43210
(Received 21 June 1991)

The flow between two horizontal coaxial cylinders with a partially filled gap, the Taylor-Dean system, is investigated for the case in which the outer cylinder rotates while the inner cylinder remains at rest. The initial instability is to a mixed state of both traveling inclined rolls and laminar base flow. At a larger rotation rate, the entire flow becomes time dependent. At a still larger rotation rate, the flow undergoes a subcritical transition to a stationary roll pattern, a process previously observed only in binary fluid mixtures.

PACS number(s): 47.20.−k

Studies of the routes to turbulence in diverse physical systems far from thermodynamic equilibrium have shown that the transition from the base state usually is to a state with a pattern that is periodic in space and/or in time [1]. The classical prototypes of such systems are Rayleigh-Bénard convection and Taylor-Couette flow. Upon increasing the relevant control parameter, temporal and spatial frequencies emerge that correspond to various state transitions, until eventually the system becomes chaotic, as indicated by the presence of broad components in the Fourier spectrum. Typically, once time dependence begins in such systems, it persists and becomes more complex until finally the state may be characterized as turbulent. However, exceptions to this common scenario are found in some systems. For example, Walden *et al.* [2] and later Moses and Steinberg [3] have observed thermally induced *stationary overturning convection* in binary fluid mixtures in a rectangular cell. In this case there is a subcritical transition from a traveling-waves state (first instability after the conducting state) to a stationary pattern (secondary instability) with an increase in the control parameter, the Rayleigh number. A similar phenomenon has been observed using an annular container [4]. The circular cell geometry has not changed the essential phenomenon but has suppressed the formerly observed hysteresis.

We report here observations of a transition from a traveling roll state to a stationary roll state in a single-component Newtonian fluid. The fluid is contained in a modified version of the Taylor-Couette geometry with broken rotational symmetry. Specifically, the system consists of flow between two horizontal coaxial cylinders with a partially filled gap, the so-called *Taylor-Dean system* [5] (see Fig. 1). In the case discussed here, only the outer cylinder rotates, with angular velocity Ω. The onset of instability is characterized by a state of three regions: inclined rolls traveling to the right (region with pattern amplitude $A \neq 0$), laminar flow ($A = 0$), and inclined rolls traveling to the left ($A \neq 0$). This transition is subcritical. For higher values of the control parameter, the time dependence disappears from the flow and the pattern becomes stationary and axisymmetric. As the Taylor-Dean system is purely hydrodynamic, this transition has a qualitatively different origin from the one that is observed in thermal convection in binary mixtures for negative values of the separation ratio [2–4].

It has been emphasized previously [5] that when only the outer cylinder rotates, Dean rolls should occur. They result from a centrifugal instability in curved Poiseuille channel flow with a constant longitudinal pressure gradient. Dean rolls have recently drawn attention because of their importance in practical systems such as channel

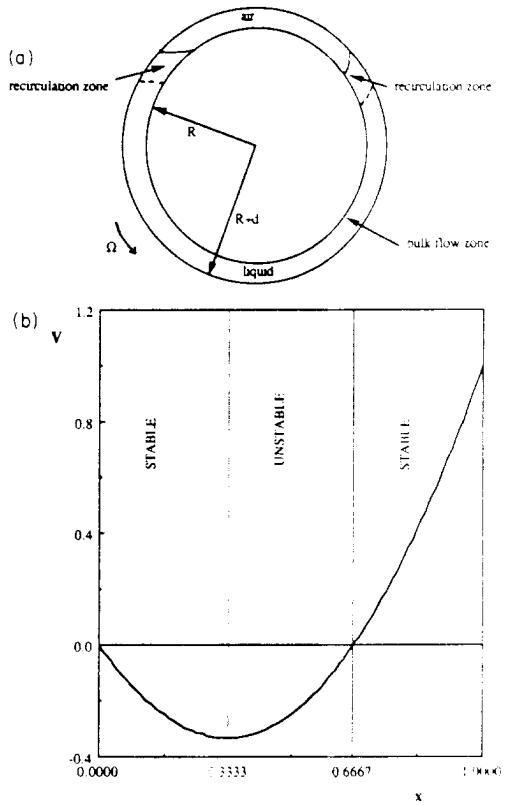

FIG. 1. Sketch of the flow geometry. The gravitational force is downward in this view, perpendicular to the axis. (a) The base flow consists of the azimuthal bulk flow and of the two-dimensional velocity field in the recirculation zone. (b) The bulk base-flow-velocity profile and Rayleigh's circulation criterion: The unstable layer is sandwiched between two stable layers. The pure Poiseuille flow has one solid boundary at $x = 0$ and one nonrigid boundary at $x = \frac{2}{3}$.

flows and pipe or duct flows [6]. The curved Poiseuille channel flow has been modeled sometimes by the flow between two coaxial cylindrical stationary surfaces under an external azimuthal pressure gradient. In that case, the base-flow state can be calculated and both the linear [7,8] and weakly nonlinear stability analyses [9,10] can be carried out. In the present case, the rotation and the free surfaces resulting from the partial filling of the system force a Poiseuille component with a constant azimuthal pressure gradient.

The main difference between the well-known Taylor vortex flow and the Dean vortex flow is that the geometry in which Dean rolls occur does not possess rotational symmetry. Therefore, the observed vortex structure must be nonaxisymmetric. One consequence of this is the potential occurrence of noninteger azimuthal wave-number modes on Dean vortices. Such modes are possible since the patterns are not constrained to obey periodic boundary conditions in the azimuthal direction, as is the case in the Taylor-Couette system.

A few experiments have been realized to study systematically the flow stability of the Dean configuration [11,12]. We have recently reported observations of Dean rolls in the Taylor-Dean system [5]. Our experimental system consists of two horizontal coaxial cylinders. The inner cylinder, made of black Delrin plastic with radius $a=4.486$ cm, is fixed, and the outer, with radius $b=5.080$ cm, is made of Duran glass and rotates with angular velocity Ω [Fig. 1(a)]. The gap between the cylinders is $d=b-a=0.594$ cm. The radius ratio $\eta=a/b=0.883$ is large enough for the small-gap approximation to be reasonable. Teflon rings are attached to the inner surface of the outer cylinder a distance $L=53.40$ cm apart, giving an aspect ratio $\Gamma=L/d=90$. The working fluid is water with 1% Kalliroscope AQ 1000 added for visualization. Its kinematic viscosity is $\nu=0.98\times10^{-2}$ cm^2/sec at the temperature $T=21$ °C. The filling-level fraction $n=\theta_f/2\pi=0.75$ weakly influences the instability threshold [15].

We define the control parameter of the system to be a modified Taylor number $\mathrm{Ta}=(\Omega bd/\nu)(d/b)^{1/2}$, defined with respect to the outer cylinder parameters. The flow-pattern wavelengths are scaled by the characteristic length d, velocities are scaled by ν/d, and the frequencies are scaled by the inverse of the radial diffusion time $\tau=d^2/\nu\simeq36$ sec. We have chosen the ramping rate (experimental variation of the Taylor number) $r=d\mathrm{Ta}/dt^*\leq3$, where $t^*=t/\Gamma$, in order to achieve quasistatic conditions and thus avoid introducing spurious hysteresis [13].

Flow frequencies are measured from the power spectrum of single-point time series obtained with laser light that is reflected off the Kalliroscope flakes onto a photodiode detector. Spatial-dependence data are obtained using a 28–85-mm variable focal length lens to form an image of the visualized flow on a 1024-pixel charge-coupled device linear array interfaced through a computer automated measurement and control (CAMAC) system to a computer. The line of 1024 pixels is oriented parallel to the cylinder axis. The output consists of intensity maxima and minima which correspond to the centers and boundaries of the rolls. Space-time diagrams are then produced by displaying intensity versus axial-position plots at regular time intervals. An analysis of these plots yields both the roll size and the dynamics of the pattern in time and space. The spatial periodicity of the flow pattern is characterized by the wave number $q=2\pi d/\lambda$, and its time dependence is characterized by the phase velocity c_{ph}. Both quantities are measured from the space-time diagrams.

Away from the Teflon end rings, the base state consists of a purely azimuthal flow in the bulk, recirculation rolls near one free surface, and a boundary-layer-type flow near the other free surface [14]. The recirculation rolls and the boundary layer flow have azimuthal extensions of about d from the free surfaces. In order to minimize the effect of the recirculation rolls, we chose a small gap in comparison with the mean radius of the system. In the small-gap approximation, the bulk base-flow-velocity profile $V(x)=3x^2-2x$, where $x=(r-a)/d$. According to the Rayleigh circulation criterion for flow stability under centrifugally driven perturbations, the profile $V(x)$ has one unstable layer of flow located between two stable layers [Fig. 1(b)] [15]. The unstable layer belongs to the Poiseuille part of the flow and so we identify the instability to be of the Dean type.

Rotating cylinder ends (Teflon rings attached to the outer cylinder) induce Ekman cells even for low values of Ta. They become observable at about Ta=25 near both ends of the system, and have an axial extension of ~1.6. At larger Ta, stationary small rolls of average size $l_E=0.8$ are formed adjacent to the Ekman end cells. The maximum number of those rolls is 6 when Ta$\simeq$80 (Fig. 2). In the following, this part of the system is referred to as the *Ekman region.*

For Ta=91, cells in the Ekman region become time dependent, oscillating with a period of approximately 7 sec or a frequency $f=0.143$ Hz (5.15 in scaled units). At the same time, 3–5 traveling inclined rolls that are moving toward the middle of the system are generated close to each Ekman region. These rolls have a wavelength $\lambda=1.584$ or a wave number $q=3.967$. The phase velocity of the traveling rolls depends on their axial position: close to an Ekman region, it is $c=0.180$ cm/sec (10.9 in scaled units). The Fourier spectrum of the reflected light intensity gives a peak frequency around $f=0.136$ Hz (4.90 in

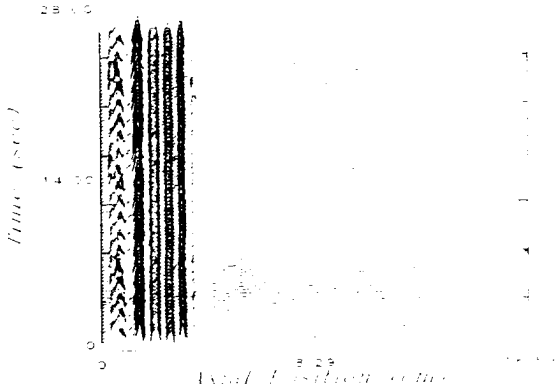

FIG. 2. Space-time diagram of the flow with stationary rolls in the Ekman region on the left, for Ta=2.7.

scaled units). The frequency of the traveling rolls is nearly identical to that of the oscillating rolls in the Ekman region. There are no rolls observed in the middle of the system [Fig. 3(a)]. The mixed state of traveling inclined rolls (perturbations of finite amplitude $A \neq 0$) and of laminar base flow (zero amplitude state) is stable, having been observed over many hours without noticeable changes. The transition has a hysteresis of about 13% in Ta. Therefore we have a *subcritical Hopf bifurcation.* While increasing Ta, the number of traveling inclined rolls increases on each side and the laminar base-flow extension decreases. For Ta=99, another set of traveling inclined rolls forms in the middle of the system (the laminar base-flow zone), with some rolls moving to the left and some to the right, separated by a dislocation source. They have both a wavelength value $\lambda = 0.889$ that is incommensurate with that of the initially formed, larger rolls, and a phase velocity that is more than two times larger than that of the larger rolls. This corresponds to a second transition to another mixed state with both different finite amplitudes and a zero amplitude [Fig. 3(b)]. The Fourier spectra obtained from single-point time series contain two different frequencies. The lower frequency corresponds to the motion of the large traveling inclined rolls and the higher frequency to the small traveling inclined rolls. The phase velocity of the large traveling rolls varies along the axis of the system. The presence of the small rolls retards the large rolls in the region of coexistence of the two types of rolls [Fig. 3(c)]. At Ta=101, the zero amplitude state disappears and the flow pattern becomes a mixture of large and small traveling inclined rolls. The front between the large and small rolls in the space-time diagram moves irregularly [Fig. 3(b)]. This state is characterized by both two frequencies and two incommensurate wavelengths and is chaotic in appearance. At Ta=109, the small rolls disappear. The resulting flow pattern consists only of large traveling rolls (usually with a dislocation), and is characterized by one frequency component and two incommensurate wavelengths ($\lambda_1 = 1.403$, $\lambda_2 = 1.733$).

At Ta=110, the flow pattern becomes stationary and axisymmetric after a transient period during which the pattern relaxes by adjusting its amplitude and phase (wavelength). The spatial evolution of the transition to the stationary state for a fixed value of the control parameter has been recorded, and we find that the front between the time-dependent and stationary states has a finite ve-

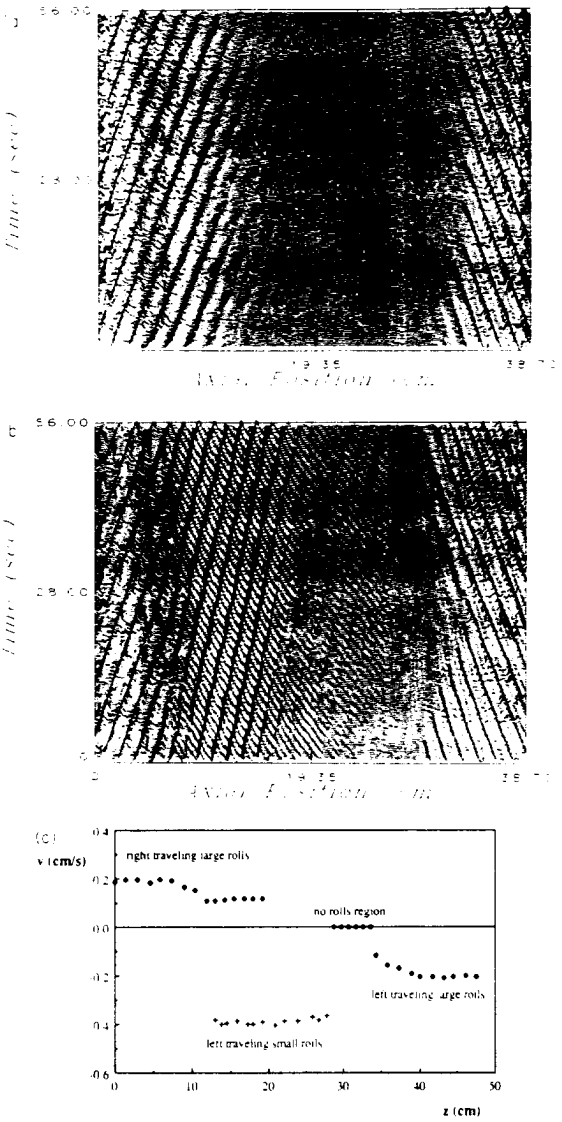

FIG. 3. Space-time diagram of the time-dependent flow patterns: (a) mixed state (Ta=91.0), (b) large traveling Dean rolls coexisting with small traveling rolls (Ta=95.9), and (c) phase velocity of rolls as a function of axial position for Ta=95.9.

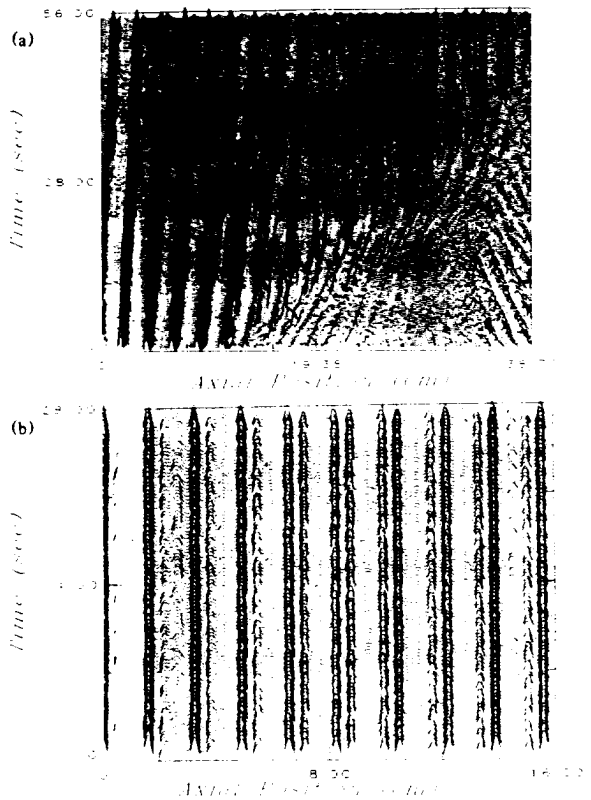

FIG. 4. Transition to the stationary state for Ta=115.8: (a) transient state with a moving front between the time-dependent pattern and the emerging stationary pattern, (b) final stationary state with wavelength modulation (only the central region of the system is shown).

locity $v_f = 0.6$ cm/sec (36.4 in scaled units) which is larger than that of the traveling rolls themselves [Fig. 4(a)]. The phase velocity of the traveling rolls has a large discontinuity at the transition, as shown by varying the control parameter Ta in steps of $\delta \mathrm{Ta} = 0.165$. Furthermore, the transition is subcritical, as it exhibits a large hysteresis of about 20% in Ta. As a result of this transition, the rolls become axisymmetric and the wavelength changes to $\lambda = 1.80$, corresponding to the wave number $q = 3.53$ together with a two-roll modulation wavelength $\Lambda = 2.81$ or wave number $Q = 2.24$ [Fig. 4(b)].

A linear-stability analysis of the base flow shows that the critical state is stationary and is characterized by $q_c = 2.875$ and $\mathrm{Ta}_c = 89.7$ [15]. Rolls in the Ekman regions become oscillatory near the theoretical value for the onset of Dean rolls. We speculate that they perturb the flow in regions close to them, thus generating traveling Dean rolls. (The formation of the small traveling rolls may in turn result from a modification of the base flow by the large rolls. As yet there is no theoretical indication that they should come from the unperturbed base flow.) As the control parameter increases, centrifugally driven perturbations in the bulk of the system become dominant, forcing the time dependence (induced by oscillations in the Ekman regions) from the pattern. Therefore, the time-dependent roll pattern may be considered as a metastable phase, possibly induced by the ends of the system, between the laminar base flow and the stationary Dean vortex flow.

The transition from a traveling roll pattern to a stationary pattern is unusual for hydrodynamic flows. It has been observed so far only in convection with binary mixtures of ethyl alcohol and water for negative values of the separation ratio [2–4]. This phenomenon was explained by the homogenization of the fluid mixture due to the elimination of the Soret-effect-induced concentration gradient for sufficiently large convective amplitude. Recent experiments conducted in an annular container [4] have shown that the transition is continuous, without hysteresis, and that the phase velocity vanishes with the reduced control parameter (Rayleigh number) following a power law. This is in relatively good agreement with both analytical and numerical calculations [16].

It is worthwhile to compare the flow considered in this paper with other similar systems. The pure Dean vortex flow that is observed in curved-channel Poiseuille flow consists, at the onset, of stationary almost axisymmetric rolls, except in the entrance region [11,12]. The transition to turbulence proceeds through instabilities of the rolls. In the Taylor-Couette system with a rotating outer cylinder and an inner cylinder at rest, no roll-forming instability is found and the flow becomes turbulent for very large values of the control parameter Ta. Moreover, all states observed thus far in the Taylor-Couette system for general rotation rates of the inner and outer cylinders always keep their time dependence [17], although reemergent periodic states [18] and periodic components in chaotic states [19] have been reported. Finally, the Taylor-Couette system subjected to a Coriolis force undergoes a transition from a disordered to an ordered, but still time-dependent, state [20].

In summary, the flow pattern in the Taylor-Dean system with the inner cylinder fixed undergoes an unusual transition from the laminar base flow to a complex time-dependent state which, in turn, bifurcates to a stationary state by a highly hysteretic transition process. Linear-stability theory applied to the bulk base flow does not capture the basic features of the initial transition. A potential approach would be to use model amplitude equations with forcing to mimic the important end regions observed in this system.

The authors would like to thank J. E. Wesfreid, L. Fourtune, and J. J. Hegseth for interesting discussions on the problem. This work was supported by the Office of Naval Research and NATO.

[1] *Propagation in Systems far from Equilibrium*, edited by J. E. Wesfreid, H. R. Brand, P. Manneville, G. Albinet, and N. Boccara, Springer Series in Synergetics Vol. 41 (Springer-Verlag, Berlin-Heidelberg, 1988)
[2] R. W. Walden, P. Kolodner, A. Passner, and C. M. Surko, Phys. Rev. Lett. **55**, 496 (1985).
[3] E. Moses and V. Steinberg, Phys. Rev. A **34**, 693 (1986).
[4] D. R. Ohlsen, S. Y. Yamamoto, C. M. Surko, and P. Kolodner, Phys. Rev. Lett. **65**, 1431 (1990).
[5] I. Mutabazi, J. J. Hegseth, C. D. Andereck, and J. E. Wesfreid, Phys. Rev. A **38**, 4752 (1988).
[6] S. A. Berger, L. Talbot, and L. S. Yao, Annu. Rev. Fluid Mech. **15**, 461 (1983).
[7] S. Chandrasekhar, *Hydrodynamic and Hydromagnetic Stability* (Oxford Univ. Press, Oxford, 1961), Chap. VIII.
[8] P. G. Drazin and W. H. Reid, *Hydrodynamic Stability* (Cambridge Univ. Press, Cambridge, 1981), Chap. III.
[9] Q. I. Daudpota, P. Hall, and T. Zang, J. Fluid Mech. **193**, 569 (1988).
[10] W. H. Finlay, J. B. Keller, and J. H. Ferziger, J. Fluid Mech. **194**, 417 (1988).
[11] P. M. Ligrani and R. D. Niver, Phys. Fluids **31**, 537 (1988).
[12] O. J. E. Matsson and P. H. Alfredsson, J. Fluid Mech. **210**, 537 (1990).
[13] K. Park, G. L. Crawford, and R. J. Donnelly, Phys. Rev. Lett. **47**, 1448 (1981).
[14] C. Normand, I. Mutabazi, and J. E. Wesfreid, Eur. J. Mech. B **10**, 335 (1991).
[15] I. Mutabazi, thèse de doctorat en Physique, Université de Paris 7 (unpublished).
[16] D. Bensimon, A. Pumir, and B. I. Shraiman, J. Phys. (Paris) **50**, 3089 (1989).
[17] C. D. Andereck, S. S. Liu, and H. L. Swinney, J. Fluid Mech. **164**, 155 (1986).
[18] R. J. Donnelly, K. Park, R. Shaw, and R. W. Walden, Phys. Rev. Lett. **44**, 987 (1981).
[19] R. W. Walden and R. J. Donnelly, Phys. Rev. Lett. **42**, 301 (1979).
[20] P. W. Hammer, R. J. Wiener, and R. J. Donnelly (private communication).

Eur. J. Mech., B/Fluids, **10**, n° 2 - Suppl., 239-245, 1991

Recent experimental results in the Taylor-Dean system

I. MUTABAZI* and J. E. WESFREID

Laboratoire d'Hydrodynamique et Mécanique Physique, E.S.P.C.I., U.R.A. C.N.R.S. n° 857,
10, rue Vauquelin, 75231 Paris Cedex 05, France

J. J. HEGSETH and C. D. ANDERECK**

Department of Physics, Ohio State University,
174 W 18th Avenue, Columbus OH 43210, U.S.A.

Abstract

The stability of the traveling roll pattern observed in the Taylor-Dean system is investigated for different values of the rotation ratio. The increase of the control parameter induces a periodic in space and in time modulation of the pattern. External modulation of the pattern may give rize to standing waves for a given amplitude of modulation.

1. Introduction

The phenomena of pattern formation and the transition to turbulence remain chalenging for scientists despite big progress which has been done for decades in order to obtain a better understanding of those phenomena. Two prototype fluid systems have been chosen to study the pattern formation because of their relative simplicity : the Rayleigh-Bénard convection and the Taylor-Couette system. In both systems, it has been observed that the pattern formation correspond to a symmetry breaking in the flow system which reduces the disorder and gives rise to a well organized pattern in a preferred direction. For example, in the Taylor-Couette system, the Taylor vortex flow corresponds to the breaking of the translational symmetry and the spiral vortex corresponds to the breaking of both the translational and the rotational symmetries. The wavy vortex flow is a result of the loss by Taylor vortex flow of the rotational symmetry [Golubitsky &Stewart, 1986].

The external symmetry breaking changes mainly the background state of the fluid system and leads to new types of flow pattern, the most important being the appearance at threshold of the time-dependent flow pattern. This is achieved in convection in binary

* *Present address:* Department of Physics, Ohio State University, 174 W 18th Avenue, Columbus OH 43210.
** *Present address:* S.P.S.R.M., C.E.N.-C.E.A., Orme des Mersiers, F-91101 Gif-sur-Yvette Cedex, France.

EUROPEAN JOURNAL OF MECHANICS, B FLUIDS, VOL. 10, N° 2-SUPPL., 1991
0997-7546/91/ 239 7/$ 2.70/

mixtures[Kolodner &Surko, 1988], in Taylor-Dean system[Mutabazi, Hegseth, Andereck &Wesfreid, 1988], in liquid crystals [Rehberg,Rasenat &Steinberg, 1989], in printing instability[Rabaud, Michalland &Couder, 1990]. The advantage of the flow with time-dependent pattern at threshold is that the transition to chaos is more direct than in systems with stationary pattern at the onset of instability. In the Taylor-Dean system, the rotational symmetry is broken by partially filling the gap between two coaxial horizontal cylinders. The rotation of the cylinders and the free surfaces impose the flow to be reversed into the gap for sufficiently low rotation velocities. In the small gap approximation, the obtained base flow profile is a superposition of the Couette flow due to the rotation and the Poiseuille flow due to the azimuthal pressure gradient. The Taylor-Dean system has been subject of intense investigation very recently because of the rich variety of pattern observed in it : traveling inclined rolls, stationary axisymmetric Dean and Taylor rolls[M&H&A&W, 1988]. The stability of traveling inclined rolls is of great interest because it leads to a new phenomenon called *spatio-temporal modulation* which has never been observed in other known systems[Mutabazi Mutabazi, Hegseth, Andereck &Wesfreid, 1990].

When the inner cylinder rotation velocity is modulated with a periodic external force, a standing wave roll pattern is observed for R_i values less than the critical value for traveling inclined roll.

2. Description of experimental apparatus and procedure

The system consists of the two horizontal coaxial cylinders, the inner cylinder of radius $a = 4.486$ cm rotates at angular velocity $2\pi f_i$, the outer cylinder of radius $b = 5.080$ cm may rotate at angular velocity $2\pi f_o$. The gap between the cylinders is $d = 0.594$ cm and the radius ration $\eta = 0.883$. The system has been conceived as an extended system with the aspect ratio $\Gamma = L/d = 90$. The working fluid is water with 1% of Kalliroscope AQ1000 for visualization. The filling level fraction $n = \theta_f/2\pi$ has been fixed at 0.75 where θ_f is the filling angle. The onset of the instability depends only weakly on the filling level and it has been verified that for $n \in [0.5, 0.8]$, the variation of the R_{ic} is within the experimental precision (≈1%). The control parameters of the flow are the Reynolds numbers defined respectively for the inner and the outer cylinder : $R_i = 2\pi f_i\, ad/\nu$, $R_o = 2\pi f_o bd/\nu$. We fix the outer cylinder Reynolds number R_o and vary the inner cylinder Reynolds number R_i, so that one may define the reduced control parameter $\epsilon = (R_i - R_{ic})/R_{ic}$.

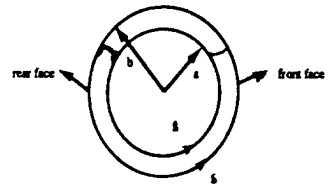

Fig.1 : Schematic experimental geometry

Time-dependent properties of the flow pattern may be characterized by the frequency measurements at a single position using the light-reflectance technique which has been described previously. Spatial periodicity is obtained by using a 28-35 mm variable focal-length lens to image the flow pattern onto a 1024 pixel charge-coupled device (CCD) array element. The array is controlled by a CAMAC module, which also serves as the data gateway to the PDP-11 computer. This system is able to continuously process up to one frame every 0.07 sec. The output of the CCD camera gives the instantaneous reflected light intensity along the axis of the cylinders, the maximum corresponding to roll centers and the minima corresponding to inflow and outflow boundaries. Space-time diagrams I(z,t) are then produced by displaying intensity versus axial position plots at regular intervals along a time axis.

3. Experimental results

We describe the main steps of the transition from laminar flow to chaotic regime observed for the traveling roll pattern.

3.1. Characteristics of the first instability

The first instability from laminar base flow to traveling rolls is, within our experimental precision, a supercritical Hopf bifurcation. Because of the asymmetry of the base flow induced by the presence of recirculation rolls which has been recently described by Normand et *al* [Normand&Mutabazi&Wesfreid, 1990], the intensity of the rolls decreases along the azimuth such that they are weaker in the rear face than in the front face (Fig.1). The observed traveling rolls are inclined by an angle of 20° from the vertical and they move along the axis of the system. As the rolls have no preferred direction of propagation at the onset, they may move either left or right of the system axis, and the direction of the propagation is the same as the roll inclination. Depending on initial conditions for the state above threshold (how the state is reached), both right and left traveling rolls may exist in the system separated by a vertical (non inclined) dislocation line. It represents a source which emits rolls traveling to the right and to the left. The wavelength of the roll pattern at the onset of instability is constant : $\lambda = 1.416$. The frequency of the pattern, for fixed R_0, increases with R_i with different slopes corresponding to the linear growth of the perturbations and to their saturation.

The figure 2 gives the distribution of the reflected roll intensity I(z,t) along the axis of the cylinders for regular time intervals (space-time diagram). The line of the same phase (roll line) are called *characteristics*, their slope gives the inverse of the roll propagation velocity. From the figure 2, it is observed that the roll propagation velocity varies along the axial coordinate z. This is a manifestation of the phase variation of the pattern which should lead to the phase instability.

In fact, increasing the control parameter, the phase variation is enhanced and the high velocity rolls can collide with low velocity rolls, resulting in lost of a roll. This phenomenon is

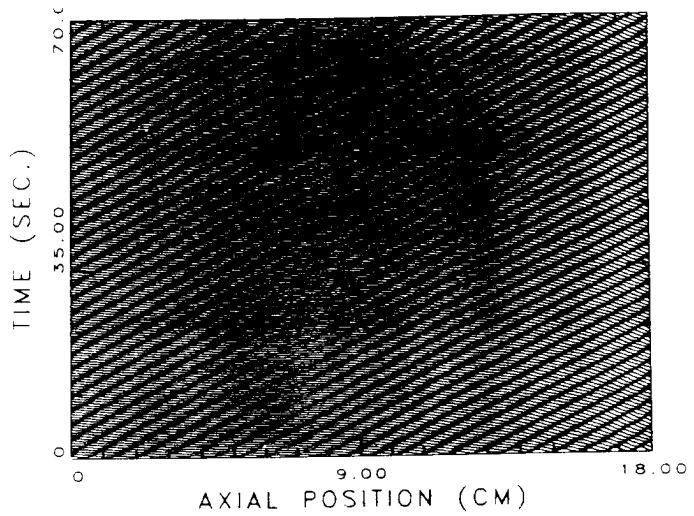

Fig.2 : Space-time for traveling inclined roll close to the onset of instability $R_o = 0$, $R_i = 263$

accompanied by the mechanism of adjustement (relaxation) of the wavelength, but because of the characteristic time $\tau = d^2/\nu$, which differs of the period $T = 1/f_1$ of the pattern, the relaxation is not finished when another collision may occur, this leads to an erratic succession in time and space of the collision events in the pattern. These phenomena are sometimes referred to the phase turbulence and are common to time -dependent patterns in extended systems[Kolodner et al, Joets &Ribotta].

3.2. Excitation of standing waves by external modulation

If the inner cylinder rotation velocity is modulated with a frequency f_M and an amplitude A_M, the threshold of the instability is decreased with increasing A_M, and for $f_M \approx 2f_1$, the roll pattern appears in form of standing wave pattern (Fig.3). This is in good agreement with the calculations of Riecke et al[Riecke&Crawford&Knobloch,1988]. The standing wave pattern becomes unstable to traveling roll pattern with increasing R_i.

3.3. Spatio-temporal modulation of the roll pattern

The second instability of the traveling roll pattern appears in the form of a short-wavelength modulation of the traveling rolls with a lower frequency $f_2 \approx f_1/20$ and a nonaxisymmetric envelope of wavelength $\Lambda \approx 3\lambda$. The ratio f_1/f_2 is function of R_o, while Λ/λ is constant for a large range of values R_o. The modulation envelope moves with a weak velocity

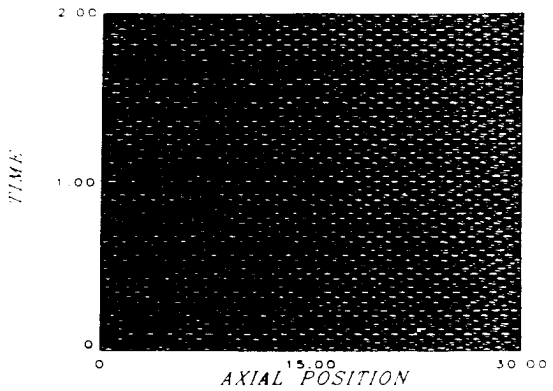

Fig.3 : Space-time diagram for standing wave excited by external modulation of the inner cylinder angular velocity : $R_o = 0$, $R_i = 265$, $R_M/R_{ic} = 0.2$, the detunning parameter e = 0

depending on the value of R_o (Fig.4). The second instability is also a supercritical Hopf bifurcation within the experimental precision of 1% on R_i. The short-wavelength modulation may be due to the wavy modes which occur in the roll pattern because of the roll distorsion observed along their axis.

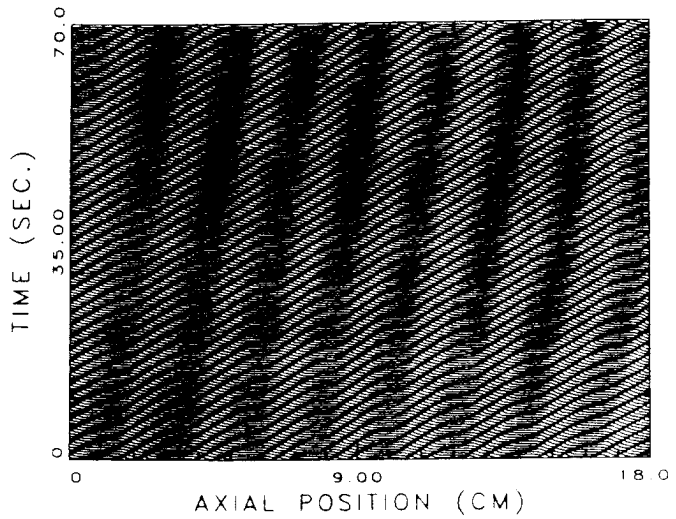

Fig. 4 : Space-time diagram for short-wavelength modulated pattern $R_o = 0$, $R_i = 303$

In fact, for given values of R_i and inclination angle value, one can estimate the number of waves in the azimuthal direction to be 2.9 for $R_o = 0$ and we observe 2 waves in the front face while the third remain unobserved because of the decreasing intensity of the rolls along the azimuth.

3.3. Transition to weak chaos from traveling roll pattern

With further increase of the control parameter R_i, the power spectrum becomes flat and no leading frequency may be detected. But the space-time diagram shows that even individual rolls have lost coherence, the pattern conserves a spatial coherence around the modulating envelope wavelength. Increasing R_i, the space-time diagram shows a succession of traveling rolls zones separated irregularly by sources and sinks. In figure 5, we observe also that the modulating envelope pattern exhibits spatio-temporal defects due to the macroscopic phase variation with the time and the axial coordinate.

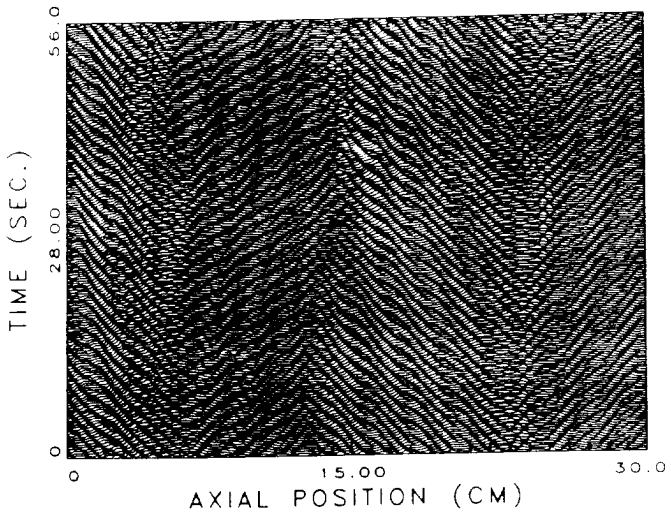

Fig.5 : Space-time diagram for weak chaotic pattern $R_o = 0$, $\varepsilon = 0.176$

4.Conclusion

The traveling roll pattern in Taylor-Dean system with a large aspect ratio undergoes a sequence of transition : phase instability with spatio-temporal defects, short-wavelength modulation, appearance of sources and sinks in the pattern leading to a chaos. The standing wave pattern should be excited in the system by external modulation of the inner cylinder rotation velocity.

Acknowledgement: This work has been supported by the Office of Naval Research and NATO.

References

M.Golubitsky and I.Stewart , SIAM (1986)
A.Joets and R.Ribotta, *J.Phys.(Paris), Colloq.***50**, C3-171(1989)
P.Kolodner, C.M.Surko, Phys.Rev.Lett.**61**, 842 (1988)
P.Kolodner,D.Bensimon and C.M. Surko, *Phys.Rev.Lett* .**60**, 1723 (1988)
I.Mutabazi, J.J.Hegseth,C.D.Andereck and J.E.Wesfreid, *Phys.Rev.A*. **38**, 4762(1988)
I.Mutabazi, J.J.Hegseth,C.D.Andereck and J.E.Wesfreid, *Phys.Rev.Lett*. **64**, 1729(1990)
C.Normand, I.Mutabazi and J.E.Wesfreid, *Eur.J.Mech. B(Fluids)*, to appear (1990)
M.Rabaud, S.Michalland and Y.Couder, Phys.Rev.Lett. **64**, 184 (1990)
I.Rehberg, S.Rasenat and V.Steinberg, Phys.Rev.Lett. **62**, 756 (1989)
H.Riecke,J.D.Crawford , E.Knobloch, *Phys.Rev.Lett*. **61**, 1942 (1988)

A MODEL OF THE DISAPPEARANCE OF TIME-DEPENDENCE IN THE FLOW PATTERN IN THE TAYLOR-DEAN SYSTEM

Laurent Fourtune[1], Innocent Mutabazi, C. David Andereck

Department of Physics, the Ohio State University,
174 W 18th Avenue, Columbus, OH 43210, USA

INTRODUCTION

The transition to chaos in diverse physical systems far from thermodynamic equilibrium is one of the challenging problems of modern physics. The most commonly studied models in hydrodynamics are the Rayleigh-Bénard thermal convection system and the Taylor-Couette instability[1, 2], both of which have been intensively investigated during the last two decades. The transition to chaos has been characterized and various scenarios have been discovered experimentally and in numerical simulations of those systems[3]. These two systems possess several symmetries, the breaking of which gives rise to new patterns. However, the real world is far from these simple cases and an effort is underway to study more complicated systems such as thermal convection in superposed layers of immiscible fluids[4], the horizontal Taylor-Couette system with a partially filled gap[5], the flow in curved channel[6] or the boundary layer flow over a concave wall[2].

The flow between two horizontal cylinders with a partially filled gap also known as the Taylor-Dean system, exhibits a rich variety of patterns of stationary and traveling rolls[5]. In the case when the outer cylinder is fixed, the initial instability occurs in the form of traveling inclined rolls, and upon increasing the control parameter, the roll pattern exhibits a spatio-temporal modulation[7]. In the case when the inner cylinder is fixed, the transition occurs as traveling inclined rolls which undergo a subcritical bifurcation to stationary axisymmetric rolls[8]. In this paper, we will describe in detail this transition and will give a tentative explanation using the Ginzburg-Landau equation model.

The experimental system consists of two horizontal coaxial cylinders, a stationary inner cylinder made of black Delrin plastic with radius a = 4.486 cm, and an outer cylinder made of Duran glass with radius b = 5.08 cm, which rotates with angular velocity Ω. Teflon rings are attached to the inner surface of the outer cylinder a distance L = 53.40 cm apart, giving an aspect ratio Γ = L/d = 90. The working fluid is water with 1% Kalliroscope AQ 1000 added for visualization, and its kinematic viscosity is 0.98 cstokes at the temperature T = 21C. The filling level fraction v = 0.75 weakly influences the instability threshold[9].

The control parameter of the system is the Taylor number $Ta = (\Omega R d/\nu)(d/R)^{1/2}$ defined with respect to the outer cylinder parameters. The flow-pattern wavelengths are

---

[1]Present address : Elève de l'Ecole Normale Supérieure, 24 rue Lhomond, F-75231 Paris Cedex 05, France

Ordered and Turbulent Patterns in Taylor-Couette Flow
Edited by C.D. Andereck and F. Hayot, Plenum Press, New York, 1992

scaled by the characteristic length d (gap size), the phase velocity is scaled by v/d and the frequencies are scaled by the inverse of the radial diffusion time d^2/ν = 36 sec. We have chosen the ramping rate (experimental variation of the Taylor number) r = dTa/dt < 3 in order to achieve the quasistatic condition.

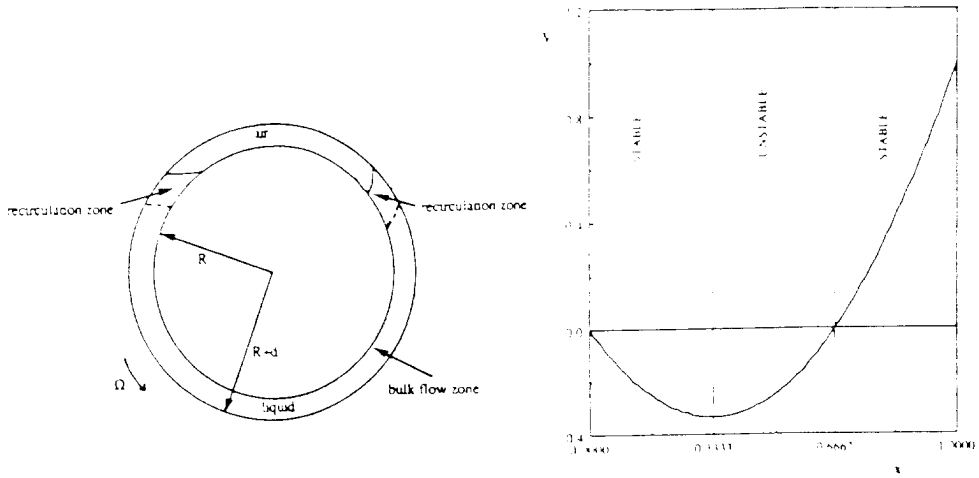

Figure 1. Flow configuration : a)Experimental geometry b) Base bulk flow velocity profile

Flow frequencies are measured from the power spectra of single point series obtained with laser light reflected off the Kalliroscope flakes onto a photodiode detector. Spatial dependence data are obtained using a 28-85 mm variable focal length lens to form an image of the visualized flow on a 1024 pixel charge coupled device (CCD) linear array interfaced through CAMAC to a computer. The line of 1024 pixels is oriented parallel to the cylinder axis. The output consists of intensity maxima and minima which correspond to the centers and boundaries of the rolls. Space-time diagrams are then produced by displaying intensity versus axial position plots at regular time intervals. Analysis of these plots yields the roll size and the dynamics of the pattern in time and space. The spatial periodicity of the flow pattern is characterized by the wavenumber $q = 2\pi\, d/\lambda$ and its time-dependence by the phase velocity, both quantities measured from the space-time diagrams.

EXPERIMENTAL RESULTS

Rotating cylinder ends, in our case Teflon rings attached to the outer cylinder, induce Ekman cells even for low values of Ta. They become visible at Ta = 25 near both ends of the system and have an axial extension of 0.95 cm. At larger Ta, smaller stationary small rolls of average size λ_E = 0.48 cm are formed adjacent to the Ekman end cells. The maximum number of those rolls is 6 when Ta = 80. As they are localized in space and their spatial extent does not increase, this part of the system is referred to as the Ekman region in the following. For Ta = 91, cells in the Ekman region become oscillatory with a frequency f = 0.143 Hz, and at the same time, 3 to 5 traveling inclined rolls moving toward the middle of the system are generated close to each Ekman region. These rolls have a wavelength λ = 1.584 or wavenumber q = 3.967.

The phase velocity of the traveling rolls depends on their axial position : close to an Ekman region, it is v = 0.180 cm/sec. The Fourier spectrum of reflected light intensity gives a frequency peak around f = 0.136 Hz (4.90 in scaled units). The traveling rolls frequency is nearly identical to that of the oscillating rolls in the Ekman region. There are no rolls observed in the middle of the system. The mixed state of traveling inclined rolls (perturbations of finite amplitude $A \neq 0$) and of laminar base flow (zero amplitude state) is stable, having been observed over many hours without noticeable changes. The transition

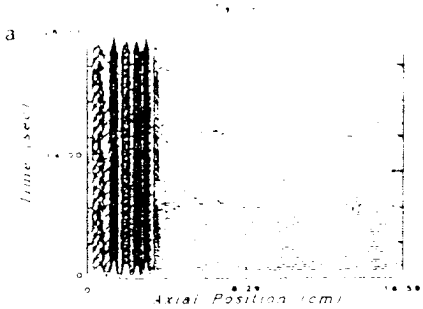

Figure 2-a . Stationary Ekman region (Ta=82.7)

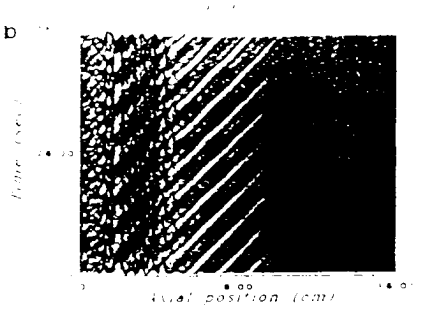

Figure 2-b . Oscillatory Ekman region and emission of traveling rolls (Ta=91)

has a hysteresis of about 13% in Ta, and is a subcritical Hopf bifurcation. Increasing Ta, the number of traveling inclined rolls increases on each side and the laminar base flow extension decreases. At Ta = 110, the flow pattern becomes stationary and axisymmetric after a transient period during which the pattern relaxes by adjusting its amplitude and phase (wavelength). The spatial evolution of the transition to the stationary state for a fixed value of the control parameter shows that there exists a front between the time-dependent and stationary states, moving with a finite velocity v_f = 0.65 cm/sec, larger than that of the traveling rolls themselves. The phase velocity of the traveling rolls has a large discontinuity at the transition. Furthermore, the transition exhibits a large hysteresis, about 14% in Ta. The rolls become axisymmetric and the wavelength changes to λ = 1.80, corresponding to the wavenumber q = 3.53, together with a two-roll modulation wavelength Λ = 2.81 or wavenumber Q = 2.24.

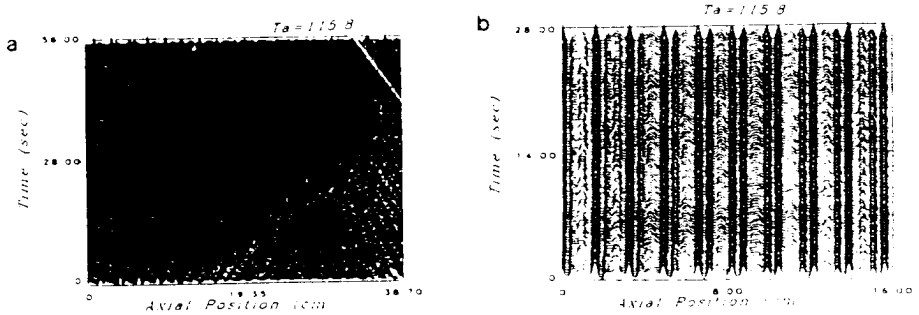

Figure 3 . a)Disappearance of time-dependence and b)stationary Dean rolls with spatial modulation

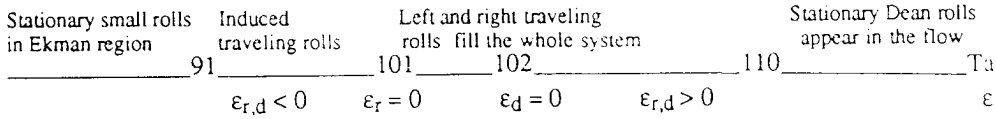

Figure 4 . Transition sequence for the control parameter (Ta or ε)

DISCUSSION OF RESULTS

In order to understand the previous results, we analyze the structure of the base flow when only the outer cylinder rotates. The base flow consists of the azimuthal bulk flow, of the flow in the recirculation zone and of the flow in the Ekman region. The flow in the recirculation zone has an extension comparable to the gap size d and chosing the small gap approximation, we are able to reduce its influence. The Ekman region is small compared to the whole length of the flow extension (l_E = 0.05 L). The velocity profile of the azimuthal bulk base flow (in the small gap approximation) is given by $V(x) = 3x^2 - 2x$ (Fig.1-a) and as deduced from Rayleigh's stability criterion, it has one unstable layer sandwiched between two stable layers. The unstable layer is subject to the Dean instability as it belongs to the Poiseuille part of the profile. The linear stability theory applied to this velocity profile V(x) gives a stationary critical state with the following characteristics : $q_c = 2.875$, $Ta_c = 89.74$. The stationary state appears at Ta = 110 with the wavenumber q = 3.53, therefore we consider that the transition to stationary rolls is the true Dean instability, the difference in critical parameters and the prexisting observed states are due to the boundary effects, mainly the flow in the Ekman region. The time-dependent roll pattern observed close to the Ekman region is a metastable phase due to the excitation by the Ekman region into a propagating medium (flow in our case). When the small rolls in the Ekman region become oscillating, the Ekman region can be considered as an oscillatory localized source (with frequency ω) which emits traveling rolls in the flow.The time dependent structure is inclined for symmetry arguments and has a wavenumber which is evidently selected by the frequency in the Ekman region.

Amplitude equation and emission of rolls in subcritical regime ($\varepsilon < 0$)

In order to understand these results, we represent the perturbative velocity in the time-dependent flow pattern (right traveling) in the separable form :

$$v'(t,x,y,z) = A(t,z)\, F(x) \exp\{i(\omega_c t - q_c z - p_c y)\}$$

where F(x) is the structure function and the envelope A(t,z) satisfies the one dimensional complex Ginzburg-Landau amplitude equation :

$$\frac{\partial A}{\partial t} - v_g \frac{\partial A}{\partial z} = \varepsilon (1+ic_0)A + \xi_0^2(1+ic_1)\frac{\partial^2 A}{\partial z^2} - g(1+ic_2)|A|^2 A \qquad (1)$$

where $\varepsilon = (Ta-Ta_c)/Ta_c$ is the relative distance from the onset of instability,
v_g is the group velocity of the flow pattern,
ξ_0 is the coherence length of the perturbations,
c_0, c_1 and c_2 are respectively the corrections to the frequency due to the control parameter, the wavelength and amplitude variations, and
g is the Landau constant of the nonlinear saturation.

We consider the Ekman region as a localized source emitting at the same frequency ω_c at z = 0 and z = L where L is the whole length of the flow extension. Far from the Ekman region, the amplitude of one induced traveling roll pattern is decreasing to zero. We therefore impose the boundary condition on the Ginzburg-Landau equation at one end, for example z = 0, without loss of generality : $A(t, z=0) = A_0 \exp\{i(\omega-\omega_c)t\}$, where A_0 represents the strength of the source. The spatial dependence of the envelope is chosen as follows $A(t,z) \sim \exp(ikz)$ where the wavenumber k is a complex number whose real part k_r is the correction to the wavenumber q_c and the imaginary part k_i gives the spatial damping length of the perturbation induced by the localized source. A similar problem formulation has been successfully applied to open flows such as wakes and jets[10]. The problem stated in this way contains many

parameters : ε, v_g, c_1,c_2 and A_0, while ξ_0 and g can be removed by scaling of the axial coordinate z and of the amplitude A. The group velocity cannot be removed since the system does not possess the Galilean invariance because of the boundaries. For simplicity of the analysis, we consider $c_1 = 0 = c_2$; numerical simulations with different values have shown no qualitative difference with the results given here. For $\varepsilon < 0$, all perturbations are damped, but for small $|\varepsilon|$, the damping is slow and some strong external excitation (in our case oscillatory Ekman rolls) may lead to observable stable solutions of the CGL equation. The results are then :

1. When $\omega = 0$, $v_g = 0$ and we obtain the trivial solution $A(t,z) = 0$, which means that the stationary Ekman region does not induce a propagating flow pattern.

2. When $\omega \neq 0$, $v_g \neq 0$, $A \neq 0$: any external time-dependent excitation can propagate in the system with a $v_g = (\omega-\omega_c)/(q_c+k_c)$. The amplitude of the perturbative envelope A exhibits two successive regimes in z-dependence : nonlinear $A \sim z^{-1/2}$ and linear where $A \sim e^{(\varepsilon/v_g)z}$ (Figure 5-a shows A(z) for different values of ε). For fixed A_0 and v_g, the spatial damping coefficient k_i is estimated from our numerical calculations (from distance at which the excitation damps by a factor of 10) : it is a linear function of ε except for small values when the dependence becomes nonlinear.

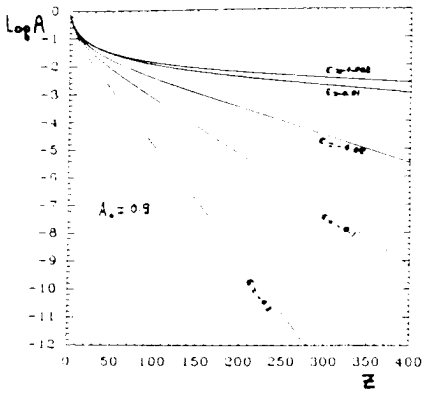

Figure 5-a . Spatial amplitude variation for different values of ε

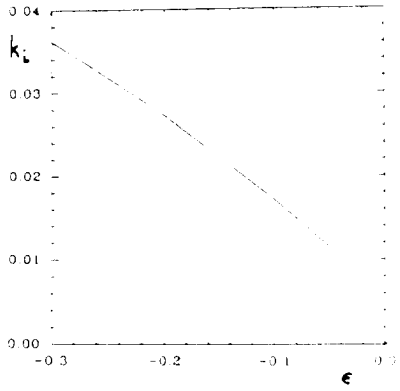

Figure 5-b . Spatial damping coefficient k_i as function ε

Hysteresis as result of modes interaction

In the flow regime between Ta = 101 and Ta = 110, both traveling inclined and Dean rolls interact, therefore the flow pattern may be described by 3 amplitudes : A_r for right traveling inclined rolls, A_l for left traveling inclined rolls and A_d for Dean rolls. Without loss of generality and for simplicity, we analyze the interaction between the right traveling A_r and Dean rolls A_d. Experimentally, the bifurcation to traveling rolls is supercritical and that to Dean rolls is subcritical, therefore we have the Ginzburg-Landau equations at 5th order, neglecting the spatial dependence :

$$\frac{\partial A_r}{\partial t} = \varepsilon_r A_r - (g_r|A_r|^2 + g_{rd}|A_d|^2)A_r - h_r|A_r|^4 A_r - k_{rd}|A_d|^4 A_r - f_{rd}|A_d|^2|A_r|^2 A_r \qquad (2\text{-a})$$

$$\frac{\partial A_d}{\partial t} = \varepsilon_d A_d - (g_{dr}|A_r|^2 + g_d|A_d|^2)A_d - h_d|A_d|^4 A_d - k_{rd}|A_r|^4 A_d - f_{rd}|A_r|^2|A_d|^2 A_d \qquad (2\text{-b})$$

where $g_r > 0$, $g_d < 0$, $d_r > 0$, $d_d > 0$ after the nature of the bifurcations, and the coupling constants g_{rd}, g_{rd}, k_{rd}, $f_{rd} < 0$, as the interaction between modes is only destructive. By assumption $g_r << (g_d, g_{rd}, g_{dr})$, i.e., the right traveling rolls are dominated by linear growth as maintained by the external source.

Ramping up, the amplitude $|A_d|$ of the Dean rolls is very small so that all terms in equation (2-a) containing $|A_d|^{n>2}$ are negligible, and therefore the right traveling rolls have amplitude $|A_r|$ given by :

$$|A_r|^2 = -\frac{\varepsilon_r}{g_r} \qquad \text{for small } \varepsilon_r$$

and

$$|A_r|^2 = -\frac{g_r}{h_r} + \left(\frac{\varepsilon_r}{h_r}\right)^{1/2}\left(1+\frac{g_r^2}{4\varepsilon_r h_r}\right)^{1/2} \qquad \text{for large } \varepsilon_r$$

The equation for Dean rolls can be written in the form, where we have neglected the spatial variations :

$$\frac{\partial A_d}{\partial t} = \varepsilon_d^{eff} A_d - g_d^{eff}|A_d|^2 A_d - h_d |A_d|^4 A_d \qquad (3)$$

with $\varepsilon_d^{eff} = \varepsilon_d - g_{dr}|A_r|^2 - k_{dr}|A_r|^4$ $g_d^{eff} = g_d + f_{dr}|A_r|^2$

For small ε_r, $\varepsilon_d^{eff} < 0$, the Dean rolls are damped and the flow is dominated by the right traveling rolls. For large ε_r, the quantity ε_d^{eff} can pass through zero toward positive values and therefore, the Dean rolls can grow in the flow. The onset of Dean rolls is given by the condition $\varepsilon_d^{eff} = 0$, this condition corresponds to $Ta_c = 110$. Once the Dean rolls have appeared in the flow, the linear growth and the nonlinear interaction coefficient become more important because of the coupling with the right traveling rolls. If for large ε_r, $g_d^{eff} = 0$, the transition to Dean rolls should change from subcritical to supercritical. This would explain the long time needed for the transition from the time-dependent to stationary Dean rolls.

The right traveling rolls equation becomes :

$$\frac{\partial A_r}{\partial t} = \varepsilon_r^{eff} A_r - g_r^{eff}|A_r|^2 A_r - d_r |A_r|^4 A_r \qquad (4)$$

where

$$\varepsilon_r^{eff} = \varepsilon_r A_r - g_{rd}|A_d|^2 - d_{rd}|A_d|^4 \quad \text{and} \quad g_r^{eff} = g_r + f_{rd}|A_d|^2$$

With the growth of the Dean rolls, ε_r^{eff} can pass through zero to negative values and as the quantity $g_r << g_d$, the traveling rolls are overturned by the Dean rolls through nonlinear interaction. So we have shown that the transition to Dean rolls is highly hysteretic because of the interaction with the right traveling rolls.

CONCLUSION

The flow between two horizontal coaxial cylinders with a partially filled gap, when only the outer cylinder rotates, exhibits an unusual transition from time-dependent patterns induced by the Ekman regions to a stationary axisymmetric pattern flow. This transition and its hysteretic nature is understood using the Ginzburg-Landau equation, with an external source. There is still an open problem concerning the spatial modulation of the stationary rolls.

ACKNOWLEDGMENT

We would like to thank J.E. Wesfreid for suggesting the approach taken here and P. Laure for the fruitful discussions. L.F. acknowledges the support from the Ecole Normale

Supérieure (France) and the hospitality of the Physics Department of the Ohio State University. This project is supported by ONR and NATO.

REFERENCES

1. S. Chandrasekhar, "Hydrodynamic and Hydromagnetic Stability", Oxford University Press, (1961)
2. P.G. Drazin and W.H. Reid, "Hydrodynamic Stability", Cambridge University Pres (1981)
3. P. Manneville, "Dissipative Structures and Weak Turbulence", Academic Press, N. Y. (1990)
4. S. Rasenat, Busse and I.Rehberg, A theoretical and experimental study of double-layer convection, J. Fluid Mech.199 : 519 (1989)
5. I. Mutabazi, J.J. Hegseth, C.D. Andereck and J.E. Wesfreid, Pattern Formation in the flow between two horizontal coaxial cylinders with a partially filled gap, Phys. Rev. A 38: 4752 (1988)
6. P.M. Ligrani and R. D. Niver, Flow visualization of Dean votices in a curved channel with 40 to 1 aspect ratio, Phys. Fluids 31: 3605 (1988)
7. I. Mutabazi, J.J. Hegseth, C.D. Andereck and J.E. Wesfreid, Spatio-temporal pattern modulation in the Taylor-Dean system, Phys.Rev. Lett. 64: 1729 (1990)
8. I. Mutabazi and C.D. Andereck, Transition from time-dependent to stationary flow patterns in the Taylor-Dean system, Phys. Rev.A 44: 6169 (1991)
9. I. Mutabazi, Etude théorique et expérimentale de l'instabilité centrifuge de Taylor-Dean, thèse de doctorat en Physique, Université de Paris 7 (1990)
10. P. Huerre and P. Monkevitz, Local and global instabilities in spatially developing flows, Ann. Rev. Fluid Mech. 22: 473 (1990)

Drift Instability and Second Harmonic Generation in a One-Dimensional Pattern-Forming System

Innocent Mutabazi[a] and C. David Andereck

Department of Physics, The Ohio State University, 174 W18th Avenue, Columbus, Ohio 43210

(Received 25 September 1992)

The transition to spatiotemporal chaos in the neighborhood of a codimension-two point observed in the Taylor-Dean system is investigated. The initial instability is to stationary Dean vortex flow, which becomes unstable to a drift instability, followed by a wavelength-halving instability. This sequence of transitions may be explained in terms of the interaction between the first and second spatial harmonics of the basic pattern.

PACS numbers: 47.52.+j, 47.32.−y

The formation of patterns in systems far from equilibrium has been intensively investigated in the last few years because of the diversity and richness of the states resulting when the stress applied to the system varies. Recently, particular attention has been drawn to those one-dimensional extended systems in which oscillatory states occur from the onset of either the first instability or as the secondary instability [1–4]. This has been motivated by the leading role played by the breaking of symmetries (such as the occurrence of a frequency in the pattern, drifting, or localized traveling pulses) in the transition to chaos. Recent developments in the nonlinear Ginzburg-Landau theory for dissipative systems have provided fresh insight into some of the experimental phenomena such as the localized pulselike structures in cellular patterns and the dynamics of defects [5,6]. In particular, a model of the interaction of the second harmonic with the fundamental mode in dissipative systems, developed in the context of the Kuramoto-Sivashinsky equation [7], has been adapted to explain the drift instability observed in the above experiments [8]. Moreover, spatial period halving (followed in some cases by spatial period doubling from the new fundamental wavelength) has been observed in directional solidification when the interface is rapidly driven above the drift threshold and then rapidly driven back to a stationary cellular regime [2]. The spatial second harmonic in that case is thus a consequence of a "forced" wavelength selection process. Therefore the question of the second harmonic generation and of its stability, familiar from other fields such as nonlinear optics [9], may also be investigated in dissipative systems far from equilibrium. The problem of resonant wave interaction between the fundamental mode and the second harmonic has been addressed in the Taylor-Couette system [10], in directional solidification [11], and in double-layer thermal convection [12,13].

We report here recent experimental results from a one-dimensional pattern-forming hydrodynamic system in which the underlying features of the second harmonic generation and its stability arise naturally (without a "forcing procedure") when the control parameter driving the system is increased continuously from the base flow state to bifurcated states (cellular patterns). As a function of the control parameter R (to be identified below) three main regimes were observed: For $R < R_c$, the flow is patternless; for $R_c < R < R_d$, the flow consists of a stationary cellular pattern with a constant mean wavelength; and, for $R_d < R < R_h$, the cellular pattern drifts at a constant velocity. For $R = R_h$, two patterns with different spatial wavelengths coexist separated by a line. For $R > R_h$, the large wavelength pattern disappears leaving only a small wavelength pattern. For still higher values of the control parameter, the flow becomes chaotic. We will describe these results in more detail and seek an explanation for them in the context of recent theoretical developments.

We consider the *Taylor-Dean system* [4], which consists of two independently rotating horizontal coaxial cylinders with a partially fluid-filled gap. In significant contrast with the Taylor-Couette system [14], the partial filling of the gap in the Taylor-Dean system produces two free surfaces. The rotation of the cylinders drives the fluid toward the free surfaces, and, to reverse it, a pressure gradient along the azimuthal direction is created. Far away from the free surfaces, the flow velocity profile is a combination of a Couette profile due to the cylinder rotation and a Poiseuille profile due to the azimuthal pressure gradient. The streamline curvature induces a radial stratification of the fluid particle momentum. Rayleigh's stability criterion [14] predicts, in the case of negative momentum stratification, that centrifugal instabilities will occur and manifest themselves as a pattern of longitudinal rolls periodically spaced in the spanwise direction and superimposed on the base flow. The linear and nonlinear stability analyses of this flow show that, depending on the relative velocity of the rotating cylinders, the destabilization of the different potentially unstable layers gives rise to either stationary or traveling roll patterns with different wave numbers, the ratio between them varying from 1 to 2.5 [15,16]. Thus, the Taylor-Dean system realizes a quasi-one-dimensional extended system with competing instabilities with various wavelengths.

Our experimental system consists of an inner cylinder made of black Delrin plastic with radius $a = 4.486$ cm, rotating at angular velocity Ω_i, and an outer cylinder, with

radius $b = 5.080$ cm, made of Duran glass and rotating in the same direction as the inner cylinder at angular velocity Ω_o. The gap between the cylinders is $d = b - a = 0.594$ cm, and the radius ratio $\eta = a/b = 0.883$. Teflon rings are attached to the inner surface of the outer cylinder a distance $L = 53.40$ cm apart, giving an aspect ratio $\Gamma = L/d = 90$, large enough to realize a quasi-one-dimensional extended system. The working fluid is water with 1% Kalliroscope AQ 1000 added for visualization. Its kinematic viscosity is $\nu = 0.98 \times 10^{-2}$ cm^2/sec at 21 °C.

We define the flow control parameters to be the Reynolds numbers relative to the inner and outer cylinders, respectively: $R_i = \Omega_i ad/\nu$, $R_o = \Omega_o bd/\nu$. In this experiment, Ω_o was kept fixed, and we varied slowly (quasistatically) the inner cylinder speed from the base flow state to a bifurcated state, therefore the control parameter $R = R_i$. The ramping rate (experimental variation of the inner cylinder Reynolds number) $r = dR_i/dt^* \leq 3$ where $t^* = t/\Gamma$ [17]. The Reynolds numbers are measured within a precision of 2%.

Flow frequencies are measured from the power spectrum of single-point time series obtained with laser light that is reflected off the Kalliroscope flakes onto a photodiode detector. Spatial dependence data are obtained using a 28–35 mm variable focal length lens to form an image of the visualized flow on a 1024-pixel charge-coupled device linear array interfaced through a computer automated measurement and control (CAMAC) system to a computer. The line of 1024 pixels is oriented parallel to the cylinder axis. The output consists of intensity maxima and minima which correspond to the centers and boundaries of the rolls. Space-time diagrams are then produced by displaying intensity versus axial position plots at regular time intervals ($\Delta t = 0.07$ sec). The spatial periodicity of the flow pattern is characterized by the nondimensional wave number $q = 2\pi d/\lambda$, and its time dependence is characterized by the propagation velocity c or the frequency f.

The main experimental results to be described here are represented in the parameter space (R_o, R_i) of Fig. 1, where $R_o \in [205, 250]$. The critical values of the control parameter for the first and second instabilities depend sensitively on R_o. The first instability gives rise to stationary axisymmetric rolls aligned along the aximuthal direction. The second instability occurs via a supercritical bifurcation, resulting in axisymmetric rolls traveling along the axial direction. The propagation velocity of the rolls at onset is of order 10^{-2} cm/sec $= 0.6\nu/d$. This behavior is usually referred to as a *drift instability* and has been interpreted recently, for other flows, as the result of an interaction between the fundamental mode and the damped second harmonic [8]. We have found clear evidence for the importance of the second harmonic in the present work. Close to the onset of this instability (for R_i less than about 300 in the case shown in Fig. 2), the drift roll velocity is, within experimental uncertainty, a linear function of the roll amplitude in agreement with the

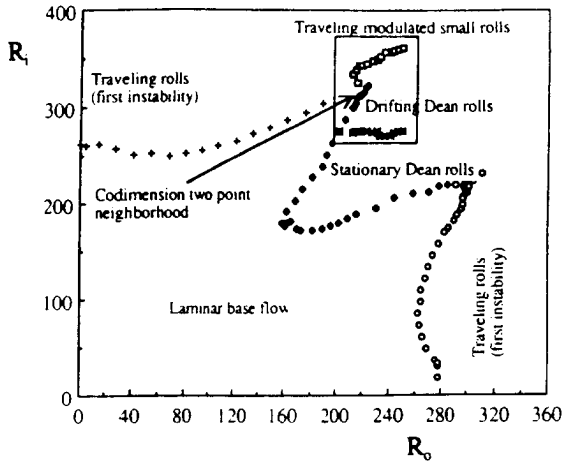

FIG. 1. The experimental parameter space (R_o, R_i) in the neighborhood of the investigated codimension-two point (located approximately by the arrow): Solid diamonds represent the onset of the stationary modes (R_{ic1}), stars represent the onset of the drift instability (R_{ic2}), and open squares refer to the onset of the halving instability (R_{ic3}).

theoretical model [8]. The traveling rolls have almost the same wavelength as the stationary rolls. Just above onset, a phase instability occurs that results in roll annihilation and creation events. For each experimental trial, these events occur at different axial positions, but consistently have a time period approximately equal to the roll drift period (Fig. 3). The points in the space-time diagram where annihilation and creation occur are spatiotemporal defects or grain boundaries [6,18]. There is always an odd, small number (1,3,5,...) of these defects, the number selected depending on the control parameter R_i and the ramping rate.

A further increase of R_i leads either to the extinction of the pattern for $205 < R_o < 213$ (by crossing the line marked by solid diamonds in Fig. 1) or to pattern weakening, detected visually by a loss of pattern contrast and quantitatively by a measured decrease of the drift frequency f_d (which is proportional to the roll amplitude near the onset of the drift instability), for $R_o > 213$. Near $R_o = 213$, there is neither roll weakening nor roll extinction, but the transition occurs for $R_i = 315$ to a state with large rolls and small rolls occupying different regions along the system axis. At the boundary or *wall* between the regions (the location of which depends on R_i), a large roll propagates and splits into two rolls of different sizes (Fig. 4) which propagate in the direction of the parent roll and with approximately the same drift velocity. Such states are observed for a finite range of the control parameter values $R_i \in [315, 330]$. The generally observed case is that where large rolls occupy a part (e.g., the left part) of the flow pattern and small rolls occupy the remainder (right); however, states with small rolls sandwiched between regions of large rolls have also been observed. The points in the parameter space (R_o, R_i) near which both roll types coexist in the system are called

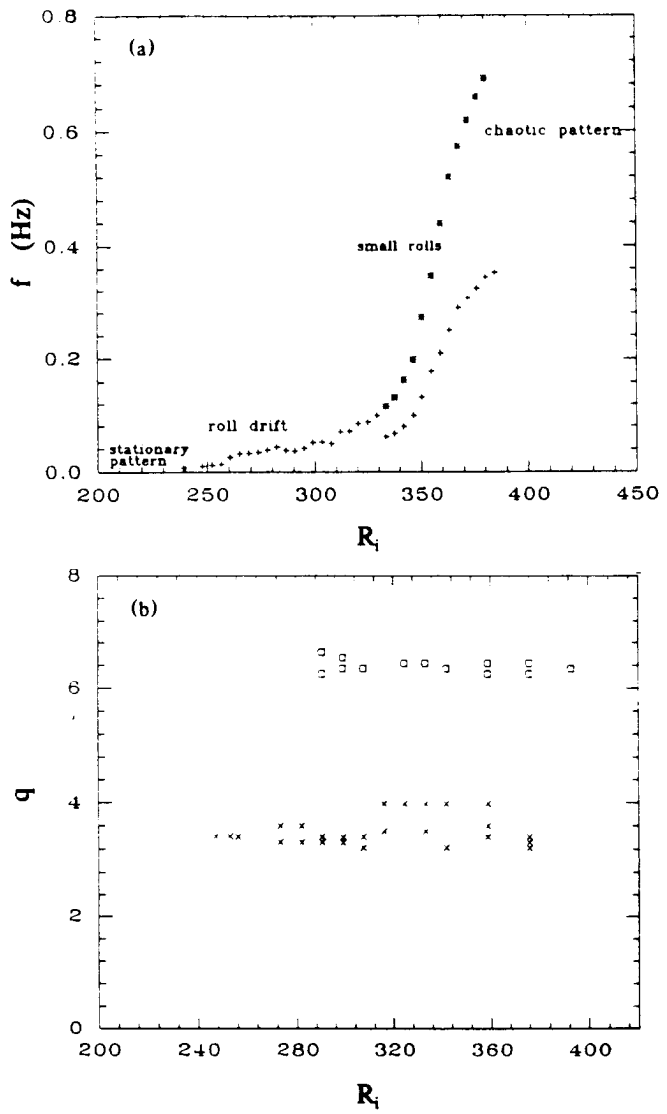

FIG. 2 (a) Drift frequency (proportional to the roll drift velocity): + represents the frequency of the fundamental mode (large roll state) and * represents the frequency of the small roll state; and (b) dimensionless roll wave number q as a function of the control parameter R_i for fixed $R_o = 242$: x represents the wave number of the fundamental mode (large rolls, whether stationary or drifting); open squares represent the average wave number of the small rolls. The pattern above $R_i \simeq 380$ is chaotic.

codimension-two points. The occurrence of small rolls reduces the domain of large rolls until they disappear entirely from the pattern when the control parameter is increased above 330. For a fixed value of R_i, the wall position fluctuates in space and time (Fig. 4) in a zone of approximately a parent roll size.

For $R_o > 213$ and less than about 250, the weak rolls again give rise to coexisting small rolls (R_{ic3} in Fig. 1), but the small rolls fill the system after only a small increase of R_i. In fact, the range of the values of R_i in which the coexistence of large and small rolls is observed

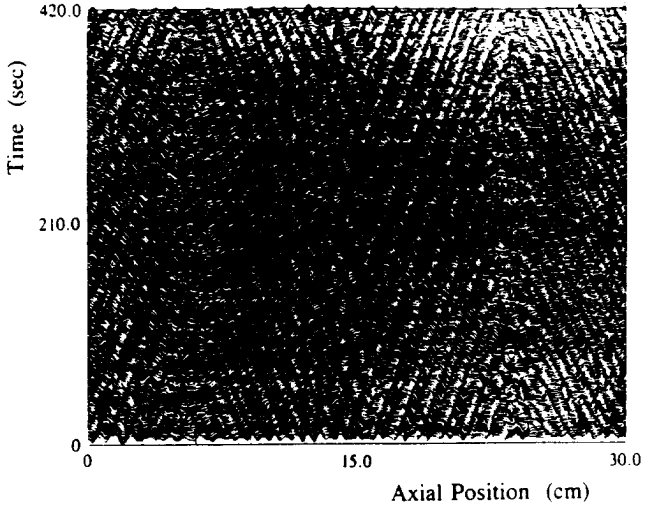

FIG. 3. Space-time diagram of traveling rolls with spatiotemporal defects for $R_o = 242$, $R_i = 282$. In this diagram, representing 60% of the whole flow pattern, there are three positions where spatiotemporal defects occur: $z_1 = 6.4$ cm $= 10.8d$, $z_2 = 12.2$ cm $= 20.5d$, $z_3 = 25.8$ cm $= 43.4d$, the left end of the pattern being located 9.7 cm $= 16.3d$ away from the origin of this plot. The period between defects at the same position is 28 sec $= 0.78d^2/\nu$ for $R_o = 242$, $R_i = 282$. The whole pattern contains five defects (three sourcelike and two sinklike). In a sourcelike defect, a roll splits to form two rolls, while in a sinklike defect, two rolls collide to form one roll.

decreases as R_o increases. The small rolls are periodically modulated in space and time (their intensity increases and then decreases as they propagate) and behave like a two-roll packet (drifting at the same velocity) in which the rolls exchange energy. In the small rolls region, we have observed localized in space and time remanent large

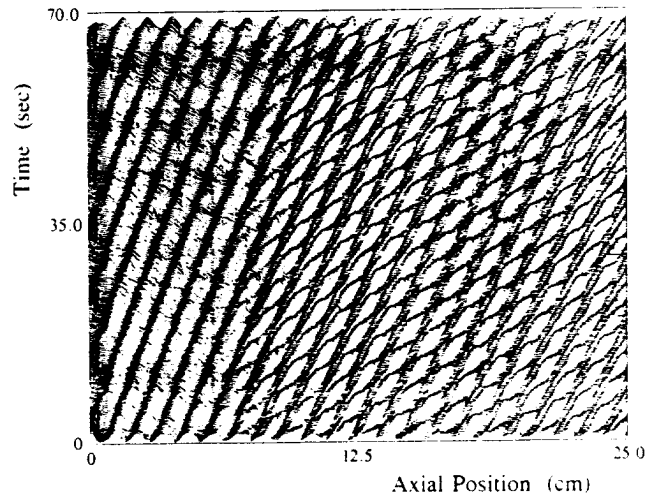

FIG. 4. Space-time diagram for coexisting large and small traveling rolls in the vicinity of the codimension-two point ($R_o = 213$, $R_i = 326$). Each large roll splits into two rolls of different sizes which propagate in the same direction forming a two-roll packet.

rolls. For $R_o < 213$, a transition occurs as indicated by the crosses in Fig. 1 from the now patternless flow to traveling rolls which are about half the size of the former, extinct, rolls.

In all cases, the spatial Fourier spectra show that the frequencies and the mean wave numbers of the small roll and superseded large roll pattern states are in ratios close to 2:1; the differences $\delta f = f_h - 2f_d \sim 0.01$ and $\delta q = q_2 - 2q_1 \sim 0.20$ evidently are due to the spatiotemporal modulations of the small rolls, and other temporal and spatial phase gradient related instabilities. Since the second frequency f_h is almost twice the former drift frequency ($f_h \simeq 2f_d$) and the small rolls have a size almost a half of the former rolls (Fig. 4), this transition may be called a *halving instability*.

The linear stability analysis of the Taylor-Dean system shows that [16], near the particular value of the relative rotation velocity $\mu = \Omega_o/\Omega_i = 0.714$, which is in the range of values of (R_o, R_i) considered here, the marginally stable modes are stationary and have wave numbers which are quite resonant (2:1). Therefore, following the general nonlinear analysis of resonant stationary modes [8,12], we may conclude that their interaction leads to the predominance of either the fundamental mode (axisymmetric stationary rolls) for low values of $R_i > R_{ic1}$ or the mixed states of fundamental and second harmonic modes with finite phase shifts between them, which give rise to drifting rolls for $R_i > R_{ic2}$. The effective growth rate of the drifting rolls decreases, leading to the pattern extinction or weakening observed experimentally. The generation of the small traveling rolls from the large rolls probably originates in the mechanism of the second harmonic generation, when the effective growth rate of the drifting mode crosses zero to negative values, while that of the second harmonic becomes strong enough to override the fundamental mode. This flow pattern is in turn subject to new phase instabilities and, in fact, at their onset, the small traveling rolls have at least two frequencies and are modulated in space. The simultaneous presence of large and small traveling rolls in the Taylor-Dean system constitutes an important realization of coexisting stable time-dependent states in a nonequilibrium hydrodynamic system. An understanding of the dynamics of the wall between the two stable drifting states with two different wavelengths remains for the future.

In summary, the roll patterns observed in the Taylor-Dean system near the codimension-two point undergo an unusual sequence of transitions: stationary rolls, the drift instability, pattern extinction or weakening, a halving instability, and finally a small modulated roll packet emerges. All these transitions and the properties of corresponding states suggest that they originate in the interaction between the fundamental and second harmonic mode.

The authors thank G. Iooss, P. Laure, and H. Riecke for useful discussions. This work was supported partly by the Office of Naval Research and NATO.

[a]Present address: Laboratoire de Mécanique des Fluides, Université du Havre, B.P. 265, F-76055 Le Havre CEDEX, France.

[1] R. W. Walden, P. Kolodner, A. Passner, and C. M. Surko, Phys. Rev. Lett. **55**, 496 (1985).

[2] A. J. Simon, J. Bechhoefer, and A. Libchaber, Phys. Rev. Lett. **61**, 2574 (1988).

[3] M. Rabaud, S. Michalland, and Y. Couder, Phys. Rev. Lett. **64**, 184 (1990).

[4] I. Mutabazi, J. J. Hegseth, C. D. Andereck, and J. E. Wesfreid, Phys. Rev. Lett. **64**, 1729 (1990). See also I. Mutabazi, Thèse de Doctorat en Physique, Université Paris 7, 1990 (unpublished).

[5] O. Thual and S. Fauve, J. Phys. (Paris) **49**, 1829 (1988).

[6] R. E. Goldstein, G. H. Gunaratne, L. Gil, and P. Coullet, Phys. Rev. A **43**, 6700 (1991).

[7] B. A. Malomed and M. I. Tribelsky, Physica (Amsterdam) **14D**, 67 (1984).

[8] S. Fauve, S. Douady, and O. Thual, J. Phys. II (France) **1**, 311 (1991).

[9] L. D. Landau and E. M. Lifshitz, *Electrodynamics of Continuous Media* (Pergamon, New York, 1988). A thorough classical description of the second harmonic generation in a nonlinear dielectric is given in J. A. Armstrong, N. Bloembergen, J. Ducuing, and P. S. Pershan, Phys. Rev. **127**, 1918 (1962).

[10] H.-G. Paap and H. Riecke, Phys. Rev. A **41**, 1943 (1990); H. Riecke and H.-G. Paap, Phys. Rev. A **45**, 8605 (1992); R. J. Wiener and D. F. McAlister, Phys. Rev. Lett. **69**, 2915 (1992).

[11] H. Levine, W. J. Rappel, and H. Riecke, Phys. Rev. A **43**, 1122 (1991).

[12] M. R. Proctor and C. A. Jones, J. Fluid Mech. **188**, 301 (1988).

[13] S. Rasenat, F. H. Busse, and I. Rehberg, J. Fluid Mech. **199**, 519 (1989).

[14] S. Chandrasekhar, *Hydrodynamic and Hydromagnetic Stability* (Oxford Univ. Press, Clarendon, 1961). See also *Ordered and Turbulent Taylor Vortex Flow*, edited by C. D. Andereck and F. Hayot (Plenum, New York, 1992).

[15] I. Mutabazi, J. J. Hegseth, C. D. Andereck, and J. E. Wesfreid, Phys. Rev. A **38**, 4752 (1988).

[16] I. Mutabazi, C. Normand, H. Peerhossaini, and J. E. Wesfreid, Phys. Rev. A **39**, 452 (1989). The nonlinear analysis of these modes has been completed recently by P. Laure and I. Mutabazi (to be published).

[17] K. Park, G. L. Crawford, and R. J. Donnelly, Phys. Rev. Lett. **47**, 1448 (1981).

[18] A. Joets and R. Ribotta, in *New Trends in Nonlinear Dynamics and Pattern-Forming Phenomena*, edited by P. Coullet and P. Huerre, NATO ASI Ser. B, Vol. 237 (Plenum, New York, 1990), p. 125.

Effects of External Noise on the Fréedericksz Transition in a Nematic Liquid Crystal

Mingming Wu and C. David Andereck
Department of Physics, The Ohio State University, Columbus, Ohio 43210
(Received 3 November 1989)

We have determined the effects of imposing dichotomous noise on the magnetic Fréedericksz transition in the nematic liquid crystal MBBA. Various states of the nematic orientation occur, depending on the magnitude of the dc field and the amplitude and correlation time of the noise component. The resultant phase diagrams are in partial agreement with the analytic results of Horsthemke, Doering, Lefever, and Chi for $H > H_c$. A substantial deviation of the experimental result from computer simulations based on their model for low magnetic field ($H < H_c$) is observed.

PACS numbers: 61.30.Gd, 05.40.+j, 64.60.Ht, 64.70.Md

The effects of imposing external noise on nonlinear systems has been investigated in situations as diverse as the Briggs-Rauscher chemical reaction[1] and superfluid turbulence.[2] Under certain conditions such systems may show extreme sensitivity to noise. It has been shown that multiplicative external noise can induce a variety of transitions (or affect transitions already present), but rarely have observations of noise-induced behaviors been amenable to quantitative theoretical understanding. For example, Kai, Kai, and Takata[3] and Brand, Kai, and Wakabayashi[4] carried out experiments to study the effects of external noise on the electrohydrodynamic instabilities of a nematic liquid crystal. They found that imposing noise can shift transition thresholds and stabilize the system against turbulence. However, quantitative agreement with existing theory was not possible. In their experiments, external noise affected the liquid-crystal system in two ways: directly, by the fluctuations of the control parameter, and indirectly, by the dependence of the spatial-pattern wavelength on the noise intensity. The spatial inhomogeneities introduced both theoretical and experimental difficulties for the study. These difficulties are overcome in the present study of the Fréedericksz transition of a nematic liquid crystal, which was suggested by the theoretical work of Horsthemke, Doering, Lefever, and Chi.[5] The Fréedericksz transition consists simply of a rotation of the nematic director; no roll pattern or other flow is generated. This makes possible a more complete theoretical treatment than for the earlier, more complex, experimental situations.

The Fokker-Planck equation has been the usual starting point for studies of the effects of colored noise on nonlinear systems,[6-8] but no analytic results have been obtained except for dichotomous noise. Dichotomous noise consists of a signal which jumps between two levels at random times. It is a special case of colored noise with an exponentially decreasing correlation function.[9] Horsthemke *et al.*[5] investigated theoretically the effects of dichotomous noise on the Fréedericksz transition. In their study, the state of the stochastic system was characterized by the probability density function of the rotation angle of the liquid-crystal molecules. The general form of the probability density was obtained analytically as a function of noise amplitude and correlation time. It was found that various distinct states of the system (as indicated by the form of the probability density function) could be induced by changing the control parameters.

Stocks, Mannella, and McClintock[10] studied this model system with an analog simulator. Generally, they obtained good agreement with the predicted transition locations, not unexpected since they were solving by a different method the same equation that Horsthemke *et al.*[5] proposed. By contrast, our experiment was designed to investigate the effects of dichotomous noise on the Fréedericksz transition in the actual physical system. The experiment verified qualitatively the analytic prediction for one case, although the data are in better agreement with a computer simulation based on a more exact version of the model. We also found a parameter region where only partial agreement between the experiment and our simulation exists.

We studied the Fréedericksz transition with a layer of a nematic liquid crystal [N-(*p*-methoxybenzylidene)-*p'*-butylaniline (MBBA), in our case] sandwiched between two glass plates lying parallel to the x-y plane. The inner surfaces of the glass plates are coated with polyvinyl alcohol (PVA) and rubbed along the x axis. The resultant grooves give a surface topography such that the lowest surface energy will be reached when the director aligns with the groove pattern[11] [see Fig. 1(a)]. The magnetic field, which is perpendicular to the initial orientation of the molecules, produces a torque on the molecules due to their anisotropic susceptibility. The magnetic torque tends to align the molecules in the direction of the field. It is counteracted by viscous and elastic torques. Assuming that the orientations of the molecules are uniform across the x-y plane the following equation, with boundary conditions at the plates ($z = \pm d/2$), can be obtained by balancing these three torques:

$$\lambda_1 \partial_t \theta = K_{22} \partial_{zz} \theta + \chi_a H^2 \sin\theta \cos\theta , \qquad (1)$$
$$\theta(\pm d/2) = 0 ,$$

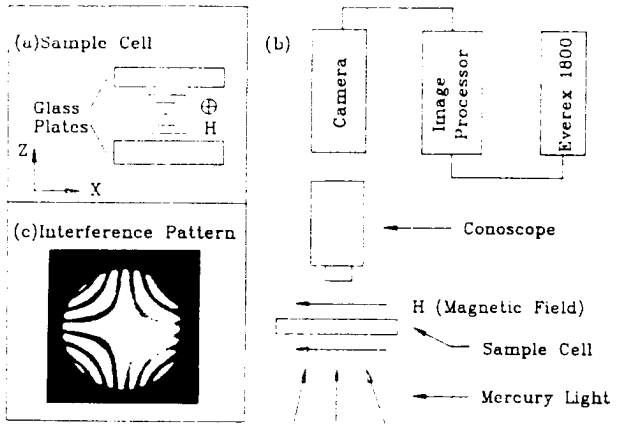

FIG. 1. (a) The molecules close to the plates are in approximate alignment with the x axis; those near the middle of the layer rotate in the x-y plane when $H > H_c$. (b) Schematic diagram of the experiment. (c) Typical interference pattern for $H = 0$.

where $\theta(z,t)$ is the angle between the director and the x axis, λ_1 is the twist viscosity, K_{22} is the twist elastic constant, χ_a is the anisotropic susceptibility, H is the applied magnetic field, and d is the sample thickness.

Equation (1) can be written in dimensionless form as follows:

$$\partial_\tau \theta = \partial_{z'z'}\theta + h^2 \sin\theta\cos\theta , \tag{2}$$

where

$$H_c \equiv \frac{\pi}{d}\left(\frac{K_{22}}{\chi_a}\right)^{1/2}, \quad h \equiv \frac{H}{H_c}, \quad \tau_0 \equiv \frac{\lambda_1 d^2}{K_{22}\pi^2},$$
$$\tau \equiv \frac{t}{\tau_0}, \quad z' \equiv \frac{\pi z}{d}. \tag{3}$$

τ_0 is the relaxation time of the sample. H_c is the critical field for the transition, found by solving $\partial_\tau\theta = 0$. θ is obtained implicitly as a function of the magnetic field[12] as follows:

$$h = \frac{2}{\pi} F\left(\sin\theta_m, \frac{\pi}{2}\right), \quad h > 1,$$
$$\theta_m = 0, \quad h < 1. \tag{4}$$

Here, $F(\sin\theta_m,\pi/2)$ is the complete elliptic integral of the first kind and θ_m is the rotation angle of the molecules halfway between the plates. Equation (4) shows that the liquid-crystal molecules start to rotate when the magnetic field exceeds a threshold magnetic field H_c. This is the Fréedericksz transition for this geometry.

With the noise signal added to the magnetic field, h in Eq. (2) is replaced by $h = h + \delta_t$, where δ_t is the noise signal divided by H_c. Equation (2) becomes

$$\partial_\tau \theta = \theta_{z'z'} + (h+\delta_t)^2 \sin\theta\cos\theta . \tag{5}$$

Retaining the lowest spatial mode $\theta \simeq \hat{\theta}(t)\cos(\pi z/d)$, Eq. (5) becomes

$$\partial_\tau \theta = -\theta + (h+\delta_t)^2 \sin\theta\cos\theta . \tag{6}$$

Horsthemke *et al.*[5] further simplified this equation by expanding $\sin\theta\cos\theta$ for small θ and obtained

$$\partial_\tau \theta = -\theta + (h+\delta_t)^2(\theta - \tfrac{1}{2}\theta^3) . \tag{7}$$

The probability density function of θ_m is introduced to describe the state of this stochastic system and it is analytically obtained by solving the Fokker-Planck equation resulting from Eq. (7). By examining the solution for divergences and local extrema, the locations of transitions between different probability density functions were determined.

Figure 1(b) shows the experimental setup. The sample cell is mounted on the stage of a conoscopic microscope located in a magnetic field. The conoscope forms an interference pattern consisting of symmetric hyperbolas [Fig. 1(c)] due to the birefringence of the nematic liquid crystal.[12] The interference pattern rotates with the rotation of the director. If the rotation angle of the interference pattern is ϕ and that of the director at $z = 0$ is θ_m, then[13]

$$\tan 2\phi = \frac{2\sin\theta_m}{2E(\sin\theta_m,\pi/2) - F(\sin\theta_m,\pi/2)}, \tag{8}$$

where $E(\sin\theta_m,\pi/2)$ is the complete elliptic integral of the second kind. Thus the director's rotation angle can be obtained by measuring the rotation angle of the interference pattern. To do this, the interference pattern is imaged in a charge-coupled-device array camera which is connected to an Imaging Technology FG-1024 image processor. The image of one of the hyperbolas corresponding to the lowest light intensity is stored and the director orientation obtained later by fitting a hyperbolic curve to the intensity profile and then extracting the principal axis. This gives ϕ, and hence by Eq. (8), θ_m. The magnetic field is provided by an electromagnet driven by an amplified signal from a digital-analog converter in the personal computer. The time intervals of the dichotomous noise are obtained from Poisson-distributed random numbers.

Table I gives the values of d, τ_0, and H_c for the samples we used in our experiment. The H_c values were obtained by measuring the director orientation as the applied dc magnetic field was varied and then fitting Eq. (4) to the data. The relaxation time and the sample thickness were obtained from the measured H_c and Eq. (3). The parameters χ_a, λ_1, and K_{22} for MBBA were taken from Ref. 13.

In order to use the optical technique to determine the molecular orientation, the initial angle between the di-

TABLE I. Characteristics of the three samples used in our experiment.

Sample	d (μm)	τ_0 (s)	H_c (G)
1	143	50.3	373
2	178	77.5	301
3	158	61.3	338

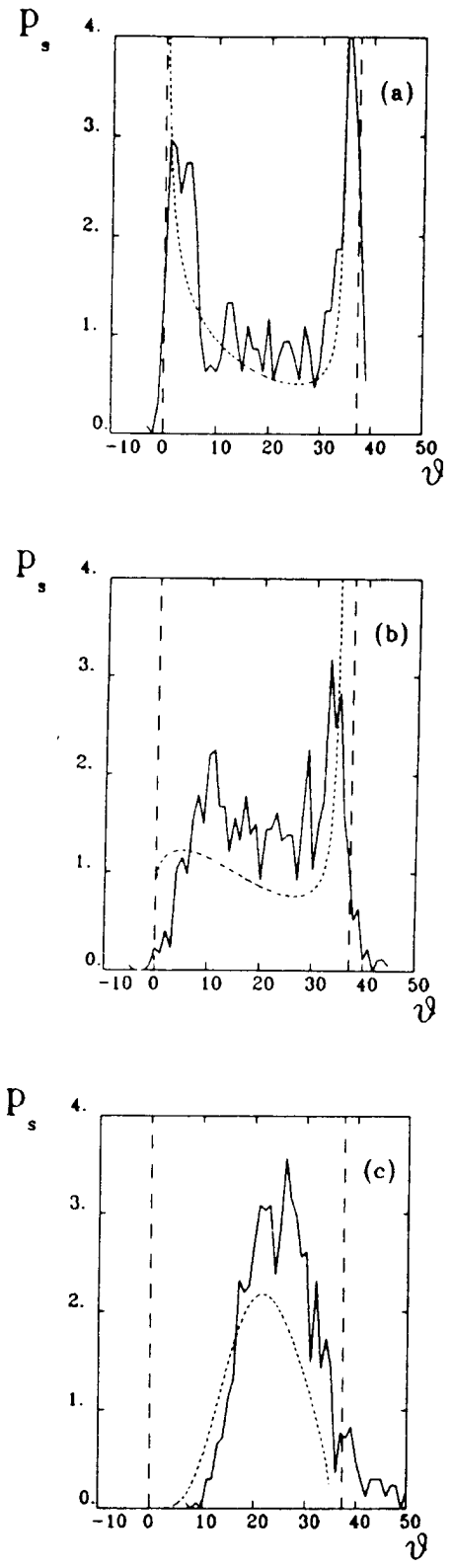

FIG. 2. Typical probability density functions for MBBA when driven by dichotomous noise with $h=1.09$ and $\delta=0.225$: Solid lines are experimental measurements, dotted lines analytic results, and dashed lines the rotation angles under $h+\delta$ and $h-\delta$. (a) $\gamma\tau_0=0.414$, (b) $\gamma\tau_0=0.836$, and (c) $\gamma\tau_0=4.182$. Here $1/\gamma$ is the correlation time of the noise signal.

rector and the magnetic field was $\sim 88°$ rather than 90°. If the initial angle was 90°, as assumed in the analytic calculation, the initial orientations of the molecules would be in metastable equilibrium within $\pm\theta_0$ ($\theta_0 \leq 0.5°$) of the x axis. Subjected to a large enough magnetic field, molecules would rotate both clockwise and counterclockwise depending on their original orientations. The interference pattern would be destroyed and the optical technique could not be used.

A typical set of probability density functions of the rotation angle of the director is shown in Fig. 2 for the same noise amplitude but different correlation times for $h=1.09$. Each probability density function was obtained from about 10 h of data acquisition with 30 s between each data point (1200 points total). The analytic probability density functions were calculated from the model of Horsthemke *et al.*[5] The simulation density was calculated from a time series of length $80000\tau_0$, based on Eq. (6) and an initial angle of $\sim 2°$.

The phase diagrams are displayed in Fig. 3, along with the analytic and simulation results. In the analytic calculation, transitions occur when the density at one end of the support changes from infinity to zero.[5] However, the observed transitions in both the experiment and the simulation were not as sharply defined. Therefore, we chose to mark the experimental transitions by displaying only points that were clearly in one state or the other. Figure 3(a) shows the experiment definitely disagrees with the analytic results for $\delta < 0.15$, while showing much better agreement with the simulation. The analytic results, simulations, and the experiments for Fig. 3(a) all show not only the intuitively expected bimodal (small $\gamma\tau_0$, with divergences at each end of the support) and unimodal (large $\gamma\tau_0$) densities, but also a nontrivial bimodal intermediate state. The deviation of the simulation and the experimental transitions from those of the analytical results [Fig. 3(a)], in particular, can be attributed to both the approximation $\sin\theta\cos\theta \simeq \theta - \frac{1}{2}\theta^3$ of the analytic calculation and the nonzero initial angle introduced in the simulation and the experiment.

A comparison of the experimentally observed transition boundary for $h=0.905$ with the simulation results is given in Fig. 3(b). (The analytic calculation in this parameter range is not available yet but is in progress.[14]) The bimodal intermediate states were not observed in the experiment; rather we observed transitions from bimodal states directly to unimodal states. This gives rise to a large discrepancy between the experimental and simulated transition to the unimodal states when δ exceeds ~ -0.2.

No evidence of soft-mode transitions (in which the extrema of the density function coalesce or split) were observed in a limited number of experiments for $h \geq 1.2$, whereas they appeared prominently in the analytic phase diagrams.[5] Simulations do show soft-mode transitions, though they are not as easy to detect as those in the analytic study and they have been found only at higher δ

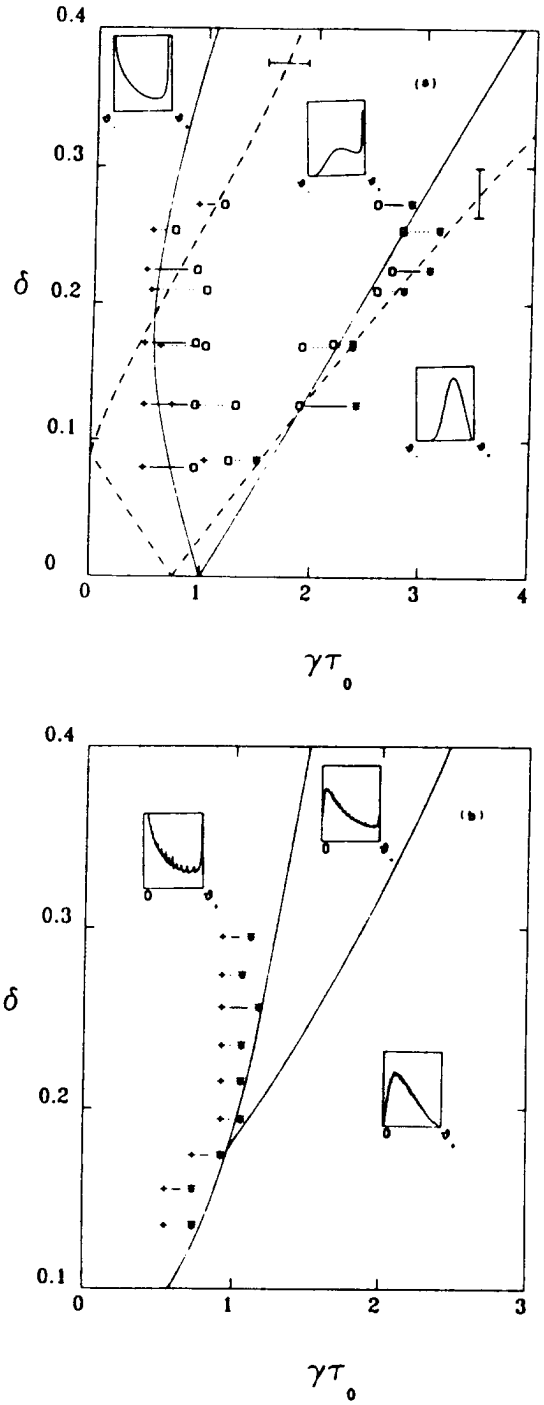

FIG. 3. Phase diagrams. + indicates a definite bimodal state is observed; □, intermediate state; *, unimodal state. (a) $h=1.09$, solid lines are from sample 1, dashed lines from sample 2. (b) $h=0.905$, data are taken from sample 3. The dashed curves are from the analytic solution to the model (Ref. 5), the solid curves are from the simulations. The curves are not fits to the data, there being no independently adjustable parameters, as described in the text. Error bars indicate the errors in the predicted transitions due to the uncertainty in H_c. Insets: Representative analytic probability densities for (a) and probability densities from the simulations for (b) in the different regions of the δ-$\gamma\tau_0$ plane.

and h. We believe that these discrepancies may be due to the use of the small-angle approximation in the analytic calculation. Further work is in progress to determine the true large-h phase diagram.

In summary, our experiment has confirmed the main predictions of the model of Horsthemke *et al.*[5] for the effects of a specific type of colored noise on a real physical system. The observed transitions are in agreement with simulations based on the model for $h=1.09$. The discrepancy in the phase diagram for $h=0.905$ for large noise amplitud[illegible] >0.2) [Fig. 3(b)] suggests that a more complete [illegible] may be necessary to fully account for our results. Such a model could include spatial effects across the x-y plane,[15,16] and more realistic boundary conditions, in which the strict $\theta(z=\pm d/2)=0$ is relaxed to allow for some response to the fluctuations at the surfaces.

We thank Werner Horsthemke for bringing this problem to our attention, and Stuart Collins and David Johnson for helpful discussions. This work was supported by the Office of Naval Research, under Contract No. N00014-86-K-0071 and Grant No. N00014-89-J-1352, and by an Ohio State University Small Grant and a Graduate Student Alumni Research Award.

[1]W. Horsthemke and R. Lefever, *Noise Induced Transitions: Theory and Applications in Physics, Chemistry and Biology*, Springer Series in Synergetics Vol. 15 (Springer-Verlag, Berlin, 1984).

[2]D. Griswold and J. T. Tough, Phys. Rev. A **36**, 1360 (1987).

[3]S. Kai, T. Kai, and M. Takata, J. Phys. Soc. Jpn. **47**, 1379 (1979).

[4]H. R. Brand, S. Kai, and S. Wakabayashi, Phys. Rev. Lett. **54**, 555 (1985).

[5]W. Horsthemke, C. R. Doering, R. Lefever, and A. S. Chi, Phys. Rev. A **31**, 1123 (1985).

[6]M. San Miguel and J. M. Sancho, Z. Phys. B **43**, 361 (1981).

[7]A. Fulinski, Phys. Lett. A **126**, 84 (1987).

[8]W. Horsthemke and R. Lefever, Z. Phys. B **40**, 241 (1980).

[9]Dichotomous noise is certainly a very special form of colored noise, and not all of our results will generalize [N. G. Stocks, R. Mannella, and P. V. E. McClintock, J. Stat. Phys. **54**, 1383 (1988)]. However, its use has experimental advantages and analytic results are possible.

[10]Stocks, Mannella, and McClintock, Ref. 9.

[11]W. H. De Jeu, *Physical Properties of Liquid Crystalline Materials*, Liquid Crystal Monographs Vol. 1 (Gordon and Breach, New York, 1980).

[12]P. G. de Gennes, *The Physics of Liquid Crystals* (Oxford Univ. Press, London, 1974).

[13]P. E. Cladis, Phys. Rev. Lett. **28**, 1629 (1972).

[14]W. Horsthemke (private communication).

[15]G. Srajer, S. Franden, and R. B. Meyer (to be published).

[16]F. Lonberg, S. Franden, A. Hurd, and R. E. Meyer, Phys. Rev. Lett. **52**, 1903 (1984).

EUROPHYSICS LETTERS 1 July 1992

Europhys. Lett., **19** (5), pp. 391-395 (1992)

Ring Pattern Formation in 2-*d* Shear of Freely Suspended Films of a Smectic *C* Liquid Crystal.

I. MUTABAZI[1,2], P. L. FINN[1], J. T. GLEESON[1,3](*), J. W. GOODBY[4]
C. D. ANDERECK[2] and P. E. CLADIS[1]

[1] *AT&T Bell Laboratories - Murray Hill, NJ 07974, USA*
[2] *Department of Physics, Ohio State University - Columbus, OH 43210, USA*
[3] *Department of Physics, Kent State University - Kent, OH 44242, USA*
[4] *School of Chemistry, Hull University - Hull HU6 7RX, Great Britain*

(received 6 September 1991; accepted in final form 18 May 1992)

PACS. 61.30 – Liquid crystals.
PACS. 47.20 – Hydrodynamic stability and instability.

Abstract. – Space-time diagrams are used to analyze the dynamics of the liquid-crystal smectic *C* director in two-dimensional shear. We find a steady-state ring pattern only persists if there are no broken rings. A pair of defects, disclinations, is created when a ring breaks. With broken rings, the pattern dynamics is a sensitive balance between phase winding by shearing and unwinding by defect motion. Because the film is a 2-*d* elastic medium, low-frequency elastic oscillations occur in the ring pattern in the absence of shear. Using dimensional analysis and measurements of the in-plane orientational diffusion constant, estimates are obtained for an in-plane elastic constant and rotational viscosity that are consistent with bulk measurements.

In recent years, new ideas have emerged in the understanding of fundamental and universal features of the dynamics of macroscopic system driven far from equilibrium by external fields [1]. Particular attention has been paid to systems that exhibit spatial patterns at a bifurcation. Examples of such systems are: ferrofluids in electric or magnetic fields [2] and thermal [3] and shear instabilities in simple [4] or complex fluids such as liquid crystals [5]. Space-time diagrams are a useful experimental tool to obtain quantitative information of the time evolution of simple spatial patterns. In this paper, we report experimental results of the space-time behavior of freely suspended smectic *C* liquid-crystal films in circular shear.

Nematic liquid crystals are anisotropic 3-dimensional liquids characterized by an optic axis, $\boldsymbol{n}$, whose coupling to external forces is well known [6]. With modern image analysis techniques, their highly contrasted optical patterns observed with a polarizing microscope are an ideal source of quantitative information for such nonlinear, nonequilibrium processes as electrohydrodynamic convection [7] and directional growth [8]. However, far from

(*) Present address: Department of Physics, Princeton University, Princeton, NJ 08544, USA.

equilibrium, the 3-dimensional fluidity and strong coupling between $\boldsymbol{n}$ and external forces typically result in complicated patterns not easily described in quantitative terms. For this reason, we chose freely suspended films of smectic C liquid crystal that have a microscopic structure of parallel layers and are 2-d anisotropic liquids in the plane of the layers [6].

In smectic C, the molecular long axis (roughly speaking parallel to $\boldsymbol{n}$) is at an angle θ to the layer normal. To conserve layer spacing, θ is constant at fixed temperature, however, cooperative rotations in the plane of the layers are allowed. Thus, a 2-d director, $\boldsymbol{c}$, is sufficient to describe macroscopic changes in molecular orientation in the smectic C phase. While 3-d nematic liquid crystals have the symmetry $\boldsymbol{n} \leftrightarrow -\boldsymbol{n}$, the layer structure in smectic C liquid crystals distinguishes between $\boldsymbol{c}$ and $-\boldsymbol{c}$. Nevertheless, it has been formally shown for an ideal smectic C geometry—dislocation-free parallel layers—that the curvature elasticity [9] and hydrodynamics [10] for $\boldsymbol{c}$ is identical to that for $\boldsymbol{n}$ constrained to 2-dimensions. As the magnitude of $\boldsymbol{c}$ is constant at fixed temperature, it is characterized by a phase variable, Φ, that depends on space and time.

Here, we investigated the phase winding regime of smectic C liquid crystals in a 2-dimensional shear field Ω [11]. A glass needle with tip diameter $2r_0 \sim 150\,\mu$m is inserted into the center of a circular film of radius $R \sim$ mm. Needle rotation at constant angular velocity exerts a shear on the film. Starting from a uniform $\boldsymbol{c}$, the initial director response to shear is continuous rotation of $\boldsymbol{c}$ at the needle (phase winding) resulting in the appearance of concentric rings when the film is observed in an optical microscope with crossed polarizers [11]. There is no threshold for ring formation.

Freely suspended smectic C films in 2-d shear, Ω, were first studied by Cladis *et al.* [11]. They studied the structure of the ring pattern and observed that it could be destroyed by ring breaking resulting in disclination pair creation and subsequent phase unwinding. Using image analysis and 1-d space-time (r-t) diagrams, the purpose of our experiments is to address the question: is there a steady state for the ring pattern? The four r-t plots in fig. 1

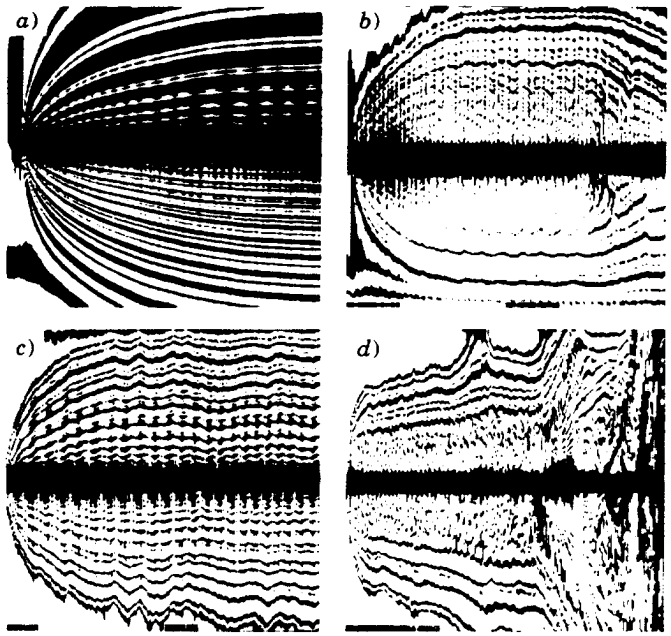

Fig. 1. – Space-time plots of ring pattern dynamics at different shear. In the images, the vertical axis is a diameter of the film and is 1.57 mm. In *a)* $\nu \equiv \Omega/2\pi = 0.6\,\mathrm{s}^{-1}$ and the horizontal (time) axis covers $\Delta t = 194$ s; *b)* $\nu = 0.6\mathrm{s}^{-1}$, $\Delta t = 385$ s; *c)* $\nu = 1.2\,\mathrm{s}^{-1}$, $\Delta t = 1000$ s; and *d)* $\nu = 3.0\,\mathrm{s}^{-1}$, $\Delta t = 500$ s.

give an overview of ring patterns observed at different shearing rates. In fig. 1, t is the horizontal axis and r, the vertical axis, is a diameter of the film. The needle is the black horizontal band in the middle of each picture.

To optimize 2-*d* spatio-temporal behavior and minimize boundary effects at the top and bottom film-air boundaries [12], films of thickness $e \sim (15 \div 20)\,\mu\text{m} \sim 5 \cdot 10^3$ layers and diameter $2R = 2.8\,\text{mm}$ are used. The material is 10E6 (4-hexyloxyphenol 4'-decyloxybenzoate) [13] which exhibits the smectic C phase between 43.5 °C and 78.3 °C. Above 78.3 °C, continuous rotational symmetry in the plane of the layers is restored. This is the smectic A phase that is also layered. Experiments are carried out at fixed temperature $T = 73\,°\text{C}$.

In polar coordinates (r, ϕ) the director $\boldsymbol{c}$ has two components that can be expressed in terms of a phase [11] $\Phi(r, \phi, t)$ as $\boldsymbol{c} = (\cos\Phi, \sin\Phi)$. At $r = R$, $\Phi = 0$. Every 2π rotation of the needle results in a 2π increase in Φ at the needle compared to the boundary R. Lines of constant Φ have circular symmetry about the center of the film. When Φ is perpendicular or parallel to the polarizers, a dark ring is observed by a videocamera attached to a polarizing microscope. Because of the high symmetry of the pattern, real-time image processing is used to study the dynamics of Φ by space-time plots with the sampling space a diameter of the film (fig. 1). We now describe the time dependence of Φ as a function of shear.

At a given needle rotation rate, Ω, Φ continuously increases in time at r_0 with Φ decreasing logarithmically [11] with distance from r_0. At R, $\Phi \equiv 0$. In fig. 1*a*), $\Omega/2\pi \equiv \nu = 0.6\,\text{s}^{-1}$. It is clearly observed that a line of constant Φ starts at the needle, a source for the pattern. Figure 2 shows that the radial distance from the needle edge for a line of constant Φ initially grows like $\sqrt{t}$, where t is time, after which saturation occurs. The time to reach saturation, τ_s, is shorter for larger ν: $1/\tau_s \sim 0.013\nu$.

Figure 1*b*) is also for $\nu = 0.6\,\text{s}^{-1}$ with 385 s along the time axis. Here, a ring has broken before saturation leading to oscillations in the pattern. Eventually, one of a pair of disclinations reaches the needle, resulting in phase unwinding and destruction of the saturated state [14]. Thus, a disclination at the needle is a sink of Φ even though the needle still rotates. The ring oscillation amplitude is small in fig. 1*b*) and larger in fig. 1*c*) where the time axis is now 1000 s and $\nu = 1.2\,\text{s}^{-1}$.

In fig. 1*a*), a steady-state regime persists as long as there are no broken rings. A broken

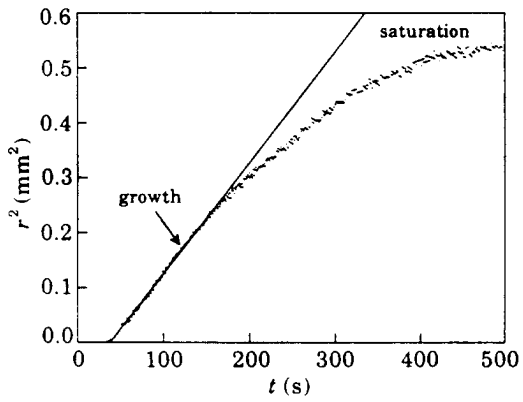

Fig. 2.

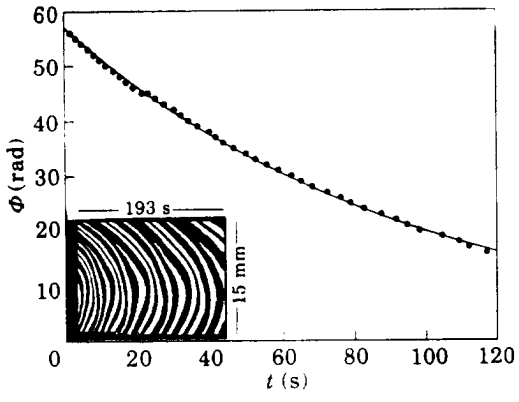

Fig. 3.

Fig. 2. – Growth and saturation of a line of constant phase Φ, *i.e.* one of the lines shown in fig. 1*a*). The slope in the initial stage is $2.2 \cdot 10^{-3}\,\text{mm}^2/\text{s}$.

Fig. 3. – Φ at the film center as a function of time as the ring pattern relaxes after the needle has been pulled from the film.

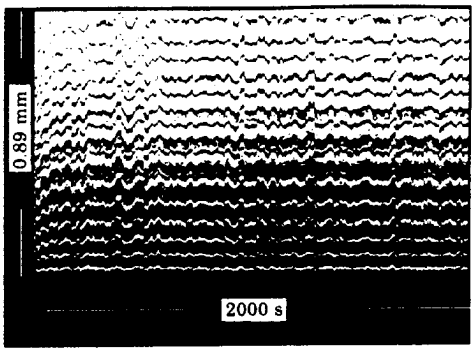

Fig. 4. – Oscillations in the ring pattern when the needle is stopped but kept in the film. The pattern was generated at $\nu = 1.2\,s^{-1}$.

ring destroys the circular symmetry of the ring pattern and oscillations are then observed in the space-time plots (fig. 1*b*) and *c*)). The ring pattern is more robust when a ring breaks close to the needle (fig. 1*c*)) than when it breaks further from the needle (fig. 1*b*)).

In fig. 1*d*), $\nu = 3s^{-1}$. Here, more than one pair of defects has been created in the film before saturation is reached. Local phase winding and unwinding is more rapid. The coexistence of these two competing mechanisms results in irregular sequences of phase winding and unwinding and ring breaking creating more disclination pairs. Sometimes, the ring pattern completely disappears from the film. These processes occur irregularly in space and time suggesting a picture of spatio-temporal intermittency.

The dynamics of Φ is characterized by diffusion of the director phase with diffusion constant D_0, that is the ratio of an elastic constant K (dyn) to the rotational viscosity, γ_1 (dyn/cm^2/s = P): $D_0 = K/\gamma_1$. A way to measure D_0 is to remove the needle from the film and measure the phase unwinding process [11]. The space previously occupied by the needle is replaced by a circular region of uniform Φ that rotates in time as rings vanish at the center of the film.

After phase winding, we removed the needle from the film and measured the time dependence of Φ at the center of the film. Figure 3 shows Φ at the film center as a function of t. Inset in fig. 3 is a typical binarized r-t plot with the vertical axis of the plot a film diameter. From such measurements, we found for 10E6 that $D_0 = 2 \pm 0.1 \cdot 10^{-4}\,cm^2/s$. In another liquid-crystal compound (TB9A) with a higher-temperature smectic C phase (170 °C), Cladis *et al.* [11] found $D_0 = 1.3 \cdot 10^{-4}\,cm^2/s$.

If the shearing process is stopped before phase saturation, the number of rings does not change but their size increases until the whole film is filled: there is a dilation of existing rings. When the needle is stopped and retained in the film after saturation is reached, rings dilate and contract in phase (fig. 4). In fig. 4, the vertical axis is a radius of the film. After filtering, the power spectrum for a line of constant Φ in fig. 4 shows a broad peak centered at $\nu_0 \sim 1/(90 \pm 10\,s)$. The oscillations are in phase along the radial direction leading to the picture that the ring pattern is an elastic medium with a frequency response ν_0 given by $\nu_0 = D_0/R^2$. Thus, with $D_0 = 2 \cdot 10^{-4}\,cm^2/s$ and $R = 0.14\,cm$, $1/\nu_0 = 98\,s$, the same order of magnitude as observed.

We use dimensional analysis [6] to obtain an estimate for the magnitude of the elastic constant in smectic C:

$$K \sim \frac{k_B T_c}{d_c}, \tag{1}$$

where T_c is the transition temperature to the phase where continuous rotational symmetry in the plane of the layers is restored and the microscopic layered structure is retained, the smectic A phase. k_B is Boltzmann's constant, K is a Frank elastic constant and d_c is the layer spacing at T_c. Putting $T_c = 78.3\,°C = 351.3\,K$, the transition temperature from smectic A to smectic C, $d_0 = 31.5\,Å$, the layer spacing in 10E6 [13] at T_c into eq. (1), we obtain $K \sim 1.5 \cdot 10^{-7}$ dyn. From the measured diffusion constant, then $\gamma_1 \sim 7.7 \cdot 10^{-4}$ P. We note that while these estimates for K and γ_1 are smaller than found in nematic liquid crystals, this is consistent with bulk measurements for K and γ_1 on oriented nematic and smectic C phases [15].

In conclusion, using space-time diagrams, we investigated the phase saturation and relaxation of the director in freely suspended circular smectic liquid-crystal films in two-dimensional shear. We found that a steady ring pattern persisted as long as there were no broken rings. Spatio-temporal intermittency is observed when several rings are broken, resulting in the creation of disclinations that act as sinks for the pattern. In the absence of shear, we observed low-frequency relaxation oscillations in the ring pattern. Dimensional analysis combined with measurements of the director diffusion constant gives estimates for K and γ_1 consistent with bulk measurements on oriented smectic C samples.

* * *

We thank Y. COUDER, H. R. BRAND and B. YURKE for stimulating discussions. IM thanks the Office of Naval Research and the Ohio State University Office of Research and Graduate Studies, and JTG thanks NSERC (Canada) for support.

REFERENCES

[1] BUSSE F. H. and KRAMER L. (Editors), *Nonlinear Evolution of Spatio-Temporal Structures in Dissipative Continuous Systems, NATO ASI Series* (Plenum Press, New York, N.Y.) 1990.
[2] BERCEGOL H., CHARPENTIER E., COURTY J. M. and WESFREID J. E., *Phys. Lett. A*, **121** (1987) 311.
[3] See, for example, WESFREID J. E. and ZALESKI S. (Editors), *Cellular Structures and Instabilities* (Springer Lectures Notes in Physics, Berlin) 1984.
[4] ANDERECK C. D., LIU S. S. and SWINNEY H. L., *J. Fluid. Mech.*, **164** (1986) 155.
[5] CLADIS P. E. and TORZA S., *Phys. Rev. Lett.*, **35** (1975) 1283; CLADIS P. E., in *Nematics, Mathematical and Physical Aspects*, edited by J.-M. MICHEL, J.-M. GHIDAGLIA and F. HELEIN (Kluwer Academic Publishers) 1990.
[6] DE GENNES P. G., *Physics of Liquid Crystals* (Oxford University Press) 1974.
[7] REHBERG I., RASENAT S., DE LA TORRE JAUREZ M., SCHOPF W., HORNER F., AHLERS G. and BRAND H. R., *Phys. Rev. Lett.*, **67** (1991) 596; see also: ZIMMERMANN W., *MRS Bulletin*, **16** (1991) 46.
[8] FLESSELLES J. M., SIMON A. J. and LIBCHABER A., *Adv. Phys.*, **30** (1991) 1.
[9] LANGER S. A. and SETHNA J. P., *Phys. Rev. A*, **34** (1986) 5035.
[10] BRAND H. and PLEINER H., *J. Phys. (Paris)*, **41** (1980) 553; **43** (1982) 853.
[11] CLADIS P. E., COUDER Y. and BRAND H. R., *Phys. Rev. Lett.*, **55** (1985) 2945.
[12] SIROTA E. B., PERSHAN P. S., SORENSON L. B. and COLLET J., *Phys. Rev. Lett.*, **55** (1985) 2039.
[13] KELLER P., CLADIS P. E., FINN P. L. and BRAND H. R., *J. Phys. (Paris)*, **46** (1985) 2203.
[14] A more detailed study of defect dynamics in this system has recently been made by COUDER Y., BRAND H. R. and CLADIS P. E., preprint (1991).
[15] PELZL G., SCHILLER P. and DEMUS D., *Liq. Cryst.*, **2** (1987) 131. See also: MEIBOOM S. and HEWITT R. C., *Phys. Rev. A*, **15** (1977) 2444.

Biological scattering particles for laser Doppler velocimetry

Diane A. Jacobs
Department of Physics, The Ohio State University, Columbus, Ohio 43210 and Department of Physics and Astronomy, Eastern Michigan University, Ypsilanti, Michigan 48197

Charles W. Jacobs
Department of Molecular Genetics, The Ohio State University, Columbus, Ohio 43210

C. David Andereck
Department of Physics, The Ohio State University, Columbus, Ohio 43210

(Received 24 May 1988; accepted 24 August 1988)

The use of formaldehyde-killed single-cell organisms as scattering particles for laser Doppler velocimetry studies in water and salt solutions is discussed. Advantages over traditional scattering particles include ready availability in large quantities, uniformity in size, monodispersity, and the ability to stay suspended in solution for several days. The tracers are colloidal sols for a wide range of densities of aqueous solutions. The microorganisms can be easily stained with a large variety of fluorescent and nonfluorescent dyes before they are used as tracer particles.

I. INTRODUCTION

Laser Doppler velocimetry (LDV) is a well-established and widely used technique in fluid dynamics studies. One of the primary difficulties with LDV is in finding suitable scattering particles for each application. In our case, we are using LDV to study spatial and temporal properties of the flow that precedes the onset of weak turbulence in a fluid contained between eccentric cylinders with the inner cylinder rotating. The outer cylinder, through which the laser beams and the scattered signal must pass, is 1.7 cm thick glass. This is a necessary feature of the design, but it introduces a few difficulties. First, the curved surfaces of the cylinder introduce beam path distortions and second, the air–glass and water–glass interfaces scatter the incident laser beams. These distortions and scatterings drastically decrease the signal-to-noise ratio. We found it impossible, under these conditions, to work in a LDV backscattering mode, and a forward scattering mode was not optimized. We therefore had to introduce a fluid between the cylinders, and on the outside of the glass cylinder, that provided refractive index matching with the glass. Unfortunately the chosen fluid was incompatible with the usual scattering particles, thus forcing a search for new ones. We evaluated a number of biological particles with seemingly appropriate characteristics and found several that worked extremely well. We will discuss the specific properties of the biological particles we have selected, compare our LDV results with previous work employing other techniques, and suggest further applications of these particles.

II. EXPERIMENTAL APPARATUS

The cylindrical annulus used in the experiment has inner and outer radii of 4.486 and 5.080 cm, respectively. The inner cylinder is stainless steel and the outer cylinder is precision bore glass tubing.[1] These cylinders are surrounded by a tank consisting of a stainless steel frame supporting optical quality glass plates. Backscattering LDV was achieved by mounting the transmitting and receiving optics together on a motor-driven track, which allows the sample volume to be scanned vertically through the system. The backscattering mode is convenient for setting up a particular flow state; however, the forward scattering mode was generally used to obtain the highest signal-to-noise ratio in detailed studies. To optimize the forward scattering signal, the fluid in the tank and in the space between the cylinders must have an index of refraction of 1.47 to match that of the glass cylinder. Preferably this fluid should be nontoxic, noncorrosive, and have nearly the same dynamical parameters as water. We employed a solution of aqueous NaI (~ 1.5 gm NaI/cm^3 of distilled water).[2] If necessary, the salt concentration was adjusted by adding very small amounts of solid NaI until good index matching was achieved. The specific gravity of the fluid is 1.77, and the kinematic viscosity is $\sim 1.02 \times 10^{-2}$ cm^2/sec. The fluid is nontoxic and does not detectably react with stainless steel, glass, or plastic. The iodine tends to precipitate over long periods of time, but the addition of ~ 0.02 g of ascorbic acid per cubic centimeter of fluid will cause it to dissolve.

Once we chose the NaI solution as our working fluid an appropriate seed particle was needed. The standard ones were not acceptable. Polystyrene spheres are too light (specific gravity = 1.05) and titanium dioxide and other paint pigments are either too heavy and sediment too rapidly, or they have been found to clump. There were several criteria for selecting new tracer particles. We wanted particles with diameter close to the 632.8 nm wavelength of light from our He–Ne laser. The particles had to be stable in the aqueous NaI solution and be as close as possible to the density of the working fluid in order to reduce sedimentation and to ensure close tracking of the fluid velocity fluctuations. In addition, the particles of a given type had to be spherical, monodisperse, and as homogenous as possible in size, yet a range of sizes should be available so that optimum conditions could

 0031-9171/88/123457-05$01.90

be achieved for either forward or backscattering LDV modes. Most of these criteria were met with certain biological particles. For these experiments we used three different kinds of formaldehyde-killed, single-celled organisms as tracer particles, giving us a range of sizes: a bacterial strain, two yeast strains, and conidia from a mold (Fig. 1).

The bacterium, *Staphlyococcus epidermidis* OSU253, was obtained from a local culture collection.[3] A small quantity was inoculated into 50 ml of LB broth medium[4] and incubated at 37 °C for 18 h with shaking at 250 rpm. The culture was removed from the incubator and 5.5 ml of 37% formaldehyde solution was added. The culture was swirled to mix the formaldehyde and then left at room temperature for 2 h. The fixed cells were harvested by (i) centrifuging at $6000 \times g$ for 10 min, (ii) decanting the formaldehyde and culture medium, (iii) resuspending the cells in distilled water to wash away residual culture medium, (iv) centrifuging again at $6000 \times g$ for 10 min, and, finally, (v) resuspending the cells in 5 ml of distilled H_2O. Dilutions of this suspension were used as tracer particles.

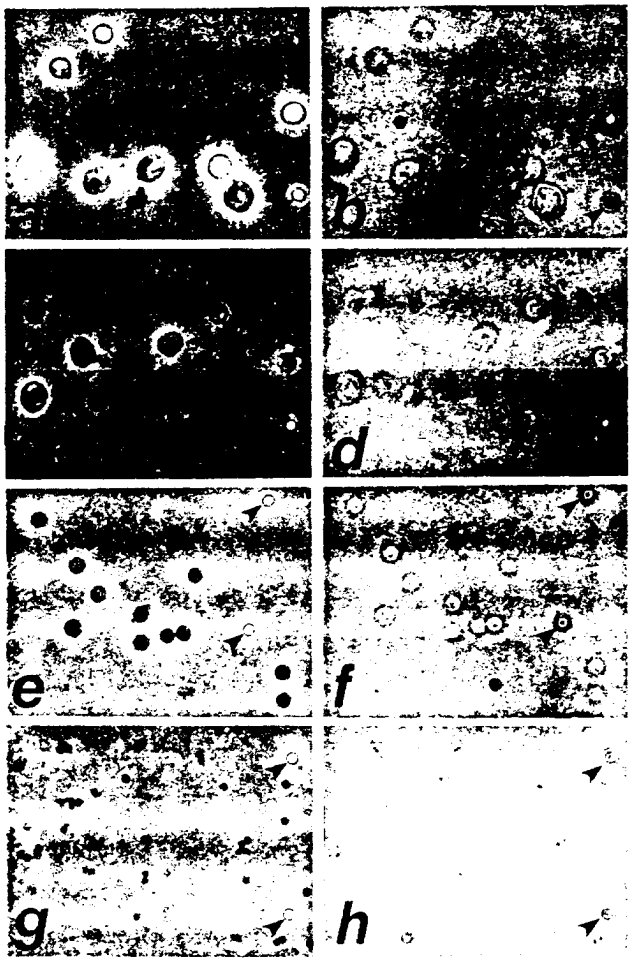

FIG. 1. Phase contrast-enhanced (a, c, e, g) and bright-field (b, d, f, h) micrographs of the particles suspended in NaI solution. The bright-field micrographs approximate the interaction of light with the particles in the experimental system; the phase contrast micrographs are to aid in identifying the particles in the bright-field micrographs. From top to bottom: yeast C276.4A (a, b); yeast D273.10B (c, d); conidia (e, f); bacteria (g, h). At the right of each frame are 2.02 μm diameter polystyrene spheres (arrows) to indicate scale.

We used two strains of baker's yeast: *Saccharomyces cerevisiae* D273.10B,[5] and *S. cerevisiae* C276.4A.[6] These strains were inoculated into 100 ml of YPD broth medium[7] and incubated for two days at 37 °C with shaking at 200 rpm. The cultures were harvested and prepared for use as seed particles as described for the bacteria. The C276.4A yeast was more spherical than the D273.10B strain.

The conidia we used were from *Aspergillus nidulans* R153.[8] This strain carries a mutation that causes white conidial color. Conidia were inoculated into a petri dish containing YG agar medium[7] and grown for five days at 37 °C. The conidia were harvested by adding sterile glass beads (4 mm diam) to the petri dish and shaking gently. Then 15 ml of a 0.15 molar solution of NaCl and 0.1% (by volume) Tween 80 was added.[9] *A. nidulans* conidia cannot be killed by the simple addition of formaldehyde; we incubated them at room temperature for 16 h in YG broth[7] and 1 μg/ml Myacide SP (Inolex) prior to formaldehyde fixation. The formaldehyde suspension was incubated for 2 h at room temperature and the conidia recovered and prepared for use as tracer particles as described for the bacteria.

III. RESULTS

The bacteria had an average diameter of 0.8 μm, the yeasts 4.2–5.1 μm, and the conidia 3.0 μm, based on measurements of photographic images (Fig. 1). The concentration of particles shown in Fig. 1 is much greater than that in the working fluid so that a good sample of the microorganisms can be seen. In our application there were about 3 to 10 particles in the measuring volume to obtain optimal signal. The apparent densities of the organic constituents of the particles, as judged by sedimentation equilibrium centrifugation and density gradient sedimentation in cesium chloride,[10] were 1.35–1.45 g/cm^3. The microorganisms were all in a colloidal suspension in the NaI solution and there was no observable sedimentation over the course of five days. Likewise, when the microorganisms were suspended in NaI solutions ranging from 1.37 g/cm^3 to 1.84g/cm^3 and centrifuged for 15 min at $12\,000 \times g$, they could not be sedimented from solutions with densities greater than that of the organic components. Neither did the particles rise to the top of the solution, as did the polystyrene spheres (density 1.05 g/cm^3); instead, they remained in colloidal suspension. The rate of aggregation, which will enhance sedimentation, of uncharged lyophobic sols is inversely proportional to their initial concentration. The aggregate half-life for the particle concentration used in our experiments is calculated to be about five days. In addition, all the microorganisms have a net negative charge on their surfaces[11,12] which will prevent clumping and further decrease the sedimentation rate.[13] The particles will settle out of motionless distilled water within several hours, but may be kept in suspension indefinitely by even very mild agitation.

The index of refraction of the yeast is 1.45, that of the conidia and bacterium is about 1.44. These values were determined by observing the organisms in a glycerol–water mixture under a phase contrast microscope. The index of refraction of the fluid is a known function of the concentration of the glycerol in water. The percent by volume of glyc-

erol in the fluid was varied until the shade of the cell wall (likely the primary light scatterer in the particle) matched the shade of the surrounding fluid; the index of refraction was then determined to be equal to that of the fluid.

The conidia had a tendency to clump somewhat because of the hydrophobic nature of their cell walls, a property not unique to the strain of mold we chose. The bacteria were also found to clump, but this could be alleviated by adding the ascorbic acid to the solution. This result is not surprising. The charged double layer on the bacteria that prevents aggregation is neutralized by positive ions in the solution, such as excess Na^+. These ions will bind more readily to the ascorbic acid, preventing flocculation of the bacteria. The use of nonaqueous solvents such as alcohols, ketones, and hydrocarbons will dehydrate the cell walls of all the particles and cause them to stick together. It should be possible, however, to use the particles in ethanol–water mixtures as long as the ethanol concentration is below 10%.

The spectral results obtained using these particles were quite good and agree well with those of Gorman and Swinney.[14] The system was kept in the concentric mode, with radius ratio of 0.883 and aspect ratio of 20, so comparisons could be made with their study. The data from all the particles were obtained while the fluid was in a wavy vortex flow state with 17 vortices. The number of vortices was determined by scanning the entire length of the fluid, while operating in the backscattering mode, and noting the inflow and outflow boundaries on a strip chart recording of the analog output of the frequency tracker. Figure 2 shows typical spectra obtained using the various particles. Frequencies are normalized to the inner cylinder frequency, f_i, and the power is plotted on a log scale. The Reynolds number in all the cases shown here was $6.08R_c$, where R_c is the critical value for onset of time-independent Taylor vortices. The azimuthal wavenumber of the states shown is 6 and the fundamental frequency is clearly visible at $2.157f_i$, several orders of magnitude above the background noise. Each spectrum was obtained by subdividing a 24 576 point time series into 24 equal segments, calculating a fast Fourier transform for each, and then finding the average. This technique reduced contributions to the frequency spectrum from random fluctuations in the background noise and enhanced the signal-to-noise ratio.

The primary peak in each spectrum corresponds to the frequency of traveling azimuthal waves passing a point of observation in the laboratory. The primary frequency we observe is 6% higher than the value obtained by Gorman and Swinney. The difference in fundamental frequencies may be explained on the basis of the work of King *et al.*[15] on wave speeds in circular Couette systems. The spatial state of a flow with traveling azimuthal waves is specified, in part, by the average axial wavelength, which is defined by $\bar{\lambda} = 2H/N$, where H is the height of the fluid contained between the cylinders and N is the number of Taylor vortices. King *et al.* have found that there is a dependence of the primary wave speed on $\bar{\lambda}$; the difference between our $\bar{\lambda}$ and that of Gorman and Swinney can account for about one-third of the difference in our fundamental frequency values. After the onset of wavy vortex flow, the azimuthal wave speed decreases monotonically with increasing Reynolds number.[15] The lowest Reynolds number for which Gorman and Swinney present wave-speed data is $\sim 9.4R_c$. Our measurements were made at $6.08R_c$, which will again have the effect of raising the fundamental frequency we observe.

The background noise remains at about the same level at higher frequencies [Fig. 3(a)]. Only a high frequency spec-

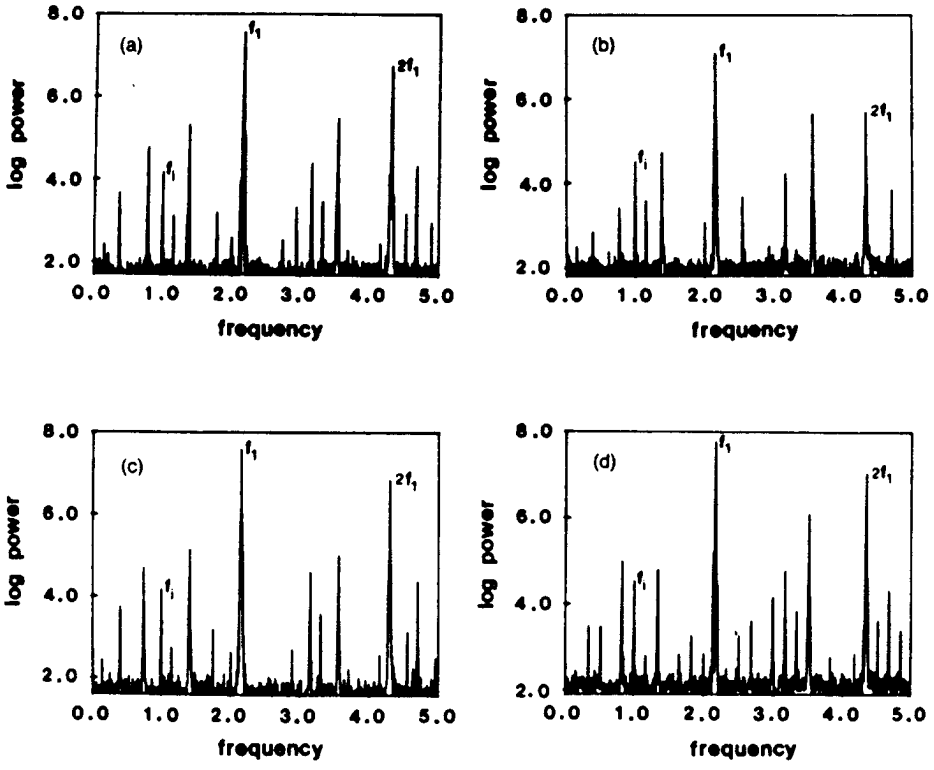

FIG. 2. Power spectra of the axial component of the velocity measured in the center of the gap between the cylinders using the following tracer particles: (a) bacteria; (b) yeast D273.10B; (c) yeast C276.4A; (d) conidia. The data were obtained in the forward scattering mode. The fundamental frequency at $2.157f_i$ is labeled as f_1; all other frequency components are linear combinations of f_i and f_1, harmonics or aliases.

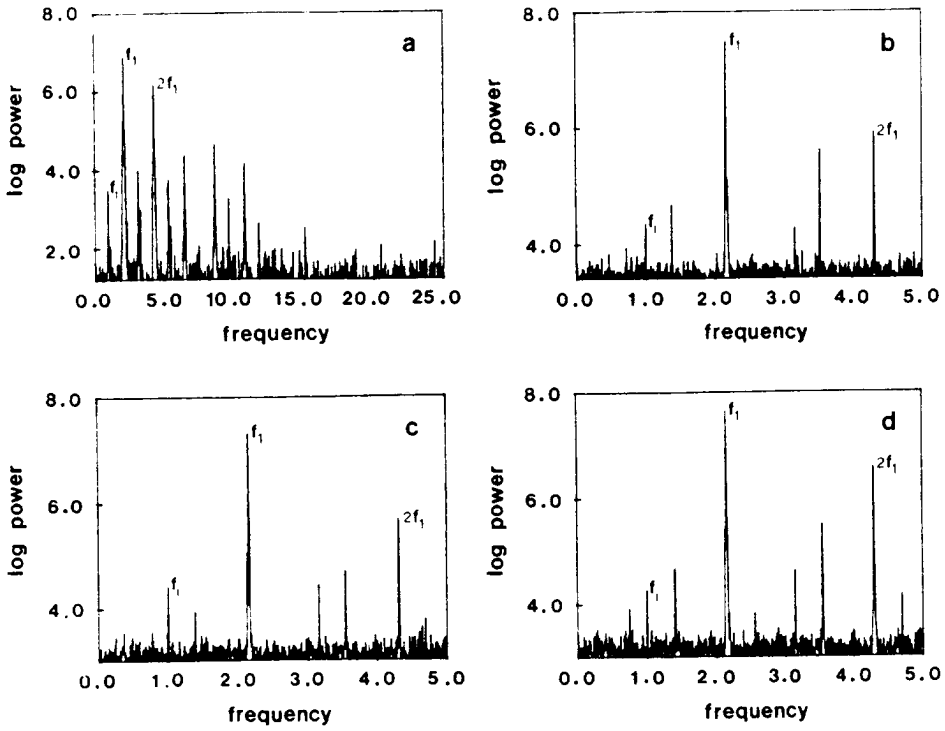

FIG. 3. Power spectra of the axial component of the velocity measured in the center of the gap with the following scattering particles: (a) yeast C276.4A with high Nyquist frequency; (b) bacteria and (c) yeast D273.10B in the backscattering mode; (d) yeast D273.10B dyed with Saffranin in the backscattering mode.

trum with yeast C276.4A is shown, but it is representative of the results obtained for all the different particles. The highest Nyquist frequency we used is still well below that at which Brownian motion may introduce error in the velocity measurements,[16] and indeed we see no such contribution in the spectra. Figures 3(b) and 3(c) show spectra using the bacterium and yeast D273.10 B as tracer particles, respectively; in both cases the data were obtained in the backscattering mode. The signal-to-noise ratio of the fundamental peak has dropped slightly more than an order of magnitude; this is consistent with the Mie scattering theory for particles of these dimensions.[17] The primary peak is still clearly visible at least four orders of magnitude above the background noise, but the secondary peaks are harder to discern. We dyed each of the biological particles with Saffranin, a red dye, to increase their reflectance of the red laser light. The resulting spectra showed little change from the undyed case, with perhaps a slight difference in favor of the dyed particles when using the backscattering mode. Again a representative spectrum of the dyed particles is shown [Fig. 3(d)]; the results were similar in all cases.

IV. DISCUSSION

The organisms we selected are certainly not the only ones that could yield potentially useful tracer particles. We rejected the use of blood cells and particulate suspensions such as milk because they are heterogeneous in size, and they are either not particularly spherical or they do not maintain their shape in this application. The organisms we have chosen are encased in a rigid cell wall and can maintain their shapes under a variety of conditions: in fact, drastic physical or chemical means are required to break the walls, even of the dead organisms. The cell walls are molecular cages, composed mostly of polymers of sugars or their derivatives, that allow the passage of small molecules. The exact size of the molecules varies with the particular cell wall, but most walls will allow the diffusion of molecules with a molecular weight of a few thousand. In the living cell the passage of small molecules and ions is regulated by a membrane that lies inside the cell wall; the integrity of this membrane requires the expenditure of energy and it ceases to function upon the death of the cell. The formaldehyde kills the cells and converts them, for the present purposes, to rigid molecular cages containing inactivated, high-molecular weight cellular constituents. We will refer to the interior contents of the cell as the cell matrix, the major components of which are DNA, cellular proteins, and RNA, retained in their normal structures. The free exchange of small molecules, such as the salt water, through the cell wall and into the cell matrix allows the density of the particles to be matched fairly closely to that of the working fluid. This density matching may play a role in permitting the long term suspension of the particles. Fluid exchange is by simple diffusion through the cell wall and matrix. For ions the size of Na^+ and I^-, equilibrium should be established within seconds.

The presence of the cellular matrix within the killed cells allows its exploitation in staining the particles. Since formaldehyde killing preserves most of the intracellular structure of the organisms, dyes that stain specific cell constituents can be used. For example, one could stain the surface or various interior components of the cells with fluorescent dyes such as acridine orange, aniline blue, DAPI (blue), rhodamine, or fluorescein that have affinity for carbohydrates, nucleic acids, or proteins. The cell matrices may also be stained a particular color to reduce their transmittance and increase the reflectance of the specific laser light being used. As stated earlier, we used Saffranin for this purpose.

It is not difficult to achieve a homogeneity in the size of the cells. Certain organisms, grown under defined conditions, will produce populations of cells of about the same size. Since the cells reproduce by dividing, and they accumulate mass between divisions, cells that have just divided ("young" cells) tend to be smaller than cells just about to divide ("old" cells). Most of the heterogeneity of size in a population will be due to the distribution of young and old cells. It is important to pick an organism whose size differential is not extreme. Not all strains of a given organism have the same growth characteristics or cell shape; for example, the one yeast strain we worked with was more spherical than the other. One must not assume that all microorganisms within a particular class will work equally as well.

A most attractive benefit of these seed particles is that they are extremely inexpensive. The procedures for growing the organisms and preparing them for use are standard in most microbiology laboratories. Strains of organisms can be obtained locally from departmental culture collections or from the collections of individual investigators. Sufficient quantities of particles for several months work can be grown in a day to a week, depending on the organism, using less than 100 ml of standard microbiological media. Processing of the samples (harvesting, killing, washing, and delivery) is accomplished in less than 3 h; most of that time is occupied in the 2 h formaldehyde-killing step that requires no manipulations. It is also possible to filter the index matching fluid containing the particles through an inexpensive membrane filter to remove the biological tracer particles, and any stray dust or dirt, so that a different type of particle can be substituted. A similar filtering sytem, or a centrifugation process, may be used to recover the particles for reuse in an open flow system. However, the labor involved to recover the particles, in contrast to the minimal expense of replacing them, may not be cost effective.

It should be noted that although the particles we used had been killed with formaldehyde, they were chosen from organisms that pose minimal health hazard and are found in the normal working environment. Before biological particles are used, even in the formaldehyde-treated form, prudence would dictate consulting with a knowledgeable biologist concerning possible health risks involved in dealing with the live form of the organisms. This point cannot be stressed enough, since conidia, in particular, are resistant to killing.

We have demonstrated that light-scattering particles derived from several microorganisms are useful in LDV studies of fluid flow. We evaluated these particles under very specific conditions, i.e., in a concentrated NaI solution in a circular Couette flow system. However, there are several reasons that these particles are likely to be useful for studying flow of a wide range of aqueous fluids. First, the particles themselves are compatible with many aqueous solutions. In fact, the organisms from which they are derived thrive in aqueous environments. Second, the particles can be suspended in distilled water or dilute solutions of salts and the settling time is measured in hours per centimeter. They can be maintained in suspension by minimal agitation. The particles behaved as colloids in a wide range of concentrations of NaI solutions with virtually no observable sedimentation over several days. These observations suggest that the particles may be effective in LDV scattering in aqueous fluids of vastly different specific gravities and compositions. Third, the particles can be very useful in applications where expensive fluorescent tracers are currently employed. Finally, the particles we used were not selected after an exhaustive search. Rather, they were derived from conveniently available microorganisms that were likely to meet the initial criteria we established. Since all four organisms we tested gave acceptable LDV signals, there may be many more potentially useful light scattering particles currently residing in local microbiological culture collections.

ACKNOWLEDGMENTS

We thank Doug Dolfinger and Paul Murphy for their help in the design and construction of our apparatus; Bill Swoager, John Pringle, and Phil Perlman for providing organisms; Berl Oakley for furnishing organisms and microscope facilities; and Phil Farina for the gift of Myacide SP.

This work was supported in part by the Office of Naval Research Contract No. N00014-86-K-0071.

[1]P. B. Duran glass, Wilmad Glass Company, Inc., Buena, NJ.
[2]A. Fraser and H. L. Swinney (private communication).
[3]Bacterial strain obtained from W. Swoager, Department of Microbiology, The Ohio State University.
[4]T. Maniatis, E. F. Fritsh, and J. Sambrook, *Molecular Cloning, a Laboratory Manual* (Cold Spring Harbor Laboratory, New York, 1982).
[5]F. Sherman, J. W. Stewart, J. H. Parker, E. Inhaber, N. A. Shipment, G. J. Putterman, R. L. Gardinsky, and E. Margoliash, J. Biol. Chem. **243**, 5446 (1968); yeast strain obtained from P. Perlman, Department of Molecular Genetics, The Ohio State University.
[6]L. E. Wilkinson and J. R. Pringle, Exp. Cell Res. **89**, 175 (1974); yeast strain obtained from J. Pringle, Department of Biology, The University of Michigan.
[7]Media used in cultivating the various organisms were YPD broth: yeast extract, 10 g; peptone, 20 g; glucose, 20 g; H_2O to a final volume of 1000 cm^3. YG broth: yeast extract, 10 g; glucose, 20 g; H_2O to 1000 cm^3. YG agar: YG broth + 15 g agar per 1000 cm^3.
[8]This strain was obtained from B. Oakley, Department of Molecular Genetics, The Ohio State University; originally obtained from C. Roberts, University of Leichester, United Kingdom.
[9]A. J. Clutterbuck, in *Handbook of Genetics*, edited by R. C. King (Plenum, New York, 1974), p. 447.
[10]M. Meselson and F. Stahl, Proc. Natl. Acad. Sci. **44**, 671 (1958).
[11]C. E. Ballou, in *The Molecular Biology of the Yeast Saccharomyces Metabolism and Gene Expression*, edited by J. N. Strathern, E. W. Jones, and J. R. Broach (Cold Spring Harbor Laboratory, New York, 1982), pp. 335–360.
[12]L. Leive, *Bacterial Membranes and Walls* (Marcel Dekker, New York, 1973).
[13]S. Voyutsky, *Colloid Chemistry*, translated by N. Bobrov (MIR, Moscow, 1978), Chap. 7.
[14]M. Gorman and H. L. Swinney, J. Fluid Mech. **117**, 123 (1982).
[15]G. P. King, Y. Li, W. Lee, and H. L. Swinney, J. Fluid Mech. **141**, 365 (1984).
[16]E. F. C. Somerscales, in *Methods of Experimental Physics*, edited by L. Marton and C. Marton (Academic, New York, 1981), Vol. 18, Part A, pp. 39–41.
[17]H. C. van de Hulst, *Light Scattering by Small Particles* (Wiley, New York, 1962), pp. 151–153.

Appendix B: Invited Seminars, Colloquia and Conference Talks

Invited Seminars and Colloquia:

Eastern Michigan University
University of Akron
Duke University
Ohio University
Ohio State University
Naval Surface Weapons Center
Michigan State University
ESPCI, University of Paris
University of Michigan-Dearborn
Kent State University
Case Western Reserve University
University of California-Santa Barbara

Invited Conference Presentations:

AAPT Summer Meeting, Columbus, Ohio, 1986
Workshop at Les Houches, France, 1987
Ohio Section APS Meeting, Akron, 1987
National Science Teachers Association Area Convention, Columbus, Ohio, 1988
Spring Meeting of the APS, Baltimore, 1989
Aspen Center for Physics Workshop, Aspen, Colorado, 1989
Gordon Research Conference, Ventura, California, 1992
Conference on Nonlinear Problems of Hydrodynamic Stability Theory, Moscow, Russia, 1992
Spring Meeting of the APS, Washington, 1992

Appendix C: Students and Postdoctoral Research Associates

Selected M. S. and Doctoral Students

1. G. William Baxter, *"An Experimental Study of Dynamical Domain Formation in a Circular Couette System,"* M.S., August 1986. Now at Behrend College, of Pennsylvania State University.
2. John J. Hegseth, *"Spatiotemporal Patterns in Flow Between Two Independently Rotating Cylinders,"* Ph.D., January 1990. Now at the University of New Orleans.
3. Innocent Mutabazi, *"Etude Theorique et Experimentale de l'Instabilite Centrifuge de Taylor-Dean,"* Ph.D., January 1990. Degree from ESPCI, Paris, primary advisor J. E. Wesfreid, work partially done at OSU under my supervision. See 4. below.
4. Mingming Wu, *"A Study of External Modulation of Nonlinear Systems,"* Ph.D., Autumn 1991. Now at the University of California-Santa Barbara.

Postdoctoral Research Associates

1. Donald Griswold [Ph.D., Ohio State University (1986)], September 1986 to April 1987. Now at Lawrence Livermore Laboratory.
2. Diane A. Jacobs [Ph.D., University of Texas-Austin (1983)], August 1986 to August 1988. Now at Eastern Michigan University.
3. S. Scott Courts [Ph.D., Ohio State University (1988)], September 1988 to October 1989. Now at Lake Shore Cryotronics.
4. Innocent Mutabazi [Ph.D., ESPCI, University of Paris (1990)], May 1990 to September 1991. Now at University of LeHavre, France.